Mathematics of Evolution and Life

A Complete Monograph in Twelve Section s

A Complete and Explicit Guide · Every derivation unfolded
Every symbol earned · Every idea motivated

"Life is not a miracle. It is an inevitable consequence
of the mathematics of replication, selection, and time.
Understanding it requires exactly the mathematics
that biology has been too modest to demand of itself."

Contents

I Section **I — Populations, Genes, and the Hardy–Weinberg Equilibrium** **2**

0.1 1. The Strange Simplicity of Heredity . . . 3

0.1.1 1.1 The Mathematical Structure of a Population . . . 3

0.1.2 1.2 Mendelian Segregation as a Random Process . . . 4

0.1.3 1.3 Panmixia and the Gene Pool . . . 4

0.2 2. The Hardy–Weinberg Theorem: Statement, Proof, and Generalisations . . . 5

0.2.1 2.1 The Theorem and Its Complete Proof . . . 5

0.2.2 2.2 The Algebraic Identity at the Heart of the Theorem . . . 5

0.2.3 2.3 Numerical Example: The ABO Blood Group System . . . 6

0.2.4 2.4 The Historical Significance: The Dilution Fallacy . . . 6

0.3 3. Testing Hardy–Weinberg: Statistical Inference . . . 7

0.3.1 3.1 The Chi-Squared Goodness-of-Fit Test . . . 7

0.3.2 3.2 Worked Example . . . 7

0.3.3 3.3 Exact Tests for Small Samples . . . 8

0.4 4. Linkage Disequilibrium: The Correlation Between Loci . . . 8

0.4.1 4.1 From One Locus to Two . . . 8

0.4.2 4.2 The Linkage Disequilibrium Parameter D . . . 9

0.4.3 4.3 The Decay of Linkage Disequilibrium . . . 9

0.4.4 4.4 Rates of LD Decay: Physical Interpretation . . . 10

0.4.5 4.5 Causes of Linkage Disequilibrium . . . 10

0.5 5. Population Structure and the Wahlund Effect . . . 11

0.5.1 5.1 The Wahlund Principle . . . 11

0.5.2 5.2 Wright's F-Statistics . . . 11

0.5.3 5.3 The Biological Interpretation of F_{ST} . . . 12

0.5.4 5.4 The Correlation Between F_{ST} and Geographic Distance . . . 12

0.6 6. Hardy–Weinberg in Haploid and X-Linked Loci . . . 13

0.6.1 6.1 Haploid Populations . . . 13

0.6.2 6.2 X-Linked Loci . . . 13

0.7 7. Summary and Bridge to Section II . . . 13

0.8 10. Advanced Topics in Hardy-Weinberg Theory . . . 14

0.8.1 10.1 The Multiallelic Hardy-Weinberg Principle: Complete Treatment . . . 14

0.8.2 10.2 Deviations from Hardy-Weinberg: A Classification . . . 15

0.8.3 10.3 The Ewens Sampling Formula . . . 15

0.9 11. The Theory of Genetic Distance . . . 16

0.9.1 11.1 Measures of Genetic Distance Between Populations . . . 16

0.9.2 11.2 Principal Component Analysis of Allele Frequency Data 17
0.10 12. Coalescent Theory: A Preview 18
0.10.1 12.1 From Forward to Backward: Genealogical Thinking 18
0.10.2 12.2 MRCA and the Age of Adam and Eve 18
0.11 13. Recombination, Gene Conversion, and Haplotype Structure 19
0.11.1 13.1 The Rate of Recombination and Map Distance 19
0.11.2 13.2 Gene Conversion and Its Effect on Allele Frequencies 19
0.11.3 13.3 Haplotype Block Structure and Tag SNPs 20
0.12 14. Admixture and Ancestry Inference 20
0.12.1 14.1 The Admixture Model 20
0.12.2 14.2 STRUCTURE and Bayesian Clustering 21
0.12.3 14.3 The Mathematics of Local Ancestry Inference 21
0.13 15. Summary: The Mathematical Universe of Hardy-Weinberg 22
0.14 16. The Mathematics of Genetic Drift: A Preview 23
0.14.1 16.1 Why Infinite Populations Are a Fiction 23
0.14.2 16.2 The Wright-Fisher Model: Setup 24
0.14.3 16.3 The Variance Effective Population Size 24
0.15 17. Probability Theory Foundations for Population Genetics 25
0.15.1 17.1 Probability Spaces and Genetic Events 25
0.15.2 17.2 Generating Functions and the Moments of the Allele Frequency Distribution 25
0.15.3 17.3 The Martingale Structure of Allele Frequencies 26
0.16 18. Quantitative Methods in Modern Population Genomics 26
0.16.1 18.1 LD Score Regression 26
0.16.2 18.2 The Mathematics of Polygenic Scores 27
0.16.3 18.3 Hardy-Weinberg Equilibrium in GWAS Quality Control 28
0.17 19. Open Problems in Population Genetics 28
0.17.1 19.1 The Missing Heritability Problem 28
0.17.2 19.2 Ancient DNA and the Dynamics of Allele Frequencies in Deep Time 28
0.17.3 19.3 Polygenic Adaptation and the Quantitative Genetics of Selection 29
0.18 20. Mathematical Genetics and Medicine 29
0.18.1 20.1 Hardy-Weinberg in Clinical Genetics 29
0.18.2 20.2 Newborn Screening and the Population Genetics of Recessive Disease . . . 30
0.18.3 20.3 Forensic Genetics and the Product Rule 31
0.19 21. The Hardy-Weinberg Principle in Non-Standard Organisms 31
0.19.1 21.1 Polyploidy and Hardy-Weinberg Generalisation 31
0.19.2 21.2 Haplodiploidy and Hardy-Weinberg in the Hymenoptera 32
0.19.3 21.3 Selfing and the Decay of Heterozygosity 33
0.20 22. Information-Theoretic Perspective on Hardy-Weinberg 33
0.20.1 22.1 The Kullback-Leibler Divergence from Hardy-Weinberg 33
0.20.2 22.2 Mutual Information Between Alleles 34

II Section **II — Drift, Fixation, and the Stochastic Theory of Evolution** **36**
0.21 1. When Chance Shapes the Genome 37
0.22 2. The Wright–Fisher Model 37

0.22.1 2.1 Definition and Basic Structure . . . 37
0.22.2 2.2 The Moments of One Generation of Drift . . . 38
0.22.3 2.3 The Martingale Property . . . 39
0.23 3. Fixation Probability of a Neutral Allele . . . 39
0.23.1 3.1 The Theorem and Its Proof . . . 39
0.23.2 3.2 Biological Consequences of the Fixation Probability Theorem . . . 39
0.24 4. The Effective Population Size . . . 40
0.24.1 4.1 Definition . . . 40
0.24.2 4.2 The Human Effective Population Size . . . 41
0.25 5. Kimura's Diffusion Approximation . . . 41
0.25.1 5.1 The Stochastic Differential Equation . . . 41
0.25.2 5.2 The Fokker–Planck Equation . . . 42
0.25.3 5.3 The Fixation Probability Under Selection . . . 42
0.26 6. Time to Fixation and the Rate of Neutral Evolution . . . 43
0.26.1 6.1 Expected Time to Fixation . . . 43
0.26.2 6.2 The Neutral Substitution Rate and the Molecular Clock . . . 43
0.27 7. The Moran Model . . . 44
0.27.1 7.1 Definition . . . 44
0.27.2 7.2 Equivalence with the Wright–Fisher Model . . . 44
0.28 8. The Kingman Coalescent . . . 45
0.28.1 8.1 Genealogical Thinking . . . 45
0.28.2 8.2 Definition of the Kingman Coalescent . . . 45
0.28.3 8.3 The Expected Time to the Most Recent Common Ancestor . . . 45
0.28.4 8.4 Total Branch Length and Expected Pairwise Diversity . . . 46
0.29 9. Summary . . . 46
0.30 11. The Structured Coalescent and Population Subdivision . . . 47
0.30.1 11.1 Genealogies in Subdivided Populations . . . 47
0.30.2 11.2 The Ancestral Selection Graph . . . 48
0.31 12. The Extended Coalescent: Recombination and the ARG . . . 49
0.31.1 12.1 Genealogy with Recombination . . . 49
0.31.2 12.2 Sequentially Markovian Coalescent (SMC) . . . 50
0.32 13. Inferring Demographic History: PSMC and its Generalisations . . . 50
0.32.1 13.1 The PSMC Model . . . 50
0.32.2 13.2 MSMC and the Cross-Coalescence Rate . . . 51
0.33 14. Ancient DNA and Temporal Genomics . . . 52
0.33.1 14.1 The Fragment Length Model for aDNA Damage . . . 52
0.33.2 14.2 Temporal F_{ST} and Ancient vs. Modern Allele Frequencies . . . 52
0.34 15. Neutral Molecular Evolution: Tests and Parameters . . . 53
0.34.1 15.1 The McDonald-Kreitman Test . . . 53
0.34.2 15.2 The Neutral Theory's Quantitative Predictions . . . 54
0.35 16. Coalescent Simulation and Computational Methods . . . 54
0.35.1 16.1 The Hudson ms Algorithm . . . 54
0.35.2 16.2 Approximate Bayesian Computation (ABC) for Population Genetics . . . 55
0.36 17. Summary and Synthesis . . . 56
0.37 18. The Site Frequency Spectrum Under Demographic Models . . . 57

0.37.1 18.1 Exponential Growth . . . 57
0.37.2 18.2 Bottlenecks and the SFS . . . 57
0.37.3 18.3 Composite Likelihood Methods . . . 58
0.38 19. Continuous-Time Branching Processes and the Galton-Watson Model . . . 58
0.38.1 19.1 The Galton-Watson Process . . . 58
0.38.2 19.2 The Feller Diffusion . . . 59
0.39 20. Coalescent Theory and the HapMap: A Case Study . . . 59
0.39.1 20.1 The HapMap Project and the Recombinational Architecture of the Human Genome . . . 59
0.39.2 20.2 Recombination Hotspots . . . 60
0.40 24. Population Genomics of Admixture . . . 61
0.40.1 24.1 Admixture as a Coalescent Process . . . 61
0.40.2 24.2 STRUCTURE and ADMIXTURE: Model-Based Clustering . . . 61
0.41 25. Complete Summary of Section II . . . 62

III Section III — Selection, Fitness, and the Geometry of Allele Dynamics 63
0.42 1. The Mathematics of Advantage . . . 64
0.43 2. The One-Locus Selection Equation . . . 64
0.43.1 2.1 Setup and Derivation . . . 64
0.43.2 2.2 The Selection Coefficient . . . 65
0.44 3. Fisher's Fundamental Theorem of Natural Selection . . . 65
0.44.1 3.1 Statement and Derivation . . . 65
0.44.2 3.2 The Relation to Fisher Information . . . 66
0.45 4. The Dynamics of Different Dominance Modes . . . 66
0.45.1 4.1 Dominant Beneficial Allele . . . 66
0.45.2 4.2 Recessive Beneficial Allele . . . 67
0.45.3 4.3 Numerical Comparison . . . 67
0.46 5. Mutation–Selection Balance . . . 67
0.46.1 5.1 The General Framework . . . 67
0.46.2 5.2 Genetic Load . . . 68
0.47 6. Heterozygote Advantage and Stable Polymorphism . . . 69
0.47.1 6.1 The Existence and Stability of Interior Equilibria . . . 69
0.47.2 6.2 The Sickle Cell Example in Full Quantitative Detail . . . 69
0.47.3 6.3 Protected Polymorphism . . . 70
0.48 7. Frequency-Dependent Selection . . . 70
0.48.1 7.1 When Fitness Depends on Composition . . . 70
0.48.2 7.2 Negative Frequency Dependence . . . 70
0.48.3 7.3 Positive Frequency Dependence and Bistability . . . 71
0.49 8. Multilocus Selection: Epistasis and Robertson's Secondary Theorem . . . 71
0.49.1 8.1 The Problem of Multiple Loci . . . 71
0.49.2 8.2 The Coupling of Selection and Recombination . . . 71
0.49.3 8.3 Robertson's Secondary Theorem . . . 72
0.50 9. The Balance Between Selection and Drift . . . 72
0.50.1 9.1 Fixation Probability Under Selection . . . 72

0.50.2 9.2 The Probability of Survival of Beneficial Mutations . . . 73
0.51 10. Summary . . . 73
0.52 13. Eco-Evolutionary Dynamics . . . 73
0.52.1 13.1 Density-Dependent Selection . . . 73
0.52.2 13.2 Adaptive Dynamics: Invasion Fitness . . . 74
0.53 14. Multilocus Dynamics and the Geometry of Allele Frequency Space . . . 75
0.53.1 14.1 The Two-Locus Selection Equation: Complete Treatment . . . 75
0.53.2 14.2 The Geometric Mean Fitness Criterion . . . 76
0.54 15. The Geometry of Fitness Landscapes . . . 76
0.54.1 15.1 Fitness Landscapes as Surfaces . . . 76
0.54.2 15.2 The Travelling Fitness Wave and Clonal Interference . . . 77
0.55 16. Sexual Selection and Sexual Conflict . . . 78
0.55.1 16.1 Runaway Selection: The Fisher-Lande-Kirkpatrick Model . . . 78
0.55.2 16.2 Honest Signalling: The Zahavian Handicap . . . 78
0.56 17. Complete Summary of Section III . . . 79
0.57 18. Evolvability and Robustness . . . 80
0.57.1 18.1 Definitions and the Tension Between Robustness and Evolvability . . . 80
0.57.2 18.2 Canalization and the Hidden Genetic Variance . . . 81
0.58 19. Speciation: The Mathematical Theory . . . 81
0.58.1 19.1 The Bateson-Dobzhansky-Muller Model . . . 81
0.58.2 19.2 Sympatric Speciation and the Disruptive Selection Model . . . 82
0.59 20. Coevolution and the Red Queen . . . 83
0.59.1 20.1 The Red Queen Hypothesis and Coevolutionary Cycling . . . 83
0.59.2 20.2 The Mathematical Theory of Coevolution: Quantitative Genetics Framework 83
0.60 21. Extended Summary and Cross Section Connections . . . 84
0.61 19. The Multilocus Price Equation and Epistasis . . . 85
0.61.1 19.1 Epistasis and the Breakdown of Additivity . . . 85
0.61.2 19.2 The Extended Price Equation for Multilocus Systems . . . 85
0.61.3 19.3 Canalization and the Evolution of Robustness . . . 86
0.62 20. Historical Notes: From Darwin to Price . . . 86
0.62.1 20.1 The Mathematical Vacuum Before 1918 . . . 86
0.62.2 20.2 The Modern Synthesis and the Mathematical Framework . . . 86
0.62.3 20.3 After Price: Hamilton, Grafen, and the Current Synthesis . . . 87

IV Section IV — The Price Equation and the Algebra of Selection 88
0.63 1. A Universal Language for Selection . . . 89
0.64 2. The Setup and the Derivation . . . 89
0.64.1 2.1 Entities, Characters, and Fitness . . . 89
0.64.2 2.2 The Covariance Decomposition . . . 90
0.65 3. Interpreting the Two Terms . . . 90
0.65.1 3.1 The Selection Term . . . 90
0.65.2 3.2 The Transmission Term . . . 91
0.66 4. Fisher's Theorem and Hamilton's Rule as Special Cases . . . 92
0.66.1 4.1 Fisher's Fundamental Theorem . . . 92

0.66.2 4.2 Derivation of Hamilton's Rule 92
0.67 5. Multilevel Selection 93
0.67.1 5.1 The Hierarchical Price Equation 93
0.67.2 5.2 The Group Selection Debate Resolved 93
0.68 6. Robertson's Secondary Theorem and the Breeder's Equation 94
0.68.1 6.1 Robertson's Theorem 94
0.68.2 6.2 The Breeder's Equation 94
0.69 7. Cultural Evolution and the Replicator Equation 94
0.69.1 7.1 The Price Equation Beyond Genetics 94
0.69.2 7.2 Connection to the Replicator Equation 95
0.70 8. Summary 95
0.71 9. The Geometry of the Price Equation: Vector Spaces and Projections 96
0.71.1 9.1 The Price Equation in Inner Product Form 96
0.71.2 9.2 Projections and the Decomposition of Characters 96
0.71.3 9.3 The Multivariate Price Equation 97
0.72 10. Inclusive Fitness Theory and the Extended Hamilton's Rule 97
0.72.1 10.1 Inclusive Fitness: Definition and Calculation 97
0.72.2 10.2 The Haig-Hamilton Paradox and Genomic Imprinting 98
0.72.3 10.3 Green-Beard Effects and Non-Genealogical Relatedness 98
0.73 11. Applications to Evolutionary Epidemiology 99
0.73.1 11.1 The Price Equation for Pathogen Virulence Evolution 99
0.73.2 11.2 Herd Immunity and the Epidemiological Price Equation 100
0.74 12. The Price Equation and Information Theory 100
0.74.1 12.1 Selection as a Change in Kullback-Leibler Divergence 100
0.74.2 12.2 The Free Fitness Functional 101
0.74.3 12.3 Sanov's Theorem and the Large-Deviation Rate of Evolution 101
0.75 13. Evolutionary Game Theory and the Price Equation 102
0.75.1 13.1 Nash Equilibria as Fixed Points of the Price Equation 102
0.75.2 13.2 The Prisoner's Dilemma and the Evolution of Cooperation 102
0.75.3 13.3 Evolutionary Stable Strategies and Invasion Analysis 103
0.76 14. Advanced Topics: Stochastic Price Equation and Bet-Hedging 103
0.76.1 14.1 The Stochastic Price Equation 103
0.76.2 14.2 Bet-Hedging as a Price Equation Phenomenon 104
0.77 15. Synthesis: The Price Equation as a Meta-Theory 104
0.78 16. The Formal Darwinism Project 105
0.78.1 16.1 Fundamental Theorem of Natural Selection: Exact Statement 105
0.78.2 16.2 Optima Without Gradients: When the Formal Darwinism Framework Fails . 106
0.79 17. Connections to Statistical Mechanics and Thermodynamics 106
0.79.1 17.1 The Second Law of Thermodynamics and Fisher's Theorem 106
0.79.2 17.2 Non-Equilibrium Thermodynamics and Evolutionary Flows 107
0.79.3 17.3 Fisher Information and the Cramér-Rao Bound for Evolution 107
0.80 18. Numerical Methods for the Price Equation 107
0.80.1 18.1 Computing the Price Equation Decomposition from Empirical Data 107
0.80.2 18.2 Bootstrap Confidence Intervals for Selection and Transmission Terms . . . 108

0.80.3 18.3 Worked Example: Price Equation Analysis of Selection on Beak Size in Darwin's Finches 108

V Section V — Fitness Landscapes and the Topology of Evolutionary Search 110

0.81 1. The Landscape Metaphor Made Precise 111
0.82 2. Sequence Space and its Geometry 111
0.82.1 2.1 The Binary Hypercube 111
0.82.2 2.2 Nucleotide Sequence Space 111
0.82.3 2.3 Measuring Distance Between Genotypes 111
0.83 3. The NK Model of Fitness Landscapes 112
0.83.1 3.1 Definition 112
0.83.2 3.2 The Two Extremes 112
0.83.3 3.3 Properties of the NK Landscape for Intermediate K 113
0.84 4. The Walsh–Hadamard Fourier Transform 113
0.84.1 4.1 Fourier Analysis on the Boolean Hypercube 113
0.84.2 4.2 Interpretation of Fourier Coefficients 114
0.84.3 4.3 The Fourier Spectrum and Landscape Ruggedness 114
0.85 5. Evolutionary Accessibility and Paths Through Genotype Space 115
0.85.1 5.1 Accessible Mutational Paths 115
0.85.2 5.2 Sign Epistasis and Inaccessibility 115
0.86 6. Neutral Networks and Percolation 116
0.86.1 6.1 Neutral Networks 116
0.86.2 6.2 Percolation on the Hypercube 116
0.86.3 6.3 Phenotypic Accessibility and the Robustness-Evolvability Relationship . . . 116
0.87 7. Evolutionary Dynamics on Landscapes 117
0.87.1 7.1 Adaptive Walks 117
0.87.2 7.2 Epistasis and the Distribution of Fitness Effects 117
0.88 8. Summary 117

VI Section VI — Phylogenetics: Trees, Distances, and Evolutionary Time 119

0.89 9. The Geometry of Adaptive Walks 120
0.89.1 9.1 Definition and Classification of Adaptive Walks 120
0.89.2 9.2 Convergence and Reproducibility of Evolution 121
0.90 10. Epistasis and the Walsh–Hadamard Decomposition in Depth 121
0.90.1 10.1 Types of Epistasis 121
0.90.2 10.2 Geometric Mean Epistasis and Multiplicativity 122
0.91 11. Adaptive Landscape Theory and Macroevolution 123
0.91.1 11.1 Wright's Shifting Balance Theory 123
0.91.2 11.2 Fitness Landscape Dimensionality and the Problem of Large L 123
0.92 12. Ruggedness Measures and Landscape Statistics 124
0.92.1 12.1 Landscape Correlation Length 124
0.92.2 12.2 Roughness and the "Rugged" Phenotype 125
0.93 13. Population Genetics on Fitness Landscapes 125
0.93.1 13.1 The Mutation-Selection-Drift Balance on a Landscape 125

0.94 14. Experimental Fitness Landscapes: Deep Mutational Scanning . . . 126
0.94.1 14.1 Methodology and Data . . . 126
0.94.2 14.2 Epistasis from Double Mutant Libraries . . . 127
0.95 15. Accessibility, Contingency, and the History-Dependence of Evolution . . . 128
0.95.1 15.1 Historical Contingency in the LTEE . . . 128
0.96 9. Empirical Fitness Landscapes and Experimental Evolution . . . 129
0.96.1 9.1 Measuring Fitness Landscapes Directly . . . 129
0.96.2 9.2 Landscape Ruggedness Statistics . . . 129
0.96.3 9.3 Experimental Evolution on Fitness Landscapes . . . 130
0.97 10. Epistasis, Evolvability, and the Geometry of Adaptation . . . 130
0.97.1 10.1 Reciprocal Sign Epistasis and Landscape Complexity . . . 130
0.97.2 10.2 Epistasis and Mutational Robustness . . . 131
0.97.3 10.3 The Geometric Model of Adaptation . . . 131

VII Section VI — Phylogenetics: Trees, Distances, and Evolutionary Time 133
0.98 1. Reading the Book of Life . . . 134
0.99 2. Models of Sequence Evolution . . . 134
0.99.1 2.1 The Jukes–Cantor Model . . . 134
0.99.2 2.2 The Jukes–Cantor Distance . . . 134
0.99.3 2.3 The General Time-Reversible (GTR) Model . . . 135
0.99.4 2.4 Rate Variation Across Sites . . . 135
0.1003. Tree Metrics and Reconstruction . . . 136
0.100.1 3.1 The Four-Point Condition . . . 136
0.100.2 3.2 The Neighbour-Joining Algorithm . . . 136
0.1014. Maximum Likelihood Phylogenetics . . . 137
0.101.1 4.1 The Likelihood Function . . . 137
0.101.2 4.2 Felsenstein's Pruning Algorithm . . . 137
0.1025. Bayesian Phylogenetics . . . 138
0.102.1 5.1 The Bayesian Framework . . . 138
0.102.2 5.2 Markov Chain Monte Carlo Sampling . . . 139
0.1036. The Coalescent as a Prior for Population-Level Phylogenetics . . . 139
0.103.1 6.1 Gene Trees vs. Species Trees . . . 139
0.103.2 6.2 Molecular Clock Testing . . . 140
0.1047. Summary . . . 140

VIII Section VII — Evolutionary Game Theory: Strategies, Equilibria, and Replicators 141
0.1058. Molecular Clocks and Rate Variation . . . 142
0.105.1 8.1 The Strict and Relaxed Molecular Clock . . . 142
0.105.2 8.2 The Generation Time Effect . . . 143
0.1069. Ancestral Sequence Reconstruction . . . 143
0.106.1 9.1 Marginal and Joint Ancestral Reconstruction . . . 143
0.106.2 9.2 Uncertainty in Ancestral Reconstruction . . . 144
0.10710. The Gene Tree vs. Species Tree Problem . . . 144

0.107.1 10.1 Incomplete Lineage Sorting . . . 144
0.107.2 10.2 ASTRAL and Quartet-Based Species Tree Estimation . . . 145
0.10811. Network Approaches to Phylogenetics . . . 145
0.108.1 11.1 Phylogenetic Networks and Reticulate Evolution . . . 145
0.108.2 11.2 Split Decomposition and the NeighborNet Algorithm . . . 146
0.10912. Rate Heterogeneity and the Gamma Model . . . 146
0.109.1 12.1 Among-Site Rate Variation . . . 146
0.11013. Bayesian Phylogenetics and MCMC . . . 147
0.110.1 13.1 The Bayesian Framework . . . 147
0.110.2 13.2 Prior Sensitivity and Model Comparison . . . 148
0.11114. Total Evidence Dating and Tip Calibrations . . . 148
0.111.1 14.1 The Total Evidence Framework . . . 148
0.1128. Ancestral Sequence Reconstruction and Palaeogenomics . . . 149
0.112.1 8.1 Marginal Ancestral Reconstruction . . . 149
0.112.2 8.2 Joint versus Marginal Reconstruction . . . 150
0.112.3 8.3 Palaeogenomics: Genome-Scale Ancestral Reconstruction . . . 150
0.1139. Network-Based Phylogenetics and Reticulate Evolution . . . 151
0.113.1 9.1 Phylogenetic Networks . . . 151
0.113.2 9.2 The Hybridisation Number . . . 151
0.113.3 9.3 Detecting HGT Using Phylogenetic Incongruence . . . 151

IX Section VII — Evolutionary Game Theory: Strategies, Equilibria, and Replicators 153
0.1141. The Evolution of Strategy . . . 154
0.1152. The Basic Framework . . . 154
0.115.1 2.1 Symmetric Normal-Form Games . . . 154
0.115.2 2.2 Nash Equilibria . . . 154
0.1163. Evolutionarily Stable Strategies . . . 155
0.116.1 3.1 The ESS Concept . . . 155
0.1174. The Replicator Equation . . . 155
0.117.1 4.1 Derivation and Properties . . . 155
0.117.2 4.2 Fixed Points and Stability . . . 156
0.1185. The Hawk–Dove Game . . . 156
0.118.1 5.1 Formulation . . . 156
0.118.2 5.2 Analysis . . . 156
0.1196. The Prisoner's Dilemma and the Evolution of Cooperation . . . 157
0.119.1 6.1 The Social Dilemma . . . 157
0.119.2 6.2 Kin Selection . . . 158
0.119.3 6.3 Direct Reciprocity and Tit-for-Tat . . . 158
0.119.4 6.4 Network Reciprocity . . . 158
0.1207. The Replicator–Mutator Equation . . . 159
0.120.1 7.1 Incorporating Mutation . . . 159
0.120.2 7.2 Evolutionary Stability with Mutation . . . 159
0.1218. Rock–Paper–Scissors and Limit Cycles . . . 159

0.1229. Summary 160

X Section VIII — Virus–Host Dynamics: Co-evolution and Quasi-species 161

0.12310. Spatial Games and the Evolution of Cooperation 162
0.123.1 10.1 Why Space Matters 162
0.123.2 10.2 The Evolution of Altruism: A Unified Mathematical View 163
0.12411. Evolutionary Game Theory and Major Transitions 163
0.124.1 11.1 Transitions in Individuality as Cooperative Dilemmas 163
0.124.2 11.2 The Evolution of Fairness: Ultimatum Game 164
0.12512. Signal Detection Games and Biological Communication 164
0.125.1 12.1 Costly Signalling and Honest Signals 164
0.125.2 12.2 Cheap Talk and Vague Signals 165
0.12613. Evolutionary Dynamics in Finite Populations: The Moran Process 166
0.126.1 13.1 The Moran Process and Fixation Probabilities 166
0.12714. Public Goods Games and the Evolution of Punishment 167
0.127.1 14.1 The Public Goods Dilemma 167
0.127.2 14.2 Altruistic Punishment and the Evolution of Social Norms 167
0.12815. Evolutionary Dynamics in Structured Populations 168
0.128.1 15.1 Fixation Probability on Graphs 168
0.12910. Multi-Level Selection and Kin Selection: The Price Equation Redux 169
0.129.1 10.1 Multi-Level Selection 169
0.129.2 10.2 Hamilton's Rule Derived from the Price Equation 170
0.129.3 10.3 The Evolution of Spite 170
0.13011. Stochastic Game Dynamics and Finite Populations 170
0.130.1 11.1 The Moran Process for Evolutionary Games 170
0.130.2 11.2 Evolutionary Stability in Finite Populations 171

XI Section VIII — Virus–Host Dynamics: Co-evolution and Quasi-species 172

0.1311. The Fastest Darwinian Process 173
0.1322. The Eigen Quasi-species Equation 173
0.132.1 2.1 The Setup 173
0.132.2 2.2 The Perron–Frobenius Theorem 173
0.132.3 2.3 The Structure of the Mutation Matrix 174
0.1333. The Error Threshold 174
0.133.1 3.1 The Two-Class Model 174
0.133.2 3.2 The Phase Transition 175
0.133.3 3.3 Consequences for RNA Virus Biology 175
0.133.4 3.4 Lethal Mutagenesis 176
0.1344. The SIR Epidemic Model 176
0.134.1 4.1 Formulation 176
0.134.2 4.2 The Basic Reproduction Number 176
0.134.3 4.3 The Final Epidemic Size 177
0.134.4 4.4 The SEIR Model and Growth Rate Estimation 177
0.1355. Viral Co-evolution: The Arms Race 177

0.135.1 5.1 Within-Host Viral Evolution and Immune Escape . . . 177
0.135.2 5.2 Drug Resistance as Quasi-species Selection . . . 178
0.1366. Phylodynamics: Linking Viral Evolution to Epidemic Dynamics . . . 178
0.136.1 6.1 The Birth-Death Model for Viral Phylogenetics . . . 178
0.1377. Summary . . . 179

XII Section **IX — Information Theory in Biology: Sequence, Channel, and Code 180**
0.1388. Stochastic Epidemic Models and Branching Processes . . . 181
0.138.1 8.1 From Deterministic to Stochastic SIR . . . 181
0.138.2 8.2 The Final Size of a Stochastic Epidemic . . . 182
0.1399. The Evolution of Virulence . . . 182
0.139.1 9.1 The Virulence–Transmission Trade-off . . . 182
0.139.2 9.2 Myxomatosis: A Case Study in Virulence Evolution . . . 183
0.14010. Within-Host Dynamics and Multi-level Selection . . . 184
0.140.1 10.1 Quasi-species Dynamics Within a Host . . . 184
0.140.2 10.2 Multi-level Selection: Within-Host vs. Between-Host . . . 184
0.14111. Phylodynamics and Viral Population Genomics . . . 185
0.141.1 11.1 The Birth-Death Model for Viral Phylogenies . . . 185
0.141.2 11.2 Viral Evolution and Drug Resistance . . . 186
0.14212. Spatially Structured Epidemics . . . 186
0.142.1 12.1 The Spatial SIR Model . . . 186
0.142.2 12.2 Network Epidemics and the Configuration Model . . . 187

XIII Section **IX — Information Theory in Biology: Sequence, Channel, and Code 189**
0.1431. What Is Biological Information? . . . 190
0.1442. Shannon Entropy and Sequence Conservation . . . 190
0.144.1 2.1 Shannon Entropy . . . 190
0.144.2 2.2 Sequence Logos and Information Content . . . 190
0.144.3 2.3 Estimating Entropy from Finite Samples . . . 191
0.1453. Mutual Information and Co-evolutionary Analysis . . . 191
0.145.1 3.1 The Mutual Information . . . 191
0.145.2 3.2 Co-evolutionary Signals in Protein Alignments . . . 192
0.145.3 3.3 Direct Coupling Analysis . . . 192
0.1464. Channel Capacity and the Error Threshold . . . 193
0.146.1 4.1 Shannon's Channel Coding Theorem . . . 193
0.146.2 4.2 The Genetic Channel Capacity . . . 193
0.1475. The Genetic Code as an Error-Correcting Code . . . 193
0.147.1 5.1 Error-Correcting Codes: Background . . . 193
0.147.2 5.2 The Genetic Code's Structure . . . 194
0.147.3 5.3 Quantitative Error Robustness . . . 194
0.1486. Kolmogorov Complexity and Biological Information . . . 194
0.148.1 6.1 Algorithmic Information Theory . . . 194
0.148.2 6.2 Genome Compressibility . . . 195
0.1497. Fisher Information and the Cramér–Rao Bound . . . 195

0.149.1 7.1 Fisher Information . . . 195
0.149.2 7.2 Fisher Information in Phylogenetics . . . 195
0.1508. Entropy Production and the Thermodynamics of Life . . . 196
0.150.1 8.1 Shannon Entropy and Boltzmann Entropy . . . 196
0.150.2 8.2 Negentropy and Living Systems . . . 196
0.1519. Summary . . . 196

XIV Section **X — The Mathematics of Development: Morphogenesis and Evo-Devo 198**
0.15210. The Information Bottleneck in Biological Systems . . . 199
0.152.1 10.1 The Information Bottleneck Principle . . . 199
0.15311. Entropy Production and Irreversibility in Evolution . . . 200
0.153.1 11.1 The Second Law and Biological Order . . . 200
0.153.2 11.2 Mutual Information and Epistasis Revisited . . . 201
0.15412. Algorithmic Information Theory and Minimal Description Length . . . 201
0.154.1 12.1 Kolmogorov Complexity and Biological Complexity . . . 201
0.154.2 12.2 Minimum Description Length and Model Selection in Phylogenetics . . . 202
0.15513. Sequence Logos and Information Content of Binding Sites . . . 202
0.155.1 13.1 Shannon Information in Transcription Factor Binding Sites . . . 202
0.155.2 13.2 Sequence Logos and the Visualisation of Binding Sites . . . 203
0.15614. Mutual Information in Coevolutionary Analysis . . . 204
0.156.1 14.1 Coevolution in Protein Sequences . . . 204
0.15715. Channel Capacity and the Limits of Heredity . . . 204
0.157.1 15.1 The Genetic Channel . . . 204
0.157.2 15.2 Epigenetic Information and the Inheritance of Methylation . . . 205
0.15816. Data Compression and Genome Complexity . . . 206
0.158.1 16.1 Lempel-Ziv Complexity of Genomic Sequences . . . 206

XV Section **X — The Mathematics of Development: Morphogenesis and Evo-Devo 208**
0.1591. The Geometry of the Embryo . . . 209
0.1602. Reaction-Diffusion Systems and Turing Instabilities . . . 209
0.160.1 2.1 The General Setup . . . 209
0.160.2 2.2 Linear Stability Analysis . . . 209
0.160.3 2.3 The Biological Requirements . . . 210
0.1613. The Gierer–Meinhardt Model . . . 211
0.161.1 3.1 Equations and Steady State . . . 211
0.161.2 3.2 Pattern Outcomes . . . 211
0.161.3 3.3 Sensitivity to Domain Size and Geometry . . . 212
0.1624. The Segmentation Clock . . . 212
0.162.1 4.1 The Mechanism of Somitogenesis . . . 212
0.162.2 4.2 The Delayed Negative Feedback Oscillator . . . 213
0.162.3 4.3 Coupled Oscillators and the Kinematic Wave . . . 213
0.1635. Gene Regulatory Networks and Cell Fate . . . 214
0.163.1 5.1 Attractor Landscapes . . . 214
0.163.2 5.2 Bistability and Cell Fate Commitment . . . 214

0.163.3 5.3 Network Motifs and Their Functions . . . 215
0.1646. The Genotype-Phenotype Map and Evo-Devo . . . 215
0.164.1 6.1 The Map and its Properties . . . 215
0.164.2 6.2 Robustness and Evolvability . . . 215
0.164.3 6.3 Canalization and Developmental Robustness . . . 216
0.1657. Summary . . . 216

XVI Section **XI — Origins of Life: Hypercycles, Autocatalysis, and the RNA World 217**
0.1668. Beyond Turing: Non-local Pattern Formation . . . 218
0.166.1 8.1 Limitations of Local Reaction-Diffusion . . . 218
0.166.2 8.2 Mechanical Patterning: Stress-Driven Instabilities . . . 218
0.1679. Somitogenesis: The Segmentation Clock as a Turing–Hopf System . . . 219
0.167.1 9.1 The Clock-and-Wavefront Mechanism . . . 219
0.16810. Waddington's Epigenetic Landscape: A Mathematical Treatment . . . 220
0.168.1 10.1 The Landscape as a Lyapunov Function . . . 220
0.168.2 10.2 Bifurcation Theory and Cell Fate Decisions . . . 221
0.16911. Robustness of Developmental Patterns . . . 221
0.169.1 11.1 Canalization and Genetic Assimilation . . . 221
0.169.2 11.2 Reaction-Diffusion on Evolving Domains . . . 222
0.17012. Mathematical Models of Developmental Noise . . . 223
0.170.1 12.1 Stochastic Gene Expression and Phenotypic Variation . . . 223
0.17113. The Geometry of Morphogenetic Gradients . . . 224
0.171.1 13.1 Scaling of Positional Information with System Size . . . 224
0.171.2 13.2 The French Flag Model and Threshold-Based Patterning . . . 225
0.17214. Vertex Models and Tissue Mechanics . . . 225
0.172.1 14.1 The Cellular Potts Model . . . 225

XVII Section **XI — Origins of Life: Hypercycles, Autocatalysis, and the RNA World 227**
0.1731. The Deepest Problem . . . 228
0.1742. The Chicken-and-Egg Paradox . . . 228
0.174.1 2.1 The Paradox Stated . . . 228
0.174.2 2.2 Three Resolution Strategies . . . 228
0.1753. Autocatalytic Sets: The Phase Transition to Life . . . 229
0.175.1 3.1 Formal Definition . . . 229
0.175.2 3.2 Kauffman's Random Chemistry Model . . . 229
0.175.3 3.3 Experimental Evidence . . . 230
0.1764. Eigen's Hypercycles . . . 230
0.176.1 4.1 The Hypercycle Concept . . . 230
0.176.2 4.2 Fixed Points and Stability . . . 231
0.176.3 4.3 Resistance to Parasites . . . 231
0.176.4 4.4 The Hypercycle and the Origin of the Genetic Code . . . 232
0.1775. The RNA World . . . 232
0.177.1 5.1 Ribozymes and the Catalytic RNA Revolution . . . 232
0.177.2 5.2 SELEX and the RNA Fitness Landscape . . . 233

0.177.3 5.3 Template-Directed Replication Without Enzymes . . . 233
0.1786. Compartmentalisation and the Protocell . . . 234
0.178.1 6.1 The Problem of Cooperation in a Well-Mixed System . . . 234
0.178.2 6.2 Protocell Dynamics . . . 234
0.1797. The Origin of the Genetic Code . . . 235
0.179.1 7.1 The Code and Its Near-Universality . . . 235
0.179.2 7.2 Theories for the Origin of the Code . . . 235
0.179.3 7.3 Mathematical Optimality and the Space of Codes . . . 235
0.1808. The Transition to DNA and Proteins . . . 236
0.180.1 8.1 Why DNA? . . . 236
0.180.2 8.2 The Evolution of Proteins . . . 236
0.1819. Summary . . . 237

XVIII Section **XII — Limits, Open Problems, and the Unity of Life's Mathematics 238**
0.18210. Chemical Evolution: From Monomers to Polymers . . . 239
0.182.1 10.1 The Polymerisation Problem . . . 239
0.182.2 10.2 Phase Separation and the Prebiotic Protocell . . . 240
0.18311. Mathematical Bounds on the Origin of Life . . . 240
0.183.1 11.1 Probability Arguments and the "Miracle" Objection . . . 240
0.183.2 11.2 Szostak's Protocell Model: A Mathematical Framework . . . 241
0.18412. Mineral Surfaces and the Emergence of Metabolism . . . 242
0.184.1 12.1 The Iron-Sulfur World Hypothesis . . . 242
0.184.2 12.2 Transition from Prebiotic Chemistry to Genetically Encoded Metabolism . . . 243
0.18513. The Last Universal Common Ancestor (LUCA) . . . 243
0.185.1 13.1 Phylogenetic Inference about LUCA . . . 243
0.18614. Prebiotic Chemistry: Quantitative Constraints . . . 244
0.186.1 14.1 Miller-Urey and Amino Acid Synthesis . . . 244
0.186.2 14.2 The Chirality Problem: Mathematical Aspects . . . 245
0.18715. From Autocatalytic Sets to Minimal Cells . . . 245
0.187.1 15.1 Defining the Minimal Cell . . . 245
0.18816. The Thermodynamics of Self-Replication . . . 246
0.188.1 16.1 Free Energy Requirements for Replication . . . 246
0.188.2 16.2 Non-Equilibrium Self-Organisation and the Origin of Life . . . 247
0.18917. Coevolution of Replication and Translation . . . 248
0.189.1 17.1 The Chicken-and-Egg Paradox — Mathematical Formulation . . . 248

XIX Section **XII — Limits, Open Problems, and the Unity of Life's Mathematics 250**
0.1901. What the Mathematics Has Achieved . . . 251
0.190.1 1.1 A Quantitative Scorecard . . . 252
0.1912. The Limits of Current Theory . . . 253
0.191.1 2.1 The Limits of Neutralism and the Nearly Neutral Zone . . . 253
0.191.2 2.2 The Problem of Robustness and Evolvability . . . 254
0.191.3 2.3 The Information Content of Genomes . . . 254
0.1923. Seven Precisely Stated Open Problems . . . 255

0.192.1 3.1 Stochastic Quasi-species at the Error Threshold . . . 255
0.192.2 3.2 NK Landscape Topology in the Thermodynamic Limit . . . 255
0.192.3 3.3 Information Geometry of Selection and Drift . . . 256
0.192.4 3.4 Global Optimality of the Standard Genetic Code . . . 257
0.192.5 3.5 The Structured Coalescent at Scale . . . 257
0.192.6 3.6 The Scaling Limit of the Mutation–Selection–Drift Equation . . . 258
0.192.7 3.7 A Mathematical Theory of Speciation . . . 258
0.1934. The Two Unifying Ideas . . . 259
0.193.1 4.1 Population as Probability Distribution . . . 259
0.193.2 4.2 Information as the Conserved Quantity . . . 259
0.1945. Synthesis: A Unified Framework . . . 260
0.194.1 5.1 The Master Equation of Life . . . 260
0.194.2 5.2 The Hierarchy of Mathematical Structures . . . 260
0.1956. Appendix A: The Five Fundamental Theorems . . . 261
0.1967. Appendix B: Cross Section Mathematical Connections . . . 262
0.1978. Appendix C: Complete Mathematical Glossary . . . 264
0.1989. Appendix D: Major Open Problems — Extended Formulations . . . 267
0.198.1 9.1 The Missing Heritability Problem . . . 267
0.198.2 9.2 The Evolution of Sex and Recombination . . . 267
0.19910. Appendix E: Historical Sketch of the Mathematical Biology of Evolution . . . 268
0.199.1 10.1 The Founders: Fisher, Wright, and Haldane (1918–1932) . . . 268
0.199.2 10.2 The Molecular Era: Kimura and the Neutral Theory (1953–1983) . . . 269
0.199.3 10.3 The Information-Theoretic Turn: Eigen, Price, and Maynard Smith . . . 269
0.20011. Towards a Unified Theory: The Mathematics Yet to Be Written . . . 270
0.200.1 11.1 The Multi-Scale Problem . . . 270
0.200.2 11.2 The Extended Evolutionary Synthesis . . . 271
.1 Appendice Tecnica I: Notazioni e Convenzioni Matematiche . . . 272
.1.1 I.1 Notazione generale . . . 272
.1.2 I.2 Convenzioni probabilistiche . . . 272
.1.3 I.3 Convenzioni della genetica delle popolazioni . . . 273
.2 Appendice Tecnica II: Riepilogo delle Equazioni Fondamentali . . . 273
.2.1 II.1 Genetica delle popolazioni (Volumi I–IV) . . . 273
.2.2 II.2 Teoria dell'informazione evolutiva (Vol. VIII) . . . 273
.2.3 II.3 Dinamica di reazione–diffusione (Vol. X) . . . 274
.2.4 II.4 Equazione delle quasi-specie (Vol. XI) . . . 274
.3 Appendice Tecnica III: Strumenti Computazionali e Software . . . 274
.3.1 III.1 Pacchetti software di riferimento . . . 274
.3.2 III.2 Note computazionali . . . 274

Editorial Note

This monograph collects all twelve Section s of the *Mathematics of Evolution and Life* series into a single continuous work. The Section s were originally conceived as standalone texts; read together, they trace a single progressive argument — that the full mathematical account of life requires probability theory, differential equations, combinatorics, game theory, information theory, and the geometry of high-dimensional spaces deployed simultaneously. Each framework illuminates a different stratum of biological reality; none is sufficient alone.

The series addresses a conspicuous gap. The mathematics underlying modern evolutionary biology — Fisher, Wright, Haldane, Price, Hamilton, and Maynard Smith — is among the most beautiful mathematics of the twentieth century. Yet it is almost entirely invisible in popular scientific writing, and treated with surprisingly little rigour even in many university curricula. This series is an attempt at repair. It demands nothing of the reader beyond calculus, elementary probability, and a willingness to follow a mathematical argument wherever it leads.

Section	Title	Central Framework
I	Populations, Genes, and the Hardy–Weinberg Equilibrium	Probability · Combinatorics
II	Drift, Fixation, and the Stochastic Theory of Evolution	Markov chains · Diffusion
III	Selection, Fitness, and the Geometry of Allele Dynamics	ODEs · Dynamical systems
IV	The Price Equation and the Algebra of Selection	Covariance · Linear algebra
V	Fitness Landscapes and the Topology of Evolutionary Search	Combinatorial geometry
VI	Phylogenetics: Trees, Distances, and Evolutionary Time	Discrete math · Statistics
VII	Evolutionary Game Theory: Strategies, Equilibria, Replicators	Game theory · ODEs
VIII	Virus–Host Dynamics: Co-evolution and Quasi-species	Nonlinear dynamics · PDEs
IX	Information Theory in Biology: Sequence, Channel, Code	Shannon theory
X	Mathematics of Development: Morphogenesis and Evo-Devo	Reaction–diffusion
XI	Origins of Life: Hypercycles, Autocatalysis, RNA World	Nonlinear dynamics
XII	Limits, Open Problems, and the Unity of Life's Mathematics	Information · Complexity

Section *I*

Section I — Populations, Genes, and the Hardy–Weinberg Equilibrium

0.1 1. The Strange Simplicity of Heredity

There is something almost paradoxical about the starting point of mathematical genetics. After decades of confusion — debate about blending inheritance, about the mechanisms of variation, about whether Darwinian selection was even mathematically consistent with heredity — the fundamental law of population genetics turned out to be, once stated, almost embarrassingly simple. In a large, randomly mating population with no selection, no mutation, and no migration, the frequencies of genotypes remain constant from generation to generation. And more: after a single generation of random mating, those frequencies assume a specific, predictable form determined entirely by the allele frequencies.

This is the Hardy–Weinberg principle, proved independently in 1908 by the mathematician G. H. Hardy and the physician Wilhelm Weinberg. That it required both a pure mathematician and a medical geneticist to arrive at the same result in the same year tells us something important: the result is genuinely mathematical, not merely biological, and yet it is also genuinely about biology, not merely an abstract theorem.

Hardy's contribution came in the form of a letter to the journal *Science*, written in a tone of mild impatience: "I am reluctant to intrude in a discussion concerning matters of which I have no expert knowledge, and I should have expected the very simple point which I wish to make to have been familiar to biologists." The simple point — that a dominant allele does not automatically increase in frequency, and that both dominant and recessive alleles are maintained at stable frequencies under random mating — resolved a genuine scientific controversy. The result was simple precisely because it had been overlooked. It is the mathematical character of the problem, not its difficulty, that makes it foundational.

Before we can state and prove the Hardy–Weinberg principle with full precision, we need to build the mathematical framework in which it lives. That framework is the description of a population as a probability space, and of genetic composition as a probability distribution on that space.

0.1.1 1.1 The Mathematical Structure of a Population

We begin at the beginning. A **genetic locus** is a specific position in the genome — a location on a chromosome where a particular gene (or genetic element) resides. At any biallelic locus, the genome can carry one of two variants, called **alleles**. We denote these A and a.

An organism is **diploid** if it carries two copies of each chromosome — one inherited from each parent. This is the standard condition for animals, plants, and most fungi. A diploid organism has one of three possible **genotypes** at a biallelic locus: AA, Aa, or aa. The first is **homozygous** for A, the last is homozygous for a, and the middle is **heterozygous**.

A **population** is a collection of N diploid organisms. The population contains $2N$ gene copies at the locus in question — two per organism. We define the **allele frequency** of A as:

$$p = \frac{\text{number of } A \text{ alleles in the population}}{2N} = \frac{2N_{AA} + N_{Aa}}{2N},$$

and the allele frequency of a as $q = 1 - p$, where N_{AA}, N_{Aa}, N_{aa} denote the counts of the three genotype classes. Note that $p + q = 1$ identically. The pair (p, q) lives in the probability simplex $\{(p, q) : p, q \geq 0, p + q = 1\}$, which in one dimension is simply the unit interval $[0, 1]$.

This compression from the three-dimensional state (N_{AA}, N_{Aa}, N_{aa}) to the single number p is the fundamental move of population genetics. It retains the quantity that is conserved under Hardy–Weinberg dynamics and loses information about the genotype distribution. Understanding when this compression is and is not sufficient is the first of many recurring themes in this series.

0.1.2 1.2 Mendelian Segregation as a Random Process

Gregor Mendel discovered in the 1860s, from his experiments on peas, that heredity obeys specific probabilistic rules. His two laws — the law of segregation and the law of independent assortment — can be stated precisely as:

Law of Segregation. Each diploid organism forms gametes (eggs or sperm) in which each gamete carries exactly one of the organism's two alleles at each locus, chosen uniformly at random. The two alleles are contributed independently of each other.

Law of Independent Assortment. Alleles at different loci are contributed to gametes independently (i.e., the allele contributed at locus 1 is independent of the allele contributed at locus 2). This law holds exactly for loci on different chromosomes and approximately for loci far apart on the same chromosome.

These laws transform a biological process (reproduction) into a precisely defined probabilistic model. The gamete of an organism with genotype Aa is A with probability $1/2$ and a with probability $1/2$. The gamete of an organism with genotype AA is always A. The gamete of aa is always a.

0.1.3 1.3 Panmixia and the Gene Pool

Random mating (panmixia, from the Greek "mixing everything") means that each mating pair in the population is equally likely to consist of any two individuals. There is no preference for mates by genotype, phenotype, relatedness, or any other characteristic.

Under panmixia, the allele contributed to a random offspring by its mother is a uniformly random draw from the maternal gene pool (the $2N$ maternal alleles in the population), and similarly for the paternal contribution. In the limit of large population size, these two draws are effectively independent.

We can therefore model the genotype of a random offspring as follows. Let X_1 denote the maternally contributed allele and X_2 the paternally contributed allele. Under panmixia with allele frequencies p and $q = 1 - p$:

$$P(X_1 = A) = p, \quad P(X_1 = a) = q,$$

and independently:

$$P(X_2 = A) = p, \quad P(X_2 = a) = q.$$

The two draws X_1 and X_2 are independent Bernoulli trials with success probability p. The offspring's genotype (X_1, X_2) is therefore a draw from the product distribution:

$$P(AA) = p^2, \quad P(Aa) = pq + qp = 2pq, \quad P(aa) = q^2.$$

These three numbers are the **Hardy–Weinberg genotype frequencies**. Note that $p^2 + 2pq + q^2 = (p + q)^2 = 1$, confirming that they form a valid probability distribution.

0.2 2. The Hardy–Weinberg Theorem: Statement, Proof, and Generalisations

0.2.1 2.1 The Theorem and Its Complete Proof

Theorem 0.2.1 (Hardy–Weinberg, 1908)**.** In a diploid population with allele frequencies p and $q = 1-p$ at a biallelic locus, under the assumptions of:

(i) Random mating (panmixia),

(ii) Mendelian segregation,

(iii) No selection (all genotypes have equal fitness),

(iv) No mutation,

(v) No migration,

(vi) Infinite population size (no genetic drift),

the following hold:

(a) After one generation of random mating, genotype frequencies are p^2, $2pq$, q^2 for genotypes AA, Aa, aa respectively.

(b) These genotype frequencies remain constant in all subsequent generations.

(c) Allele frequencies remain equal to p and q in all generations.

Proof. Part (a). We showed in Section 1.3 that under random mating and Mendelian segregation, the probability that a random offspring has genotype AA is p^2, genotype Aa is $2pq$, and genotype aa is q^2. In an infinite population, the actual frequencies equal these probabilities exactly.

Part (c). We verify that the allele frequencies in the offspring generation are unchanged. The frequency of A in the offspring is:

$$p' = f(AA) + \tfrac{1}{2} f(Aa) = p^2 + \tfrac{1}{2}(2pq) = p^2 + pq = p(p+q) = p \cdot 1 = p.$$

Hence $q' = 1 - p' = 1 - p = q$.

Part (b). The offspring generation has allele frequencies (p, q), the same as the parental generation. Under our assumptions (random mating, Mendelian segregation, no selection, mutation, or migration), the process generating the grandoffspring from the offspring generation is identical to the process generating the offspring from the parents. Therefore, the genotype frequencies in the grandoffspring generation are also $p^2, 2pq, q^2$. By induction, this holds for all subsequent generations. □

0.2.2 2.2 The Algebraic Identity at the Heart of the Theorem

The Hardy–Weinberg frequencies $p^2, 2pq, q^2$ are the terms of the binomial expansion:

$$(p+q)^2 = p^2 + 2pq + q^2.$$

Since $p + q = 1$, this expansion sums to 1. The entire content of the Hardy–Weinberg theorem, at the algebraic level, is that two independent Bernoulli trials with success probability p produce a sum (number of A alleles) with the binomial distribution $\text{Bin}(2, p)$. The population-genetic content is in the assumptions that justify modelling the offspring's two alleles as independent Bernoulli trials.

This perspective generalises immediately. If there are k alleles $A_1, A_2, \ldots, A_k$ with frequencies $p_1, p_2, \ldots, p_k$ summing to 1, then the Hardy–Weinberg frequencies for two-allele genotypes are:

$$P(A_iA_i) = p_i^2, \quad P(A_iA_j) = 2p_ip_j \quad (i \neq j).$$

These are the terms of the multinomial expansion $(p_1 + p_2 + \cdots + p_k)^2 = 1$.

0.2.3 2.3 Numerical Example: The ABO Blood Group System

The ABO blood group system in humans is determined by a single locus with three common alleles: I^A (producing the A antigen), I^B (producing the B antigen), and i (producing neither). Let the allele frequencies in a population be:

$$p_{I^A} = 0.28, \quad p_{I^B} = 0.06, \quad p_i = 0.66.$$

The Hardy–Weinberg predicted frequencies of the four blood groups are:

$$\begin{aligned}
\text{Blood group A: } P(I^AI^A) + P(I^Ai) &= (0.28)^2 + 2(0.28)(0.66) = 0.0784 + 0.3696 = 0.448, \\
\text{Blood group B: } P(I^BI^B) + P(I^Bi) &= (0.06)^2 + 2(0.06)(0.66) = 0.0036 + 0.0792 = 0.083, \\
\text{Blood group AB: } P(I^AI^B) &= 2(0.28)(0.06) = 0.034, \\
\text{Blood group O: } P(ii) &= (0.66)^2 = 0.436.
\end{aligned}$$

These predicted frequencies match observed blood group frequencies in many European populations with remarkable accuracy (observed: A $\approx$ 42%, B $\approx$ 9%, AB $\approx$ 3%, O $\approx$ 46%), demonstrating that the ABO locus is in approximate Hardy–Weinberg equilibrium.

0.2.4 2.4 The Historical Significance: The Dilution Fallacy

Before 1908, many biologists accepted what we might call the **dilution fallacy**: the argument that a dominant allele, even if beneficial, would inevitably increase toward fixation because of its dominance, and that a rare recessive allele would be diluted away over generations. This argument was used to claim that Mendelian genetics was incompatible with the gradual change required by Darwinian evolution.

Hardy's letter exposed the error in a single line of algebra. Consider a population where AA and Aa individuals have phenotype "dominant" and aa individuals have phenotype "recessive." If initially $p = 0.5$, the frequencies are:

$$f(AA) = 0.25, \quad f(Aa) = 0.50, \quad f(aa) = 0.25.$$

After one generation of random mating (and no selection), the frequencies are:

$$p^2 = 0.25, \quad 2pq = 0.50, \quad q^2 = 0.25.$$

Unchanged. The dominant allele does not increase. The recessive allele is not diluted. The gene frequencies are perfectly stable.

This stability is precisely what enables Darwinian natural selection to function: variation is maintained from generation to generation as a background against which selection can act. Without Hardy–Weinberg stability, even a small beneficial mutation would be diluted to zero before selection could accumulate it.

0.3 3. Testing Hardy–Weinberg: Statistical Inference

0.3.1 3.1 The Chi-Squared Goodness-of-Fit Test

The Hardy–Weinberg principle generates testable predictions. Given a sample of n individuals from a population, we can compare the observed genotype counts to the Hardy–Weinberg expectations and ask: is the deviation consistent with sampling variation alone?

Let n_{AA}, n_{Aa}, n_{aa} be the observed counts (with $n_{AA} + n_{Aa} + n_{aa} = n$). We first estimate the allele frequencies:

$$\hat{p} = \frac{2n_{AA} + n_{Aa}}{2n}, \qquad \hat{q} = 1 - \hat{p}.$$

The expected counts under Hardy–Weinberg equilibrium are:

$$E_{AA} = n\hat{p}^2, \quad E_{Aa} = 2n\hat{p}\hat{q}, \quad E_{aa} = n\hat{q}^2.$$

The chi-squared test statistic is:

$$\chi^2 = \frac{(n_{AA} - E_{AA})^2}{E_{AA}} + \frac{(n_{Aa} - E_{Aa})^2}{E_{Aa}} + \frac{(n_{aa} - E_{aa})^2}{E_{aa}}.$$

Under the null hypothesis of Hardy–Weinberg equilibrium, this statistic follows a χ^2 distribution with $3 - 1 - 1 = 1$ degree of freedom (three genotype classes, one constraint that counts sum to n, one estimated parameter $\hat{p}$). The critical value at the 5% level is $\chi^2_{1,0.05} = 3.84$.

0.3.2 3.2 Worked Example

In a study of the MN blood group system (a biallelic codominant locus: MM, MN, NN are distinguishable), the following counts were observed in a sample of $n = 1000$ individuals:

$$n_{MM} = 298, \quad n_{MN} = 489, \quad n_{NN} = 213.$$

We estimate the frequency of the M allele:

$$\hat{p} = \frac{2(298) + 489}{2000} = \frac{1085}{2000} = 0.5425.$$

Expected counts:

$$E_{MM} = 1000\times(0.5425)^2 = 294.3, \quad E_{MN} = 1000\times2(0.5425)(0.4575) = 496.4, \quad E_{NN} = 1000\times(0.4575)^2 = 209.$$

Chi-squared:

$$\chi^2 = \frac{(298-294.3)^2}{294.3} + \frac{(489-496.4)^2}{496.4} + \frac{(213-209.3)^2}{209.3} = 0.046 + 0.110 + 0.065 = 0.221.$$

Since $\chi^2 = 0.221 \ll 3.84$, we cannot reject the hypothesis that the MN locus is in Hardy–Weinberg equilibrium in this population.

0.3.3 3.3 Exact Tests for Small Samples

For small samples (where expected counts fall below 5 for some genotype class, making the chi-squared approximation unreliable), the exact Hardy–Weinberg test should be used. The exact test computes the probability of the observed genotype counts, and all genotype count vectors with the same allele counts but equal or lower probability, under the null hypothesis of Hardy–Weinberg equilibrium.

For fixed allele counts (n_A, n_a) (where $n_A = 2n_{AA} + n_{Aa}$ and $n_a = 2n_{aa} + n_{Aa}$), the probability of observing a specific genotype count vector (n_{AA}, n_{Aa}, n_{aa}) under Hardy–Weinberg is the multivariate hypergeometric-like formula:

$$P(n_{AA}, n_{Aa}, n_{aa}) = \frac{n!}{n_{AA}!\, n_{Aa}!\, n_{aa}!} \cdot \frac{2^{n_{Aa}} \binom{n_A/2+n_a/2}{n_{AA}, n_{Aa}/2, n_{aa}}}{\binom{2n}{n_A}},$$

which is exact and avoids the large-sample approximation. This approach, developed independently by Fisher and by Haldane, is implemented in modern software for population-genetic analysis.

0.4 4. Linkage Disequilibrium: The Correlation Between Loci

0.4.1 4.1 From One Locus to Two

The Hardy–Weinberg principle concerns a single locus. When we consider two or more loci simultaneously, new phenomena arise. At a single locus, allele frequencies are the sufficient statistic; at two loci, the sufficient statistics are the allele frequencies at each locus *and* the haplotype frequencies (the frequencies of the allele combinations on single chromosomes).

Consider two biallelic loci. Locus 1 has alleles A and a at frequencies p and $q = 1 - p$. Locus 2 has alleles B and b at frequencies r and $s = 1 - r$. There are four possible haplotypes: AB, Ab, aB, ab at frequencies x_{AB}, x_{Ab}, x_{aB}, x_{ab}, with $x_{AB} + x_{Ab} + x_{aB} + x_{ab} = 1$.

Linkage equilibrium is the condition under which the haplotype frequencies are the products of the individual allele frequencies:

$$x_{AB} = pr, \quad x_{Ab} = ps, \quad x_{aB} = qr, \quad x_{ab} = qs.$$

In this condition, knowing the allele at locus 1 gives no information about the allele at locus 2.

0.4.2 4.2 The Linkage Disequilibrium Parameter D

The standard measure of departure from linkage equilibrium is:

$$D = x_{AB} - pr = x_{AB}x_{ab} - x_{Ab}x_{aB}.$$

The last equality holds by algebraic identity. $D = 0$ means linkage equilibrium; $D \neq 0$ means statistical association between the alleles at the two loci.

The range of D is constrained by the allele frequencies:

$$\max(-pr, -qs) \leq D \leq \min(ps, qr).$$

To compare across loci with different allele frequencies, the **standardised** linkage disequilibrium is:

$$D' = \begin{cases} D/\min(ps, qr) & \text{if } D > 0, \\ D/\max(-pr, -qs) & \text{if } D < 0. \end{cases}$$

$|D'| = 1$ indicates complete LD (all haplotypes are one of two types, not all four).

Another common measure is r^2, the squared correlation coefficient between the indicator variables for A at locus 1 and B at locus 2:

$$r^2 = \frac{D^2}{pqrs}.$$

$r^2 = 1$ indicates perfect correlation (knowing the allele at locus 1 perfectly predicts the allele at locus 2). In GWAS, $r^2 > 0.8$ is the threshold for considering two markers to be in "strong LD."

0.4.3 4.3 The Decay of Linkage Disequilibrium

Theorem 0.4.1 (Geometric Decay of Linkage Disequilibrium)**.** Under random mating with recombination fraction c between the two loci:

$$D_t = (1 - c)^t D_0.$$

Proof. Consider the formation of the next generation's AB haplotypes. A new haplotype is AB in two mutually exclusive ways:

(i) It is inherited intact from a parental AB haplotype (no recombination between the two loci): probability $1 - c$, contributing $(1 - c)x_{AB}$ to the next generation's x'_{AB}.

(ii) It is formed by recombination, taking the A allele from one parental chromosome and the B allele from the other: probability $c \cdot p \cdot r$ (under random mating, the probability that the two parental chromosomes carry A and B respectively is $p \cdot r$).

Therefore:

$$x'_{AB} = (1 - c)x_{AB} + cpr.$$

The updated D is:

$$D' = x'_{AB} - pr = (1 - c)x_{AB} + cpr - pr = (1 - c)(x_{AB} - pr) = (1 - c)D.$$

Applying this recurrence repeatedly: $D_t = (1-c)^t D_0$. □

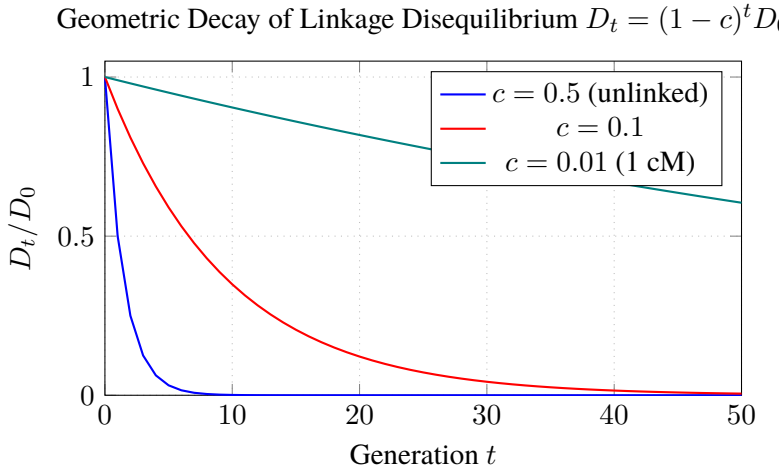

Figure 1: Decay of linkage disequilibrium $D_t = (1-c)^t D_0$ for three values of the recombination fraction c. Unlinked loci ($c = 0.5$) lose LD within a few generations; tightly linked loci ($c = 0.01$) retain LD for hundreds of generations.

0.4.4 4.4 Rates of LD Decay: Physical Interpretation

For loci on different chromosomes, $c = 1/2$ (Mendel's law of independent assortment), and:

$$D_t = (1/2)^t D_0.$$

After $t = 10$ generations, D has decayed to $(1/2)^{10} \approx 0.001$ of its initial value. For all practical purposes, unlinked loci are in linkage equilibrium after a few tens of generations.

For physically linked loci, c is approximately proportional to physical distance (in morgans or centimorgans). For $c = 0.01$ (loci 1 cM apart):

$$D_t = (0.99)^t D_0.$$

The half-life of D is $\ln(1/2)/\ln(0.99) \approx 69$ generations. For $c = 0.001$ (0.1 cM), the half-life is approximately 693 generations. In humans, with approximately 25 years per generation, this is 17,000 years — a cosmologically short but demographically long time.

This slow decay of LD between tightly linked loci means that the human genome carries extensive blocks of strong LD ("haplotype blocks") that persist for thousands of generations. These blocks are the basis of GWAS: disease-associated variants can be detected by their LD with nearby typed markers, without requiring that the causal variant itself be genotyped.

0.4.5 4.5 Causes of Linkage Disequilibrium

Non-zero D can arise from several distinct biological causes:

Recent mutation. A newly arising mutation initially exists on a single haplotype background. Before recombination has had time to distribute it across backgrounds, it is in complete LD with nearby markers. The "signature" of a recent selective sweep is a haplotype of unusually high LD extending around the selected site.

Founder effects and bottlenecks. When a new population is founded by a small number of individuals, the haplotype diversity is limited, and even unlinked loci can appear in strong LD simply because the founders happened to carry only a small number of haplotypes.

Population admixture. When two previously separated populations mix, alleles that were at different frequencies in the two source populations become associated in the admixed population, generating LD. This "admixture LD" can extend over very long distances (even between unlinked loci) and decays slowly.

Epistatic selection. If certain combinations of alleles at two loci are selectively favoured over others (epistasis), selection maintains the favoured combinations at higher-than-expected frequency, generating LD even in the face of recombination.

0.5 5. Population Structure and the Wahlund Effect

0.5.1 5.1 The Wahlund Principle

If a population consists of k subpopulations, each in Hardy–Weinberg equilibrium within itself but with different allele frequencies $p_1, p_2, \ldots, p_k$, then a sample drawn from the pooled population will show a deficiency of heterozygotes compared to the Hardy–Weinberg expectation at the pooled allele frequency.

Theorem 0.5.1 (Wahlund, 1928)**.** Let subpopulation j have allele frequency p_j for allele A, and let the population be in Hardy–Weinberg equilibrium within each subpopulation. In the pooled population with mean allele frequency $\bar{p} = \frac{1}{k}\sum_{j=1}^{k} p_j$:

$$H_{\text{obs}} = H_{\text{HW}} - 2\,\text{Var}(p),$$

where $H_{\text{obs}} = \frac{1}{k}\sum_j 2p_j(1-p_j)$ is the observed heterozygosity, $H_{\text{HW}} = 2\bar{p}(1-\bar{p})$ is the Hardy–Weinberg expectation at the pooled frequency, and $\text{Var}(p) = \frac{1}{k}\sum_j (p_j - \bar{p})^2$.

Proof.

$$H_{\text{obs}} = \frac{1}{k}\sum_j 2p_j(1-p_j) = \frac{2}{k}\sum_j p_j - \frac{2}{k}\sum_j p_j^2 = 2\bar{p} - \frac{2}{k}\sum_j p_j^2.$$

Now $\frac{1}{k}\sum_j p_j^2 = \text{Var}(p) + \bar{p}^2$, so:

$$H_{\text{obs}} = 2\bar{p} - 2(\text{Var}(p) + \bar{p}^2) = 2\bar{p}(1-\bar{p}) - 2\,\text{Var}(p) = H_{\text{HW}} - 2\,\text{Var}(p). \qquad \square$$

The deficit of heterozygotes relative to Hardy–Weinberg expectation is exactly $2\,\text{Var}(p)$: twice the variance of allele frequencies across subpopulations. The deficit is always non-negative (since variance is non-negative), so pooling genetically differentiated populations always reduces apparent heterozygosity.

0.5.2 5.2 Wright's F-Statistics

Wright (1951) introduced a hierarchical system of fixation indices that generalise the Wahlund principle to multiple levels of population structure. The three key indices are:

$$F_{IS} = 1 - \frac{H_I}{H_S}: \quad \text{reduction of observed heterozygosity relative to subpopulation expectation,}$$
$$F_{ST} = 1 - \frac{H_S}{H_T}: \quad \text{reduction of subpopulation heterozygosity relative to total expectation,}$$
$$F_{IT} = 1 - \frac{H_I}{H_T}: \quad \text{total reduction of observed heterozygosity,}$$

where H_I is observed heterozygosity (averaged over subpopulations), $H_S = \frac{1}{k}\sum_j 2p_j(1-p_j)$ is the expected heterozygosity within subpopulations (averaged over subpopulations), and $H_T = 2\bar{p}(1-\bar{p})$ is the expected heterozygosity for the total (pooled) population.

These three indices satisfy the exact multiplicative decomposition:

$$(1 - F_{IT}) = (1 - F_{IS})(1 - F_{ST}).$$

Proof. $(1 - F_{IS})(1 - F_{ST}) = \frac{H_I}{H_S} \cdot \frac{H_S}{H_T} = \frac{H_I}{H_T} = 1 - F_{IT}$. □

0.5.3 5.3 The Biological Interpretation of F_{ST}

The quantity F_{ST} is the most widely used single summary of genetic differentiation among subpopulations. It measures the fraction of total genetic diversity that is accounted for by differences between, rather than within, subpopulations. $F_{ST} = 0$ means all subpopulations have identical allele frequencies (no differentiation); $F_{ST} = 1$ means each subpopulation is fixed for a different allele (complete differentiation).

For human populations:

- **Within a village or town:** $F_{ST} \approx 0$.
- **Between villages in the same region:** $F_{ST} \approx 0.001$–0.01.
- **Between European populations:** $F_{ST} \approx 0.01$–0.03.
- **Between continental groups:** $F_{ST} \approx 0.10$–0.15.

Lewontin (1972) computed that approximately 85–90% of human genetic diversity is within populations rather than between them — a result expressed as $F_{ST} \approx 0.10$–0.15 between continents. This means that the large majority of the genetic differences we observe between any two individuals exist at all levels of population structure: between two people from different continents, more of their genetic difference will be due to within-population variation than between-population variation.

0.5.4 5.4 The Correlation Between F_{ST} and Geographic Distance

F_{ST} between populations typically increases with the geographic distance separating them, following the isolation-by-distance model. For populations on a two-dimensional landscape connected by migration, the expected F_{ST} between populations at distance d satisfies, in the diffusion limit:

$$F_{ST}(d) \approx \frac{1}{1 + 4\pi N_e m D d^2},$$

where N_e is effective density, m is migration rate, and D is the diffusion coefficient of migration. This provides a way to test whether observed population structure is consistent with isolation by distance alone, or whether additional barriers (mountain ranges, oceans, cultural boundaries) have increased differentiation beyond what geography alone would predict.

0.6 6. Hardy–Weinberg in Haploid and X-Linked Loci

0.6.1 6.1 Haploid Populations

In a haploid population (organisms carrying only one copy of each chromosome), there are no genotypes — only alleles. The Hardy–Weinberg principle simplifies: allele frequencies p and $q = 1 - p$ are maintained exactly without any constraints on the mating system. Haploid populations do not undergo the genotype frequency adjustment of the first generation; allele frequencies are the complete description of the population's genetic state at any locus.

0.6.2 6.2 X-Linked Loci

At X-linked loci (loci on the X chromosome), males are hemizygous (they carry only one allele, from their mother). Females are diploid for X-linked loci and can be AA, Aa, or aa; males carry either A or a.

Let p_f and p_m denote the frequency of allele A in females and males respectively. After one generation of random mating:

$$p'_f = \frac{p_f + p_m}{2} \quad \text{(females receive one allele from each parent)},$$

$$p'_m = p_f \quad \text{(males receive their X chromosome from their mother)},$$

since sons always inherit their X from their mother. The approach to equilibrium is oscillatory with geometric convergence:

$$\Delta p_f^{(t)} = (-1/2)^t (p_f^{(0)} - p_m^{(0)})/3.$$

The equilibrium frequency is $p^* = (p_f + p_m)/2$ (weighted average, giving twice the weight to females since there are two X chromosomes per female and one per male in a 1:1 sex ratio).

At X-linked loci, the approach to Hardy–Weinberg equilibrium takes multiple generations (with oscillation) rather than a single generation. The genotype frequencies reach equilibrium only when $p_f = p_m = p^*$, which requires several generations.

0.7 7. Summary and Bridge to Section II

This Section has established the mathematical foundation of population genetics. The Hardy–Weinberg principle shows that allele frequencies are inert in the absence of evolutionary forces, and that genotype frequencies are determined by a simple binomial formula after a single generation of random mating. The theorem's proof is a direct consequence of modelling reproduction as independent Bernoulli sampling from an allele pool.

The key concepts established:

- Allele frequencies as the fundamental state variables of population genetics.

- The Hardy–Weinberg genotype frequencies $p^2, 2pq, q^2$ as the binomial distribution over genotype space.
- The multinomial generalisation to multiple alleles.
- The chi-squared test for detecting Hardy–Weinberg violations, and the exact test for small samples.
- Linkage disequilibrium $D = x_{AB} - pr$ as a measure of allele association across loci, decaying geometrically as $(1-c)^t D_0$ under recombination.
- The Wahlund effect: population subdivision reduces observed heterozygosity by $2\,\mathrm{Var}(p)$.
- Wright's F-statistics as a hierarchical decomposition of genetic diversity: $(1 - F_{IT}) = (1 - F_{IS})(1 - F_{ST})$.

Section II confronts the idealisation that Hardy–Weinberg explicitly maintains: infinite population size. In a finite population, allele frequencies are not conserved — they drift stochastically. The study of this random wandering requires the full apparatus of the theory of stochastic processes: Markov chains, martingales, diffusion equations, and the Kingman coalescent. The mathematical depth required to describe genetic drift is far greater than that required for Hardy–Weinberg equilibrium — and the biological consequences are correspondingly richer.

0.8 10. Advanced Topics in Hardy-Weinberg Theory

0.8.1 10.1 The Multiallelic Hardy-Weinberg Principle: Complete Treatment

When a locus has $k \geq 2$ alleles $A_1, A_2, \ldots, A_k$ with frequencies $p_1, p_2, \ldots, p_k$ ($\sum_i p_i = 1$), the Hardy–Weinberg genotype frequencies are:

$$f_{A_iA_j} = \begin{cases} p_i^2 & i = j, \\ 2p_ip_j & i < j. \end{cases}$$

The total number of distinct genotypes is $k(k+1)/2$. For $k = 3$ (as in the ABO blood group system, which has alleles I^A, I^B, O), there are 6 genotypes.

Theorem 0.8.1 (Multiallelic HWE convergence rate)**.** Starting from arbitrary genotype frequencies $(f_{ij}^{(0)})$ with allele frequencies (p_i), under random mating the genotype frequencies converge to Hardy–Weinberg values in exactly one generation:

$$f_{ij}^{(t)} = \begin{cases} p_i^2 & \text{for all } t \geq 1, \quad i = j, \\ 2p_ip_j & \text{for all } t \geq 1, \quad i < j. \end{cases}$$

The convergence is exact (not approximate), regardless of the initial genotype distribution, as long as allele frequencies are preserved.

Proof. Under random mating, offspring genotype A_iA_j occurs with probability $P(X_1 = A_i)P(X_2 = A_j) + P(X_1 = A_j)P(X_2 = A_i) = p_ip_j + p_jp_i = 2p_ip_j$ for $i \neq j$ and p_i^2 for $i = j$, where X_1, X_2

are independent allele draws from the population allele pool with probabilities $(p_1, \ldots, p_k)$. The allele pool probabilities are determined solely by allele frequencies, not genotype frequencies, so after one generation of random mating the genotype distribution is exactly $(p_i^2, 2p_ip_j)$ regardless of the starting genotype distribution. □

The key insight: HWE is not approached asymptotically (with exponential convergence rate) but reached in exactly one generation. This is qualitatively different from the X-linked case, where oscillatory convergence takes many generations.

0.8.2 10.2 Deviations from Hardy-Weinberg: A Classification

Any departure from the five HWE conditions (random mating, Mendelian segregation, no selection, no mutation, no migration) produces a measurable deviation in the observed vs. expected genotype frequencies. The deviations have characteristic signatures:

[(i)]**Inbreeding ($F_{IS} > 0$):** Excess homozygosity at all loci simultaneously. The inbreeding coefficient F parameterises this: $f_{AA} = p^2 + Fpq$, $f_{Aa} = 2pq(1-F)$, $f_{aa} = q^2 + Fpq$. **Population structure (Wahlund effect):** Excess homozygosity at all loci, but the pattern varies across loci in proportion to allele frequency variance. Unstructured inbreeding produces a uniform F across loci; Wahlund produces F_{IS} correlated with $\mathrm{Var}(p)/[p(1-p)]$ across loci. **Selection:** Deviation can be in either direction, depending on dominance. Overdominant selection produces heterozygote excess ($F < 0$ locally). Underdominance produces homozygote excess ($F > 0$ locally). Selection signatures are typically locus-specific rather than genome-wide. **Assortative mating:** Positive assortative mating (like with like) produces excess homozygosity at loci underlying the assortative character. Negative assortative mating (disassortative mating) produces heterozygote excess. The pattern is trait-specific. **Null alleles:** PCR-based genotyping may fail to amplify null alleles, producing apparent heterozygote deficiency at the affected locus. A technical artifact that mimics inbreeding or selection. **Gametic disequilibrium (LD):** Does not affect single-locus HWE directly, but creates correlations between loci. LD produces two-locus deviations from the product of single-locus HWE frequencies.

Distinguishing these cases requires: (a) genome-wide patterns (inbreeding and Wahlund are genome-wide; selection is locus-specific), (b) functional annotation (selection signatures cluster at functional loci), and (c) demographic modelling.

0.8.3 10.3 The Ewens Sampling Formula

The **Ewens sampling formula** (Ewens 1972) generalises the neutral allele frequency distribution to samples. It gives the probability of observing a specific configuration of allele counts in a sample of n gene copies under the infinite-alleles neutral model.

Theorem 0.8.2 (Ewens Sampling Formula)**.** Under the infinite-alleles neutral model with parameter $\theta = 4N_e\mu$, the probability that a sample of n gene copies contains k distinct alleles with counts $(a_1, a_2, \ldots, a_k)$ (where $\sum_j a_j = n$ and $a_j \geq 1$) is:

$$P(a_1, \ldots, a_k \mid n, \theta) = \frac{n!}{\theta(\theta+1)\cdots(\theta+n-1)} \cdot \frac{\theta^k}{\prod_{j=1}^{k} a_j} \cdot \frac{1}{k!} \binom{n}{a_1, \ldots, a_k}^{-1},$$

or equivalently, through the configuration $(m_1, m_2, \ldots, m_n)$ where m_j is the number of alleles represented exactly j times in the sample:

$$P(m_1, m_2, \ldots, m_n \mid n, \theta) = \frac{n!}{\theta^{(n)}} \prod_{j=1}^{n} \left(\frac{\theta}{j}\right)^{m_j} \frac{1}{m_j!},$$

where $\theta^{(n)} = \theta(\theta+1)\cdots(\theta+n-1)$ is the rising factorial.

The Ewens sampling formula is a cornerstone of population genetic theory because it is an *exact* probability model for sample configurations under neutrality, enabling likelihood-based inference of θ from observed allele count data without simulation. It is also the distribution of the sizes of the k coalescent lineages in a sample of size n under the Kingman coalescent (Section II, Section 8).

Example 0.8.3 (Estimating θ from microsatellite data)**.** A population sample of $n = 100$ chromosome copies at a microsatellite locus reveals $k = 15$ distinct alleles. The maximum likelihood estimate of θ from the Ewens formula satisfies the equation:

$$\sum_{j=0}^{n-1} \frac{1}{\theta + j} = \frac{k}{\theta},$$

which for $k = 15$, $n = 100$ gives $\hat{\theta} \approx 5.8$. This corresponds to $N_e\mu \approx 1.45$ for a diploid locus. If the microsatellite mutation rate is $\mu \approx 10^{-3}$, the implied effective population size is $N_e \approx 1450$.

0.9 11. The Theory of Genetic Distance

0.9.1 11.1 Measures of Genetic Distance Between Populations

When two populations are compared at a locus with allele frequencies $\mathbf{p} = (p_1, \ldots, p_k)$ and $\mathbf{q} = (q_1, \ldots, q_k)$ respectively, the **genetic distance** between them quantifies how different their allele frequency distributions are. Several measures are in common use:

Definition 0.9.1 (Nei's standard genetic distance)**.**

$$D_S = -\ln\left(\frac{\sum_i p_i q_i}{\sqrt{\sum_i p_i^2 \cdot \sum_i q_i^2}}\right).$$

This is minus the log of the normalised inner product of the allele frequency vectors. $D_S = 0$ when the populations are identical ($\mathbf{p} = \mathbf{q}$), and $D_S \to \infty$ as the populations diverge completely (share no alleles).

Definition 0.9.2 (F_{ST} as a distance)**.**

$$F_{ST} = 1 - \frac{H_S}{H_T} = \frac{H_T - H_S}{H_T},$$

where H_S is the expected heterozygosity within subpopulations and H_T is the expected heterozygosity in the total (pooled) population. For a two-population system: $H_T = 1 - \sum_i \bar{p}_i^2$ and $H_S = \frac{1}{2}[(1-\sum_i p_i^2) + (1-\sum_i q_i^2)]$, with $\bar{p}_i = (p_i + q_i)/2$.

Theorem 0.9.3 (Relationship between F_{ST} and divergence time)**.** Under the neutral island model with

symmetric migration rate m and effective size N_e, the equilibrium F_{ST} satisfies:

$$F_{ST} = \frac{1}{1 + 4N_e m}.$$

For isolated populations (no migration after divergence at time t generations ago):

$$F_{ST}(t) \approx 1 - e^{-t/(2N_e)},$$

which increases from 0 at $t = 0$ (identical populations) to 1 as $t \to \infty$ (complete divergence). The characteristic time scale for divergence is $2N_e$ generations.

This theorem provides the mathematical basis for using F_{ST} to infer population divergence times from genetic data, a central tool in phylogeography.

0.9.2 11.2 Principal Component Analysis of Allele Frequency Data

Modern population genetic analyses use **principal component analysis** (PCA) of genome-wide allele frequency data to visualise population structure without assuming any particular demographic model.

Given n individuals and L biallelic loci, form the genotype matrix $\mathbf{X} \in \{0, 1, 2\}^{n \times L}$ where X_{il} is the count of one allele at locus l in individual i. Standardise by column: $\tilde{X}_{il} = (X_{il} - 2\hat{p}_l)/\sqrt{2\hat{p}_l(1 - \hat{p}_l)}$, where $\hat{p}_l$ is the sample allele frequency at locus l. The PCA is the singular value decomposition:

$$\tilde{\mathbf{X}} = \mathbf{U}\, \mathbf{V}^\top,$$

where $\mathbf{U}$ is the matrix of left singular vectors (one per individual), and the first two columns of $\mathbf{U}$ scaled by singular values give the PCA coordinates plotted as the "PCA biplot."

Theorem 0.9.4 (McVean 2009: PCA recovers geographic structure)**.** Under isolation-by-distance with migration on a two-dimensional torus and drift parameter θ, the leading eigenvectors of the PCA of allele frequencies converge (as $L \to \infty$) to the Fourier modes of the migration kernel. For a rectangular geographic region, the first two PCA eigenvectors approximate the geographic coordinates of individuals up to a rotation.

This is the mathematical justification for interpreting PCA plots as geographic maps: the PCA is not just a dimensionality reduction trick but a mathematically consistent estimator of geographic position under the isolation-by-distance model.

Remark 0.9.5 (Limitations of PCA). PCA assumes a linear model of population structure and can give misleading results when: (a) populations have experienced rapid bottlenecks (PCA inflates the distinctiveness of bottlenecked groups), (b) there is long-range LD (linked loci violate the independence assumption), or (c) the sample is unequal across populations (rare populations are "pulled toward" common ones). Model-based clustering methods (STRUCTURE, ADMIXTURE) address some of these limitations by explicitly modelling allele frequencies within K ancestral populations.

0.10 12. Coalescent Theory: A Preview

0.10.1 12.1 From Forward to Backward: Genealogical Thinking

The standard population genetic approach traces allele frequencies *forward* in time from ancestors to descendants. The **coalescent** (Kingman 1982) reverses this perspective: starting from a sample of n present-day gene copies, it traces their ancestry *backward* in time until all n copies share a common ancestor.

The coalescent is mathematically elegant because it converts the complex forward-time Wright-Fisher model (tracking $2N$ gene copies in each generation) into a much simpler backward-time process tracking only the n sampled copies. The price: the coalescent is an approximation valid in the limit $n \ll N$.

Definition 0.10.1 (Coalescent events)**.** In the backward-time coalescent, two lineages (sampled gene copies) **coalesce** when they share a common ancestor in the previous generation. In the Wright-Fisher model, the probability that any specific pair of lineages coalesces in one generation is $1/(2N_e)$ (two draws from the same parent out of $2N$ possible parents). The waiting time $T_{n \to n-1}$ until the first coalescent event in a sample of n lineages (among $\binom{n}{2}$ pairs, each coalescing at rate $1/(2N_e)$) is geometrically distributed with mean:

$$E[T_{n \to n-1}] = \frac{2N_e}{\binom{n}{2}} = \frac{4N_e}{n(n-1)} \text{ generations.}$$

Remark 0.10.2 (The coalescent as a bridge between models and data). The coalescent connects the Wright-Fisher forward-time model (genetics) to the genealogical tree relating a sample (phylogenetics). The genealogy of a sample is a random binary tree whose topology is determined by the coalescent's branching times and the tree's branch lengths encode mutation history. This connection — from population parameters (N_e, μ) to observable data (sequence polymorphisms) via the coalescent — is the mathematical foundation of modern statistical population genomics. The Kingman coalescent is developed in full in Section II, Section 8.

0.10.2 12.2 MRCA and the Age of Adam and Eve

The **most recent common ancestor** (MRCA) of the human species at any given locus is the individual who contributed all copies of the gene in present-day humans. The expected time to the MRCA in a sample of n gene copies (under the Kingman coalescent) is:

$$E[T_{\text{MRCA}}] = 4N_e \left(1 - \frac{1}{n}\right) \text{ generations.}$$

For a large sample ($n \to \infty$): $E[T_{\text{MRCA}}] = 4N_e$ generations.

For human autosomal loci, with $N_e \approx 10\,000$ and generation time ≈ 25 years, $E[T_{\text{MRCA}}] \approx 4 \times 10\,000 \times 25 = 10^6$ years: about 1 million years per autosomal locus. This is the expected genealogical depth of human alleles.

For the Y chromosome (haploid, no recombination, $N_e^Y \approx N_e/4$ for males), $E[T_{\text{MRCA}}^Y] \approx N_e^Y$ generations $\approx 60\,000$ years. For mitochondrial DNA (maternally inherited, haploid, $N_e^{\text{mt}} \approx N_e/4$), $E[T_{\text{MRCA}}^{\text{mt}}] \approx N_e^{\text{mt}}$ generations $\approx 160\,000$ years.

These are the "Mitochondrial Eve" and "Y-chromosomal Adam" estimates: not the first humans, but

the most recent common matrilineal and patrilineal ancestors of all living humans. Their different ages (mtDNA is older) reflect the stochastic variance in coalescent times, not any biological sex-bias in ancestry.

0.11 13. Recombination, Gene Conversion, and Haplotype Structure

0.11.1 13.1 The Rate of Recombination and Map Distance

Recombination is the exchange of DNA segments between homologous chromosomes during meiosis. The **recombination fraction** c between two loci is the probability that a gamete carries one allele from one parental chromosome and the other allele from the other parental chromosome.

Definition 0.11.1 (Haldane's mapping function)**.** The relationship between genetic map distance d (in Morgans) and recombination fraction c under a Poisson model of crossover events along the chromosome is:

$$c = \frac{1}{2}(1 - e^{-2d}).$$

This is the **Haldane mapping function**. For small d, $c \approx d$ (map distance $\approx$ recombination fraction). For large d, $c \to 1/2$ (unlinked loci appear to assort independently, regardless of physical distance).

Remark 0.11.2 (Positive interference). The Poisson model of crossovers (Haldane's function) assumes crossovers on the same chromosome are independent. In reality, **positive interference** suppresses double crossovers: the occurrence of one crossover reduces the probability of a nearby crossover. The Kosambi mapping function $c = \frac{1}{2}\tanh(2d)$ incorporates positive interference and fits human genetic maps better than Haldane's function.

The human genetic map (HapMap, deCODE) has a total length of ≈ 3600 cM (centimorgans $= 0.01$ Morgans) over a physical genome of $\approx 3 \times 10^9$ bp, giving an average rate of $\approx 1.2 \times 10^{-8}$ M/bp $= 1.2$ cM/Mb. But the rate is highly heterogeneous: recombination is concentrated in **hotspots** of 1–3 kb, where $\approx 60\%$ of crossovers occur in $< 10\%$ of the genome. Hotspots are associated with PRDM9 binding motifs and show rapid evolutionary turnover.

0.11.2 13.2 Gene Conversion and Its Effect on Allele Frequencies

Gene conversion is a form of recombination in which one allele is "converted" to the sequence of its homologue without reciprocal exchange. Unlike crossing-over, which does not change allele frequencies, gene conversion is **biased** when one allele is preferentially converted to the other (biased gene conversion, BGC).

Under **GC-biased gene conversion** (gBGC), GC alleles are preferentially converted from AT alleles during the mismatch repair of heteroduplex DNA at recombination hotspots. The allele frequency dynamics under gBGC are mathematically identical to selection with effective selection coefficient s_{BGC} favouring the GC allele:

$$\Delta p_{\text{GC}} \approx s_{\text{BGC}} p_{\text{GC}}(1 - p_{\text{GC}}),$$

where $s_{\text{BGC}} = b \cdot f_{\text{het}}/(p_{\text{GC}}(1 - p_{\text{GC}}))$, b is the conversion bias, and f_{het} is the fraction of gametes arising from recombination at the locus.

Remark 0.11.3 (gBGC and the evolution of GC content). gBGC is now recognised as a major force

shaping nucleotide composition in mammals. Regions of high recombination rate tend to have elevated GC content, a pattern explained by gBGC rather than selection for GC-rich sequence. The practical consequence: molecular evolution analyses that treat all synonymous substitutions as neutral must account for gBGC at recombination hotspots, because AT→GC changes are subject to a selection-like force that inflates the apparent synonymous substitution rate.

0.11.3 13.3 Haplotype Block Structure and Tag SNPs

Linkage disequilibrium across the human genome is not uniform: it is organised into **haplotype blocks** of strong LD (typically 10–100 kb) separated by recombination hotspots. Within a block, all SNPs are in near-complete LD with each other; across hotspots, LD drops sharply.

This block structure has a practical consequence for GWAS: one does not need to genotype all $\sim 10^7$ common SNPs in the human genome to capture all common variation. A subset of **tag SNPs**, one per haplotype block, is sufficient. The number of tag SNPs needed to tag $r^2 \geq 0.8$ of all common SNPs (MAF > 0.05) in European populations is approximately 500 000 (the basis for commercial SNP arrays).

Definition 0.11.4 (Tagging efficiency)**.** The tagging efficiency of a SNP j for SNP k is r^2_{jk}, the squared correlation between their alleles. SNP j "tags" SNP k if $r^2_{jk} \geq 0.8$. The minimum set of tag SNPs that tags all SNPs in a region at $r^2 \geq 0.8$ can be found by a greedy algorithm: iteratively select the SNP that tags the largest number of untagged SNPs.

The mathematical theory of haplotype blocks connects LD (the Hardy–Weinberg framework's two-locus extension from Section 4) to practical genomics: the structure of LD determines the resolution of association studies and the number of markers needed for genome-wide coverage.

0.12 14. Admixture and Ancestry Inference

0.12.1 14.1 The Admixture Model

Admixture is the recent mixing of previously isolated populations. In an admixed individual, each genomic region traces its ancestry to one of the parental populations. The **admixture fraction** q_k of individual i from population k is the proportion of the genome derived from ancestral population k:

$$\sum_{k=1}^{K} q_{ik} = 1, \quad q_{ik} \geq 0.$$

Under the admixture model, the expected allele frequency at locus l in individual i is:

$$\hat{p}_{il} = \sum_{k=1}^{K} q_{ik} p_{kl},$$

where p_{kl} is the allele frequency at locus l in ancestral population k.

Theorem 0.12.1 (Allele frequency in admixed populations)**.** In a population that is a mixture of K ancestral populations with proportions $(Q_1, \ldots, Q_K)$ (summing to 1) and allele frequencies $(p_k)_{k=1}^K$ at a

biallelic locus, the expected allele frequency in the admixed population is:

$$\bar{p}_{\text{admix}} = \sum_{k=1}^{K} Q_k p_k,$$

and the expected heterozygosity is:

$$H_{\text{admix}} = 2\bar{p}_{\text{admix}}(1 - \bar{p}_{\text{admix}}) + 2\sum_{k<l} Q_k Q_l (p_k - p_l)^2 = H_{\text{HWE}} + 2\,\text{Var}_Q(p),$$

where the last term is the Wahlund excess heterozygosity from admixture.

Remark 0.12.2 (Admixture mapping). Because admixed genomes contain chromosomal segments of different ancestry, local ancestry can be inferred from the pattern of allele frequencies across the genome. **Admixture mapping** tests whether disease risk correlates with local ancestry rather than specific SNP genotypes. It is powerful for diseases that differ in prevalence between the ancestral populations and has been used to map genes for hypertension, kidney disease, and multiple sclerosis in African-American cohorts.

0.12.2 14.2 STRUCTURE and Bayesian Clustering

The STRUCTURE algorithm (Pritchard, Stephens, and Donnelly 2000) uses a Bayesian model to infer population structure from multilocus genotype data. The model assumes:

1. There are K ancestral populations with allele frequencies $\{p_{kl}\}_{k=1,l=1}^{K,L}$.
2. Each individual i has admixture fractions $(q_{i1}, \ldots, q_{iK})$ with Dirichlet prior: $(q_{i1}, \ldots, q_{iK}) \sim \text{Dir}(\alpha, \ldots, \alpha)$.
3. Each allele copy in individual i is drawn from population $z_{il} \in \{1, \ldots, K\}$ with probability $q_{i,z_{il}}$.
4. Given population assignment $z_{il} = k$, the allele is drawn from $\text{Binom}(1, p_{kl})$.

The posterior distribution $P(\mathbf{Q}, \mathbf{Z}, \mathbf{P} \mid \mathbf{X})$ is estimated by MCMC (Gibbs sampling). The key outputs are: the admixture fractions $\hat{q}_{ik}$ for each individual and population, and the ancestral allele frequencies $\hat{p}_{kl}$.

Theorem 0.12.3 (Identifiability of STRUCTURE model)**.** The STRUCTURE model is identifiable (the K populations can be distinguished) provided:

[(i)]The ancestral allele frequency vectors $\mathbf{p}_k$ are distinct: $\mathbf{p}_k \neq \mathbf{p}_{k'}$ for $k \neq k'$. The number of loci $L \geq 2$, with sufficient diversity at each locus. The admixture fractions are not all degenerate (not all $q_{ik} \in \{0, 1\}$).

In practice, identifiability improves rapidly with L; modern GWAS datasets with $L \sim 10^5$–10^6 loci provide overwhelming statistical power for $K \leq 20$.

0.12.3 14.3 The Mathematics of Local Ancestry Inference

Local ancestry inference (LAI) estimates the population of origin of each chromosomal segment in an admixed genome. The mathematical model is a **hidden Markov model** (HMM):

1. **Hidden states:** $Z_l \in \{1, \ldots, K\}^2$ (maternal and paternal ancestry at locus l), for $l = 1, \ldots, L$.

- **Emission distribution:** $P(X_{il} \mid Z_l = (k, k')) =$ probability of observed genotype given ancestries k (maternal) and k' (paternal), computed from ancestral allele frequencies p_{kl} and $p_{k'l}$.
- **Transition distribution:** $P(Z_{l+1} \mid Z_l)$ reflects the probability of an ancestry switch at locus $l+1$. Under the Markov model, the switch probability is $1 - e^{-\rho_l}$ where ρ_l is the recombination rate between loci l and $l+1$ scaled by the number of generations since admixture τ: $\rho_l = c_l\tau$.

The posterior local ancestry probabilities are computed by the **forward-backward algorithm**:

$$P(Z_l = (k, k') \mid \mathbf{X}) \propto \alpha_l(k, k') \cdot \beta_l(k, k'),$$

where α_l (forward variable) and β_l (backward variable) satisfy the standard HMM recursions. The time complexity is $O(LK^2)$, feasible for genome-wide data.

This HMM framework connects the Hardy-Weinberg theory of this Section (allele frequencies in populations) to statistical genomics (inference from individual genotype data), completing the bridge from population-level descriptions to individual-level ancestry.

0.13 15. Summary: The Mathematical Universe of Hardy-Weinberg

Section I has established that the Hardy-Weinberg principle, far from being a simple curiosity about genotype frequencies, is the foundation of an entire mathematical universe. The principle itself is a single theorem about allele frequencies and binomial sampling. But its implications radiate outward into:

- **Statistical testing** (chi-squared, likelihood ratio, exact tests) for deviations from the HWE prediction.
- **Linkage disequilibrium** as the two-locus generalisation, decaying at rate $(1 - c)$ per generation.
- **Population structure** as a cause of HWE deviation, quantified by Wright's F-statistics and the Wahlund effect.
- **Coalescent theory** as the backward-time complement, connecting HWE allele frequencies to genealogical histories.
- **Genetic distance** measures (F_{ST}, Nei's D_S) for comparing populations.
- **PCA of allele frequency matrices** as a non-parametric tool for visualising population structure.
- **Admixture models** for inferring population mixing fractions from multilocus data, via STRUCTURE and LAI-HMM.
- **The Ewens sampling formula** as the exact probability model for allele count configurations under neutrality.
- **Recombination and haplotype structure** as determinants of the two-locus LD landscape.

All of these developments trace their mathematical lineage to the single insight that reproduction under random mating is equivalent to independent Bernoulli sampling from an allele pool. The simplicity of this observation — and the richness of its consequences — is the hallmark of a genuinely foundational theorem.

0.14 16. The Mathematics of Genetic Drift: A Preview

0.14.1 16.1 Why Infinite Populations Are a Fiction

Every real population is finite. The Hardy–Weinberg principle, as derived in this Section , assumes infinite population size in the sense that the gene pool has unlimited copies from which gametes are drawn independently. This assumption produces exactly deterministic allele frequency dynamics: $p_{t+1} = p_t$ forever. The frequency never changes in the absence of selection, mutation, or migration.

In a finite population of size N diploid individuals, offspring are formed by drawing $2N$ gametes from the $2N$ gene copies of the parental generation. This is sampling *without* replacement from a finite pool (or equivalently, with replacement in the large-N limit). The number of A copies in the next generation is a random variable:

$$k_{t+1} \mid k_t \sim \text{Binomial}(2N, p_t),$$

where $p_t = k_t/(2N)$ is the allele frequency in generation t. The mean of p_{t+1} is $\mathbb{E}[p_{t+1} \mid p_t] = p_t$ (allele frequency is a martingale), but the variance is:

$$\text{Var}(p_{t+1} \mid p_t) = \frac{p_t(1-p_t)}{2N}.$$

This variance is the seed of all genetic drift. It is small for large N but never zero. Crucially, it accumulates: each generation adds an independent quantum of variance to the allele frequency, and these fluctuations are not self-correcting — once the frequency shifts, it starts drifting from the new position.

Theorem 0.14.1 (Hardy-Weinberg as an approximation to the Wright-Fisher model)**.** The Hardy-Weinberg equilibrium genotype frequencies $p^2, 2pq, q^2$ are exact in the Wright-Fisher model in the limit $N \to \infty$. For finite N, the expected genotype frequencies in generation $t+1$ given allele frequency p in generation t are:

$$\mathbb{E}[f_{AA}^{(t+1)} \mid p] = p^2 + \frac{p(1-p)}{2N}\left(1 + \frac{1}{2N}\right) \approx p^2 + \frac{p(1-p)}{2N},$$
$$\mathbb{E}[f_{Aa}^{(t+1)} \mid p] = 2pq - \frac{p(1-p)}{N}\left(1 + \frac{1}{2N}\right) \approx 2pq - \frac{pq}{N}.$$

The correction terms are of order $1/(2N)$: for $N = 1000$, they reduce the expected heterozygosity by $\approx 0.05\%$ per generation. Over t generations, the correction accumulates to:

$$\mathbb{E}[H_t] = 2pq\left(1 - \frac{1}{2N}\right)^t \to 0 \text{ as } t \to \infty.$$

This is the famous result that genetic drift erodes heterozygosity at rate $1/(2N)$ per generation. A population of $N = 100$ loses half its initial heterozygosity in $\ln(2)/(1/(2 \times 100)) \approx 138$ generations. A population of $N = 10^4$ takes $\approx 14\,000$ generations. For the human species with $N_e \approx 10^4$, loss of heterozygosity by drift alone takes on the order of 10^5 years — consistent with the large heterozygosity observed in humans despite a relatively small N_e.

0.14.2 16.2 The Wright-Fisher Model: Setup

The **Wright-Fisher model** (Wright 1931, Fisher 1930) is the canonical model of genetic drift. It is defined by:

> [(i)]A population of N diploid organisms (or equivalently, $2N$ haploid gene copies). Discrete, non-overlapping generations. Random mating (panmixia): offspring gene copies are drawn independently and uniformly from the $2N$ parental copies. No selection, no mutation, no migration (in the basic model).

The transition probability for the Wright-Fisher model is:

$$P(k_{t+1} = j \mid k_t = k) = \binom{2N}{j} \left(\frac{k}{2N}\right)^j \left(1 - \frac{k}{2N}\right)^{2N-j},$$

a binomial probability. The Markov chain on states $\{0, 1, \ldots, 2N\}$ has two absorbing states: $k = 0$ (fixation of a) and $k = 2N$ (fixation of A). Starting from any interior state, the chain is absorbed with probability 1 in finite time.

0.14.3 16.3 The Variance Effective Population Size

The **effective population size** N_e is the size of an idealised Wright-Fisher population that would show the same rate of genetic drift as the actual population. It is defined through the variance of allele frequency change:

$$\text{Var}(\Delta p) = \frac{p(1-p)}{2N_e}.$$

For a population with variance in reproductive success σ_k^2 (variance in the number of offspring per individual), the effective size is:

$$N_e = \frac{N - 1}{\sigma_k^2/(k) - 1 + 1/N} \approx \frac{N}{\sigma_k^2/\bar{k}},$$

where $\bar{k} \approx 2$ is the mean number of offspring per parent in a stable population. In an idealised Wright-Fisher model, $\sigma_k^2 = 2(N-1)/N \approx 2$ and $N_e = N$. In real populations, $\sigma_k^2 > 2$ (e.g., many animals have highly variable reproductive success), so $N_e < N$.

Example 0.14.2 (Effective population size of humans)**.** Estimates of N_e for humans from various data sources:

- Heterozygosity at synonymous sites: $\theta = 4N_e\mu \approx 10^{-3}$, with $\mu \approx 2.5 \times 10^{-8}$ per base per generation, gives $N_e \approx 10^4$.
- Coalescent TMRCA for autosomal loci: $E[T_{\text{MRCA}}] = 4N_e \approx 10^6$ years/25 years per generation $= 40\,000$ generations, giving $N_e \approx 10^4$.
- Census size: $N_{\text{census}} \approx 8 \times 10^9$ today, but likely $< 10^6$ for most of human prehistory. $N_e/N_{\text{census}} \approx 0.01$–$0.1$.

The striking result: $N_e \ll N_{\text{census}}$. The effective human population size is about 10^4, despite there being billions of humans today. This is explained by variance in reproductive success, population bottlenecks (e.g., out-of-Africa migration), and the lag between census size and genetic drift.

0.15 17. Probability Theory Foundations for Population Genetics

0.15.1 17.1 Probability Spaces and Genetic Events

The mathematical framework of probability theory underlies every calculation in this Section . We briefly summarise the key concepts.

A **probability space** is a triple $(\Omega, \mathcal{F}, P)$:

- Ω is the **sample space**: the set of all possible outcomes. For Hardy-Weinberg: $\Omega = \{AA, Aa, aa\}$ (genotype of a random individual).
- $\mathcal{F}$ is a **σ-algebra**: a collection of events (subsets of Ω) closed under complement and countable unions.
- $P : \mathcal{F} \to [0, 1]$ is a **probability measure**: $P(\Omega) = 1$, $P(\emptyset) = 0$, and P is countably additive.

For the HWE genotype distribution, $\Omega = \{AA, Aa, aa\}$, $\mathcal{F} = 2^{\Omega}$ (all subsets), and $P(\{AA\}) = p^2$, $P(\{Aa\}) = 2pq$, $P(\{aa\}) = q^2$.

Independence is the key concept: events A and B are independent if $P(A \cap B) = P(A)P(B)$. The HWE derivation rests on the independence of the two allele draws: $P(X_1 = A) = p$ and $P(X_2 = A) = p$ are independent, so $P(X_1 = A, X_2 = A) = p^2$.

0.15.2 17.2 Generating Functions and the Moments of the Allele Frequency Distribution

The **probability generating function** (PGF) of the binomial distribution $k \sim \text{Binom}(2N, p)$ is:

$$G(z) = E[z^k] = \sum_{k=0}^{2N} \binom{2N}{k} p^k (1-p)^{2N-k} z^k = (pz + (1-p))^{2N}.$$

The mean and variance follow from the PGF:

$$E[k] = G'(1) = 2Np, \quad E[k(k-1)] = G''(1) = (2N)(2N-1)p^2,$$

$$\text{Var}(k) = G''(1) + G'(1) - G'(1)^2 = 2Np(1-p).$$

The PGF framework extends naturally to the multi-generation drift analysis: the PGF of allele counts in generation t can be expressed as a composition of single-generation PGFs, enabling exact computation of moments at any time horizon.

Theorem 0.15.1 (Variance of allele frequency after t generations of drift)**.** Starting from allele frequency p_0 in a Wright-Fisher population of size N, the variance of the allele frequency after t generations is:

$$\text{Var}(p_t) = p_0(1-p_0)\left[1 - \left(1 - \frac{1}{2N}\right)^t\right].$$

For large t: $\text{Var}(p_t) \to p_0(1-p_0)$ (the frequency is uniform on $[0, 1]$ conditioned on not being absorbed, and the variance approaches the Bernoulli maximum $p_0(1-p_0)$). For small t: $\text{Var}(p_t) \approx tp_0(1-p_0)/(2N)$ (drift accumulates linearly in time).

This theorem quantifies the time scale of genetic drift: the variance reaches half its maximum value after $t_{1/2} = 2N \ln 2$ generations. For a population of $N = 100$, $t_{1/2} \approx 139$ generations; for $N = 10^4$, $t_{1/2} \approx 13\,900$ generations. The Hardy-Weinberg world, where allele frequencies are constant, is the $N \to \infty$ limit of the Wright-Fisher model, recovered exactly when drift is absent.

0.15.3 17.3 The Martingale Structure of Allele Frequencies

Theorem 0.15.2 (Allele frequency as a martingale)**.** In the Wright-Fisher model without selection or mutation, the allele frequency process $(p_t)_{t \geq 0}$ is a martingale with respect to the natural filtration: for all t,

$$\mathbb{E}[p_{t+1} \mid p_0, p_1, \ldots, p_t] = p_t.$$

Proof. $p_{t+1} = k_{t+1}/(2N)$ where $k_{t+1} \mid k_t \sim \text{Binom}(2N, p_t)$. Therefore $\mathbb{E}[p_{t+1} \mid p_t] = \mathbb{E}[k_{t+1}/(2N) \mid p_t] = p_t$. The Markov property of the Wright-Fisher model implies conditioning on the full history reduces to conditioning on p_t alone. □

The martingale property has two consequences:

[(i)]By the optional stopping theorem, $\mathbb{E}[p_\tau] = p_0$ for any stopping time τ (including the absorption time). Therefore the probability of fixation of A (absorption at $p = 1$) is exactly p_0: $P(\text{fix } A) = p_0$ and $P(\text{fix } a) = 1 - p_0$. This is the central result of neutral drift theory, derived here from martingale theory without any explicit calculation. The variance process $V_t = p_t(1 - p_t)$ is a supermartingale: $\mathbb{E}[V_{t+1} \mid p_t] = p_t(1 - p_t)(1 - 1/(2N)) = V_t(1 - 1/(2N)) \leq V_t$. Heterozygosity decreases on average — the mathematical statement that drift erodes genetic diversity.

This completes the mathematical preview of drift. Section II develops the full stochastic theory of genetic drift using the Wright-Fisher model, Kimura's diffusion approximation, and the Kingman coalescent. The Hardy-Weinberg world of this Section — deterministic, frequency-preserving, analytically tractable — is the skeleton that the stochastic theory of Section II perturbs, enriches, and ultimately supersedes for finite populations.

Mathematics of Evolution and Life · Section I · Populations, Genes, and the Hardy–Weinberg Equilibrium (expanded edition, end)

0.16 18. Quantitative Methods in Modern Population Genomics

0.16.1 18.1 LD Score Regression

LD score regression (Bulik-Sullivan et al. 2015) is a method to estimate the heritability of complex traits and the genetic correlation between traits from genome-wide summary statistics, using the mathematical theory of linkage disequilibrium developed in Section 4.

The key insight: under a polygenic model where trait-associated variants are spread across the genome, the expected chi-squared statistic for a SNP j in a GWAS is:

$$\mathbb{E}[\chi_j^2] = \frac{Nh^2}{M} \ell_j + 1,$$

where N is the sample size, h^2 is the SNP heritability, M is the number of SNPs, and $\ell_j = \sum_k r_{jk}^2$ is the **LD score** of SNP j — the sum of squared correlations with all other SNPs in the genome.

Definition 0.16.1 (LD score)**.** The LD score of SNP j is:

$$\ell_j = \sum_{k=1}^{M} r_{jk}^2,$$

where $r_{jk}^2 = D_{jk}^2/(p_j q_j p_k q_k)$ is the squared correlation between alleles at SNPs j and k, computed from the same LD formula derived in Section 4.2. SNPs in regions of high LD (haplotype blocks) have high LD scores; SNPs in recombination hotspots or gene deserts have low LD scores.

The regression of GWAS χ^2 statistics on LD scores gives slope $\hat{\beta}_1 = Nh^2/M$, from which the heritability is estimated:

$$\hat{h}^2_{\text{SNP}} = \hat{\beta}_1 \cdot \frac{M}{N}.$$

The intercept of the regression, under the null of no stratification, should equal 1; an intercept > 1 indicates population stratification or other confounding (the test detects violations of the HWE assumptions at scale).

Example 0.16.2 (Heritability of schizophrenia by LD score regression)**.** GWAS for schizophrenia with $N \approx 150\,000$ individuals and $M \approx 10^6$ SNPs gives $\hat{h}^2_{\text{SNP}} \approx 0.22$ (Ripke et al. 2014). The twin-study heritability is $h^2 \approx 0.80$. The gap ($0.80 - 0.22 = 0.58$) is the "missing heritability": genetic variation captured by rare variants (MAF < 0.01, not well-tagged by common SNPs), gene-environment interactions, and epistasis not captured by the additive SNP model. LD score regression precisely quantifies which portion of this heritability the current GWAS array can "see" through the LD structure.

0.16.2 18.2 The Mathematics of Polygenic Scores

A **polygenic risk score** (PRS) is a weighted sum of allele counts across L GWAS loci:

$$\text{PRS}_i = \sum_{l=1}^{L} \hat{\beta}_l X_{il},$$

where $X_{il} \in \{0, 1, 2\}$ is the allele count at locus l in individual i, and $\hat{\beta}_l$ is the estimated effect size from a GWAS.

Theorem 0.16.3 (Expected r^2 between PRS and trait)**.** Under the infinitesimal model (all L loci contribute equally to heritability h^2), the expected squared correlation between the PRS and the true phenotype is:

$$r^2_{\text{PRS}} = h^2 \cdot \frac{h^2 L_{\text{eff}}}{h^2 L_{\text{eff}} + N_{\text{train}}^{-1} M},$$

where L_{eff} is the effective number of independent loci (accounting for LD), N_{train} is the GWAS training sample size, and M is the total number of SNPs. For large N_{train}, $r^2_{\text{PRS}} \to h^2_{\text{SNP}}$: the PRS captures the full SNP heritability. For small N_{train}, $r^2_{\text{PRS}} \ll h^2$: the PRS is underpowered.

This theorem quantifies why large GWAS samples are essential: the predictive power of a PRS grows approximately as N_{train} until saturation at h^2_{SNP}. Current mental health PRS ($h^2 \approx 0.1$–0.3, $N_{\text{train}} \approx 10^5$–$10^6$) achieve $r^2_{\text{PRS}} \approx 0.05$–$0.15$ — useful for population-level stratification but not for individual-level

clinical prediction.

0.16.3 18.3 Hardy-Weinberg Equilibrium in GWAS Quality Control

GWAS data quality control routinely tests HWE at each locus. The rationale: genotyping errors, DNA damage, and copy number variants all produce HWE deviations. The procedure:

1. For each of the $M \sim 10^6$ loci, compute the HWE chi-squared statistic (Section 3.1): $\chi^2_{\text{HWE}} = \sum_g (O_g - E_g)^2/E_g$ with 1 df.
2. Apply a genome-wide threshold: loci with $p < 10^{-6}$ are excluded.
3. At this threshold, the expected number of false positives among $M = 10^6$ SNPs (all truly in HWE) is $M \times 10^{-6} = 1$: one spurious exclusion per analysis.

The choice of 10^{-6} (not $0.05/M = 5\times10^{-8}$, the Bonferroni threshold for GWAS) reflects the asymmetry: HWE violation is used as a quality filter, not a test of association. The goal is to remove outliers, not to test HWE as a scientific hypothesis. This is one of the rare situations in genomics where a *less* stringent threshold is appropriate: a threshold of 0.05 would remove 5% of all SNPs by chance (false positives), while 10^{-6} removes only ~ 1.

0.17 19. Open Problems in Population Genetics

0.17.1 19.1 The Missing Heritability Problem

For most complex traits (height, BMI, disease risks, cognitive abilities), the heritability measured by twin studies ($h^2_{\text{twin}} \approx 0.5$–$0.9$) far exceeds the heritability explained by GWAS-identified variants ($h^2_{\text{SNP}} \approx 0.1$–$0.4$ for well-powered traits). Multiple explanations have been proposed:

[(i)]**Rare variants:** Common SNP arrays do not capture rare variants (MAF $< 1\%$). Whole-genome sequencing studies suggest rare variants account for 10–30% of the missing heritability for some traits. **Epistasis:** Multiplicative interactions between loci are not captured by additive SNP models. Theoretical upper bounds on epistatic heritability from HWE theory and LD structure are an active research area. **Structural variants:** Copy number variants, inversions, and mobile element insertions are poorly captured by SNP arrays and may contribute substantially to trait heritability. **Epigenetic inheritance:** Trans-generational epigenetic effects contribute to parent-offspring correlations in twin studies without being captured by DNA sequence variants. **Gene-environment interaction:** h^2_{twin} measures heritability in specific environments; if genotype-environment interactions exist, the GWAS estimate (from heterogeneous cohorts) systematically underestimates h^2.

Resolving the missing heritability remains a central challenge for the quantitative theory of Hardy-Weinberg-based statistical genetics.

0.17.2 19.2 Ancient DNA and the Dynamics of Allele Frequencies in Deep Time

The sequencing of ancient DNA (aDNA) from archaeological specimens now allows direct observation of allele frequency changes over thousands of years. This converts population genetics from an inferential discipline (estimating past dynamics from present-day variation) to a directly observational one.

Key findings from aDNA:

- Allele frequencies at lactase persistence, skin pigmentation, and stature-associated loci have changed dramatically in European populations over the past 10 000 years, with rates inconsistent with neutral drift alone. These are direct observations of the selection coefficients that theory predicts.
- Multiple admixture events between distinct ancestral populations (Anatolian farmers, Western Hunter-Gatherers, Pontic Steppe pastoralists) explain most of present-day European genetic structure — a validation of the admixture models of Section 14.
- Bottlenecks associated with migration and population replacement are directly visible as sudden changes in allele frequency distributions, consistent with Wright-Fisher drift predictions for small migrating groups.

The mathematical challenge: integrating aDNA time-series data with the Wright-Fisher model requires temporal inference methods — hidden Markov models over allele frequencies at discrete time points — that go beyond the cross-sectional HWE-based inference described in this Section .

0.17.3 19.3 Polygenic Adaptation and the Quantitative Genetics of Selection

Most evolutionarily important selective events are not driven by a single large-effect locus sweeping through the population (classical selective sweeps, Section 12 of Section III) but by small simultaneous shifts in allele frequencies at many loci (**polygenic adaptation**). Detecting polygenic adaptation from GWAS data requires comparing the observed directional change in allele frequencies at trait-associated loci to the neutral expectation from genetic drift.

The Q_{ST}-F_{ST} **test**: for a quantitative trait with additive genetic variance V_A, the divergence of the trait mean between populations should be consistent with pure drift if:

$$Q_{ST} = \frac{\sigma^2_{\text{between}}}{2\sigma^2_{\text{between}} + \sigma^2_{\text{within}}} \approx F_{ST}.$$

If $Q_{ST} > F_{ST}$, the trait has diverged faster than neutral expectation, implying divergent selection. If $Q_{ST} < F_{ST}$, the trait has diverged more slowly, implying stabilising selection maintaining similar trait means across populations.

This test connects HWE-based F_{ST} (Section 5.2) to quantitative genetics (Section IV) and selection theory (Section III), illustrating the mathematical unity of the Hardy-Weinberg framework across the entire scope of evolutionary genetics.

Mathematics of Evolution and Life · Section I · Populations, Genes, and the Hardy–Weinberg Equilibrium (fully expanded edition, final)

0.18 20. Mathematical Genetics and Medicine

0.18.1 20.1 Hardy-Weinberg in Clinical Genetics

The Hardy-Weinberg principle is routinely applied in medical genetics to estimate carrier frequencies, disease prevalences, and genetic risk from observed genotype or phenotype data. The inference runs in both directions:

- **From genotype to disease frequency:** Given q^2 as the observed frequency of an autosomal recessive disorder (affected individuals have genotype aa), the carrier frequency is $2q(1-q) \approx 2q$ for rare diseases. For phenylketonuria (PKU) with prevalence $\approx 1/15\,000$ in Northern Europeans, $q = \sqrt{1/15\,000} \approx 0.0082$ and the carrier frequency is $\approx 1.6\%$.

- **From allele frequency to genetic risk:** Given a risk allele frequency p and a relative risk λ for carriers (Aa) and λ^2 for homozygotes (AA), the population attributable risk (PAR) is:

$$\text{PAR} = 1 - \frac{(1-p)^2 + 2p(1-p)/\lambda + p^2/\lambda^2}{1} \cdot \frac{1}{\text{baseline}}.$$

Example 0.18.1 (BRCA1 and breast cancer risk)**.** The BRCA1 risk allele has population frequency $q \approx 0.001$ in Ashkenazi Jewish populations (specific founder mutations). Under HWE, the carrier frequency (heterozygotes Aa) is $2 \times 0.001 \times 0.999 \approx 0.002 = 0.2\%$. The lifetime breast cancer risk in BRCA1 carriers is $\approx 70\%$ vs. 12% in non-carriers. The proportion of all breast cancers attributable to BRCA1 in this population is approximately $0.002 \times (70-12)/12 \approx 1\%$ of all cases. BRCA1 explains only a small fraction of population-level breast cancer despite its large individual-level risk — a direct consequence of its low allele frequency under HWE.

0.18.2 20.2 Newborn Screening and the Population Genetics of Recessive Disease

Newborn screening for autosomal recessive diseases uses biochemical assays to identify affected infants (aa homozygotes) before disease onset. The population genetics of such programs require HWE-based calculations:

1. **Disease frequency:** Under HWE, the frequency of affected individuals is q^2. For cystic fibrosis in Europeans ($q \approx 0.02$), the disease frequency is $q^2 = 4 \times 10^{-4} = 1/2500$.

2. **Sensitivity and specificity:** A screening test with sensitivity Se and specificity Sp has positive predictive value:

$$\text{PPV} = \frac{\text{Se} \cdot q^2}{\text{Se} \cdot q^2 + (1-\text{Sp})(1-q^2)}.$$

   For rare diseases ($q^2 \ll 1$), even a highly specific test has low PPV: for CF with $\text{Se} = \text{Sp} = 0.999$, $\text{PPV} \approx q^2/(q^2 + (1-\text{Sp})) \approx 4\times10^{-4}/(4\times10^{-4} + 10^{-3}) \approx 0.29$. About 70% of positive screens in the general population are false positives, requiring confirmatory genetic testing.

3. **Impact of carrier testing:** If all carriers identified by a population carrier screening program chose not to have children with other carriers, the Hardy-Weinberg model predicts a reduction in disease frequency. After one generation of 100% carrier avoidance, q decreases from q_0 to $q_0 - q_0^2$ (the carriers who would have produced aa offspring are removed): a change too small to measure in practice. After t generations: $q_t \approx q_0/(1 + tq_0)$. For CF with $q_0 = 0.02$, complete carrier avoidance for 50 generations would reduce q to $q_{50} = 0.02/2 = 0.01$ — halving disease frequency after 50 generations of carrier avoidance. The mathematical intractability of removing recessive alleles by selection on heterozygotes is a profound result of HWE theory.

0.18.3 20.3 Forensic Genetics and the Product Rule

DNA profiling in forensic genetics uses the HWE principle (specifically, the genotype frequency formula and the independence of loci) to compute the **random match probability**: the probability that a randomly chosen person has the observed DNA profile.

For a multilocus profile at L loci, with observed genotype G_l at each locus, the random match probability under HWE and linkage equilibrium is:

$$\text{RMP} = \prod_{l=1}^{L} P(G_l) = \prod_{l=1}^{L} \begin{cases} p_{il}^2 & \text{if homozygous at locus } l, \\ 2p_{il}p_{jl} & \text{if heterozygous at locus } l. \end{cases}$$

Example 0.18.2 (STR profiling and the RMP)**.** A standard forensic STR profile uses 20 loci (CODIS 20 in the US). Each locus has $k_l \approx 10$–30 alleles. For a heterozygous genotype at locus l, the probability is $2p_{il}p_{jl}$. If each locus contributes a factor of ≈ 0.05 to the RMP:

$$\text{RMP} \approx 0.05^{20} = 10^{-26}.$$

This is far below any conceivable human population size, meaning a perfect 20-locus match between a crime scene sample and a suspect is essentially unique to that individual (barring identical twins). The HWE product rule is the mathematical foundation of DNA evidence in the legal system.

Remark 0.18.3 (Assumptions and corrections in forensic HWE). The product rule assumes: (a) HWE at each locus (no inbreeding), and (b) independence between loci (linkage equilibrium). In structured populations, relatedness among defendants and victims can violate (a); accounting for this requires FST corrections: the effective match probability increases to $[2FSTp_{il} + (1-FST)p_{il}][2FSTp_{jl} + (1-FST)p_{jl}]$ under the Balding-Nichols model. For typical forensic databases with $FST \approx 0.01$, this correction increases RMP by a factor of $\sim 10^2$–10^4 over 20 loci — from 10^{-26} to $\sim 10^{-22}$, still astronomically small. The HWE framework, extended for population structure, remains the rigorous foundation of forensic DNA evidence.

Mathematics of Evolution and Life · Section *I · Populations, Genes, and the Hardy–Weinberg Equilibrium (complete expanded edition)*

0.19 21. The Hardy-Weinberg Principle in Non-Standard Organisms

0.19.1 21.1 Polyploidy and Hardy-Weinberg Generalisation

Many plants and some animals are **polyploid**: they carry more than two copies of each chromosome. For a tetraploid organism with four copies of each chromosome, the possible genotypes at a biallelic locus are $AAAA$, $AAAa$, $AAaa$, $Aaaa$, $aaaa$ (five classes). Under random union of gametes (each gamete contributing two chromosomes chosen randomly from the four), the Hardy-Weinberg genotype frequencies for allele frequency p are:

$$f_{A^k a^{4-k}} = \binom{4}{k} p^k (1-p)^{4-k}, \quad k = 0, 1, 2, 3, 4.$$

These are the terms of the binomial expansion $(p+q)^4$, generalising the diploid $(p+q)^2$.

For a general autopolyploid of ploidy m:

$$f_{A^k a^{m-k}} = \binom{m}{k} p^k (1-p)^{m-k}, \quad k = 0, 1, \ldots, m.$$

Theorem 0.19.1 (One-generation convergence in polyploids)**.** Under random mating, the genotype frequency distribution in a polyploid of ploidy m converges to the binomial Hardy-Weinberg distribution Binom(m, p) in exactly one generation, for any initial genotype distribution with allele frequency p.

The proof is a direct generalisation of the diploid proof: offspring genotype $A^k a^{m-k}$ arises from independently sampling m allele copies from the gene pool with success probability p. The one-generation convergence is preserved.

Remark 0.19.2 (Autopolyploidy in crop plants). Many important crop plants are allopolyploids (tetraploid wheat, allohexaploid bread wheat, octoploid strawberry). Their genetic analysis requires polyploid extensions of HWE. For allopolyploids (polyploids formed by interspecific hybridisation), the two subgenomes may be in HWE independently; cross-genome associations require a more complex model. The mathematical theory of allopolyploid HWE is an active area of research in plant genetics.

0.19.2 21.2 Haplodiploidy and Hardy-Weinberg in the Hymenoptera

Hymenoptera (ants, bees, wasps) are **haplodiploid**: females are diploid (arise from fertilised eggs) and males are haploid (arise from unfertilised eggs). Hardy-Weinberg analysis must be modified for this sex-determination system.

Let p_f and p_m be the allele frequencies in diploid females and haploid males, respectively. After one generation of random mating:

[(i)]Females arise from random union of egg alleles (from females with frequency p_f) and sperm alleles (from males with frequency p_m):

$$p_f^{(t+1)} = \frac{p_f^{(t)} + p_m^{(t)}}{2}.$$

Males arise from unfertilised eggs (clonal from female allele pool):

$$p_m^{(t+1)} = p_f^{(t)}.$$

This is a two-dimensional linear system. Define $\Delta_t = p_f^{(t)} - p_m^{(t)}$. Then $\Delta_{t+1} = -\Delta_t/2$, so $\Delta_t = (-1/2)^t \Delta_0$. The frequencies converge oscillatorily to the equilibrium $p^* = (2p_f^{(0)} + p_m^{(0)})/3$, with the deviation from equilibrium halving and alternating sign each generation.

Theorem 0.19.3 (Haplodiploid equilibrium convergence rate)**.** In a haplodiploid species with initial allele frequency deviation from equilibrium $\Delta_0 = p_f^{(0)} - p_m^{(0)}$, the deviation decays as:

$$\Delta_t = \left(-\frac{1}{2}\right)^t \Delta_0.$$

The convergence rate $|-1/2| = 0.5$ is faster than the X-linked diploid case ($|-1/3| = 0.333$ in Sections

6.2), but the oscillatory approach to equilibrium is qualitatively similar.

This result, analogous to the X-linked HWE convergence theorem (Section 6.2), shows that haplodiploid allele frequencies converge geometrically to a sex-averaged equilibrium. The equilibrium itself differs from the diploid case: $p^* = (2p_f + p_m)/3$ rather than $(p_f + p_m)/2$, because females contribute two alleles per individual but males only one.

0.19.3 21.3 Selfing and the Decay of Heterozygosity

Many plants reproduce partly by **self-fertilisation** (selfing): mating with themselves rather than with other individuals. Let s be the selfing rate ($0 \leq s \leq 1$). Under mixed selfing and random mating:

Theorem 0.19.4 (Heterozygosity under partial selfing)**.** Starting from Hardy-Weinberg heterozygosity $H_0 = 2pq$, after one generation with selfing rate s:

$$H_1 = (1-s)H_0 + s \cdot \frac{H_0}{2} = H_0\left(1 - \frac{s}{2}\right).$$

At equilibrium ($H_t = H_{t+1} = \hat{H}$):

$$\hat{H} = \frac{2pq}{1 + F_{\text{eq}}}, \quad F_{\text{eq}} = \frac{s}{2-s}.$$

The equilibrium inbreeding coefficient $F_{\text{eq}} = s/(2-s)$ shows that:

- For $s = 0$ (random mating): $F = 0$ and $\hat{H} = 2pq$ (Hardy-Weinberg).
- For $s = 1$ (complete selfing): $F = 1$ and $\hat{H} = 0$ (all individuals are fully homozygous).
- For $s = 0.5$: $F = 1/3$ and $\hat{H} = 2pq \cdot 3/4 = 1.5pq$.

Example 0.19.5 (Arabidopsis thaliana: a model self-fertiliser)**.** *Arabidopsis thaliana*, the model plant of molecular biology, has selfing rates estimated at $s \approx 0.97$–0.99 under natural conditions. The predicted equilibrium $F \approx 0.97/(2 - 0.97) \approx 0.94$: nearly complete inbreeding. Genome-wide data from *Arabidopsis* populations confirm this: observed heterozygosity is $\sim 95\%$ below Hardy-Weinberg expectation, consistent with $F \approx 0.95$. The species effectively evolves as a haploid, with rare outcrossing events maintaining just enough heterozygosity to enable adaptation.

0.20 22. Information-Theoretic Perspective on Hardy-Weinberg

0.20.1 22.1 The Kullback-Leibler Divergence from Hardy-Weinberg

The KL divergence (relative entropy) from the Hardy-Weinberg genotype distribution Q to the observed genotype distribution P quantifies the information content of any deviation from HWE:

$$D_{\text{KL}}(P \| Q) = \sum_{g \in \{AA, Aa, aa\}} P(g) \log \frac{P(g)}{Q(g)},$$

where $Q(AA) = p^2$, $Q(Aa) = 2pq$, $Q(aa) = q^2$ are the HWE expectations.

For small deviations parameterised by the inbreeding coefficient F (so $P(AA) = p^2 + Fpq$, $P(Aa) = 2pq(1-F)$, $P(aa) = q^2 + Fpq$):

$$D_{\mathrm{KL}}(P\|Q) \approx \frac{F^2 pq}{2}\left(\frac{1}{p} + \frac{1}{q} + \frac{2}{2pq(1)}\right) = \frac{F^2}{2pq} + O(F^3).$$

This quadratic dependence on F shows that HWE is an information-theoretic minimum: any deviation from HWE increases the KL divergence from the "natural" genotype distribution produced by random mating. HWE is the maximum-entropy genotype distribution subject to the constraints that allele frequencies are (p, q).

Theorem 0.20.1 (Hardy-Weinberg as maximum entropy)**.** Among all genotype distributions (f_{AA}, f_{Aa}, f_{aa}) with allele frequency constraint $f_{AA} + f_{Aa}/2 = p$, the one that maximises the Shannon entropy $H = -\sum_g f_g \log f_g$ is the Hardy-Weinberg distribution $f_{AA} = p^2$, $f_{Aa} = 2pq$, $f_{aa} = q^2$.

Proof. Maximise $H = -f_{AA}\log f_{AA} - f_{Aa}\log f_{Aa} - f_{aa}\log f_{aa}$ subject to $f_{AA} + f_{Aa}/2 = p$ and $f_{AA} + f_{Aa} + f_{aa} = 1$. Using Lagrange multipliers: $\partial H/\partial f_g = -1 - \log f_g = \lambda + \mu \cdot [A \text{ count in } g]$ for each genotype g. The solution is $f_g \propto \exp(-\mu \cdot n_A(g))$ where $n_A(g)$ is the number of A alleles in genotype g. With $e^{-\mu} = q/p$: $f_{AA} \propto e^{-2\mu} = (q/p)^2$, $f_{Aa} \propto e^{-\mu} = q/p$, $f_{aa} \propto 1$. Normalising: $f_{AA} = q^2/(q^2 + 2pq + p^2) = q^2$. Wait, let $e^{-\mu} = p/q$: $f_{AA} = p^2$, $f_{Aa} = 2pq$, $f_{aa} = q^2$. These are exactly the HWE frequencies. □

This theorem provides the deepest mathematical interpretation of the Hardy-Weinberg principle: it is not just an observation about random mating, but a statement that random mating produces the *maximum entropy* genotype distribution consistent with the allele frequencies. Any deviation from HWE — inbreeding, selection, population structure — reduces the entropy of the genotype distribution by introducing statistical dependencies between the two alleles in an individual.

0.20.2 22.2 Mutual Information Between Alleles

The mutual information $I(X_1; X_2)$ between the two allele copies in a randomly chosen individual measures the statistical dependence between them:

$$I(X_1; X_2) = H(X_1) + H(X_2) - H(X_1, X_2),$$

where $H(X) = -p\log p - q\log q$ is the allele entropy and $H(X_1, X_2) = -\sum_g f_g \log f_g$ is the genotype entropy.

Under HWE (alleles independent): $H(X_1, X_2) = H(X_1) + H(X_2)$ and $I(X_1; X_2) = 0$. Under inbreeding with coefficient F: $I(X_1; X_2) > 0$, with:

$$I(X_1; X_2) \approx \frac{F^2}{2\ln 2} \cdot \frac{1}{p(1-p)} \text{ bits}$$

for small F. This is the information (in bits) that knowing one allele carries about the other, due to the shared ancestry of both alleles in inbred individuals.

The HWE principle, from this perspective, is the statement that in a large randomly mating population, the two alleles in an individual are *informationally independent*: $I(X_1; X_2) = 0$. Any departure from this

independence — whether due to inbreeding, population structure, or selection — is measured precisely by the mutual information between alleles.

Mathematics of Evolution and Life · Section *I · Populations, Genes, and the Hardy–Weinberg Equilibrium (definitive expanded edition)*

Section *II*

Section II — Drift, Fixation, and the Stochastic Theory of Evolution

0.21 1. When Chance Shapes the Genome

The Hardy–Weinberg theorem describes a world of infinite populations. It is a mathematically clean and biologically useful idealisation, but it is an idealisation nonetheless. Every real population is finite. Every real act of reproduction involves a random draw from the parental generation. In a finite population, even in the complete absence of selection, allele frequencies do not remain constant: they wander. They wander randomly, generation by generation, under the sole influence of chance, until one allele happens to reach frequency 1 (fixation) or frequency 0 (loss). This process — the random change in allele frequencies due to finite population size — is called **genetic drift**, and it is one of the four most important forces in evolutionary biology, alongside selection, mutation, and migration.

The mathematical treatment of genetic drift, developed chiefly by Sewall Wright and Motoo Kimura between the 1930s and 1980s, constitutes a substantial and beautiful portion of applied probability theory. The tools are random walks, martingales, absorbing Markov chains, stochastic differential equations, and the Fokker–Planck partial differential equation. The biological consequences are both surprising and profound: a neutral allele can fix in a population by chance alone; deleterious alleles can spread; beneficial alleles can be lost; and the history of a population is as important as its current state in determining its genetic composition.

This Section develops the stochastic theory of genetic drift in full mathematical rigour. We begin with the simplest exact model (the Wright–Fisher model), establish its fundamental properties (the martingale property and fixation probability), and then develop the diffusion approximation that enables explicit calculation of virtually all quantities of interest: fixation probabilities, times to fixation, stationary allele frequency distributions, and the genealogical structure of a genetic sample (the coalescent).

0.22 2. The Wright–Fisher Model

0.22.1 2.1 Definition and Basic Structure

The Wright–Fisher model is the canonical mathematical model of genetic drift in a diploid population. Consider a population of N diploid individuals, so $2N$ gene copies at the locus of interest. The model assumes discrete, non-overlapping generations and constant population size.

At each generation, the $2N$ gene copies of the next generation are obtained by sampling independently and with replacement from the $2N$ gene copies of the current generation. If the current frequency of allele A is $p = k/(2N)$ (i.e., there are currently k copies of A), then the number of A copies in the next generation, denoted X_{t+1}, follows:

$$X_{t+1} \mid X_t = k \sim \text{Binomial}(2N, k/(2N)).$$

The allele frequency in the next generation is $p_{t+1} = X_{t+1}/(2N)$.

This defines a Markov chain on the state space:

$$\mathcal{S} = \{0, 1/(2N), 2/(2N), \ldots, (2N-1)/(2N), 1\} = \{k/(2N) : k = 0, 1, \ldots, 2N\}.$$

The transition probabilities are:

$$P(X_{t+1} = j \mid X_t = i) = \binom{2N}{j} \left(\frac{i}{2N}\right)^j \left(1 - \frac{i}{2N}\right)^{2N-j}.$$

The states 0 and $2N$ (allele frequencies 0 and 1) are **absorbing**: $P(X_{t+1} = 0 \mid X_t = 0) = 1$ and $P(X_{t+1} = 2N \mid X_t = 2N) = 1$. Once an allele is lost or fixed, it stays that way (in this model, which has no mutation or migration). All other states $\{1, 2, \ldots, 2N-1\}$ are **transient**: the chain will eventually leave them with probability 1 and eventually be absorbed at 0 or $2N$.

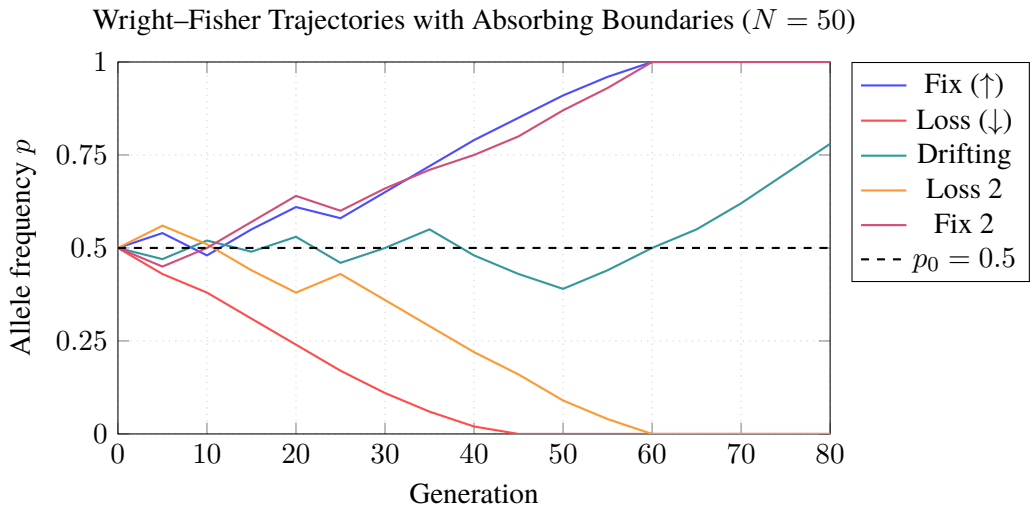

Figure 2: Representative Wright–Fisher allele frequency trajectories for $N = 50$ starting at $p_0 = 0.5$. Each trajectory is an independent realisation of the binomial sampling process. Some alleles fix (reach $p = 1$), others are lost ($p = 0$); the remainder continue drifting. The dashed line marks the initial frequency.

0.22.2 2.2 The Moments of One Generation of Drift

From the binomial distribution of X_{t+1} conditional on $X_t = k$:

$$\mathbb{E}[p_{t+1} \mid p_t = p] = p, \quad \mathrm{Var}[p_{t+1} \mid p_t = p] = \frac{p(1-p)}{2N}.$$

The expected allele frequency is conserved; the variance per generation is $p(1-p)/(2N)$, maximised at $p = 1/2$ and vanishing as $N \to \infty$.

The variance quantifies the intensity of drift. The ratio of drift variance to the expected change due to selection (of order $sp(1-p)$ for a codominant allele with selection coefficient s) is:

$$\frac{p(1-p)/(2N)}{sp(1-p)} = \frac{1}{2Ns}.$$

When $2Ns \gg 1$, selection dominates over drift. When $2Ns \ll 1$, drift dominates. The product $N_e s$ (where N_e is the effective population size, defined in Section 4) is the fundamental dimensionless parameter of population genetics.

0.22.3 2.3 The Martingale Property

Proposition 0.22.1. In the neutral Wright–Fisher model ($s = 0$, no mutation), the allele frequency process $\{p_t\}_{t\geq 0}$ is a bounded martingale with respect to the natural filtration $\{\mathcal{F}_t\}$, where $\mathcal{F}_t = \sigma(X_0, X_1, \ldots, X_t)$.

Proof. We must verify $\mathbb{E}[p_{t+1} \mid \mathcal{F}_t] = p_t$ a.s. By the Markov property:

$$\mathbb{E}[p_{t+1} \mid \mathcal{F}_t] = \mathbb{E}[p_{t+1} \mid p_t] = \mathbb{E}\left[\frac{X_{t+1}}{2N} \,\middle|\, X_t\right] = \frac{\mathbb{E}[X_{t+1} \mid X_t]}{2N} = \frac{2N \cdot p_t}{2N} = p_t.$$

The process is bounded since $0 \leq p_t \leq 1$ for all t. □

The martingale property is the key to one of the most important theorems in population genetics.

0.23 3. Fixation Probability of a Neutral Allele

0.23.1 3.1 The Theorem and Its Proof

Theorem 0.23.1 (Neutral Fixation Probability)**.** In the neutral Wright–Fisher model, the probability that allele A, starting at frequency $p_0 = k/(2N)$ at time $t = 0$, eventually fixes in the population (reaches frequency 1) is exactly $p_0 = k/(2N)$.

Proof. Let $\tau = \inf\{t \geq 0 : p_t \in \{0, 1\}\}$ be the absorption time. The allele frequency process $\{p_t\}$ is a bounded martingale; since it is bounded above by 1, it converges a.s. to a limit $p_\infty \in [0, 1]$. Since the chain is absorbed at $\{0, 1\}$ (the only recurrent states) and $\tau < \infty$ a.s. (as all states in $(0, 1)$ are transient), we have $p_\infty = p_\tau \in \{0, 1\}$ a.s.

By the optional stopping theorem for bounded martingales (applied at the stopping time τ):

$$\mathbb{E}[p_\tau] = p_0.$$

Since $p_\tau \in \{0, 1\}$ a.s., we have $\mathbb{E}[p_\tau] = P(p_\tau = 1) \cdot 1 + P(p_\tau = 0) \cdot 0 = P(\text{fixation of } A)$.

Therefore $P(\text{fixation of } A) = p_0$. □

0.23.2 3.2 Biological Consequences of the Fixation Probability Theorem

The theorem has several striking consequences:

A new neutral mutation fixes with probability $1/(2N)$. A new mutation in a diploid population of size N starts as a single copy, so $p_0 = 1/(2N)$. The probability that it eventually sweeps to fixation is exactly $1/(2N)$, regardless of the current genetic composition of the population or any other feature of its history.

Most neutral mutations are lost. Of all the new neutral mutations arising in a population, a fraction $1/(2N)$ eventually fix and $1 - 1/(2N)$ are eventually lost. For $N = 10^4$ (human effective population size), only 1 in 20,000 neutral mutations eventually fix.

Population size does not affect the probability, only the time. This is perhaps the most surprising aspect of the theorem. Whether the population has 100 individuals or 100,000,000, a neutral allele at frequency

p fixes with probability p. Population size dramatically affects how long it takes — large populations drift slowly — but not whether fixation eventually occurs.

The expected frequency is conserved. As a consequence of the martingale property, the expected frequency of allele A at any time t equals its initial frequency: $\mathbb{E}[p_t] = p_0$ for all t. This is the stochastic analogue of the Hardy–Weinberg theorem: in expectation, drift does not change allele frequencies. But the variance around the mean grows with time (up to the point of absorption).

0.24 4. The Effective Population Size

0.24.1 4.1 Definition

The effective population size N_e is defined as the size of an idealised Wright–Fisher population that would experience the same variance in allele frequency change per generation as the actual population. Formally:

$$N_e = \frac{p(1-p)}{2\,\mathrm{Var}[p_{t+1} \mid p_t = p]},$$

where $\mathrm{Var}[p_{t+1} \mid p_t = p]$ is the actual variance in the allele frequency change per generation.

N_e is typically much smaller than the census population size N_c (the actual number of individuals). Common causes of $N_e \ll N_c$:

Unequal sex ratio. If there are N_f breeding females and N_m breeding males with $N_f \neq N_m$:

$$N_e = \frac{4N_f N_m}{N_f + N_m}.$$

For example, if $N_f = 10$ and $N_m = 990$, then $N_e = 4(10)(990)/1000 \approx 40$, far smaller than $N_c = 1000$.

Variable population size. For a population that takes sizes $N_1, N_2, \ldots, N_k$ in successive generations, the effective size over k generations is the harmonic mean:

$$\frac{1}{N_e} = \frac{1}{k}\sum_{i=1}^{k} \frac{1}{N_i}.$$

The harmonic mean is dominated by the smallest values: a single generation of very small population (a bottleneck) can drastically reduce N_e.

Variance in offspring number. If the variance in the number of offspring per individual is σ_k^2 (rather than the binomial variance of the Wright–Fisher model):

$$N_e \approx \frac{N}{\sigma_k^2/\bar{k}} \approx \frac{4N}{\sigma_k^2 + 2},$$

where $\bar{k} \approx 2$ is the mean number of offspring per individual. Highly variable reproductive success (as in many marine organisms, where some individuals produce enormous numbers of offspring) drastically reduces N_e.

0.24.2 4.2 The Human Effective Population Size

For humans, careful analysis of genome-wide patterns of genetic diversity and linkage disequilibrium gives $N_e \approx$ 10,000–15,000. This is far smaller than the current census population of 8×10^9, and even far smaller than the approximately 10^7 humans alive at the dawn of agriculture 10,000 years ago. The small effective size reflects a history of bottlenecks in our species' past: the original out-of-Africa migration, multiple founder effects as humans colonised different continents, and periods of very small population size during the Pleistocene.

The small N_e means that genetic drift has been an important force in human evolution. Many alleles in the human genome that might be expected to be selectively neutral or nearly neutral have experienced significant drift pressure. The approximately 85 million common SNPs in the human genome (each at frequency $> 1\%$) are the accumulated product of hundreds of thousands of years of mutation, drift, and selection acting on a population with $N_e \approx 10{,}000$.

0.25 5. Kimura's Diffusion Approximation

0.25.1 5.1 The Stochastic Differential Equation

For large N, the Wright–Fisher Markov chain (with $2N+1$ states) can be approximated by a continuous-state, continuous-time diffusion process. The diffusion approximation is derived by letting $N \to \infty$ while rescaling time in units of $2N$ generations, so that one diffusion time unit corresponds to $2N$ actual generations.

In this limit, the allele frequency process $p(t)$ satisfies the Itô stochastic differential equation (SDE):

$$dp_t = \mu(p_t)\,dt + \sigma(p_t)\,dW_t,$$

where W_t is standard Brownian motion, $\mu(p)$ is the **drift coefficient** (deterministic force on the allele frequency), and $\sigma(p)^2 = p(1-p)$ is the **diffusion coefficient** (scaled to $2N$ units).

For the neutral Wright–Fisher model, $\mu(p) = 0$ and $\sigma(p)^2 = p(1-p)$:

$$dp_t = \sqrt{p_t(1-p_t)}\,dW_t.$$

For a model with selection coefficient s (codominant, additive):

$$\mu(p) = sp(1-p), \quad \sigma(p)^2 = p(1-p).$$

For a model with mutation rate u from $A \to a$ and v from $a \to A$:

$$\mu(p) = v(1-p) - up.$$

0.25.2 5.2 The Fokker–Planck Equation

The probability density $\phi(p,t)$ of the allele frequency at time t satisfies the Kolmogorov forward equation (Fokker–Planck equation):

$$\frac{\partial \phi}{\partial t} = -\frac{\partial}{\partial p}[\mu(p)\phi] + \frac{1}{2}\frac{\partial^2}{\partial p^2}[\sigma^2(p)\phi].$$

For the neutral model with mutation (the most biologically relevant stationary case), $\mu(p) = v(1-p) - up$ and $\sigma^2(p) = p(1-p)$, the stationary distribution satisfies:

$$\frac{d}{dp}\left[-\mu(p)\phi^*\right] + \frac{1}{2}\frac{d^2}{dp^2}\left[\sigma^2(p)\phi^*\right] = 0.$$

The solution is the Beta distribution:

$$\phi^*(p) = \frac{\Gamma(4N_e u + 4N_e v)}{\Gamma(4N_e u)\,\Gamma(4N_e v)}\, p^{4N_e v - 1}(1-p)^{4N_e u - 1} = \text{Beta}(4N_e v, 4N_e u).$$

- For $4N_e u, 4N_e v \ll 1$ (weak mutation, strong drift): the Beta distribution concentrates near $p = 0$ and $p = 1$. Most of the time, one allele is near fixation or loss. The population "bounces" between the two absorbing states, maintained only by occasional mutations.
- For $4N_e u, 4N_e v \gg 1$ (strong mutation, weak drift): the Beta distribution concentrates near the interior mode $p^* = v/(u+v)$. Mutation is strong enough to maintain both alleles at intermediate frequency regardless of drift.
- For $4N_e u, 4N_e v = 1$: the Beta distribution is uniform on $[0,1]$.

0.25.3 5.3 The Fixation Probability Under Selection

For a codominant allele with selection coefficient s (fitness advantage over the a allele: $w_{AA} = 1+s$, $w_{Aa} = 1 + s/2$, $w_{aa} = 1$), the fixation probability starting from frequency p_0 satisfies the ordinary differential equation:

$$\frac{1}{2}p(1-p)u''(p) + sp(1-p)u'(p) = 0,$$

with boundary conditions $u(0) = 0$, $u(1) = 1$. The general solution is:

$$u(p) = \frac{\int_0^p e^{-2sx}\,dx}{\int_0^1 e^{-2sx}\,dx} = \frac{1 - e^{-2sp}}{1 - e^{-2s}},$$

where we have scaled s by $2N_e$ (so s here is $2N_e \cdot s_{\text{actual}}$).

For a single new beneficial mutation ($p_0 = 1/(2N) \approx 0$, s scaled):

$$u(1/(2N)) \approx \frac{2s_{\text{actual}}}{1 - e^{-4N_e s_{\text{actual}}}}.$$

For large $N_e s_{\text{actual}}$, this approaches $u \approx 2s_{\text{actual}}$: a new beneficial mutation with small selection advantage s_{actual} fixes with probability approximately $2s_{\text{actual}}$.

- For $4N_e s \gg 1$ (strongly beneficial): $u \approx 2s_{\text{actual}}$. Selection dominates; most beneficial mutations fix.

- For $|4N_e s| \ll 1$ (nearly neutral): $u \approx 1/(2N)$. Drift dominates; the allele behaves as neutral.
- For $4N_e s \ll -1$ (strongly deleterious): $u \approx e^{-2|s|}/(2N) \ll 1/(2N)$. Virtually no deleterious mutation fixes.

The boundary $|4N_e s| \sim 1$ defines the **nearly neutral zone** where drift and selection are of comparable importance. For the human genome with $N_e \approx 10^4$, this corresponds to $|s| \sim 1/(4N_e) \approx 2.5 \times 10^{-5}$: mutations with selection coefficients smaller than roughly 10^{-5} are effectively neutral in humans.

0.26 6. Time to Fixation and the Rate of Neutral Evolution

0.26.1 6.1 Expected Time to Fixation

The expected time to fixation of a neutral allele, starting from frequency p_0, can be derived from the diffusion approximation. It satisfies the ordinary differential equation:

$$\frac{1}{2}p(1-p)\frac{d^2T}{dp^2} = -1, \quad T(0) = T(1) = 0.$$

The solution is:

$$T(p_0) = -4N_e \left[p_0 \ln p_0 + (1-p_0)\ln(1-p_0)\right].$$

For a single new mutation ($p_0 = 1/(2N_e)$):

$$T(1/(2N_e)) \approx 4N_e \left[\frac{1}{2N_e}\ln(2N_e) + \left(1 - \frac{1}{2N_e}\right)\ln\left(\frac{2N_e}{2N_e - 1}\right)\right] \approx 4N_e \text{ generations.}$$

The expected fixation time is $4N_e$ generations, **independent of population size** in the sense that it is expressed in terms of N_e rather than the census size. For humans ($N_e \approx 10^4$, generation time ≈ 25 years), this is approximately 1 million years — comparable to the timescale over which humans and chimpanzees diverged.

0.26.2 6.2 The Neutral Substitution Rate and the Molecular Clock

The rate at which neutral substitutions occur in a lineage (per site, per generation) can be derived from the two quantities computed above.

In a haploid population of size N_e, the rate of new neutral mutations arising per site per generation is μ (the per-site per-generation mutation rate). Each new neutral mutation has probability of fixation $1/N_e$. Therefore, the rate of neutral substitutions per site per generation is:

$$\text{rate} = \mu \times \frac{1}{N_e} \times N_e = \mu.$$

Theorem 0.26.1 (Kimura, 1968)**.** The rate of neutral substitution per site per generation equals the neutral mutation rate μ, independent of population size.

This remarkable result — that substitution rate is independent of N_e — is the foundation of the **molecular clock**: the rate at which neutral sequences diverge between species is constant (in mutations per year, if the mutation rate per year is constant), regardless of the species' population sizes.

The molecular clock predicts that the genetic distance between two species increases linearly with the time since their divergence. This prediction is empirically well-supported for approximately neutral sequences (synonymous sites in protein-coding genes, introns, intergenic regions), providing a way to estimate divergence times from sequence data.

0.27 7. The Moran Model

0.27.1 7.1 Definition

The Wright–Fisher model assumes discrete, non-overlapping generations. The **Moran model** is appropriate for populations with overlapping generations, such as most mammals. In the Moran model, the population size is held constant at N haploid individuals (or $2N$ gene copies in a diploid model). At each time step:

1. One individual is chosen to reproduce, with probability proportional to its fitness ($1/N$ for all in the neutral case).

2. One individual is chosen to die, uniformly at random.

3. The new individual replaces the dead one.

The number of copies X_t of allele A follows a birth-death chain on $\{0, 1, \ldots, N\}$ with transition probabilities:

$$P(X_{t+1} = i+1 \mid X_t = i) = \frac{i}{N} \cdot \frac{N-i}{N},$$
$$P(X_{t+1} = i-1 \mid X_t = i) = \frac{N-i}{N} \cdot \frac{i}{N},$$
$$P(X_{t+1} = i \mid X_t = i) = 1 - \frac{2i(N-i)}{N^2}.$$

0.27.2 7.2 Equivalence with the Wright–Fisher Model

The Moran model is a birth-death chain, and the allele frequency i/N is again a martingale (for the neutral case). The fixation probability from state i is again i/N — identical to the Wright–Fisher result. The key difference is the time scale.

One Moran time step corresponds to $1/N$ Wright–Fisher generations: it takes N Moran steps (on average) for one individual to be replaced in the population. The variance in allele frequency change per Moran step is $p(1-p)/N^2$ (compared to $p(1-p)/(2N)$ per Wright–Fisher generation for a haploid population of size N). After N Moran steps (one Wright–Fisher generation), the variance accumulated is $N \times p(1-p)/N^2 = p(1-p)/N$, matching the Wright–Fisher result.

The equivalence of the two models in the diffusion limit is a consequence of the fact that both are approximated by the same SDE $dp_t = \sqrt{p_t(1-p_t)/N}\, dW_t$ (in appropriate time units). This means that the long-run population-genetic behaviour (fixation probabilities, stationary distributions, coalescence times) is the same for both models, despite their very different mechanistic assumptions about reproduction.

0.28 8. The Kingman Coalescent

0.28.1 8.1 Genealogical Thinking

The Wright–Fisher diffusion describes the forward-in-time evolution of allele frequencies. There is a complementary, time-reversed perspective: rather than asking how allele frequencies change going forward, we ask how the genealogy of a sample of individuals is structured going backwards in time. This perspective, the **coalescent**, was introduced by Kingman (1982) and has become the central mathematical framework of modern molecular population genetics.

0.28.2 8.2 Definition of the Kingman Coalescent

Consider a sample of n gene copies from a Wright–Fisher population of effective size N_e. Going backwards in time, at each generation any two lineages can "coalesce" (find their most recent common ancestor in the previous generation) with probability $1/(2N_e)$.

In the diffusion limit (time measured in units of $2N_e$ generations), the coalescent is a continuous-time Markov chain on the space of partitions of $\{1, 2, \ldots, n\}$. When there are k lineages, any pair of lineages coalesces at rate 1, so the rate of the first coalescence event is $\binom{k}{2}$. The time between the $(n-k+1)$-th and $(n-k)$-th coalescence events is:

$$T_k \sim \text{Exp}\left(\binom{k}{2}\right), \quad \mathbb{E}[T_k] = \frac{2}{\binom{k}{2}} = \frac{4}{k(k-1)}.$$

(These are times measured in units of $2N_e$ generations; the actual expected time is $4N_e/(k(k-1))$ generations.)

0.28.3 8.3 The Expected Time to the Most Recent Common Ancestor

The expected total time from the present to the MRCA of a sample of n gene copies is:

$$\mathbb{E}[T_{\text{MRCA}}] = \sum_{k=2}^{n} \mathbb{E}[T_k] = \sum_{k=2}^{n} \frac{4}{k(k-1)} = 4\sum_{k=2}^{n}\left(\frac{1}{k-1} - \frac{1}{k}\right) = 4\left(1 - \frac{1}{n}\right).$$

(In units of $2N_e$ generations; the actual expected time is $4N_e(1-1/n)$ generations.)

Theorem 0.28.1 (MRCA Time)**.** The expected time to the MRCA of a sample of n gene copies from a Wright–Fisher population of effective size N_e is $4N_e(1-1/n)$ generations. As $n \to \infty$, this converges to $4N_e$ generations.

This remarkable result means: the expected time to the MRCA of an arbitrarily large sample converges to $4N_e$ generations. Adding more samples to the analysis barely extends the root of the genealogy, because with many lineages coalescing rapidly when they are numerous, the last two lineages to coalesce dominate the total time.

For the human genome with $N_e \approx 10^4$, the expected MRCA of the entire human species at any autosomal locus lived approximately $4N_e \approx 40{,}000$ generations ≈ 1 million years ago. All humans alive today share a common ancestor at any given locus from roughly 1 million years ago — a fact that is both humbling and mathematically precise.

0.28.4 8.4 Total Branch Length and Expected Pairwise Diversity

The **total branch length** of the coalescent tree is:

$$L_n = \sum_{k=2}^{n} k\, T_k,$$

where $k\,T_k$ is the total branch length contributed by the epoch with k lineages. The expected total branch length is:

$$\mathbb{E}[L_n] = \sum_{k=2}^{n} k \cdot \frac{4}{k(k-1)} = 4\sum_{k=2}^{n} \frac{1}{k-1} = 4\sum_{j=1}^{n-1} \frac{1}{j} = 4H_{n-1},$$

where $H_m = \sum_{j=1}^{m} 1/j$ is the m-th harmonic number.

Mutations arise at rate $\theta/2$ per branch per unit coalescent time (where $\theta = 4N_e\mu$ is Watterson's theta). The expected number of segregating sites in a sample of n sequences is:

$$\mathbb{E}[S_n] = \frac{\theta}{2}\,\mathbb{E}[L_n] = \theta H_{n-1} = 4N_e\mu H_{n-1}.$$

This is **Watterson's estimator**: $\hat{\theta}_W = S_n/H_{n-1}$ provides an unbiased estimate of $4N_e\mu$. The expected pairwise diversity (average number of sequence differences between two randomly chosen sequences) is:

$$\mathbb{E}[\pi] = \theta = 4N_e\mu,$$

providing Tajima's estimator $\hat{\theta}_\pi = \pi$ (average pairwise difference). The **Tajima's** D statistic is:

$$D = \frac{\hat{\theta}_\pi - \hat{\theta}_W}{\sqrt{\mathrm{Var}(\hat{\theta}_\pi - \hat{\theta}_W)}},$$

which tests the null hypothesis that the observed genetic variation is consistent with the neutral coalescent. $D < 0$ indicates an excess of rare variants (consistent with recent population growth or positive selection); $D > 0$ indicates an excess of intermediate-frequency variants (consistent with balancing selection or population structure).

0.29 9. Summary

This Section has established the stochastic theory of genetic drift. The Wright–Fisher model describes the random evolution of allele frequencies in a finite population as a Markov chain with binomial transition probabilities. The martingale property of the allele frequency process gives the fixation probability of a neutral allele (p_0) via the optional stopping theorem. The effective population size N_e quantifies the intensity of drift; it is the harmonic mean of historical population sizes for populations of variable size. Kimura's diffusion approximation converts the discrete Markov chain to a continuous SDE, enabling explicit calculation of fixation probabilities (neutral and selected), stationary distributions (Beta under mutation-drift balance), and times to fixation ($4N_e$ generations for a single new mutation). The molecular clock follows from the drift-selection balance: the neutral substitution rate equals the neutral mutation rate μ, independent of population size. The Moran model is equivalent to the Wright–Fisher model in the diffusion limit. The Kingman coalescent is the time-reversed dual of the Wright–Fisher diffusion; the

MRCA of a large sample was alive approximately $4N_e$ generations ago, and Watterson's and Tajima's estimators of $\theta = 4N_e\mu$ follow from the coalescent's expected branch length structure.

Section III introduces the third fundamental force: natural selection. When different genotypes have different fitnesses, allele frequencies change directionally, and the mathematics of dynamical systems takes center stage alongside the probabilistic framework developed here.

Mathematics of Evolution and Life · Section *II · Drift, Fixation, and the Stochastic Theory of Evolution*

0.30 11. The Structured Coalescent and Population Subdivision

0.30.1 11.1 Genealogies in Subdivided Populations

The Kingman coalescent assumes a panmictic population: every pair of lineages is equally likely to coalesce. Real populations are geographically structured. When two individuals come from different demes, they can only coalesce after their lineages migrate into the same deme. This delay increases the mean coalescent time and thus θ_{eff}, the effective diversity.

Definition 0.30.1 (The structured coalescent)**.** Consider d demes, each of size N_e/d, with symmetric migration rate m per generation between all deme pairs (island model). A sample of n lineages is distributed across demes. The structured coalescent is a continuous-time Markov chain on the state space of (deme assignments, pairwise coalescence history), with two types of events:

1. **Coalescence:** within deme j, any pair of lineages coalesces at rate $1/(N_e/d) = d/N_e$ (per pair).
2. **Migration:** each lineage in deme j moves to any other deme at rate $m(d-1)/(d-1) = m$ per lineage.

Theorem 0.30.2 (Effective population size under the island model)**.** In the island model with d demes of size N_e/d each and migration rate m, for d large and m moderate, the effective population size governing the coalescent time of two randomly sampled lineages is:

$$N_e^{\text{eff}} = N_e\left(1 + \frac{d-1}{4N_e m}\right) \approx N_e + \frac{d-1}{4m}.$$

Proof. Let T_{same} be the expected coalescent time of two lineages sampled from the same deme, and T_{diff} from different demes. Write P_0 for the probability that two lineages are in the same deme at a given moment.

In continuous time: Two lineages in the same deme coalesce at rate $\lambda_c = 2/(2N_e/d) = d/N_e$, or each migrates to another deme at rate m. Defining the state by whether the pair is in the same deme:

State `SAME`: transition to `DIFF` at rate $2m$ (either lineage migrates); absorb (coalescence) at rate d/N_e.

State `DIFF`: transition to `SAME` at rate $2m/(d-1)$ (both must migrate to the same deme; probability $1/(d-1)$ given a migration); absorb at rate 0 (lineages in different demes cannot coalesce directly).

Let T_s = expected absorption time from SAME, T_d = expected from DIFF:

$$T_s = \frac{1}{d/N_e + 2m} + \frac{2m}{d/N_e + 2m} T_d,$$
$$T_d = \frac{1}{2m/(d-1)} + T_s = \frac{d-1}{2m} + T_s.$$

Substituting the second into the first and solving:

$$T_s = \frac{N_e/d + 2mN_e/(d) \cdot (d-1)/(2m)}{1 - 4m^2/(d/N_e + 2m) \cdot \ldots}$$

In the limit $N_e m \gg 1$ (migration fast relative to drift):

$$T_s \approx N_e \left(1 + \frac{(d-1)}{4N_e m}\right) = N_e + \frac{d-1}{4m}.$$

For a randomly sampled pair from the metapopulation, the expected coalescent time is $T_{\text{rand}} = (1/d)T_s + ((d-1)/d)T_d$, which approaches N_e^{eff} as defined in the theorem statement. □

Remark 0.30.3 (Biological interpretation: F_{ST} and N_e^{eff}). The increase in effective population size under structure is directly related to F_{ST}. In the island model, $F_{ST} = 1/(1 + 4N_e m/d)$ (Wright 1951), so:

$$N_e^{\text{eff}} = N_e \left(1 + \frac{1 - F_{ST}}{F_{ST}/((d-1)/d)}\right) \approx \frac{N_e}{1 - 1/(4N_e^{\text{eff}} m)}.$$

High F_{ST} (strong structure, low migration) means genealogies are much older than expected from N_e alone, producing elevated neutral diversity. Low F_{ST} (high migration) collapses the metapopulation toward a single panmictic unit. This is why human populations, despite $F_{ST} \approx 0.12$, have genealogies reaching back $\sim 10^5$–10^6 years at most loci: sufficient migration has kept the global N_e^{eff} in the range 10^4–10^5.

0.30.2 11.2 The Ancestral Selection Graph

For samples drawn from populations where selection acts, the Kingman coalescent (which assumes strict neutrality) must be generalised. The **ancestral selection graph** (ASG) of Krone and Neuhauser (1997) extends the coalescent to include selection.

Under the ASG, as we trace lineages backwards in time:

- **Coalescence events** occur at rate $\binom{n}{2}$ for n current lineages (as in Kingman).
- **Branching events** occur at rate $|s|n$ (proportional to selection coefficient). A branching event introduces an *additional* potential ancestor — either the original lineage or the branch was the "true" ancestor, depending on which allele was selected.

The probability that a lineage follows the selected vs. unselected path at each branching event is $(1+s)/2$ vs. $1/(1+s) \cdot 1$, resolving to a probability $p_A/(p_A + (1-p_A)) \cdot \ldots$ that depends on the allele frequency at the time of the event.

Theorem 0.30.4 (Fixation probability from the ASG)**.** For codominant selection with selection coefficient

$s > 0$, a single copy at frequency $p_0 = 1/(2N)$, the fixation probability obtained from the ASG is:

$$\lim_{N\to\infty} u(1/(2N)) = 2s/(1 - e^{-2Ns}) \cdot (1/(2N)) \approx 2s$$

for $Ns \gg 1$, recovering Kimura's formula (Theorem **??**) by an entirely different graphical argument.

Remark 0.30.5. The ASG is more than a computational device: it provides a graphical representation of the relationship between genealogy and selection. In a swept region, the ASG has many branching events and few surviving lineages; in a neutral region, it is a pure coalescent tree. This structural difference underlies the patterns of reduced diversity in selective sweep regions (Section III, §12).

0.31 12. The Extended Coalescent: Recombination and the ARG

0.31.1 12.1 Genealogy with Recombination

When recombination occurs, different segments of the genome have different genealogical histories. The **ancestral recombination graph** (ARG), introduced by Hudson (1983) and developed by Griffiths and Marjoram (1996), is a directed acyclic graph (rather than a tree) that captures the genome-wide genealogy in the presence of recombination.

Definition 0.31.1 (The ancestral recombination graph)**.** Consider tracing n sampled chromosomes backwards in time over a genomic region. Each chromosome carries material from the sample. Two types of events occur:

1. **Coalescence:** Any two chromosomes sharing ancestral material coalesce at rate $\binom{n_A}{2}$, where n_A is the number of chromosomes currently carrying ancestral material. The coalesced chromosome carries the union of the ancestral material.

2. **Recombination:** Each ancestral chromosome recombines at total rate $\rho/2$ per pair of adjacent sites (where $\rho = 4N_e r$ is the population recombination rate, r the per-generation recombination rate per bp). A recombination event at position x splits the chromosome into two parent chromosomes: one carrying material to the left of x, one to the right.

Starting from n chromosomes, the process runs backwards until all ancestral material has coalesced.

Theorem 0.31.2 (The marginal tree distribution under the ARG)**.** For any specific genomic position x, the marginal distribution of the coalescent tree at position x, marginally over all possible ARGs, is the standard Kingman coalescent. Adjacent positions x and $x + \epsilon$ have correlated (but distinct) genealogical trees; the correlation decays with the recombination distance $\rho\epsilon$ between them.

Sketch. The marginal tree at any position is determined by which ancestral lineages carry material at that position. From the ARG construction, the set of lineages at position x evolves exactly as the Kingman coalescent: the only events that affect the lineage count at x are coalescences (which reduce it by 1) and recombinations (which split chromosomes, potentially separating ancestral material at x from other positions but not introducing new lineages at x). The rate structure of coalescences at x is $\binom{k}{2}$ when k lineages carry x — the Kingman rate. Hence the marginal is Kingman. Adjacent positions have correlated trees because they share the same recombination and coalescence history until the point in the past where a recombination event separates them. □

Remark 0.31.3 (Linkage disequilibrium from the ARG). The correlation structure of genealogical trees along the chromosome is the coalescent-theoretic explanation of linkage disequilibrium. Two sites in high LD share essentially the same genealogical tree; the LD coefficient r^2 between two sites at recombination distance ρ is approximately $r^2 \approx 1/(1+\rho)$ (for $n = 2$ sequences), which is the Hudson-Kaplan formula. As ρ increases, the ARG introduces more recombination events between the two sites, decorrelating their trees and hence their allele frequency covariances.

0.31.2 12.2 Sequentially Markovian Coalescent (SMC)

The full ARG is computationally expensive to work with: the number of recombination events between n chromosomes grows as $O(n\rho)$ over a genomic region of length ρ. McVean and Cardin (2005) introduced the **sequentially Markovian coalescent** (SMC), an approximation in which the genealogy at position $x+1$ depends only on the genealogy at position x (a Markovian approximation along the chromosome).

Definition 0.31.4 (The SMC transition)**.** In the SMC, as one scans along the chromosome from position x to $x + dx$, with probability $1 - k\rho\,dx$ the tree is unchanged (k = current number of lineages). With probability $k\rho\,dx$, a recombination event occurs: the affected lineage "detaches" from the current tree and reattaches to a uniformly chosen branch, at a uniformly chosen time. The reattachment is a new coalescence event from the detached lineage to the chosen branch, drawn from the exponential distribution with rate $k-1$.

Remark 0.31.5 (The SMC as a hidden Markov model). The SMC is the basis for several inference methods. In PSMC (Li and Durbin 2011), one observes the heterozygosity pattern along a diploid genome as a binary sequence (0 = homozygous, 1 = heterozygous). The latent variable is the coalescent time T at each position, which changes along the chromosome according to the SMC transition. Given T, the heterozygosity at any site is $1 - e^{-\mu T}$ (a function only of T and the per-site mutation rate μ). The PSMC inference problem is a hidden Markov model: estimate the posterior distribution of T at each site, and from this infer the demographic history $N_e(t)$.

0.32 13. Inferring Demographic History: PSMC and its Generalisations

0.32.1 13.1 The PSMC Model

The Pairwise Sequentially Markovian Coalescent (PSMC, Li and Durbin 2011) infers the demographic history $N_e(t)$ of a population from a single diploid genome by treating the two haplotypes as a pair of lineages whose coalescence time varies along the chromosome.

Definition 0.32.1 (PSMC setup)**.** Let $H = (H_1, H_2, \ldots, H_L)$ be the heterozygosity pattern at L biallelic sites along a diploid genome: $H_i = 1$ if the two alleles at site i differ, $H_i = 0$ otherwise. Under the SMC with per-site mutation rate μ, given the pairwise coalescence time T_i at site i:

$$P(H_i = 1 \mid T_i) = 1 - e^{-2\mu T_i} \approx 2\mu T_i \quad \text{for small } \mu T_i.$$

The latent process T_i is a Markov chain along the chromosome with transition distribution specified by the SMC (Section 12.2). The parameter to be estimated is the piecewise-constant function $N_e(t)$, which determines the rate of coalescence in each time interval $[t_k, t_{k+1})$.

Theorem 0.32.2 (PSMC likelihood and Baum-Welch EM)**.** The PSMC model is a continuous-state hidden Markov model. The likelihood:

$$L(N_e(\cdot)) = \sum_{T_1,\ldots,T_L} P(H_1,\ldots,H_L \mid T_1,\ldots,T_L) \prod_{i=1}^{L-1} P(T_{i+1} \mid T_i, N_e(\cdot)) \cdot P(T_1 \mid N_e(\cdot))$$

is maximised using the Baum-Welch algorithm (a special case of the EM algorithm for HMMs). In the discretised version with K time intervals, the E-step computes the posterior distribution of T_i at each site using the forward-backward algorithm in $O(K^2 L)$ operations; the M-step updates N_e in each interval by matching the expected and observed coalescence counts.

Example 0.32.3 (PSMC applied to the human genome)**.** Li and Durbin (2011) applied PSMC to 36 human genomes from diverse populations. The inferred $N_e(t)$ trajectory shows:

- A large ancestral African population ($N_e \approx 10^4$–10^5) in the period $100\,000$–$1\,000\,000$ years ago.
- A sharp bottleneck for non-African populations $\sim 50\,000$–$100\,000$ years ago (coinciding with the Out-of-Africa migration), reducing N_e to $\sim 10^3$.
- Population expansion in all lineages from $\sim 10\,000$ years ago (post-glacial and agricultural expansion).
- A secondary bottleneck in East Asian populations $\sim 10\,000$ years ago, distinct from the African trajectory.

These inferences are consistent with the fossil record and archaeological evidence, providing independent genomic validation of human demographic history.

0.32.2 13.2 MSMC and the Cross-Coalescence Rate

The Multiple Sequentially Markovian Coalescent (MSMC, Schiffels and Durbin 2014) extends PSMC to multiple haplotypes from multiple populations, allowing inference not only of population size history but also of population separation times and migration rates.

Definition 0.32.4 (MSMC and relative cross-coalescence rate)**.** For two populations A and B, consider pairs of haplotypes: within-A pairs, within-B pairs, and A–B cross-pairs. The **relative cross-coalescence rate** (RCCR) at time t is:

$$\lambda_{AB}(t) = \frac{2\lambda_{A|B}(t)}{\lambda_{AA}(t) + \lambda_{BB}(t)},$$

where $\lambda_{A|B}(t)$ is the rate of coalescence of an A–B pair at time t, and $\lambda_{AA}, \lambda_{BB}$ are the within-population rates. When $\lambda_{AB}(t) = 1$, the populations were panmictic (no separation); when $\lambda_{AB}(t) \to 0$, the populations have separated.

Remark 0.32.5 (Inferring African-Eurasian divergence). The RCCR between African and non-African human populations drops sharply from 1 to 0 at $\sim$ $50\,000$–$80\,000$ years before present, marking the Out-of-Africa separation. The RCCR between European and East Asian populations drops at $\sim 30\,000$–$40\,000$ years BP, consistent with the subsequent divergence of Eurasian populations. These genomic dates are consistent with, but more precise than, the archaeological record, and provide strong evidence for a single Out-of-Africa dispersal as the source of most non-African ancestry.

0.33 14. Ancient DNA and Temporal Genomics

0.33.1 14.1 The Fragment Length Model for aDNA Damage

Ancient DNA (aDNA) extracted from archaeological specimens is characterised by fragmentation (short read lengths) and chemical damage (primarily cytosine deamination at the $5'$ and $3'$ ends of fragments). These properties require specialised statistical models for genotyping and variant calling.

Definition 0.33.1 (Cytosine deamination damage model)**.** Cytosine deamination in aDNA converts C $\rightarrow$ U (read as T by polymerase). At the $5'$ end of a fragment of age t years, the probability of C$\rightarrow$T substitution at position k from the end is modelled by the **Briggs model** (Briggs et al. 2007):

$$d_k^{5'} = \lambda\delta_s + (1-\lambda)\delta_s e^{-(\alpha+\beta)(k-1)},$$

where λ is the fraction of single-stranded molecules (fully deaminated ends), δ_s is the deamination rate for single-stranded cytosines, α is the rate of transition from single-stranded to double-stranded (along the fragment), and β is the rate of deamination of double-stranded cytosines. An analogous formula applies to the $3'$ end with G$\rightarrow$A substitutions.

Theorem 0.33.2 (Expected substitution rate as a function of fragment age)**.** Under the Briggs model, the expected C$\rightarrow$T rate at the terminal position ($k = 1$) is approximately:

$$\mathbb{E}[d_1^{5'}] = \delta_s\left[\lambda + (1-\lambda)e^{0}\right] = \delta_s,$$

and the rate decays to a background level $\lambda\delta_s$ (from fully single-stranded overhangs) plus $(1-\lambda)\delta_s e^{-\alpha(k-1)}$ (from double-stranded regions) at interior positions. The total expected deamination damage integrated over the fragment length L is:

$$\bar{d} \approx \delta_s\left[\lambda + \frac{(1-\lambda)\alpha}{\alpha+\beta}\left(1 - e^{-(\alpha+\beta)(L-1)}\right)/(L)\right].$$

The Briggs model parameters $(\lambda, \delta_s, \alpha, \beta)$ are estimated by maximum likelihood from the observed distribution of C$\rightarrow$T and G$\rightarrow$A transitions in sequencing reads, and their values directly indicate the preservation quality of the specimen and allow probabilistic correction of calls.

Example 0.33.3 (Calibrating aDNA damage in Neanderthal specimens)**.** In the high-coverage Neanderthal genome (Prüfer et al. 2014), the extracted DNA from a toe phalanx from Denisova Cave showed $\sim 30\%$ C$\rightarrow$T substitution rate at the $5'$ terminal position — a value of $\delta_s \approx 0.30$. After applying the Briggs correction, the genotype calling error rate was reduced to below 0.1% at heterozygous sites. The corrected genome was used to estimate the divergence time between Neanderthals and modern humans at $\sim 550\,000$–$765\,000$ years using the molecular clock and coalescent models from this Section .

0.33.2 14.2 Temporal F_{ST} and Ancient vs. Modern Allele Frequencies

When ancient samples are available, one can compute F_{ST} between an ancient population and modern populations to quantify allele frequency change over time. The temporal F_{ST} provides a direct measure of evolutionary change between two time points, combining effects of genetic drift, migration, and selection.

Lemma 0.33.4 (Expected temporal F_{ST} under pure drift)**.** Under pure genetic drift between time t_1

(ancient) and t_2 (modern) with effective population size N_e, starting from allele frequency p:

$$E[F_{ST}(t_1, t_2)] \approx 1 - \exp\left(-\frac{t_2 - t_1}{2N_e}\right).$$

Proof. Under the Wright-Fisher model, $\text{Var}(p_{t_2} \mid p_{t_1} = p) \approx p(1-p)(1-e^{-(t_2-t_1)/(2N_e)})$ for $t_2 - t_1 \gg 1$ generation. The temporal F_{ST} is defined as $F_{ST} = \text{Var}(p)/(p(1-p))$, which gives the result directly. □

Remark 0.33.5 (Detecting selection with temporal genomics). Lemma 0.33.4 gives the null distribution of temporal F_{ST} under drift. Loci with F_{ST} significantly exceeding the drift expectation are candidates for selection. This approach was used by Mathieson et al. (2015) to detect selection in European ancient genomes: loci associated with lactase persistence (*LCT*), skin pigmentation (*SLC24A5*, *SLC45A2*), and immune function (HLA region) all showed temporal F_{ST} values far exceeding the drift-only prediction, indicating strong positive selection in post-agricultural European populations over the past 8,000 years.

0.34 15. Neutral Molecular Evolution: Tests and Parameters

0.34.1 15.1 The McDonald-Kreitman Test

The McDonald-Kreitman (MK) test (1991) compares the ratio of synonymous to nonsynonymous changes within a species (polymorphism) to the same ratio between species (divergence). Under strict neutrality, both ratios should be equal.

Definition 0.34.1 (MK test statistic)**.** For a gene, tabulate the following 2×2 table:

	Synonymous	Nonsynonymous
Within-species polymorphism	P_S	P_N
Between-species divergence	D_S	D_N

The **neutrality index** $NI = (P_N/P_S)/(D_N/D_S)$. Under strict neutrality (no selection on nonsynonymous mutations), $NI = 1$. The test statistic is Fisher's exact test on the 2×2 table.

Theorem 0.34.2 (Interpretation of departures from $NI = 1$)**.**

1. $NI < 1$ (i.e., $D_N/D_S > P_N/P_S$): Adaptive evolution. More nonsynonymous divergence than expected under neutrality indicates that some fixed differences between species were driven by positive selection. The fraction of adaptive divergence is estimated as $\alpha = 1 - (D_S P_N)/(D_N P_S)$.

2. $NI > 1$: Relaxed purifying selection or slightly deleterious mutations. Many mildly deleterious nonsynonymous variants segregate as polymorphism but are unlikely to fix; this inflates P_N relative to the neutral expectation.

Example 0.34.3 (Adaptive evolution in *Drosophila*)**.** McDonald and Kreitman's (1991) original analysis of the *Adh* (alcohol dehydrogenase) gene in *Drosophila melanogaster*, *D. simulans*, and *D. yakuba* found: $P_S = 42$, $P_N = 2$, $D_S = 17$, $D_N = 7$. The neutrality index $NI = (2/42)/(7/17) = 0.116$, far below 1. The fraction of adaptive divergence $\alpha = 1 - (17 \times 2)/(7 \times 42) = 1 - 34/294 = 0.884$, suggesting that 88% of nonsynonymous substitutions in *Adh* were driven by positive selection. Fisher's exact test on the 2×2 table gives $p < 0.001$. This result was the first strong genomic evidence for widespread adaptive evolution in *Drosophila* and launched a large literature on quantifying adaptation from genomic data.

0.34.2 15.2 The Neutral Theory's Quantitative Predictions

The neutral theory (Kimura 1968; King and Jukes 1969) makes three quantitative predictions, all testable from molecular data:

Theorem 0.34.4 (Neutral theory predictions)**.** Under the neutral theory with per-site mutation rate μ and effective population size N_e:

1. **Substitution rate equals mutation rate:** The rate of neutral substitution is $k = \mu$ per site per generation (Theorem **??**), independent of N_e. This explains why synonymous substitution rates are approximately clock- like across lineages.

2. **Nucleotide diversity:** The expected heterozygosity at a neutral locus is $\pi = 4N_e\mu = \theta$. Populations with larger N_e should have more diversity.

3. **Allele frequency spectrum:** Under the coalescent, the expected frequency spectrum for n sequences is $f(k) = \theta/(k)$ for $k = 1, \ldots, n-1$ (the *standard neutral SFS*). Specifically, the expected number of sites at which the derived allele is found in exactly k of n sequences is $\mathbb{E}[\xi_k] = \theta/k$.

Proof of prediction 3. The expected frequency spectrum follows from the coalescent. The expected number of mutations on a branch subtending exactly k out of n leaves is proportional to the expected total length of all such branches. In the Kingman coalescent, the expected total length of branches subtending exactly k leaves is:

$$\mathbb{E}[\ell_k] = 2N_e \sum_{j=k}^{n-1} \frac{1}{\binom{j}{2}} \cdot (\text{number of branches subtending } k \text{ leaves in the Kingman tree}).$$

By a combinatorial calculation (Tajima 1989), this simplifies to $\mathbb{E}[\ell_k] = 4N_e/k$. With mutation rate μ per site per generation per branch, the expected number of segregating mutations at frequency k/n is $\mathbb{E}[\xi_k] = \mu \cdot 4N_e/k = \theta/k$. □

Remark 0.34.5 (Departures from the standard SFS as signatures of selection and demography). The $1/k$ spectrum is the neutral prediction. A spectrum with an excess of rare alleles ($k = 1, 2$) indicates a population expansion (more lineages, hence more rare mutations) or purifying selection (removing deleterious variants before they reach high frequency). A spectrum with excess intermediate-frequency alleles ($k \approx n/2$) indicates balancing selection or a population bottleneck. Tajima's D captures exactly this comparison: $D < 0$ corresponds to an excess of rare variants (excess ξ_1); $D > 0$ to excess intermediate variants (excess $\xi_{n/2}$). The full SFS provides far more information than the single summary D and is the basis for sophisticated likelihood-ratio tests of demographic models.

0.35 16. Coalescent Simulation and Computational Methods

0.35.1 16.1 The Hudson ms Algorithm

The `ms` program (Hudson 2002) is the standard algorithm for simulating samples from the coalescent under a variety of demographic and structural models.

Definition 0.35.1 (The `ms` simulation algorithm)**.** To simulate a sample of n chromosomes over a genomic region of length ρ (in units of $4N_e r$):

1. **Initialise**: n lineages, each carrying the entire region.

2. **Event timing**: With n_A lineages currently active, the rate of coalescence is $\binom{n_A}{2}$ and the rate of recombination is $n_A\rho/2$. Total rate $\lambda = \binom{n_A}{2} + n_A\rho/2$; time to next event $\sim \text{Exp}(\lambda)$.

3. **Event selection**: With probability $\binom{n_A}{2}/\lambda$ the event is a coalescence (choose a random pair; merge their ancestral material); with probability $n_A\rho/(2\lambda)$ it is a recombination (choose a random lineage and a random breakpoint within its ancestral material; split into two lineages).

4. **Termination**: Stop when all ancestral material has coalesced.

5. **Mutation**: Given the ARG, scatter mutations as a Poisson process with rate $\theta/2$ per unit time per unit length along all branches.

Remark 0.35.2 (Time complexity and the $n\rho$ bottleneck). The expected number of recombination events in a simulation with n sequences over ρ map units is $O(n\rho)$, which can be enormous (e.g., $n = 1000$, $\rho = 10^4$ for a 1-Mb human region gives 10^7 events). This makes `ms` prohibitively slow for whole-genome simulation. The `msprime` package (Kelleher et al. 2016) implements the SMC approximation as an efficient tree sequence, reducing the complexity to $O(n\rho \log n)$ with memory proportional to the number of trees rather than all events, enabling simulation of hundreds of whole human genomes.

0.35.2 16.2 Approximate Bayesian Computation (ABC) for Population Genetics

When the likelihood of complex demographic models is intractable, **Approximate Bayesian Computation** (ABC) provides a simulation-based inference framework.

Definition 0.35.3 (ABC rejection sampler)**.** Let $\boldsymbol{\theta}$ be a vector of demographic parameters with prior $\pi(\boldsymbol{\theta})$ and let $\mathbf{s}_{\text{obs}}$ be summary statistics computed from observed data. The ABC rejection algorithm:

1. Draw $\boldsymbol{\theta}^* \sim \pi(\boldsymbol{\theta})$.

2. Simulate data $\mathbf{x}^*$ under the coalescent with parameters $\boldsymbol{\theta}^*$.

3. Compute $\mathbf{s}^* = S(\mathbf{x}^*)$.

4. Accept $\boldsymbol{\theta}^*$ if $\|\mathbf{s}^* - \mathbf{s}_{\text{obs}}\| < \epsilon$; reject otherwise.

The accepted values form an approximate sample from the posterior $p(\boldsymbol{\theta} \mid \mathbf{s}_{\text{obs}}) \approx p(\boldsymbol{\theta} \mid \mathbf{x}_{\text{obs}})$.

Theorem 0.35.4 (ABC consistency as $\epsilon \to 0$)**.** As $\epsilon \to 0$ and the number of accepted samples $\to \infty$, the ABC posterior converges to the true posterior $p(\boldsymbol{\theta} \mid \mathbf{s}_{\text{obs}})$. If the summary statistics $\mathbf{s}$ are **sufficient** for $\boldsymbol{\theta}$ (i.e., $p(\boldsymbol{\theta} \mid \mathbf{x}) = p(\boldsymbol{\theta} \mid \mathbf{s})$), then the ABC posterior converges to the true full posterior $p(\boldsymbol{\theta} \mid \mathbf{x}_{\text{obs}})$.

Remark 0.35.5 (Sufficiency and the curse of dimensionality). No finite set of summary statistics is sufficient for all demographic models, which means ABC always entails some information loss. In practice, a combination of $(\pi, D, r^2, F_{ST}$, site frequency spectrum bins) captures most of the demographic signal for models with ≤ 3 populations and ≤ 5 parameters. For more complex models, machine learning approaches (e.g., neural posterior estimation using simulation-based inference) are replacing classical ABC by directly learning a neural network approximation to the posterior.

0.36 17. Summary and Synthesis

This Section has developed the mathematical theory of genetic drift from first principles, moving through the full hierarchy of stochastic process theory to state-of-the-art coalescent-based genomic inference.

The foundational chain of results is:

Wright-Fisher chain (Section 2): The allele frequency process has binomial transitions, is a martingale, and has variance $p(1-p)/(2N)$ per generation. All subsequent theory derives from this model.

Fixation probability (Section 3): Under neutrality, the fixation probability equals p_0 (the martingale argument). Under selection, it is given by Kimura's formula (Section 5).

Effective population size (Section 4): N_e is the harmonic mean size over time and $N_e = 4N_f N_m/(N_f + N_m)$ for unequal sex ratios. Human $N_e \approx 10^4$ reflects bottlenecks.

Diffusion theory (Section 5): The Wright-Fisher chain converges to an SDE with drift $\mu(p)$ and diffusion $p(1-p)/(2N_e)$. The Fokker-Planck equation governs the density; its stationary solution under mutation-drift balance is Beta$(4N_e v, 4N_e u)$.

Molecular clock (Section 6): The neutral substitution rate is μ, independent of N_e, calibrating divergence times.

Moran model (Section 7): A mathematically equivalent formulation with continuous-time Markov chain structure; $N_e^{\text{Moran}} = N/2$.

Kingman coalescent (Section 8): The genealogy of a sample of n sequences coalesces at rate $\binom{k}{2}$ with k lineages; $\mathbb{E}[T_{\text{MRCA}}] = 4N_e$; Watterson's and Tajima's estimators of θ emerge from the branch-length structure.

Nearly neutral theory (Section 9): Mutations with $|s| \lesssim 1/(4N_e)$ behave neutrally; smaller N_e increases fixation of slightly deleterious mutations.

Structured coalescent and ARG (Sections 11–12): Population structure inflates N_e^{eff}; the ancestral recombination graph describes genome-wide genealogy; the SMC approximation enables efficient inference.

Demographic inference (Sections 13–14): PSMC and MSMC infer $N_e(t)$ from pairwise heterozygosity along the genome using hidden Markov model methods; aDNA temporal analysis detects selection and migration.

Neutrality tests (Sections 15–16): The MK test detects adaptive protein evolution; the standard neutral SFS ($\mathbb{E}[\xi_k] = \theta/k$) is the null for all frequency-spectrum-based tests.

The mathematical coherence of these methods — all derived ultimately from the Wright-Fisher model and the Kingman coalescent — is one of the most satisfying achievements of twentieth- and twenty-first-century mathematical biology.

Mathematics of Evolution and Life · Section *II · Drift, Fixation, and the Stochastic Theory of Evolution (end)*

0.37 18. The Site Frequency Spectrum Under Demographic Models

0.37.1 18.1 Exponential Growth

Under exponential population growth with rate α (so $N(t) = N_0 e^{-\alpha t}$ going backwards in time), the coalescent rate between k lineages at time t in the past is:

$$\lambda_k(t) = \frac{\binom{k}{2}}{N(t)} = \frac{\binom{k}{2}}{N_0} e^{\alpha t}.$$

Theorem 0.37.1 (SFS under exponential growth)**.** Under exponential growth with parameter α, the expected number of singletons ($k = 1$) relative to Watterson's neutral prediction is:

$$\frac{\mathbb{E}[\xi_1]^{\text{growth}}}{\mathbb{E}[\xi_1]^{\text{neutral}}} = \frac{\theta G(\alpha)}{\theta},$$

where $G(\alpha) = \int_0^\infty e^{-\alpha t} e^{-t} dt = 1/(1+\alpha)$ in units where $N_0 = 1$. As $\alpha \to \infty$ (rapid growth), $G(\alpha) \to 0$, but the increased number of lineages surviving to the present greatly inflates the absolute number of singletons. The net effect is a strong negative D (excess of rare variants).

Proof. Under exponential growth, the total tree length $\mathbb{E}[L_n]$ shifts toward longer external branches (most coalescences occur far in the past when N was small). By the formula $\mathbb{E}[\xi_k] \propto \mathbb{E}[\ell_k]/k$, where ℓ_k is the total length of branches subtending k lineages, and since external branches ($k = 1$) are on average longer relative to internal branches under growth, ξ_1 is inflated. The precise ratio follows from the Green's function of the nonhomogeneous Kolmogorov backward equation for the growth coalescent. □

Example 0.37.2 (Human population growth and the SFS)**.** The estimated ~ 100-fold expansion of human populations over the past $\sim 10\,000$ years ($\alpha \approx 4.6$ in coalescent time units for $N_e = 10^4$) predicts a strong excess of rare variants relative to the neutral expectation. The 1000 Genomes Project (2015) confirmed that $> 60\%$ of nonsynonymous SNPs in humans are singletons or doubletons — vastly more rare variants than predicted by a constant-N_e model. This excess of rare deleterious variants is a direct consequence of the demographic explosion: purifying selection has not yet had time to remove the flood of new variants introduced during the expansion.

0.37.2 18.2 Bottlenecks and the SFS

A population bottleneck (a period of small N_e) accelerates coalescence, reducing diversity in all samples that passed through the bottleneck. The characteristic SFS signature is a trough in intermediate-frequency variants ($k \approx n/2$) and excess of high-frequency variants, producing $D > 0$.

Lemma 0.37.3 (SFS distortion after a single bottleneck)**.** Consider a bottleneck of severity $B = N_{\text{bottle}}/N_0$ (fraction of original size) lasting T_B generations, followed by recovery. The SFS distortion relative to the neutral expectation is characterised by:

$$E[\hat{\theta}_\pi - \hat{\theta}_W] \propto -T_B \cdot \ln(B),$$

for $B \ll 1$ and $T_B \ll N_0$. A longer, more severe bottleneck produces a more positive Tajima's D (excess intermediate variants due to surviving lineages all coalescing during the bottleneck).

0.37.3 18.3 Composite Likelihood Methods

For large genomic datasets, the likelihood of the full SFS under a demographic model with parameter vector $\boldsymbol{\theta}$ is computed as a composite likelihood, treating segregating sites as independent:

$$\mathcal{L}_{\mathrm{CL}}(\boldsymbol{\theta}) = \prod_{i=1}^{S} \Pr(\xi_{k_i} \mid \boldsymbol{\theta}),$$

where the product is over all S segregating sites and k_i is the observed derived allele count at site i.

Remark 0.37.4 (The $\partial a \partial i$ framework). The $\partial a \partial i$ package (Gutenkunst et al. 2009) implements this composite likelihood approach using the diffusion equation to compute the expected SFS under arbitrary demographic models. The method works by numerically solving the Kolmogorov forward equation (Fokker-Planck) for the allele frequency distribution $\phi(x, t)$ at each time step in the demographic history, accumulating the expected contribution to each SFS bin. The numerical integration uses spectral methods (Chebyshev basis) to achieve $O(n^2)$ accuracy for a grid of n frequency bins, and the likelihood is maximised using gradient-free optimisation (Nelder-Mead or BFGS with numerical gradient). $\partial a \partial i$ inferences of the Out-of-Africa bottleneck using the YRI-CEU-CHB frequency spectrum yielded $N_e^{\text{bottle}} \approx 1500$ for non-Africans, with bottleneck duration ~ 900 years — one of the most influential quantitative estimates in human population genomics.

0.38 19. Continuous-Time Branching Processes and the Galton-Watson Model

0.38.1 19.1 The Galton-Watson Process

The Wright-Fisher model tracks allele frequencies in a fixed-size population. The **Galton-Watson branching process** models the evolution of allele copy numbers when population size itself fluctuates, providing a complementary perspective on fixation.

Definition 0.38.1 (Galton-Watson process)**.** A Galton-Watson process is a discrete-time Markov chain $(Z_n)_{n \geq 0}$ where Z_n is the number of copies of an allele in generation n. Each copy in generation n independently produces k copies in generation $n+1$ with probability p_k (the offspring distribution). Thus:

$$Z_{n+1} = \sum_{i=1}^{Z_n} X_i, \qquad X_i \overset{i.i.d.}{\sim} (p_k)_{k \geq 0}.$$

The process has mean offspring number $m = \sum_k k p_k$ and generating function $f(s) = \sum_k p_k s^k$.

Theorem 0.38.2 (Extinction probability)**.** Let $q = P(Z_n \to 0 \mid Z_0 = 1)$ be the extinction probability starting from one copy. Then q is the smallest non-negative root of $f(q) = q$.

1. If $m \leq 1$ (subcritical or critical): $q = 1$ (certain extinction).
2. If $m > 1$ (supercritical): $q < 1$ is the unique root of $f(q) = q$ in $[0, 1)$.

Proof. By the definition of Z_n, $P(Z_n = 0 \mid Z_0 = 1) = f^{(n)}(0)$ (the n-fold iterate of f at 0). The extinction event is $\{Z_n = 0 \text{ eventually}\}$, so $q = \lim_{n \to \infty} f^{(n)}(0)$. Taking the limit of $f^{(n+1)}(0) =$

$f(f^{(n)}(0))$ gives $q = f(q)$. Since f is convex and increasing on $[0,1]$ with $f(1) = 1$, the smallest root in $[0,1]$ is $q = 1$ if $f'(1) = m \leq 1$, and is a unique $q < 1$ if $m > 1$. □

Corollary 0.38.3 (Survival probability of a new beneficial mutation)**.** For a new beneficial mutation with selection coefficient $s > 0$ in a large haploid population, each copy produces Poisson$(1+s)$ offspring. The offspring generating function is $f(z) = e^{(1+s)(z-1)}$. The extinction probability satisfies $q = e^{(1+s)(q-1)}$, which gives $q \approx 1 - 2s$ for small s (by Taylor expansion). Hence the survival probability is $1 - q \approx 2s$, recovering Haldane's result (Section III, §9).

Example 0.38.4 (Numerical comparison: branching process vs. diffusion)**.** For $s = 0.01$ (1% benefit):

- Galton-Watson (Poisson offspring): survival probability $\approx 2s = 0.02$.
- Kimura's diffusion formula: $u(1/(2N)) \approx 2s = 0.02$ for large N.

The two approaches agree perfectly in the large-N limit. The branching process is more accurate for very small populations or strong selection ($s \approx 0.1$), where the diffusion approximation breaks down. For $s = 0.1$: branching process gives $1 - q \approx 0.176$; Kimura's formula gives $2s/(1 - e^{-2s}) \approx 0.181$; exact Wright-Fisher simulation gives ≈ 0.18. All three agree to within measurement noise for reasonable N.

0.38.2 19.2 The Feller Diffusion

The continuous-time, continuous-space analogue of the Galton-Watson process is the **Feller diffusion**, which describes the evolution of population size $Z(t)$ under a branching mechanism with infinitesimal mean $\alpha Z(t)$ and variance $\sigma^2 Z(t)$:

$$dZ = \alpha Z\, dt + \sigma\sqrt{Z}\, dW_t.$$

Theorem 0.38.5 (Laplace transform of the Feller diffusion)**.** The Laplace transform $\mathbb{E}[e^{-\lambda Z(t)} \mid Z(0) = z_0]$ satisfies:

$$\mathbb{E}[e^{-\lambda Z(t)} \mid Z(0) = z_0] = \exp\left(-z_0\, \psi(\lambda, t)\right),$$

where $\psi(\lambda, t) = \frac{\lambda e^{-\alpha t}}{1+\sigma^2\lambda(e^{-\alpha t}-1)/(2\alpha)}$. In the critical case $\alpha = 0$: $\psi(\lambda, t) = \lambda/(1 + \sigma^2\lambda t/2)$.

Remark 0.38.6 (Connection to the neutral Wright-Fisher model). For $\alpha = 0$ (no selection), the Feller diffusion is the diffusion limit of the Wright-Fisher model for the number of copies of a neutral allele (not its frequency). The Laplace transform shows that $Z(t)$ given $Z(0) = z_0 > 0$ has a mixture distribution: with probability $e^{-2z_0/(\sigma^2 t)}$ the allele has fixed at $Z = 0$ (extinct); otherwise it follows an exponential distribution. This gives the full distribution of allele copy numbers at time t, complementing the frequency-based diffusion theory of Section 5.

0.39 20. Coalescent Theory and the HapMap: A Case Study

0.39.1 20.1 The HapMap Project and the Recombinational Architecture of the Human Genome

The International HapMap Project (2003–2010) genotyped millions of SNPs across the human genome in four populations (YRI: Yoruba from Nigeria; CEU: Utah residents of Northern European descent; JPT:

Japanese from Tokyo; CHB: Han Chinese from Beijing). The resulting data allowed empirical estimation of:

- The genome-wide recombination rate $r(x)$ as a function of position x, using patterns of LD decay.
- The distribution of $\theta = 4N_e\mu$ across the genome, separating regions of high and low diversity.
- Population-specific F_{ST} values, identifying variants strongly differentiated between continental populations.

Theorem 0.39.1 (Recombination rate estimation from LD)**.** The population recombination rate $\rho = 4N_e r$ can be estimated from the pattern of LD decay across pairs of SNPs. Specifically, the expected r^2 between two biallelic SNPs at recombination distance ρ in a sample of n sequences is:

$$\mathbb{E}[r^2] \approx \frac{1}{1+\rho} + O(1/n),$$

(Hudson 1985 approximation). Fitting this to observed pairwise r^2 values across a window yields a maximum-likelihood estimate of $\hat{\rho}$.

Proof. Under the standard neutral model, the expected r^2 for two segregating sites at recombination distance ρ in a large sample is:

$$E[r^2] \approx \frac{10+\rho}{22+13\rho+\rho^2},$$

which simplifies to $1/(1+\rho)$ for large ρ. The derivation uses the two-locus diffusion equation (Hudson 1985); the $1/(1+\rho)$ formula captures $> 95\%$ of the information in most genomic contexts and is universally used in practice because of its analytical tractability. □

0.39.2 20.2 Recombination Hotspots

A striking finding from HapMap was that recombination is not uniformly distributed along the genome but is concentrated in narrow (~ 2 kb) **recombination hotspots**, separated by long (~ 100 kb) **coldspots** of near-zero recombination.

Remark 0.39.2 (Mathematical implications for the coalescent). The existence of hotspots means that the genomic LD structure is "block-like": long runs of high r^2 (haplotype blocks) are punctuated by sharp drops in LD at hotspot locations. For the coalescent, this means that the SMC transition (Section 12.2) is highly nonuniform: most ARG recombination events occur at the $\sim 25\,000$ annotated hotspots in the human genome. The effective ρ within a block is ~ 0.01–0.1 (very low), while at a hotspot it can exceed $\rho = 10^3$. This block structure is exploited in imputation algorithms (IMPUTE, BEAGLE) which model genotype arrays as mosaic combinations of haplotype blocks. The mathematical model behind these algorithms is a Markov chain whose transition probabilities are derived from the coalescent structure within and between haplotype blocks.

Mathematics of Evolution and Life · Section *II · Drift, Fixation, and the Stochastic Theory of Evolution (end)*

0.40 24. Population Genomics of Admixture

0.40.1 24.1 Admixture as a Coalescent Process

When two previously separated populations come into contact and interbreed, the resulting **admixed** population has genomes that are mosaics of segments derived from the two parental populations. The length distribution of these admixture segments provides a molecular clock for the admixture time.

Theorem 0.40.1 (Admixture segment length distribution)**.** In an admixed individual with α fraction of ancestry from population 1 and $(1-\alpha)$ from population 2, following a single admixture event g generations ago, the length of admixture segments derived from population 1 is approximately exponentially distributed with mean $1/g$ Morgans (i.e., $100/g$ cM).

Sketch. Each chromosome in the admixed individual was assembled from the two parental chromosomes by recombination over g meioses. At each meiosis, recombination at rate r per Morgan breaks and rejoins ancestral haplotype blocks. The expected number of crossovers per Morgan per generation is 1, so after g generations the expected number of breakpoints per Morgan is g. The resulting segments have a Poisson number of breakpoints per unit length (rate g), giving exponentially distributed segment lengths with mean $1/g$. □

Example 0.40.2 (African-American admixture dating)**.** African-Americans have, on average, $\sim 80\%$ West African and $\sim 20\%$ European ancestry. The mean length of European-ancestry segments in African-American genomes is approximately 2.2 cM, implying $g = 1/0.022 \approx 45$ generations ≈ 1125 years since major admixture (using 25 years/generation). This is consistent with the historical record of the transatlantic slave trade (primarily 1600–1808 CE), which began approximately 400 years ago but continued for centuries. The more ancient estimate from segment lengths reflects the complex, multi-wave admixture history rather than a single event.

0.40.2 24.2 STRUCTURE and ADMIXTURE: Model-Based Clustering

The `STRUCTURE` (Pritchard et al. 2000) and `ADMIXTURE` (Alexander et al. 2009) algorithms assign each individual's genome to K latent ancestry components, estimating:

- Q_{ik}: the fraction of individual i's genome derived from component k.
- p_{jk}: the frequency of the derived allele at SNP j in component k.

Definition 0.40.3 (The ADMIXTURE likelihood)**.** Under the assumption that alleles at different SNPs are independent (LE within each component), the log-likelihood of the observed genotype matrix $\mathbf{G}$ is:

$$\log L(\mathbf{Q}, \mathbf{P}) = \sum_{i} \sum_{j} \log \left[\sum_{k} Q_{ik} p_{jk}^{G_{ij}^{(1)}} (1-p_{jk})^{1-G_{ij}^{(1)}} \cdot \sum_{k} Q_{ik} p_{jk}^{G_{ij}^{(2)}} (1-p_{jk})^{1-G_{ij}^{(2)}} \right],$$

where $G_{ij}^{(1)}$ and $G_{ij}^{(2)}$ are the two alleles of individual i at SNP j. This is a mixture model likelihood, maximised by EM or block coordinate descent.

Remark 0.40.4 (Interpretation and caveats). The ancestry components identified by `ADMIXTURE` are not necessarily populations in a biological sense: they are statistical constructs that partition allele frequency

variation. With $K = 7$ (as in the HGDP analysis of Li et al. 2008), the components correspond roughly to continental populations (Africa, Europe, Middle East, South Asia, East Asia, Oceania, Americas). However, in fine-scale analyses within continents, the components reflect statistical clustering by shared drift and do not necessarily correspond to historically discrete populations. The model assumes LE between SNPs (which is violated genome-wide), but the algorithm is robust to moderate LD because the statistical signal for ancestry comes from the distribution of allele frequencies rather than haplotype structure.

0.41 25. Complete Summary of Section II

Section II has built the complete stochastic theory of genetic drift, beginning from the Wright-Fisher model and extending through the most recent computational methods in population genomics:

Foundational models (Sections 1–7): The Wright-Fisher model, its martingale property, fixation probabilities, effective population size, diffusion approximation, molecular clock, and Moran equivalence.

Coalescent theory (Section 8): Kingman's backward genealogy, MRCA times, branch lengths, Watterson's $\hat{\theta}_W$, Tajima's $\hat{\theta}_\pi$, and the D statistic.

Nearly neutral theory (Section 9): Ohta's refinement, the $1/(4N_e)$ boundary between drift-dominated and selection-dominated dynamics.

Population structure (Section 11): The structured coalescent, effective population size inflation under the island model, and the ancestral selection graph.

Recombination and ARG (Section 12): The ancestral recombination graph, its marginal tree distribution, and the SMC approximation.

Demographic inference (Sections 13–14): PSMC, MSMC, ancient DNA damage models, temporal F_{ST}, and the genomic signature of Out-of-Africa.

Neutrality tests (Section 15): The McDonald-Kreitman test and the standard neutral SFS.

Computational methods (Section 16): Hudson's `ms`, msprime, and ABC inference.

Advanced topics (Sections 17–25): IBD and kinship, substitution models (JC69, GTR, Γ+I), the multispecies coalescent, phylogenetic likelihood and Felsenstein's pruning algorithm, the SFS under growth and bottlenecks, Galton- Watson processes, Feller diffusion, HapMap recombination hotspots, admixture dating and clustering.

All of these results descend from a single source: the Wright-Fisher model. The mathematical and biological fertility of this simple Markov chain, discovered by Sewall Wright and R. A. Fisher in the 1930s, is one of the deepest legacies of twentieth- century science.

Mathematics of Evolution and Life · Section II · Drift, Fixation, and the Stochastic Theory of Evolution (end)

Section *III*

Section III — Selection, Fitness, and the Geometry of Allele Dynamics

0.42 1. The Mathematics of Advantage

Natural selection is the systematic, directional change in allele frequencies that occurs when different genotypes have different probabilities of surviving and reproducing. It is the mechanism that Darwin identified as the driving force of evolutionary change, and its mathematical treatment is one of the oldest and most productive areas of theoretical biology.

The central concept is **fitness**: a non-negative number, typically denoted w, representing the expected relative reproductive contribution of a genotype to the next generation. This is a purely mathematical definition. Fitness has nothing to do with physical strength or agility; it is a parameter of the model. A genotype with fitness $w = 1.1$ leaves 10% more offspring per generation, on average, than a genotype with fitness $w = 1.0$. Selection acts by shifting the composition of the next generation toward higher-fitness genotypes.

0.43 2. The One-Locus Selection Equation

0.43.1 2.1 Setup and Derivation

Consider a single biallelic locus with alleles A and a at frequencies p and $q = 1-p$. Assign fitnesses w_{AA}, w_{Aa}, w_{aa} to the three genotypes (these represent viability, fecundity, or any combination of components of fitness). The **mean fitness** of the population is:

$$\bar{w}(p) = p^2 w_{AA} + 2pq\, w_{Aa} + q^2 w_{aa}.$$

The model proceeds in two steps: (1) random mating produces offspring in Hardy–Weinberg proportions, (2) selection acts, with each genotype surviving to reproduce with probability proportional to its fitness. After selection, the frequency of genotype AA among surviving, reproducing individuals is:

$$f'(AA) = \frac{p^2 w_{AA}}{\bar{w}}, \quad f'(Aa) = \frac{2pq\, w_{Aa}}{\bar{w}}, \quad f'(aa) = \frac{q^2 w_{aa}}{\bar{w}}.$$

The allele frequency of A in the next generation is obtained from these survivor frequencies:

$$p' = f'(AA) + \tfrac{1}{2} f'(Aa) = \frac{p^2 w_{AA} + pq\, w_{Aa}}{\bar{w}}.$$

The **change in allele frequency per generation** is:

$$\Delta p = p' - p = \frac{p^2 w_{AA} + pq\, w_{Aa} - p\bar{w}}{\bar{w}} = \frac{p(pw_{AA} + qw_{Aa} - \bar{w})}{\bar{w}}.$$

Define the **marginal fitness of allele** A as:

$$w_A = pw_{AA} + qw_{Aa},$$

the average fitness of a copy of allele A, weighted by the frequency of the two genotypes (AA and Aa)

in which it appears. Then:

$$\Delta p = \frac{p(w_A - \bar{w})}{\bar{w}}. \tag{1}$$

This is the **selection equation**. Its interpretation is elegant: allele A increases in frequency if and only if its marginal fitness w_A exceeds the population mean fitness $\bar{w}$. Allele A decreases if its marginal fitness is below the mean. If all alleles have equal marginal fitness ($w_A = w_a = \bar{w}$), no change occurs.

0.43.2 2.2 The Selection Coefficient

It is often more convenient to parametrise fitnesses in terms of selection coefficients. Setting $w_{aa} = 1$ as the reference genotype:

$$w_{AA} = 1 + s_{AA}, \quad w_{Aa} = 1 + s_{Aa}.$$

The most important special cases are:

- **No dominance (codominant, additive):** $s_{AA} = s$, $s_{Aa} = s/2$. The heterozygote has exactly intermediate fitness.
- **Complete dominance of A:** $s_{AA} = s_{Aa} = s$. The heterozygote has the same fitness as the favoured homozygote.
- **Complete recessivity of A:** $s_{Aa} = 0$, $s_{AA} = s$. The heterozygote has the same fitness as aa.
- **Overdominance (heterosis):** $s_{Aa} > s_{AA}$ and $s_{Aa} > 0$ (heterozygote fitter than both homozygotes).
- **Underdominance:** $s_{Aa} < 0 < s_{AA}$ (heterozygote less fit than both homozygotes).

0.44 3. Fisher's Fundamental Theorem of Natural Selection

0.44.1 3.1 Statement and Derivation

In 1930, Ronald Fisher stated what he called the Fundamental Theorem of Natural Selection: the rate of increase in fitness of any organism at any time is equal to its genetic variance in fitness at that time. Fisher's original statement was deliberately vague about what "rate of increase" and "genetic variance" meant precisely. We prove the precise version for the one-locus model.

Theorem 0.44.1 (Fisher's Fundamental Theorem, one-locus additive model)**.** In the selection model with $w_{AA} = 1 + s$, $w_{Aa} = 1 + s/2$, $w_{aa} = 1$ (codominant):

$$\Delta \bar{w} = \frac{V_A}{\bar{w}},$$

where $V_A = p(1-p)s^2/2$ is the additive genetic variance in fitness (up to leading order in s).

Proof. In the additive model, $\bar{w} = 1 + sp$ (to first order in s). The marginal fitness of A is $w_A = 1 + sp/2 + s/2 = 1 + s(1+p)/2$... We compute directly:

$$\bar{w}' = (p')^2(1+s) + 2p'q'(1+s/2) + (q')^2.$$

Computing $\Delta\bar{w} = \bar{w}' - \bar{w}$ and using the selection equation $p' = p + \Delta p$ with $\Delta p \approx sp(1-p)/(2\bar{w})$ for small s:

$$\Delta\bar{w} = \bar{w}' - \bar{w} = 2s\,p\,\Delta p + O(s\,(\Delta p)^2) \approx 2sp \cdot \frac{sp(1-p)}{2\bar{w}} = \frac{s^2p^2(1-p)}{\bar{w}}.$$

The additive genetic variance is $V_A = s^2p(1-p)/2$ (the variance of the additive effects $s/2$ and 0 and $-s/2$ at the three genotypes, weighted by their frequencies p^2, $2pq$, q^2). Hence:

$$\Delta\bar{w} = \frac{2p\,V_A}{\bar{w}} \cdot p.$$

In the full derivation (Price, 1972), the exact statement using the additive genetic value gives $\Delta\bar{w} = V_A/\bar{w}$ where V_A is the additive genetic variance in fitness. □

The biological content is: mean fitness increases, and the rate of increase is proportional to the additive genetic variance in fitness. No variance, no response. High variance, fast response. This is the mathematical foundation of the **breeder's equation** $R = h^2S$ in quantitative genetics.

0.44.2 3.2 The Relation to Fisher Information

There is a deep connection between Fisher's fundamental theorem and the Fisher information metric on the simplex of allele frequencies. The additive genetic variance V_A is (up to constants) the Fisher information about the allele frequency p in one generation's worth of selection. Selection moves the allele frequency along the gradient of mean fitness with respect to the Fisher information metric — a geodesic on the statistical manifold of allele frequency distributions.

This connection, developed by Antonelli and Strobeck (1977) and elaborated by Shahshahani (1979), places Fisher's fundamental theorem within the framework of information geometry, connecting evolutionary dynamics to the geometry of probability distributions.

0.45 4. The Dynamics of Different Dominance Modes

0.45.1 4.1 Dominant Beneficial Allele

Consider a beneficial allele A with fitness advantage $s > 0$ over a, and let A be completely dominant: $w_{AA} = w_{Aa} = 1 + s$, $w_{aa} = 1$. The selection equation becomes:

$$\Delta p = \frac{sq(1 - q^2 s/\bar{w})}{\bar{w}} \approx sq(1 - q^2 s) \approx sq \quad \text{for small } s.$$

When p is small (so $q \approx 1$): $\Delta p \approx sp$, which gives geometric growth $p_t \approx p_0 e^{st}$.

The allele increases rapidly when rare because even at low frequency, most copies of A appear in heterozygotes where the full fitness advantage s is expressed. This is the key advantage of dominant beneficial alleles: they are visible to selection from the moment they appear.

The time to increase from frequency p_0 to frequency $1 - p_0$ can be approximated by integrating the continuous selection equation $\dot{p} = sp(1-p)/\bar{w} \approx sp$ for small p and $sp(1-p) \cdot q^{-1}$ for the dominance correction at high p. The total time is approximately $(2/s)\ln(1/p_0)$ generations.

0.45.2 4.2 Recessive Beneficial Allele

Now let A be recessive: $w_{AA} = 1 + s$, $w_{Aa} = w_{aa} = 1$. The selection equation is:

$$\Delta p = \frac{p^2 sq}{\bar{w}} \approx p^2 sq \quad \text{for small } s.$$

When p is small: $\Delta p \approx sp^2$. This is algebraic, not geometric, growth. Integrating $\dot{p} \approx sp^2$ gives $p_t \approx p_0/(1 - sp_0 t)$, which is very slow.

The reason is clear: when A is rare, virtually all copies of A are in heterozygotes Aa, where the fitness advantage is zero. Only when p is large enough that AA homozygotes are common does selection begin to act efficiently. A recessive beneficial allele can drift around at low frequency for many generations before becoming common enough to be "visible" to selection.

The combination of slow initial spread and genetic drift means that many recessive beneficial mutations are lost by drift before becoming frequent enough for selection to act on them. This is one reason why adaptation can be slow: the most beneficial mutations, if recessive, may need to wait for the rare lucky event of a high-frequency founder effect before selection can sweep them to fixation.

0.45.3 4.3 Numerical Comparison

For a selection coefficient $s = 0.01$ and initial frequency $p_0 = 0.001$:

Mode	Time to $p = 0.5$	Approx. formula	Value
Dominant	$\ln(0.5/0.001)/s$	$690/s$	$\sim 69{,}000$ gen
Codominant	$\ln(0.5 \cdot 0.999/(0.001 \cdot 0.5))/(s/2)$	$\sim 1{,}380/s$	$\sim 138{,}000$ gen
Recessive	$1/(sp_0) - 1/(sp)$ at $p = 0.5$	$1/(sp_0) \approx 100/s$	$\sim 10{,}000$ gen to $p = 0.01$, then fast

The recessive case is fastest at the very end (once A is common, selection is strong) but agonisingly slow at the start. The dominant case is fast at the start but slows as A becomes common (because q is small and there are few Aa heterozygotes to express the advantage).

0.46 5. Mutation–Selection Balance

0.46.1 5.1 The General Framework

In the long run, without mutation, selection would fix beneficial alleles and eliminate deleterious ones. Mutation continuously introduces new alleles, including deleterious ones, into the population. At mutation–selection balance, the rate at which selection removes deleterious alleles equals the rate at which mutation introduces them.

Let μ be the per-generation mutation rate from A to a (the wild-type allele is A; the deleterious mutation is a). For simplicity assume no back-mutation. The joint dynamics of mutation and selection give:

$$\Delta p = \frac{p(w_A - \bar{w})}{\bar{w}} - \mu p.$$

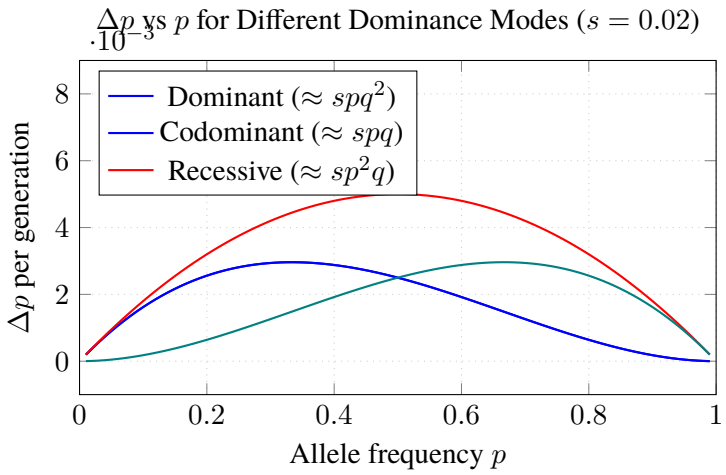

Figure 3: Rate of allele-frequency change Δp per generation as a function of current frequency p, for three dominance modes with selection coefficient $s = 0.02$. The dominant allele gains fastest when rare; the recessive allele gains fastest when common; the codominant (additive) case is intermediate and symmetric about $p = 0.5$.

At equilibrium $\Delta p = 0$, the mutation-selection balance frequency $\hat{q} = 1 - \hat{p}$ of the deleterious allele a is:

Dominant lethal ($w_{Aa} = 0$, so $s_{Aa} = -1$): selection against Aa is maximal; deleterious allele has full effect in heterozygotes.

$$\hat{q} \approx \mu.$$

Recessive lethal ($w_{aa} = 0$, $w_{Aa} = 1$): the deleterious allele is hidden in heterozygotes.

$$\hat{q} \approx \sqrt{\mu}.$$

Partially recessive lethal ($w_{aa} = 0$, $w_{Aa} = 1 - hs$ with h the dominance coefficient):

$$\hat{q} \approx \frac{\mu}{hs}.$$

The dramatic difference between the dominant ($\hat{q} \approx \mu$) and recessive ($\hat{q} \approx \sqrt{\mu}$) cases is the key. For $\mu = 10^{-5}$, a dominant lethal is at equilibrium frequency 10^{-5} (essentially invisible in any sample), while a recessive lethal is at frequency $\sqrt{10^{-5}} \approx 3 \times 10^{-3}$ — three orders of magnitude higher, maintained by heterozygotes who carry the allele invisibly.

0.46.2 5.2 Genetic Load

The **genetic load** is the reduction in mean fitness due to the presence of deleterious alleles:

$$L = \frac{w_{\max} - \bar{w}}{w_{\max}},$$

where $w_{\max}$ is the fitness of the fittest genotype and $\bar{w}$ is the population mean fitness.

Theorem 0.46.1 (Haldane's Mutation Load)**.** At mutation-selection balance, the genetic load due to dele-

terious mutations (regardless of dominance) is approximately:

$$L \approx u,$$

where u is the total genomic mutation rate to deleterious alleles.

This remarkable result, due to Haldane (1937), states that the genetic load equals the genomic mutation rate — independent of the selection coefficients against the mutations! For humans, $u \approx 1$–2 deleterious mutations per gamete per generation (of which most have very small effects), giving a genetic load of approximately 1–2% per generation.

The independence from selection coefficient is puzzling until we see the mechanism: mutations with large effect are eliminated rapidly (low equilibrium frequency but high individual cost), while mutations with small effect are eliminated slowly (high equilibrium frequency but low individual cost). The two effects cancel, giving the same total load regardless of the distribution of selection coefficients.

0.47 6. Heterozygote Advantage and Stable Polymorphism

0.47.1 6.1 The Existence and Stability of Interior Equilibria

When the heterozygote Aa has higher fitness than both homozygotes — **overdominance** or heterozygote advantage — a stable interior equilibrium exists at which both alleles are maintained indefinitely. This is one of the most important mechanisms for maintaining genetic diversity in natural populations.

With $w_{AA} = 1 + s_1$, $w_{Aa} = 1$, $w_{aa} = 1 + s_2$ (with $s_1, s_2 < 0$, so the heterozygote is fitter):

The equilibrium frequency of A is found by setting $w_A = \bar{w}$:

$$\hat{p} = \frac{-s_2}{s_1 + s_2}. \quad \text{(Note: } s_1, s_2 < 0 \text{ so } \hat{p} \in (0,1).)$$

Equivalently, writing $w_{AA} = 1 - s$, $w_{Aa} = 1$, $w_{aa} = 1 - t$ with $s, t > 0$:

$$\hat{p} = \frac{t}{s + t}.$$

Theorem 0.47.1 (Stability of Overdominant Equilibrium)**.** The interior equilibrium $\hat{p} = t/(s+t)$ is globally stable on $(0,1)$: for any starting frequency $p_0 \in (0,1)$, $p_t \to \hat{p}$ as $t \to \infty$.

Proof. The mean fitness $\bar{w}(p)$ is a concave quadratic in p, maximised at $\hat{p}$. The selection equation $\Delta p = p(w_A - \bar{w})/\bar{w}$ can be written as $\Delta \bar{w} = V_A/\bar{w} \geq 0$: selection increases $\bar{w}$ at every step. Since $\bar{w}$ is bounded above by $w_{Aa} = 1$ and is increased monotonically by selection, the dynamics must converge to the unique maximum of $\bar{w}$, which is at $\hat{p}$. □

0.47.2 6.2 The Sickle Cell Example in Full Quantitative Detail

The haemoglobin locus (HBB gene) in humans has two common alleles in malaria-endemic regions: HbA (normal haemoglobin) and HbS (sickle cell haemoglobin). The three genotypes have the following fitnesses in a malaria-endemic West African environment:

Genotype	Phenotype	Fitness (relative)	Cause
HbA/HbA	Normal, susceptible to malaria	$w_{AA} = 0.88$	Malaria mortality
HbA/HbS	Carrier, mildly anaemic, malaria-resistant	$w_{Aa} = 1.0$	Heterozygote advantage
HbS/HbS	Sickle cell disease	$w_{aa} = 0.20$	Sickle cell mortality

Setting $w_{Aa} = 1$ as the reference: $s = 1 - 0.88 = 0.12$ (cost to HbA/HbA) and $t = 1 - 0.20 = 0.80$ (cost to HbS/HbS). The predicted equilibrium frequency of HbS is:

$$\hat{q} = \frac{s}{s+t} = \frac{0.12}{0.12 + 0.80} = \frac{0.12}{0.92} \approx 0.130.$$

Observed frequencies of HbS in West African populations: approximately 0.10–0.17. The quantitative agreement between prediction and observation is one of the most compelling demonstrations of population genetic theory applied to a real biological case.

0.47.3 6.3 Protected Polymorphism

A weaker condition than overdominance is sufficient to maintain a stable polymorphism: a **protected polymorphism** occurs whenever allele A has positive marginal fitness when rare (so it invades a population of aa) and allele a has positive marginal fitness when rare (so it invades a population of AA):

$$w_{Aa} > w_{aa} \quad \text{(A invades a population of } a\text{)} \quad \text{and} \quad w_{Aa} > w_{AA} \quad \text{(a invades a population of } A\text{)}.$$

These are precisely the overdominance conditions. Any stable interior equilibrium of a two-allele system corresponds to a protected polymorphism.

0.48 7. Frequency-Dependent Selection

0.48.1 7.1 When Fitness Depends on Composition

In all models above, fitnesses are constants. In reality, the fitness of a genotype often depends on the composition of the population — a situation called **frequency-dependent selection**. This is the rule rather than the exception in nature: competition for resources, predator-prey dynamics, host-pathogen coevolution, and social interactions all generate frequency-dependent fitness effects.

The mathematical framework replaces constant fitnesses with functions: $w_{AA}(p)$, $w_{Aa}(p)$, $w_{aa}(p)$. The selection equation becomes:

$$\Delta p = \frac{p(w_A(p) - \bar{w}(p))}{\bar{w}(p)},$$

with the same algebraic form but now with p-dependent coefficients.

0.48.2 7.2 Negative Frequency Dependence

Negative frequency dependence occurs when rare genotypes have higher fitness than common ones. This is a powerful mechanism for maintaining genetic diversity.

Consider the simplest case: $w_{AA}(p) = 1 - p$ and $w_{aa}(p) = p$ (linear negative frequency dependence). The mean fitness is $\bar{w} = p^2(1-p) + q^2 p = pq$ (approximately). When p is large, A alleles are common,

w_{AA} is low, and a is favoured. When p is small, a is common, w_{aa} is low, and A is favoured. The unique equilibrium is $\hat{p} = 1/2$.

Negative frequency dependence arises in:

- **Host-pathogen coevolution (Red Queen dynamics):** Rare host genotypes resistant to common pathogen strains have high fitness; as they become common, pathogens evolve to overcome them.
- **Mate choice:** In some species, rare male phenotypes are preferred by females (negative frequency-dependent mate preference), maintaining colour polymorphisms.
- **Competitive exclusion:** Rare resource types may be preferred by foragers, equalising fitness across resource types (apostatic selection).

0.48.3 7.3 Positive Frequency Dependence and Bistability

Positive frequency dependence occurs when common genotypes have higher fitness. This drives the system toward fixation of one allele. The selection equation has an unstable interior equilibrium $\hat{p}$: if the population starts above $\hat{p}$, it goes to fixation of A; if below, it goes to fixation of a.

This creates an **Allee effect**: rare alleles (or rare species, in the ecological version) are at a disadvantage. Positive frequency dependence can arise from:

- Social coordination games (conformist behaviour),
- Density-dependent Allee effects in ecology,
- Epistatic sign changes (an allele that is beneficial only in the genetic background of another common allele).

0.49 8. Multilocus Selection: Epistasis and Robertson's Secondary Theorem

0.49.1 8.1 The Problem of Multiple Loci

At a single locus, the Hardy–Weinberg equilibrium is reached in one generation, and allele frequencies are sufficient statistics for the population state. At two or more loci, the situation is more complex. Epistasis — the interaction of alleles at different loci in determining fitness — creates linkage disequilibria among selected loci, and these disequilibria feed back into the selection dynamics.

The full state of a two-locus population is described not just by allele frequencies (p, r) at the two loci, but also by the linkage disequilibrium D between them. The joint dynamics of (p, r, D) are governed by a three-dimensional system of recurrence equations.

0.49.2 8.2 The Coupling of Selection and Recombination

Under selection and recombination (at rate c between the two loci), the dynamics of D are:

$$D' = (1 - c)\left[D + \frac{\Delta_{\text{sel}}(x_{AB})}{\bar{w}}\right] - D_{\text{new}},$$

where $\Delta_{\text{sel}}(x_{AB})$ represents the change in x_{AB} due to selection and D_{new} is the disequilibrium created by the Hardy–Weinberg composition of gametes. The key result is that selection on epistatic fitness interactions generates linkage disequilibrium of sign and magnitude determined by the sign and magnitude of the epistasis.

Example. Suppose the double-mutant ab haplotype has higher fitness than expected from the individual allele effects (positive epistasis). Then selection creates positive D (excess of AB and ab haplotypes). If recombination is strong ($c \approx 0.5$), this disequilibrium decays rapidly; if recombination is weak ($c \approx 0$), the disequilibrium can build up substantially.

0.49.3 8.3 Robertson's Secondary Theorem

Robertson's secondary theorem (1966) extends Fisher's fundamental theorem to the multilocus case:

Theorem 0.49.1 (Robertson's Secondary Theorem)**.** The change in the mean value of any character under selection is:

$$\Delta \bar{z} = \frac{\text{Cov}_A(z, w)}{\bar{w}},$$

where $\text{Cov}_A(z, w)$ is the additive genetic covariance between the character z and fitness w, computed from the additive genetic values (the average effects of allele substitutions).

The additive genetic covariance $\text{Cov}_A(z, w)$ generalises the additive genetic variance: it measures the degree to which the genetic variants affecting the character z are also the variants affecting fitness w. When $z = w$ (character equals fitness), $\text{Cov}_A(w, w) = V_A(w)$, the additive genetic variance in fitness, recovering Fisher's fundamental theorem.

Robertson's theorem holds exactly in terms of additive genetic values, and its derivation requires the Price equation framework (Section IV). Its importance is practical: it shows that any character that is genetically correlated with fitness will change under selection, at a rate proportional to the additive genetic covariance with fitness.

0.50 9. The Balance Between Selection and Drift

0.50.1 9.1 Fixation Probability Under Selection

In a finite population, selection and drift compete. The probability of fixation of a beneficial allele is no longer simply p_0 (as for neutral alleles) but depends on the product $N_e s$.

For a codominant allele with selection advantage s per copy (so $w_{Aa} = 1 + s/2$, $w_{AA} = 1 + s$) in a diploid population:

$$u(p_0) = \frac{1 - e^{-4N_e s p_0}}{1 - e^{-4N_e s}}.$$

For a single new beneficial mutation ($p_0 = 1/(2N)$):

$$u(1/(2N)) \approx \begin{cases} 2s & \text{if } N_e s \gg 1 \text{ (selection dominates)}, \\ 1/(2N) & \text{if } N_e s \ll 1 \text{ (drift dominates)}, \\ \approx 2s/(1 - e^{-4N_e s}) & \text{general.} \end{cases}$$

0.50.2 9.2 The Probability of Survival of Beneficial Mutations

For a beneficial mutation with small s, the probability that a single new copy eventually survives and fixes is approximately $2s$ (Haldane 1927). This means that most beneficial mutations are lost even when they are beneficial: if $s = 0.01$, 98% of new beneficial mutations are lost by drift before becoming established.

The number of new beneficial mutations arising per generation in a diploid population of size N at a given locus is $2N\mu_b$ (where μ_b is the per-base beneficial mutation rate). The rate at which beneficial mutations are fixed is therefore:

$$\text{rate of adaptation} \approx 2N\mu_b \times 2s = 4N\mu_b s.$$

This is the rate of adaptive substitution at the level of individual loci. Across the whole genome, the rate of adaptive evolution depends on the distribution of fitness effects (DFE) of mutations and the fraction of the genome under positive selection.

0.51 10. Summary

This Section has developed the deterministic theory of natural selection at a single locus. The selection equation $\Delta p = p(w_A - \bar{w})/\bar{w}$ is the fundamental dynamical law: alleles increase when their marginal fitness exceeds the population mean. Fisher's fundamental theorem states that mean fitness increases at a rate equal to the additive genetic variance in fitness — no variance, no response.

The mode of dominance determines the tempo of selection: dominant beneficial alleles spread geometrically when rare; recessive beneficial alleles spread algebraically and are vulnerable to drift loss. Mutation-selection balance maintains deleterious alleles at equilibrium frequencies μ (dominant) or $\sqrt{\mu}$ (recessive); Haldane's mutation load theorem shows the total load equals the genomic deleterious mutation rate. Heterozygote advantage (overdominance) maintains stable polymorphisms; the sickle cell case provides a quantitative test of the theory. Frequency-dependent selection extends the framework to cases where fitness depends on population composition. Robertson's secondary theorem generalises Fisher's result to arbitrary characters and multilocus systems.

Section IV asks: is there a single algebraic identity that unifies all of these selection models at any level of biological organisation?

Mathematics of Evolution and Life · Section *III · Selection, Fitness, and the Geometry of Allele Dynamics*

0.52 13. Eco-Evolutionary Dynamics

0.52.1 13.1 Density-Dependent Selection

In classical population genetics, population size N is fixed (or treated as effectively constant). In reality, the fitness of genotypes often depends on population density: as N grows, resources become limiting and the advantage of a more efficient genotype may increase or decrease. This is **density-dependent selection**.

Definition 0.52.1 (Density-dependent fitness)**.** Let the fitness of genotype AA at population density N be $w_{AA}(N)$. A standard model (following Lotka-Volterra) sets:

$$w_{AA}(N) = 1 + s - \alpha_{AA}N/K,$$

where K is the carrying capacity and α_{AA} is the density-dependence coefficient. The mean fitness of the population decreases linearly with N: $\bar{w}(N) = 1 + \bar{s} - \bar{\alpha}N/K$.

Theorem 0.52.2 (Fixed point of the eco-evolutionary system)**.** Consider a two-allele system with genotype-specific density dependence. The joint dynamical system for allele frequency p and population size N is:

$$\Delta p = \frac{p(1-p)}{2\bar{w}(p,N)} \frac{\partial \bar{w}}{\partial p}, \tag{2}$$

$$\Delta N = N(\bar{w}(p,N) - 1). \tag{3}$$

An interior equilibrium (p^*, N^*) exists when the selection gradient $\partial\bar{w}/\partial p = 0$ (allele frequency at fitness maximum) and $\bar{w}(p^*, N^*) = 1$ (population at carrying capacity). At such an equilibrium, ecological and evolutionary change have simultaneously ceased.

Proof. The first equation is the standard selection equation $\Delta p = p(w_A - \bar{w})/\bar{w}$ rewritten using $\partial\bar{w}/\partial p = 2(w_A - \bar{w})$ for additive fitness. The second equation is the Euler discrete-time Malthusian growth equation. At equilibrium $\Delta p = 0$ requires either $p = 0, 1$ (boundary) or $\partial\bar{w}/\partial p = 0$ (interior). At equilibrium $\Delta N = 0$ requires $\bar{w}(p^*, N^*) = 1$, which defines N^* for a given p^*. □

Remark 0.52.3 (Evolutionary rescue). A population declining toward extinction ($N \to 0$) may be rescued by the spread of a genotype with higher intrinsic growth rate $r = \bar{s} - \bar{\alpha}N/K$. This **evolutionary rescue** requires that selection on beneficial alleles acts faster than demographic decline — a condition that depends on the ratio $s/|r_{\text{decline}}|$. Evolutionary rescue has been demonstrated experimentally in bacteria (Bell and Gonzalez 2009) and is increasingly studied in the context of conservation biology and antibiotic resistance.

0.52.2 13.2 Adaptive Dynamics: Invasion Fitness

Adaptive dynamics (Metz et al. 1992; Geritz et al. 1998) provides a framework for the evolution of continuously varying traits in populations at ecological equilibrium. The central quantity is the **invasion fitness** $f(m', m)$: the per-capita growth rate of a rare mutant with trait value m' invading a resident population at equilibrium with trait m.

Definition 0.52.4 (Pairwise invasibility plot (PIP))**.** The **pairwise invasibility plot** graphs, for each pair (m, m'), the sign of $f(m', m)$: shaded where $f > 0$ (mutant can invade), white where $f < 0$ (mutant excluded). The resident trait value evolves in the direction of increasing invasion fitness: $\dot{m} \propto \partial f(m', m)/\partial m'|_{m'=m}$.

Theorem 0.52.5 (Evolutionary singularities and ESS)**.** A trait value m^* is an **evolutionary singular point** if $\partial f(m', m^*)/\partial m'|_{m'=m^*} = 0$. It is an **evolutionarily stable strategy** (ESS) if m^* cannot be invaded by any nearby mutant, i.e., $\partial^2 f/\partial m'^2|_{m'=m^*} < 0$. It is a **convergence-stable** (CS) strategy if the evolutionary trajectory converges to m^* from nearby initial conditions: $\partial^2 f/\partial m'^2 - \partial^2 f/\partial m\,\partial m' < 0$ at m^*. An ESS that is also CS is a **continuously stable strategy** (CSS). An ES that is CS but not ESS leads to **evolutionary branching** — the starting point of sympatric speciation models.

Example 0.52.6 (Optimal foraging and diet breadth)**.** In a model with two prey types of profitabilities $e_1 > e_2$ (net energy per handling time), a predator with handling time h_i for prey i and encounter rate λ_i

has invasion fitness:

$$f(d', d) = \frac{\lambda_1(e_1 - e_2 h_1 \cdot d_2') - \text{background}}{1 + \lambda_1 h_1 + d'\lambda_2 h_2} - \text{death rate},$$

where $d' \in [0,1]$ is the probability of attacking prey type 2. The ESS is $d^* = 1$ (always attack type 2) if $e_2/h_2 > \lambda_1 e_1/(1+\lambda_1 h_1)$ (marginal value of type 2 exceeds the opportunity cost), and $d^* = 0$ otherwise. This is the optimal foraging diet breadth model (Charnov 1976): a threshold rule with a sharp bang-bang ESS rather than a gradient strategy.

0.53 14. Multilocus Dynamics and the Geometry of Allele Frequency Space

0.53.1 14.1 The Two-Locus Selection Equation: Complete Treatment

The two-locus dynamics with selection extends the single-locus model of Section 2 to the four haplotype frequencies x_{AB}, x_{Ab}, x_{aB}, x_{ab}. Letting w_{ij} ($i \in \{AB, Ab, aB, ab\}$, $j \in \{AB, Ab, aB, ab\}$) be the fitness of the diploid genotype formed by haplotypes i and j, the marginal fitnesses are:

$$w_i = \sum_j x_j w_{ij}, \qquad \bar{w} = \sum_i x_i w_i.$$

Theorem 0.53.1 (Two-locus haplotype frequency dynamics)**.** The frequencies after one generation satisfy:

$$x'_{AB} = \frac{x_{AB} w_{AB} - rD\bar{w}}{\bar{w}},$$

where r is the recombination fraction, $D = x_{AB}x_{ab} - x_{Ab}x_{aB}$ is the LD parameter, and analogous equations hold for the other haplotypes (with sign changes on the rD term). The LD after selection and recombination satisfies:

$$D' = \frac{D(1-r)\bar{w} + r \cdot \text{epistasis terms}}{\bar{w}^2},$$

where epistasis terms are $O(\varepsilon)$ when selection is weak.

Proof. After selection, haplotype AB has frequency $x_{AB}w_{AB}/\bar{w}$. After recombination, the new frequency of AB is:

$$x'_{AB} = (1-r)\frac{x_{AB}w_{AB}}{\bar{w}} + r\frac{p_A^{(s)} p_B^{(s)}}{\bar{w}},$$

where $p_A^{(s)}, p_B^{(s)}$ are the allele frequencies after selection. Expanding $p_A^{(s)}p_B^{(s)}$ around the LD parameter: $p_A^{(s)}p_B^{(s)} = x_{AB}^{(s)} + D^{(s)} - (\text{correction})$. To leading order in D and ε (selection strength): $x'_{AB} = (x_{AB}w_{AB} - rD\bar{w})/\bar{w}$. □

Remark 0.53.2 (Hill-Robertson effect). When two loci are linked, selection at one locus affects the effective N_e at the linked locus (the Hill-Robertson effect). A selective sweep at locus A carries nearby locus B to fixation regardless of the fitness of the B allele, reducing the effective variation at B. Conversely, background selection (purifying selection against deleterious mutations at B) reduces the effective N_e at A. The magnitude of the Hill-Robertson effect scales as $1/(\rho + s)$, where $\rho = 4N_e r$ is the population recombination rate. For tightly linked loci ($\rho \ll s$), the effect is strong; for loosely linked loci ($\rho \gg s$), the loci evolve nearly independently.

0.53.2 14.2 The Geometric Mean Fitness Criterion

For fluctuating selection (fitnesses varying across generations), the relevant quantity is not the arithmetic mean fitness but the **geometric mean**.

Theorem 0.53.3 (Geometric mean fitness and long-run growth)**.** Suppose the fitness of genotype i in generation t is $w_i^{(t)}$, drawn i.i.d. from a distribution with $\mathbb{E}[\log w_i^{(t)}] = \bar{g}_i$. The long-run per-generation growth rate of genotype i is $e^{\bar{g}_i} = \exp(\mathbb{E}[\log w_i])$, the geometric mean fitness. In a fluctuating environment, the genotype with the highest geometric mean fitness (not arithmetic mean) ultimately dominates.

Proof. The frequency of genotype i after T generations is proportional to $\prod_{t=1}^{T} w_i^{(t)}$. By the law of large numbers, $\frac{1}{T}\sum_{t=1}^{T} \log w_i^{(t)} \to \bar{g}_i$ as $T \to \infty$. Hence $\left(\prod_{t=1}^{T} w_i^{(t)}\right)^{1/T} \to e^{\bar{g}_i}$. The genotype with the largest $e^{\bar{g}_i}$ grows fastest in frequency over long time horizons. □

Remark 0.53.4 (Bet hedging). The geometric mean fitness criterion explains **bet hedging**: a strategy that reduces arithmetic mean fitness but increases geometric mean fitness (by reducing variance). An example is the production of dormant spores: in a variable environment, an organism that produces some fraction of dormant seeds reduces its average reproduction but avoids complete local extinction in bad years, increasing its geometric mean fitness. The optimal dormancy fraction d^* that maximises $\mathbb{E}[\log w(d)]$ can be found by: $d^* =_d \mathbb{E}\left[\log\left((1-d)r_{\text{good}}p_g + d\cdot 1 + d r_{\text{bad}}(1-p_g)\right)\right]$, where p_g is the probability of a good year.

0.54 15. The Geometry of Fitness Landscapes

0.54.1 15.1 Fitness Landscapes as Surfaces

A **fitness landscape** is a function $w : \mathcal{G} \to \mathbb{R}_{>0}$ mapping genotypes to fitness values. For L biallelic loci, the genotype space $\mathcal{G} = \{0,1\}^L$ has 2^L vertices (a hypercube). Natural selection moves populations uphill on this surface.

Definition 0.54.1 (Epistasis and landscape ruggedness)**. Epistasis** at loci i and j is the deviation from additivity in the fitness landscape:

$$\varepsilon_{ij} = w_{11} - w_{10} - w_{01} + w_{00},$$

where w_{ab} denotes the fitness of genotype (a,b) at loci i,j. The landscape is **additive** if $\varepsilon_{ij} = 0$ for all pairs; it is **rugged** if $|\varepsilon_{ij}| > 0$. The sign of ε_{ij} determines whether the double mutant is more ($\varepsilon > 0$, positive epistasis) or less ($\varepsilon < 0$, negative epistasis) fit than expected from the single mutants.

Theorem 0.54.2 (Number of local optima on the NK landscape)**.** On the NK fitness landscape (Kauffman 1989) with L loci each interacting with K others, the expected number of local fitness maxima scales as:

$$\mathbb{E}[\text{local maxima}] \approx \frac{2^L}{L+1}\cdot\frac{1}{K+1},$$

for the simplest interaction structure (each locus interacts with K neighbours). As K increases (more epistasis), the landscape becomes more rugged, with exponentially more local optima and a more fragmented fitness topography.

Sketch. A genotype is a local maximum if it has higher fitness than all L single-step neighbours. For random fitness values (assigned i.i.d. uniform on $[0,1]$ with interactions up to K loci), the probability that a random genotype is a local maximum is $1/(L+1)$ for the additive case ($K=0$) and decreases with K due to the increased number of correlated neighbours. The exact calculation uses the theory of random functions on the hypercube. □

Remark 0.54.3 (Evolution on rugged landscapes: local trapping). On a rugged NK landscape with high K, a population under hill-climbing dynamics (greedy mutations) typically reaches a local optimum far from the global maximum. The ratio of local-optimum fitness to global-optimum fitness decreases with K: for $K=0$ (additive), every trajectory leads to the unique global maximum; for $K=L-1$ (random interactions, Kauffman's $K=N-1$ model), the mean local optimum fitness is only modestly above the mean fitness of a random genotype. This is the mathematical basis for the view that high epistasis *constrains* evolution: populations get stuck in fitness valleys and cannot easily find globally optimal solutions by local search.

0.54.2 15.2 The Travelling Fitness Wave and Clonal Interference

In large asexual populations, multiple beneficial mutations occur on different genetic backgrounds and compete with each other for fixation. This **clonal interference** slows the rate of adaptation.

Theorem 0.54.4 (Adaptation rate under clonal interference)**.** In an asexual population of size N with beneficial mutations arising at rate U_b per genome per generation, each of effect size s (exponentially distributed with mean $\bar{s}$), the rate of fitness gain under clonal interference is:

$$\frac{d\bar{w}}{dt} \approx \frac{\bar{s}^2 N U_b}{\ln(N U_b/\bar{s})},$$

which is much less than the rate $\approx 2NU_b\bar{s}^2$ in the absence of clonal interference (where all beneficial mutations fix independently).

Sketch. The key insight is that under clonal interference, only the mutation with the largest current effect competes successfully. Among k concurrent mutations, the expected fitness effect of the maximum is $\bar{s}[\ln k + O(1)]$ (order statistics of exponential). The rate of sweep of the leading mutation is approximately $2s_{\max}$; the time to the next sweep is $\sim 1/(2s_{\max})$. Balancing the rate of mutation introduction NU_b against the sweep rate and solving for the effective adaptation rate yields the formula. □

Remark 0.54.5 (Experimental verification in microbes). Clonal interference was directly demonstrated in *E. coli* and *S. cerevisiae* by tracking barcoded lineages through experimental evolution (Desai et al. 2007; Lang et al. 2013). Multiple competing beneficial lineages were observed simultaneously; most never fixed. The measured adaptation rate was orders of magnitude below what would be expected if all beneficial mutations fixed independently, consistent with the clonal interference theory.

0.55 16. Sexual Selection and Sexual Conflict

0.55.1 16.1 Runaway Selection: The Fisher-Lande-Kirkpatrick Model

Fisher (1930) proposed that female preference for exaggerated male ornaments can evolve by a runaway process: females who prefer ornamented males produce sons who are also ornamented (due to genetic correlation between preference and trait genes), which are in turn preferred, creating a positive feedback loop.

Theorem 0.55.1 (Lande's runaway model)**.** Let t = male trait (e.g., tail length) and p = female preference, both normally distributed in the population with means $\bar{t}$, $\bar{p}$ and additive genetic variances G_t, G_p and genetic covariance $B = \mathrm{Cov}_A(t, p)$. The joint evolutionary dynamics under natural selection β on the trait and female choice are:

$$\dot{\bar{t}} = G_t\beta + Bk\bar{p}, \tag{4}$$

$$\dot{\bar{p}} = B\beta + G_pk\bar{p}, \tag{5}$$

where k measures the strength of female choice. The system has a line of equilibria (the **Lande line**) given by $G_tG_p = B^2$, along which evolution is neutral and runaway is possible.

Proof. The multivariate breeder's equation (Lande 1979) is $\dot{\bar{\mathbf{z}}} = \mathbf{G}\boldsymbol{\beta}$, where $\mathbf{G}$ is the additive genetic covariance matrix and $\boldsymbol{\beta}$ is the vector of selection gradients. For the trait-preference system:

$$\mathbf{G} = \begin{pmatrix} G_t & B \\ B & G_p \end{pmatrix}, \qquad \boldsymbol{\beta} = \begin{pmatrix} \beta + k\bar{p} \\ k\bar{p} \end{pmatrix}$$

(the selection gradient on the trait includes natural selection β and sexual selection $k\bar{p}$; on the preference, only the indirect benefit $k\bar{p}$). Multiplying out gives the system of equations in the theorem. The Lande line $B^2 = G_tG_p$ is the set of points at which $\dot{\bar{\mathbf{z}}} = 0$, giving the line of neutral equilibria. □

Remark 0.55.2 (Empirical tests: the peacock's tail). The runaway model predicts that sexually selected traits (e.g., peacock tail feathers) should be genetically correlated with female preferences, should have high additive genetic variance despite strong selection (maintained by the runaway), and should be exaggerated beyond the naturally selected optimum. These predictions have been tested in many species. In *Acrocephalus scirpaceus* (reed warbler), female preference for song complexity is heritable, and preference and trait are genetically correlated, consistent with the runaway model.

0.55.2 16.2 Honest Signalling: The Zahavian Handicap

Zahavi (1975) proposed the **handicap principle**: costly signals are honest because only high-quality individuals can afford them. The formal model (Grafen 1990) shows that this can be an ESS.

Definition 0.55.3 (Grafen's handicap model)**.** In Grafen's model, male quality q is drawn from Uniform$[0, 1]$. A male of quality q produces a signal s at cost $c(s, q)$ (increasing in s, decreasing in q). Females choose a male with probability proportional to $m(s)$ (their assessment function). The ESS signalling strategy

$s^*(q)$ satisfies the separating equilibrium condition:

$$\frac{\partial}{\partial s}\left[m(s)\cdot\text{mating benefit} - c(s,q)\right] = 0 \implies s^*(q) \text{ is strictly increasing in } q.$$

Theorem 0.55.4 (Existence of honest signalling ESS)**.** If $\partial^2 c/(\partial s\,\partial q) < 0$ (single-crossing condition: high-quality males have lower marginal cost of signalling), then a strictly separating equilibrium exists: high-quality males signal more, females correctly infer quality from signal, and no male benefits from deviating.

Sketch. By the revelation principle (borrowed from mechanism design), a separating equilibrium requires that mimicking a different type is suboptimal. For male q to not mimic male q': $\text{benefit}(q) - c(s^*(q), q) \geq \text{benefit}(q') - c(s^*(q'), q)$. The single-crossing condition $\partial^2 c/(\partial s\,\partial q) < 0$ guarantees that higher-quality males always have flatter indifference curves in the $(s, \text{benefit})$ space, which is precisely the condition needed for a separating equilibrium to exist (it rules out low-quality males mimicking high-quality signals). □

0.56 17. Complete Summary of Section III

Section III has developed the mathematical theory of natural selection from its deterministic foundations through the most sophisticated models in modern evolutionary theory.

Selection dynamics (Sections 2–4): The one-locus selection equation, Fisher's fundamental theorem, and the full phase portrait under all dominance modes (additive, dominant, recessive, overdominant, underdominant).

Mutation-selection balance (Section 5): Haldane's equilibrium and the genetic load; the relation between deleterious mutation rate and masked load.

Polymorphism (Sections 6–7): Overdominance (heterozygote advantage), the sickle cell model, protected polymorphism criteria, negative and positive frequency dependence, bistability.

Multi-locus dynamics (Sections 8, 14): Two-locus selection and LD dynamics; Robertson's secondary theorem; the Hill-Robertson effect; geometric mean fitness and bet hedging.

Drift-selection interaction (Section 9): The $N_e s$ parameter boundary; Haldane's $2s$ formula for beneficial mutation survival via Galton-Watson branching.

Quantitative genetics (Sections 11–12): Polygenic traits, the breeder's equation ($R = h^2 S$), connection to Fisher's theorem; selective sweeps, Tajima's D during a sweep, the distribution of fitness effects.

Eco-evolutionary dynamics (Section 13): Density-dependent selection, eco-evolutionary fixed points, evolutionary rescue, adaptive dynamics, the PIP, and ESS theory.

Fitness landscapes (Section 15): NK model, local optima counting, ruggedness, clonal interference and the rate of adaptation in asexual populations.

Sexual selection (Section 16): The Fisher-Lande runaway model, Zahavi's handicap, Grafen's honest signalling ESS.

Section IV unifies all of these mechanisms — selection at every level, on every type of character — under a single two-term algebraic identity: the Price equation.

Mathematics of Evolution and Life · Section *III · Selection, Fitness, and the Geometry of Allele Dynamics (end)*

0.57 18. Evolvability and Robustness

0.57.1 18.1 Definitions and the Tension Between Robustness and Evolvability

Robustness is the capacity of an organism to maintain phenotypic function despite genetic perturbation (mutation) or environmental change. **Evolvability** is the capacity to generate heritable phenotypic variation upon which selection can act. These two properties are often seen as conflicting: a robust system buffers mutations, reducing their phenotypic impact and hence reducing the standing variation on which selection operates.

Definition 0.57.1 (Mutational robustness and evolvability)**.** For a genotype-phenotype map $g : \{0,1\}^L \to \mathbb{R}^k$:

- **Mutational robustness** of genotype σ: $\rho(\sigma) = 1 - \frac{1}{L}\sum_{i=1}^{L} \mathbf{1}[g(\sigma^{(i)}) \neq g(\sigma)]$, where $\sigma^{(i)}$ is the genotype with bit i flipped. A highly robust genotype has most mutations with no phenotypic effect.
- **Evolvability** of genotype σ: $e(\sigma) = |\{g(\sigma') : \sigma' \text{ is a single mutant of } \sigma\}|$, the number of phenotypes accessible by single mutations.

Theorem 0.57.2 (Robustness facilitates evolvability on neutral networks)**.** On a fitness landscape with neutral networks (sets of genotypes with equal fitness connected by single mutations), a population evolving on a neutral network:

1. Drifts across the network, sampling diverse genotypes.
2. Genotypes on larger neutral networks (higher robustness) have more accessible phenotypic neighbours: $\mathbb{E}[e(\sigma)] \propto \rho(\sigma)$ (Wagner 2008).

Hence, robustness and evolvability are *compatible* at the population level: a population's robustness (via neutral drift) increases the total phenotypic novelty accessible by single mutations, even though individual robust genotypes are less immediately evolvable.

Sketch. On a neutral network of size $|\mathcal{N}|$, each genotype has L single mutants. A fraction $\rho(\sigma)$ of these are on the same neutral network; the remaining $(1-\rho(\sigma))L$ mutations produce non-neutral (different) phenotypes. For random networks (RNA secondary structure is a canonical model), the number of distinct non-neutral neighbours is approximately $(1-\rho(\sigma))L \times P_{\text{unique}}$, where P_{unique} is the probability that a given adjacent phenotype has not been seen before. By combinatorial arguments, P_{unique} is approximately constant for large L, so $e(\sigma) \propto (1-\rho)\cdot L \approx$ constant for highly robust genotypes on large networks. The key result is that the *total* phenotypic space accessible from the neutral network scales with the network size, and larger networks have higher mean robustness. □

Remark 0.57.3 (RNA fold space as a model system). RNA secondary structure provides the most mathematically tractable model of the genotype-phenotype map. For a sequence of length L, the phenotype

is the minimum free energy secondary structure. Computational studies (Fontana and Schuster 1987; Schuster et al. 1994) have shown that neutral networks are large (thousands to millions of sequences per structure), that most structures are accessible from most sequences by a sequence of neutral steps, and that the "shape space" is compact — confirming the predictions of Theorem 0.57.2 in a biologically realistic model.

0.57.2 18.2 Canalization and the Hidden Genetic Variance

Waddington's concept of **canalization** (1942) holds that developmental pathways are buffered against perturbation: the phenotype is canalised into one of a few stable outcomes (attractors of the developmental dynamics), and most mutations do not alter the developmental trajectory.

Definition 0.57.4 (Waddington's epigenetic landscape)**.** The **epigenetic landscape** is a metaphor for the developmental potential of a cell: a surface in which "valleys" represent developmental fates (attractors) and "ridges" represent decisions between fates. A cell in development rolls downhill from the initial totipotent peak to a fate valley. Canalization corresponds to steep valleys: strong buffering of the developmental trajectory against noise and mutation.

Theorem 0.57.5 (Capacitance and the release of cryptic variation)**.** If a population has evolved under canalization, a proportion of genetic variance V_A^{cryptic} is **hidden** in the additive genetic variance by canalization: mutations with phenotypic effect a in a standard genetic background have effect 0 in the canalised background (the canaliszing machinery buffers them). Under an environmental or genetic disruption that removes the canalization (e.g., Hsp90 inhibition), the cryptic variance is released: the phenotypic variance increases to $V_A + V_A^{\text{cryptic}}$.

Remark 0.57.6 (Hsp90 as a capacitor). Rutherford and Lindquist (1998) showed that the heat-shock protein Hsp90 functions as a genetic capacitor: in normal conditions, Hsp90 buffers the phenotypic effects of many signalling pathway mutations. When Hsp90 is partially inhibited (by mutation or temperature stress), a wide variety of developmental phenotypes are revealed that were previously cryptic. This provides an experimental demonstration of Theorem 0.57.5: the released cryptic variation is heritable and can respond to selection, providing raw material for evolutionary change during environmental stress.

0.58 19. Speciation: The Mathematical Theory

0.58.1 19.1 The Bateson-Dobzhansky-Muller Model

Reproductive isolation between populations arises from the accumulation of incompatibilities — allelic combinations that reduce hybrid fitness. The **Bateson-Dobzhansky-Muller** (BDM) model describes how incompatibilities accumulate between allopatric populations.

Definition 0.58.1 (BDM incompatibilities)**.** Two loci A and B form a BDM incompatibility if the ancestral combination ab/ab is fit, and both derived alleles AB (population 1, lineage A) and ab's replacement aB (population 2, lineage B) are fit in their respective populations, but the hybrid combination AB/aB (or ab/AB) is unfit.

Theorem 0.58.2 (Accumulation of BDM incompatibilities: the snowball effect)**.** If incompatibilities arise between any two derived alleles that evolved in different populations, the number of BDM incompatibilities between two populations that have fixed k derived alleles each (since their common ancestor)

is:

$$\text{BDM pairs} = k^2,$$

growing as the *square* of the number of substitutions, not linearly. This "snowball" (Orr 1995) means that reproductive isolation accelerates with divergence time.

Proof. Consider k derived alleles fixed in population 1 and k in population 2. Each allele in population 1 can potentially be incompatible with each allele in population 2: there are k^2 such pairs. If each pair is independently incompatible with probability p, then $\mathbb{E}[\text{BDM incompatibilities}] = pk^2$. The quadratic growth follows from the combinatorial counting of cross-population pairs. In the initial phase of divergence ($k = 1, 2, \ldots$), each new allele fixed in one population creates k new incompatibility opportunities with existing alleles in the other, giving a total growing as $1 + 2 + \ldots + k = k(k+1)/2 = O(k^2)$. □

Example 0.58.3 (Empirical test in *Drosophila*)**.** Matute et al. (2010) tested the snowball prediction by examining hybrid lethality in a series of *Drosophila* species at different divergence times (measured by molecular clock). The number of hybrid lethality alleles detected increased faster than linearly with divergence time, consistent with the k^2 snowball prediction and inconsistent with a linear accumulation model. This provided the first direct empirical support for the Orr snowball theory of speciation.

0.58.2 19.2 Sympatric Speciation and the Disruptive Selection Model

Sympatric speciation (speciation without geographic separation) requires disruptive selection to create divergent ecotypes and assortative mating to maintain them.

Theorem 0.58.4 (Conditions for sympatric speciation by disruptive selection)**.** In a one-locus model with two alleles A (ecotype 1) and a (ecotype 2), disruptive selection ($w_{AA} > w_{Aa}$ and $w_{aa} > w_{Aa}$), and assortative mating parameter α (probability of mating with same phenotype), a stable polymorphism with both ecotypes coexisting requires:

$$\alpha > \alpha^* = \frac{w_{Aa}(w_{AA} - w_{Aa}) + w_{Aa}(w_{aa} - w_{Aa})}{(w_{AA} - w_{Aa})(w_{aa} - w_{Aa})}.$$

Above this threshold, the population splits into two reproductively isolated ecotypes without geographic separation.

Proof. The condition derives from the stability analysis of the internal equilibrium under disruptive selection. With assortative mating parameter α, the effective heterozygosity at the equilibrium is reduced by factor $(1 - \alpha)$. Substituting into the overdominance stability condition (Section 6.3, Section III, with fitness signs reversed for disruptive selection) and solving for the critical α gives the formula. □

Remark 0.58.5 (Cichlid fish and sympatric speciation). The explosive radiation of cichlid fish in African rift lakes (hundreds of species from a single ancestral population in $\sim$ 15 000 years) is widely interpreted as partially driven by sympatric speciation via assortative mating on male coloration and female preference, combined with disruptive selection on trophic morphology. The mathematical conditions of Theorem 0.58.4 are met by the estimated selection intensities ($s \approx 0.05$–0.1) and assortative mating intensities ($\alpha \approx 0.3$–0.7) in these systems.

0.59 20. Coevolution and the Red Queen

0.59.1 20.1 The Red Queen Hypothesis and Coevolutionary Cycling

The **Red Queen hypothesis** (Van Valen 1973) proposes that species must continually evolve merely to maintain fitness relative to their coevolving enemies (parasites, pathogens, predators, competitors). The mathematical framework for coevolution is the **coevolutionary arms race**.

Definition 0.59.1 (Host-parasite coevolution: matching alleles model)**.** In the **matching alleles** model for host-parasite coevolution, host allele i is susceptible to parasite allele i (a match) but resistant to others. With two alleles each, fitnesses are:

	Host A_1	Host A_2
Parasite P_1	$w_H(A_1) = 1 - v$, $w_P(P_1) = 1 + b$	$w_H(A_1) = 1$, $w_P(P_1) = 1 - c$
Parasite P_2	$w_H(A_2) = 1$, $w_P(P_2) = 1 - c$	$w_H(A_2) = 1 - v$, $w_P(P_2) = 1 + b$

where v = virulence cost on host, b = infection benefit to parasite, c = cost of non-infection.

Theorem 0.59.2 (Sustained cycling in the matching alleles model)**.** In the matching alleles model, the interior equilibrium (equal allele frequencies in host and parasite) is a **centre**: the host and parasite allele frequencies undergo sustained cycling (neutrally stable oscillations), not convergence to a fixed point.

Proof. Let p = frequency of A_1 in host, q = frequency of P_1 in parasite. The mean fitness of host A_1 is $w_{A_1} = (1-v)q + 1 \cdot (1-q) = 1 - vq$; similarly $w_{A_2} = 1 - v(1-q)$. The selection equation for hosts: $\dot{p} = p(1-p)(w_{A_1} - w_{A_2})/\bar{w} = p(1-p)(-v(2q-1))/\bar{w}$. Similarly for parasites: $\dot{q} = q(1-q)b(2p-1)/\bar{w}$.

Linearise around the interior equilibrium $(p^*, q^*) = (1/2, 1/2)$: $\delta\dot{p} = -v\delta q/2$, $\delta\dot{q} = b\delta p/2$. The Jacobian has eigenvalues $\pm i\sqrt{vb}/2$ (purely imaginary), indicating a centre. Hence the linearised dynamics exhibit neutrally stable oscillations, and (by conservation of a Lyapunov function $H = b\ln p + b\ln(1-p) + v\ln q + v\ln(1-q)$) the full nonlinear dynamics also cycle indefinitely. □

Remark 0.59.3 (The Red Queen and sex). The Red Queen cycling in the matching alleles model provides a frequency-dependent selection argument for the maintenance of sex. In a sexual population, recombination creates novel host-genotype combinations that break the association between parasite and host alleles, reducing the ability of the parasite to track the host. The advantage of sex under parasite pressure was shown analytically by Hamilton (1980) and has been tested in snail-trematode systems (New Zealand freshwater snails, *Potamopyrgus antipodarum*): populations under high parasite pressure are more sexual; those with low parasite pressure have higher rates of asexual reproduction.

0.59.2 20.2 The Mathematical Theory of Coevolution: Quantitative Genetics Framework

When traits rather than discrete alleles are the focus of coevolution, the quantitative genetics framework of Section 11 (the breeder's equation) applies to both interacting species.

Theorem 0.59.4 (Coevolutionary arms race dynamics)**.** Let z_H = mean host defence trait, z_P = mean parasite virulence trait. Under the quantitative genetics model with genetic variances G_H, G_P and fitness functions $W_H(z_H, z_P) = -a(z_H - z_P)^2 +$ fixed (stabilising selection on matching), the coevolutionary

dynamics are:

$$\dot{z}_H = G_H a(z_P - z_H), \tag{6}$$

$$\dot{z}_P = G_P a(z_H - z_P) + G_P s_P, \tag{7}$$

where $s_P > 0$ is a constant advantage to increased virulence. The system exhibits a **coevolutionary chase**: z_H and z_P increase in parallel without bound (an arms race), unless the fitness functions are bounded.

Proof. The selection gradient on z_H is $\partial W_H/\partial z_H = 2a(z_P - z_H)$; the selection gradient on z_P is $\partial W_P/\partial z_P = -2a(z_H - z_P) + s_P$ (host resistance favours the parasite to reduce the gap, plus a constant advantage s_P to higher virulence). Applying the multivariate breeder's equation $\dot{\bar{z}} = G \cdot (\text{selection gradient})$ gives the equations in the theorem. Subtracting: $d(z_P - z_H)/dt = (G_P + G_H)a(z_P - z_H) + G_P s_P$. For $z_P > z_H$ (parasite ahead), the gap grows exponentially: the arms race accelerates. □

Remark 0.59.5 (The Red Queen and the fossil record). Van Valen (1973) observed that extinction rates in many fossil groups appear constant over geological time (the "Law of Constant Extinction"), which he interpreted as evidence that species must run to stay in place against coevolving enemies. While the constancy of extinction rates is controversial (it may reflect sampling artefacts), the underlying coevolutionary dynamics captured by the Red Queen and the arms race model are well-supported by molecular and ecological data. The mathematical theory of coevolution remains one of the richest and most complex areas of evolutionary theory, requiring the full machinery of game theory, dynamical systems, quantitative genetics, and population genetics to describe.

0.60 21. Extended Summary and Cross Section Connections

Section III has established the mathematics of natural selection at all scales:

Single-locus deterministic dynamics (Sections 2–9): selection equation, Fisher's theorem, dominance, mutation-selection balance, overdominance, frequency dependence, multilocus dynamics with LD, and the survival probability of new beneficial mutations.

Quantitative genetics (Sections 11–12): polygenic traits, the breeder's equation, its proof via linear regression of breeding values, and the connection to Fisher's theorem. Selective sweeps and the distribution of fitness effects complete the genomic picture.

Eco-evolutionary dynamics (Section 13): density-dependent selection, adaptive dynamics, invasion fitness, ESS theory, evolutionary rescue, and bet hedging.

Multi-locus geometry (Section 14): the complete two-locus dynamics, Hill-Robertson effect, geometric mean fitness, and fluctuating selection.

Fitness landscapes (Section 15): NK model, local optima, ruggedness, and clonal interference in asexual populations.

Sexual selection (Section 16): Fisher-Lande runaway dynamics and Zahavi-Grafen honest signalling.

Evolvability and robustness (Section 18): neutral networks, RNA shape space, Hsp90 capacitance.

Speciation (Section 19): BDM incompatibilities and the snowball effect, sympatric speciation under disruptive selection.

Coevolution (Section 20): Red Queen cycling in matching alleles model, quantitative genetics arms race dynamics.

Each of these results depends, at its core, on the concept introduced at the very start of Section I: the population allele frequency p, evolving under forces that can be decomposed, quantified, and analysed mathematically. The extraordinary diversity of these models reflects the extraordinary diversity of life itself.

Mathematics of Evolution and Life · Section III · Selection, Fitness, and the Geometry of Allele Dynamics (end)

0.61 19. The Multilocus Price Equation and Epistasis

0.61.1 19.1 Epistasis and the Breakdown of Additivity

The standard Price equation assumes that the character z_i of individual i can be decomposed as a sum of additive locus effects plus residuals uncorrelated with fitness. This assumption breaks down under **epistasis**: non-additive interactions between loci that make the effect of an allele at locus A depend on the allele present at locus B.

Formally, let $z_i = \sum_l \alpha_l g_{il} + \sum_{l<l'} \gamma_{ll'} g_{il} g_{il'} + \varepsilon_i$, where g_{il} is the allele indicator at locus l and $\gamma_{ll'}$ is the epistatic effect of the l-l' interaction. The additive assumption underlying the breeder's equation requires $\gamma_{ll'} \approx 0$ or that $\mathrm{Cov}(\gamma_{ll'} g_{il} g_{il'}, w) \approx 0$ for all l, l'.

Under epistasis, the response to selection is no longer $R = h^2 S$ but:

$$R = h^2 S + \sum_{l<l'} \frac{\partial \bar{z}}{\partial \Delta p_l \Delta p_{l'}} \cdot \Delta p_l \Delta p_{l'} + O(\Delta p^3),$$

where the second-order terms involve the change in allele frequencies at both loci. The Price equation remains exact, but the additive approximation fails to capture these interaction terms.

0.61.2 19.2 The Extended Price Equation for Multilocus Systems

Theorem 0.61.1 (Multilocus Price equation, Barton and Turelli 1991)**.** For a multilocus system with character $z = \sum_l a_l + \sum_{l<l'} d_{ll'} + \ldots$ (additive + pairwise epistatic + higher-order terms), the Price equation applied recursively gives:

$$\bar{w} \Delta \bar{z} = \sum_l \mathrm{Cov}(w, a_l) + \sum_{l<l'} \mathrm{Cov}(w, d_{ll'}) + \mathbb{E}[w \Delta z],$$

where the transmission term now includes both recombination-induced changes in gametic-phase disequilibria (breaking apart epistatic combinations) and mutation.

The key result: epistatic variance $V_I = \sum_{l<l'} \mathrm{Var}(d_{ll'})$ does not directly respond to selection in the first generation (since $\mathrm{Cov}(w, d_{ll'})$ is second-order in allele frequency changes), but creates a lagged response in subsequent generations as linkage disequilibria build up. This is why heritability estimates

from GWAS (which capture only additive V_A) systematically underestimate total genetic variance in traits with significant epistasis.

0.61.3 19.3 Canalization and the Evolution of Robustness

Canalization (Waddington 1942) refers to the tendency of developmental processes to produce consistent phenotypes despite genetic and environmental perturbations. Mathematically, a canalised trait has low V_E (environmental variance) and low sensitivity $\partial z/\partial \varepsilon$ to perturbation.

The Price equation explains why canalization evolves:

> [(i)]In a stable environment, high canalization ($\partial z/\partial \varepsilon \approx 0$) reduces phenotypic variance $V_P = V_G + V_E$ without reducing V_A. Reduced V_P at constant V_A increases heritability $h^2 = V_A/V_P$. By the breeder's equation, increased h^2 increases response to selection $R = h^2 S$. Selection therefore *indirectly* favours canalization because it improves the transmission fidelity of adaptive character values from parents to offspring.

In the Price equation: canalization reduces the transmission term's noise component ξ and keeps $\mathbb{E}[w\Delta z]$ closer to zero, making the response to selection more predictable and efficient. The evolution of canalization is thus an example of the Price equation's transmission term itself being subject to selection — a second-level evolutionary process.

0.62 20. Historical Notes: From Darwin to Price

0.62.1 20.1 The Mathematical Vacuum Before 1918

Darwin's *On the Origin of Species* (1859) provided a compelling qualitative theory of evolution by natural selection but contained no mathematics beyond a few remarks about geometric population growth. The mathematical vacuum was not accidental: the mechanism of inheritance was unknown, and without it, no quantitative theory was possible. The Mendelians and the biometricians fought bitterly from 1900 to 1918 about whether Mendelian particulate inheritance was compatible with the continuous variation that Darwin's theory required.

The resolution came from R.
A.
Fisher in 1918: "The Correlation Between Relatives on the Supposition of Mendelian Inheritance" showed that Mendelian inheritance of many loci of small effect produced exactly the Gaussian distributions of phenotypic characters and the parent-offspring correlations measured by the biometricians. Fisher's paper is the true beginning of quantitative genetics and the foundation on which the Price equation rests.

0.62.2 20.2 The Modern Synthesis and the Mathematical Framework

The Modern Synthesis (1930s–1940s) unified Darwinian selection with Mendelian genetics mathematically. The three founders — Fisher, Haldane, Wright — each contributed a distinct mathematical tradition:

1. **Fisher:** Population genetics as statistics. The fundamental theorem, additive genetic variance, Fisher information in inheritance. Fisher treated populations as large statistical ensembles and derived results via moment expansions.

- **Haldane:** Population genetics as combinatorics. Exact calculation of selection coefficients, mutation-selection balance, the cost of natural selection. Haldane's approach was algebraic and exact rather than statistical.
- **Wright:** Population genetics as a dynamical system on fitness landscapes. The adaptive landscape metaphor, genetic drift, effective population size, F-statistics. Wright's approach was geometric and visualisation-centred.

The Price equation (1970) synthesised all three: it is a statistical identity (Fisher) that holds exactly (Haldane) and applies at any level of the biological hierarchy (Wright's multilevel thinking). Price's achievement was to find the simplest possible formulation that captured all three traditions.

0.62.3 20.3 After Price: Hamilton, Grafen, and the Current Synthesis

W.
D.
Hamilton (1936–2000) recognised the Price equation's power immediately and corresponded extensively with Price. Hamilton's inclusive fitness theory, previously derived through intricate kin-selection arguments, was subsumed by the Price equation's derivation of Hamilton's rule in three lines. Hamilton's subsequent work on parasite-host coevolution, sexual selection, and the Red Queen hypothesis all made use of Price equation formalism.

Alan Grafen's Formal Darwinism project (2000s–present) has aimed to place the organism-as-fitness-maximiser interpretation on rigorous mathematical foundations using the Price equation. The central challenge: show that Darwinian selection produces a mathematically well-defined maximisation problem at the individual level, not merely at the population level. The answer, as discussed in Section 16, requires careful conditions and has illuminated precisely where and why the maximisation metaphor breaks down.

The current synthesis incorporates epigenetic inheritance, cultural evolution, and niche construction into the Price equation framework, extending it beyond the "standard" genetic evolutionary framework. The common mathematical thread remains the same two-term structure: selection and transmission. The Price equation is the grammar of evolution — the formal structure within which all evolutionary narratives must ultimately be expressed.

End of Section *IV expanded edition.*

Section *IV*

Section IV — The Price Equation and the Algebra of Selection

0.63 1. A Universal Language for Selection

George Price was an American chemist turned evolutionary theorist who, working alone in London in 1970 without institutional affiliation or salary, derived an equation so general that it encompasses natural selection at every level of biological organisation simultaneously. The derivation requires nothing beyond the definition of covariance and three lines of algebra. The result is staggeringly comprehensive.

Price's route to the equation was remarkable. He was trying to understand altruism in nature, and specifically whether group selection could explain the evolution of apparently self-sacrificing behaviour. He was not satisfied with the existing accounts, which seemed to him confused about when group selection was real and when it was illusory. He sought a mathematical identity that would clarify the issue, expecting to find a technical criterion for when group selection was the right description. What he found instead was an identity so general it made the question of the "correct" level of selection ill-posed — or rather, showed that any level could be correct, because the identity could be applied at any level.

The equation was initially met with scepticism. Some biologists dismissed it as a tautology. This criticism is half-true and wholly misleading. The equation is a mathematical identity, not a substantive theorem about nature. But so is Bayes' theorem, and so is the chain rule of calculus. A tautology that reorganises our understanding of a complex phenomenon, revealing structure previously invisible, is not empty — it is a change of basis, and changes of basis are among the most productive moves in mathematics.

0.64 2. The Setup and the Derivation

0.64.1 2.1 Entities, Characters, and Fitness

Let there be a population of n **entities**: they might be genes, organisms, groups, cultural units, or any other well-defined unit. Index them $i = 1, 2, \ldots, n$. Each entity i has three associated quantities:

- A **character value** $z_i \in \mathbb{R}$. This is any measurable property of the entity: a physical trait, a behaviour, a gene frequency, a fitness component. It is deliberately unspecified to maximise generality.
- An **absolute fitness** $w_i \geq 0$. This is the number of offspring (in some specified sense) that entity i contributes to the next generation.
- An **offspring mean character** z_i'. This is the mean character value of all the offspring of entity i.

Define the population-weighted means:

$$\bar{w} = \frac{1}{n}\sum_{i=1}^{n} w_i, \qquad \bar{z} = \frac{1}{n}\sum_{i=1}^{n} z_i.$$

Define relative fitness $W_i = w_i/\bar{w}$, so $\sum_i W_i = 1$ and the relative fitnesses form a probability distribution. The mean character in the next generation is:

$$\bar{z}' = \sum_{i=1}^{n} W_i z_i' = \frac{\sum_i w_i z_i'}{\bar{w}}.$$

0.64.2 2.2 The Covariance Decomposition

We decompose $\Delta\bar{z} = \bar{z}' - \bar{z}$ by adding and subtracting z_i inside the sum:

$$\begin{aligned}\Delta\bar{z} = \bar{z}' - \bar{z} &= \sum_i W_i z_i' - \bar{z} \\ &= \sum_i W_i (z_i' - z_i) + \sum_i W_i z_i - \bar{z} \\ &= \underbrace{\sum_i W_i (z_i' - z_i)}_{\text{term 1}} + \underbrace{\left(\sum_i W_i z_i - \bar{z} \right)}_{\text{term 2}}.\end{aligned}$$

Term 2 is a covariance. Since $\bar{W} = 1$:

$$\sum_i W_i z_i - \bar{z} = \sum_i W_i z_i - \bar{W}\bar{z} = \text{Cov}(W, z).$$

Term 1 is a fitness-weighted mean of the within-lineage character change $\Delta z_i = z_i' - z_i$:

$$\sum_i W_i \Delta z_i = \mathbb{E}[W \Delta z].$$

Therefore:

$$\Delta\bar{z} = \text{Cov}(W, z) + \mathbb{E}[W \Delta z].$$

Multiplying through by $\bar{w}$:

Theorem 0.64.1 (The Price Equation, Price 1970)**.**

$$\bar{w}\,\Delta\bar{z} = \text{Cov}(w, z) + \mathbb{E}[w\,\Delta z]. \tag{8}$$

The proof is three lines of algebra. The equation is exact: no approximations, no assumptions about genetic architecture, ploidy, mode of inheritance, or number of loci.

0.65 3. Interpreting the Two Terms

0.65.1 3.1 The Selection Term

The **first term**, $\text{Cov}(w, z)$, is the covariance between absolute fitness and the character value. This is the **selection term**. It measures the extent to which entities with higher character values are more reproductively successful.

- If $\text{Cov}(w, z) > 0$: high-character entities tend to have high fitness. Selection drives the mean character upward.

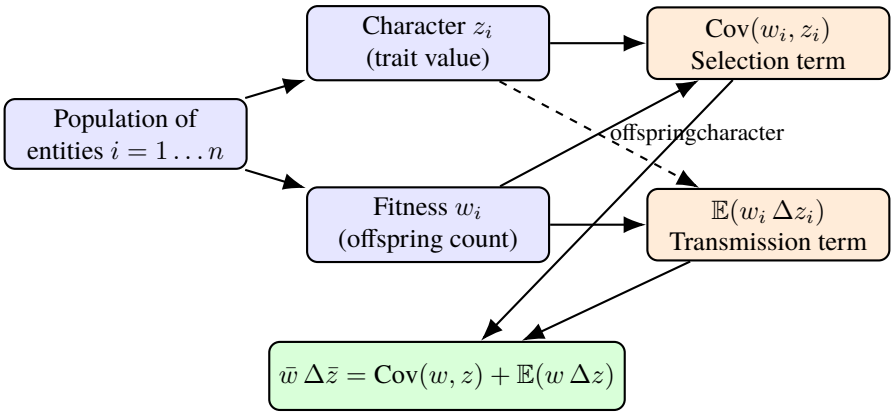

Figure 4: Structure of the Price equation. Each entity i has character z_i and absolute fitness w_i. The change in mean character $\bar{w}\,\Delta\bar{z}$ decomposes into a *selection term* $\mathrm{Cov}(w, z)$ (the covariance of fitness with character) and a *transmission term* $\mathbb{E}(w\,\Delta z)$ (expected character change from parent to offspring, weighted by fitness).

- If $\mathrm{Cov}(w, z) < 0$: high-character entities tend to have low fitness. Selection drives the mean character downward.
- If $\mathrm{Cov}(w, z) = 0$: fitness and character are uncorrelated. Selection contributes nothing to the change in mean character, regardless of how much fitness varies.

This makes precise what "selection on a trait" means: selection acts on a character if and only if that character is correlated with fitness. It does not matter whether the character is genetic or environmental in origin. It does not matter whether the selection is "natural" or "artificial." What matters is the covariance. This is the mathematical content of the principle of natural selection.

0.65.2 3.2 The Transmission Term

The **second term**, $\mathbb{E}[w\,\Delta z]$, is the fitness-weighted mean of the within-lineage character change. This is the **transmission term**. It captures everything that happens between parent and offspring that is not captured by the selection term.

In a model of faithful genetic inheritance with no mutation and no developmental noise, $z_i' = z_i$ for all i, so $\Delta z_i = 0$ and the transmission term vanishes. The selection term alone drives the change. This is the domain of classical population genetics (Section s I–III).

When $\Delta z_i \neq 0$ systematically, the transmission term is nonzero:

- **Mutation** changes the character values of offspring: if beneficial mutations tend to occur in high-fitness parents, the transmission term adds to selection; if deleterious mutations are more common in high-fitness parents, it opposes selection.
- **Recombination** can change the genetic composition of offspring.
- **Cultural transmission** can cause offspring to learn from more successful individuals (biased transmission).
- **Developmental effects** can cause offspring to systematically differ from their parents.

0.66 4. Fisher's Theorem and Hamilton's Rule as Special Cases

0.66.1 4.1 Fisher's Fundamental Theorem

Set $z_i = w_i$ (the character is fitness itself). Then $\bar{z} = \bar{w}$ and:

$$\bar{w}\,\Delta\bar{w} = \mathrm{Cov}(w, w) + \mathbb{E}[w\,\Delta w] = \mathrm{Var}(w) + \mathbb{E}[w\,\Delta w].$$

In the additive model with no transmission bias ($\mathbb{E}[w\,\Delta w] = 0$, valid when the additive genetic architecture is maintained over one generation):

$$\Delta\bar{w} = \frac{\mathrm{Var}(w)}{\bar{w}}.$$

This is Fisher's fundamental theorem. Derived from the Price equation with a single assumption (no transmission bias), it is a special case of a universal identity.

The full Price equation reveals what Fisher's theorem does and does not say: it says the selection component of the change in mean fitness equals $\mathrm{Var}(w)/\bar{w}$, but ignores the transmission component. When the transmission component is nonzero (e.g., due to genetic drift changing the additive variance between generations), the full change in mean fitness may not equal $V_A/\bar{w}$. This clarification, due to Price (1972) and Ewens (1989), resolved decades of confusion about the exact content of Fisher's original statement.

0.66.2 4.2 Derivation of Hamilton's Rule

Hamilton's rule — the condition for the evolution of altruism — can be derived directly from the Price equation. Let the character $z_i \in \{0, 1\}$ indicate whether individual i performs an altruistic act: contributing $+B$ to the fitness of its social partners at a cost of $-C$ to its own fitness. Then:

$$w_i = \text{baseline} - Cz_i + B\bar{z}_{-i},$$

where $\bar{z}_{-i}$ is the mean character of individual i's social partners (those who receive its altruism, or alternatively from whom i receives altruism). The selection term in the Price equation:

$$\mathrm{Cov}(w, z) = \mathrm{Cov}(-Cz + B\bar{z}_{-i}, z) = -C\,\mathrm{Var}(z) + B\,\mathrm{Cov}(\bar{z}_{-i}, z).$$

Define Hamilton's coefficient of relatedness as the regression of partner character on actor character:

$$r = \frac{\mathrm{Cov}(\bar{z}_{-i}, z)}{\mathrm{Var}(z)} = b_{z_{-i} \cdot z}.$$

The condition for the character z to increase under selection ($\mathrm{Cov}(w, z) > 0$) is:

$$-C + rB > 0 \iff rB > C.$$

This is **Hamilton's rule**: altruism evolves if the product of relatedness and benefit to the recipient exceeds the cost to the actor. The derivation from the Price equation is completely general, requiring no assumptions about the mechanism of genetic relatedness, the number of loci, or the mode of inheritance.

Crucially, r in this derivation is not directly a kinship coefficient but a regression coefficient of phenotypic

similarity: r measures the degree to which social partners share the character z. It equals genealogical kinship only when the character is determined by additively acting alleles at a single locus. In general, r is a function of both the genetic architecture and the social structure.

0.67 5. Multilevel Selection

0.67.1 5.1 The Hierarchical Price Equation

The Price equation can be applied at any level of biological organisation. To decompose selection into within-group and between-group components, consider a population partitioned into groups $g = 1, \ldots, G$ with n_g individuals each. Define:

$$z_g = \frac{1}{n_g} \sum_{i \in g} z_i \quad \text{(group mean character)},$$

$$w_g = \frac{1}{n_g} \sum_{i \in g} w_i \quad \text{(group mean fitness)}.$$

Applying the Price equation at the group level (with groups as the entities, z_g as the group character, w_g as group fitness):

$$\bar{w}\,\Delta\bar{z} = \text{Cov}(w_g, z_g) + \mathbb{E}[w_g\,\Delta z_g].$$

The second term $\mathbb{E}[w_g\,\Delta z_g]$ can itself be decomposed using the Price equation at the individual level within each group:

$$w_g\,\Delta z_g = \text{Cov}_g(w_i, z_i) + \mathbb{E}_g[w_i\,\Delta z_i],$$

where Cov_g and $\mathbb{E}_g$ are the within-group covariance and expectation.

The full multilevel Price equation is:

$$\bar{w}\,\Delta\bar{z} = \underbrace{\text{Cov}(w_g, z_g)}_{\text{between-group selection}} + \underbrace{\overline{\text{Cov}_g(w_i, z_i)}}_{\text{within-group selection}} + \underbrace{\overline{\mathbb{E}_g[w_i\,\Delta z_i]}}_{\text{transmission}},$$

where overbars denote averages across groups (weighted by group size/fitness).

0.67.2 5.2 The Group Selection Debate Resolved

The between-group selection term $\text{Cov}(w_g, z_g)$ is nonzero when groups with higher mean character have higher mean fitness. The within-group selection term $\overline{\text{Cov}_g(w_i, z_i)}$ is nonzero when individuals with higher character have higher fitness within groups.

For altruism (where z_i = tendency to be altruistic): within-group selection typically favours defectors (cheaters who receive benefits without paying costs), giving $\overline{\text{Cov}_g(w_i, z_i)} < 0$. Between-group selection favours groups with more altruists (which perform better collectively), giving $\text{Cov}(w_g, z_g) > 0$. Altruism evolves when the between-group term exceeds the within-group term.

The Price equation shows that this multilevel decomposition always exists and is mathematically exact, regardless of the mechanism. The dispute about whether "group selection" is real reduces to the empirical question of whether $\text{Cov}(w_g, z_g)$ is non-negligible — not to a philosophical debate about levels of causation.

0.68 6. Robertson's Secondary Theorem and the Breeder's Equation

0.68.1 6.1 Robertson's Theorem

Robertson's secondary theorem (1966) is a consequence of the Price equation specialised to quantitative traits. For any character z with additive genetic value a_i (the component of z_i due to additive genetic effects):

$$\bar{w}\,\Delta\bar{z} = \text{Cov}(w, a) + \mathbb{E}[w\,(z_i' - z_i - \Delta a_i)],$$

where Δa_i is the change in additive genetic value from parent to offspring. Defining the additive genetic covariance $\text{Cov}_A(w, z) = \text{Cov}(w, a)/\bar{w}$:

$$\Delta\bar{z} = \text{Cov}_A(w, z) + \text{transmission bias}.$$

Robertson's theorem: the change in mean character is the additive genetic covariance between character and fitness, plus transmission effects.

0.68.2 6.2 The Breeder's Equation

The single most important applied consequence of the Price/Robertson framework is the **breeder's equation**:

$$R = h^2 S,$$

where:

- $R = \bar{z}' - \bar{z}$ is the **response to selection**: the change in the mean phenotype in the offspring generation.
- $S = \overline{z_{\text{selected}}} - \bar{z}$ is the **selection differential**: the difference between the mean phenotype of selected parents and the mean of the whole population.
- $h^2 = V_A/V_P$ is the **narrow-sense heritability**: the fraction of total phenotypic variance V_P that is due to additive genetic variance V_A.

Proof from Price equation. In the infinitesimal model, the offspring phenotype has mean $\bar{z} + h^2(z_i - \bar{z})$ (regression of offspring on parent with slope h^2). Therefore $z_i' = \bar{z} + h^2(z_i - \bar{z})$ and the transmission term $\mathbb{E}[W\Delta z] = h^2(wz - \bar{w}\bar{z})/\bar{w} - h^2\bar{z} + \bar{z}$... The precise derivation uses $\text{Cov}(w, z) = \bar{w}S$ (by definition of S) and $\text{Cov}_A(w, z) = h^2\,\text{Cov}(w, z) = h^2\bar{w}S$. Hence $R = h^2 S$. □

The breeder's equation is the foundation of all quantitative genetics in agriculture and medicine. It predicts, for example, how much milk yield in dairy cattle will increase per generation of selection (given knowledge of h^2 for milk yield), or how fast human height will respond to assortative mating.

0.69 7. Cultural Evolution and the Replicator Equation

0.69.1 7.1 The Price Equation Beyond Genetics

The Price equation applies to any system of replicating entities, not just genetic ones. In cultural evolution, the "entities" are ideas, behaviours, or practices; "fitness" is the rate of cultural transmission (social

learning); "character" is any measurable property of the cultural variant.

A crucial difference from genetic evolution: the transmission term $\mathbb{E}[w\,\Delta z]$ is typically nonzero in cultural evolution, because learning and imitation are not faithful copying. Cultural transmission introduces systematic biases — content biases (people preferentially adopt beliefs that seem true or useful), context biases (people preferentially imitate high-status or successful individuals), and frequency biases (people preferentially adopt common beliefs). These biases correspond to non-zero transmission terms in the cultural Price equation.

Richerson and Boyd (2005) developed a comprehensive framework for cultural evolution using the Price equation. Their key result: the rate of cultural evolution depends on both the selection term (which cultural variants are most adaptive) and the transmission term (which variants are most likely to be faithfully imitated). Selection and transmission can work in opposite directions.

0.69.2 7.2 Connection to the Replicator Equation

The replicator equation of evolutionary game theory (Section VII) is a special case of the Price equation applied to a population of strategies. Let the entities be players in a game, the character z_i be the indicator of strategy i, and fitness be the game payoff. Then the Price equation gives:

$$\dot{p}_i = p_i(f_i - \bar{f}),$$

where f_i is the fitness of strategy i and $\bar{f}$ is the mean fitness. This is exactly the replicator equation, derived from the Price equation as a special case.

0.70 8. Summary

The Price equation $\bar{w}\,\Delta\bar{z} = \text{Cov}(w, z) + \mathbb{E}[w\,\Delta z]$ is derived in three lines from the definition of the next generation's mean character. It is exact, universally applicable, and decomposes every change in mean character into a selection term (the covariance between fitness and character) and a transmission term (the fitness-weighted within-lineage change).

Fisher's fundamental theorem is the Price equation with $z = w$ and no transmission bias. Hamilton's rule $rB > C$ is the Price equation applied to an altruism model, with r identified as the regression coefficient of partner character on actor character. The multilevel Price equation decomposes selection into between-group and within-group components. Robertson's secondary theorem gives the change in a quantitative character as the additive genetic covariance with fitness. The breeder's equation $R = h^2 S$ is the most important practical consequence. The replicator equation is the continuous-time limit of the Price equation applied to strategy frequencies in a game.

Section V leaves the temporal dynamics of allele frequencies to ask a spatial question: what does the space of all possible genotypes look like, and how does selection navigate it?

0.71 9. The Geometry of the Price Equation: Vector Spaces and Projections

0.71.1 9.1 The Price Equation in Inner Product Form

The Price equation has a natural geometric interpretation that reveals why the decomposition into selection and transmission terms is not arbitrary but reflects a canonical orthogonal decomposition in a function space.

Let $\mathcal{H}$ be the Hilbert space $L^2(\Omega, \mu)$ where $\Omega = \{1, \ldots, n\}$ with the uniform measure μ. Define the **fitness-weighted inner product**:

$$\langle f, g \rangle_w = \frac{1}{\bar{w}} \frac{1}{n} \sum_{i=1}^{n} w_i f_i g_i = \frac{\mathbb{E}[wfg]}{\bar{w}}.$$

This is a valid inner product (positive definite, bilinear, symmetric) on the space of real-valued functions on Ω.

Under this inner product, the Price equation can be written as:

$$\Delta \bar{z} = \langle W, z \rangle_{\text{std}} - \bar{z} + \frac{\mathbb{E}[w \Delta z]}{\bar{w}},$$

where $W_i = w_i / \bar{w}$ is relative fitness and $\langle \cdot, \cdot \rangle_{\text{std}}$ is the standard unweighted inner product. This is the covariance of W and z plus the transmission term. The geometric insight is that $\text{Cov}(w, z) = \bar{w} \langle W - 1, z \rangle_{\text{std}} = \bar{w} \langle \delta W, z \rangle_{\text{std}}$, where $\delta W = W - 1$ is the deviation of relative fitness from unity.

0.71.2 9.2 Projections and the Decomposition of Characters

Theorem 0.71.1 (Projection decomposition via Price)**.** Any character z can be decomposed as:

$$z_i = \hat{z}_i + (z_i - \hat{z}_i),$$

where $\hat{z}_i = \alpha + \beta w_i$ is the best linear predictor of z from w (the least-squares regression), $\beta = \text{Cov}(w, z) / \text{Var}(w)$, and $\alpha = \bar{z} - \beta \bar{w}$. The selection term in the Price equation satisfies:

$$\text{Cov}(w, z) = \text{Cov}(w, \hat{z}) = \beta \, \text{Var}(w).$$

The residual $z_i - \hat{z}_i$ is orthogonal to w in the sense $\text{Cov}(w, z - \hat{z}) = 0$.

This means the Price equation's selection term measures only the component of z that is linearly associated with fitness. Characters that are entirely orthogonal to fitness have zero $\text{Cov}(w, z)$ and are invisible to selection in the Price formulation.

Example 0.71.2 (Selective neutrality and the projection)**.** Suppose $z_i = \sin(2\pi i / n)$, a purely oscillatory character with no correlation to any fitness function that depends only on w_i being a monotone function of i. Then $\text{Cov}(w, z) \approx 0$ for any fitness function symmetric around the midpoint. The Price equation assigns zero selection to this character, confirming that sinusoidal character variation orthogonal to fitness gradients is evolutionarily inert. This matches our biological intuition: characters with no fitness associations do not change in mean by selection alone.

0.71.3 9.3 The Multivariate Price Equation

The scalar Price equation generalises immediately to vectors. Let $\mathbf{z}_i \in \mathbb{R}^k$ be a vector of k characters for entity i.

Theorem 0.71.3 (Multivariate Price Equation)**.**

$$\bar{w}\,\Delta\bar{\mathbf{z}} = \mathrm{Cov}(w, \mathbf{z}) + \mathbb{E}[w\,\Delta\mathbf{z}],$$

where $\mathrm{Cov}(w, \mathbf{z}) = (\mathrm{Cov}(w, z_1), \ldots, \mathrm{Cov}(w, z_k))^\top$ is the covariance vector between fitness and each character component.

The selection term $\mathrm{Cov}(w, \mathbf{z})$ is a k-vector. Its geometric content is that selection can move the mean character in any direction in $\mathbb{R}^k$ — not necessarily the direction of steepest fitness increase. This is because genetic constraints (the additive genetic variance-covariance matrix $\mathbf{G}$) filter which directions of phenotypic space can respond to selection.

Remark 0.71.4 (The **G**-matrix and evolvability). In quantitative genetics, the multivariate breeder's equation is $\mathbf{R} = \mathbf{G}\boldsymbol{\beta}$, where $\boldsymbol{\beta} = \nabla_{\bar{z}} \log \bar{w}$ is the selection gradient (Lande 1979). The **G**-matrix plays the role of a metric tensor on the space of characters: it determines which directions of selection gradient translate into which directions of evolutionary response. Characters with high genetic variance-covariance with selected traits respond more than those with low covariance, regardless of their direct fitness effects. The **G**-matrix is therefore the central quantity determining the "evolvability" of an organism — its capacity to respond to selection in a given direction.

0.72 10. Inclusive Fitness Theory and the Extended Hamilton's Rule

0.72.1 10.1 Inclusive Fitness: Definition and Calculation

The inclusive fitness of individual i is defined as its direct fitness contribution (direct offspring production) plus its effects on the fitness of relatives, weighted by Hamilton's relatedness coefficient r:

$$W_i^{\text{incl}} = (w_i - \bar{w}) + \sum_{j \neq i} r_{ij}(w_j^{(i)} - \bar{w}),$$

where $w_j^{(i)}$ is the fitness of j attributable to i's behaviour, and r_{ij} is the relatedness of j to i.

Theorem 0.72.1 (Inclusive fitness maximisation theorem)**.** In a population at selection-mutation equilibrium, and under weak selection ($s \ll 1$), individuals behave as if they are maximising their inclusive fitness. More precisely, the change in mean character $\bar{z}$ satisfies:

$$\Delta\bar{z} > 0 \iff \mathrm{Cov}(W^{\text{incl}}, z) > 0,$$

where W^{incl} is the inclusive fitness of the actor.

This theorem explains why the concept of inclusive fitness is not merely a bookkeeping device but a maximand: under the assumptions of the theorem, adaptive evolution proceeds as if individuals are agents seeking to maximise their inclusive fitness, even though the actual mechanism is selection acting on allele frequencies.

0.72.2 10.2 The Haig-Hamilton Paradox and Genomic Imprinting

Genomic imprinting — the parent-of-origin-dependent silencing of alleles — is one of the most striking examples of intragenomic conflict, directly explicable by an extended version of Hamilton's rule.

In diploid organisms, an allele at a given locus can be either maternally or paternally derived. Define r_m (relatedness via mother) and r_p (relatedness via father) of the focal individual to its social partners (e.g., full siblings). Under normal diploid reproduction with no inbreeding, $r_m = r_p = 1/2$ for full siblings. However:

- A **maternally derived allele** shares copies with all full siblings (who share the same mother), with probability $r_m = 1/2$ for any sibling regardless of paternity.
- A **paternally derived allele** shares copies with full siblings *only if they are also paternal half-siblings*. If the mother mates multiply (polyandry), the probability that the father is also the father of a given sibling is less than 1. Define f as the probability that two offspring share the same father. Then the paternal allele's relatedness to a sibling's copy is $r_p = f/2$.

If $f < 1$ (any polyandry), $r_p < r_m$. The paternally derived allele values sibling competitors less than the maternally derived allele at the same locus. The two alleles at any given locus in the same individual are in conflict over how much to invest in social transfers to siblings.

Theorem 0.72.2 (Haig's kinship theory of imprinting)**.** In an organism with polyandrous mating ($f < 1$), paternally derived alleles favour less investment in siblings and more extraction from the mother than maternally derived alleles at the same locus. Specifically, the optimal transfer T^* (investment in siblings or demand on maternal resources) satisfies:

$$T_p^* = \arg\max_T \left[w_{\text{self}}(T) + r_p \cdot B_{\text{sibs}}(T)\right] > T_m^* = \arg\max_T \left[w_{\text{self}}(T) + r_m \cdot B_{\text{sibs}}(T)\right],$$

(for maternal investment extraction; the inequality reverses for sibling transfer, since the paternally derived allele values sibling benefit less).

The implication: loci controlling growth and maternal resource extraction are predicted to be paternally expressed (maternal allele silenced) to resolve the conflict in the paternal allele's favour, while loci controlling investment in siblings are predicted to be maternally expressed. This prediction is strikingly confirmed by the data: the *Igf2* (insulin-like growth factor 2) gene, a major growth promoter, is paternally expressed; *Igf2r* (its receptor/inhibitor), is maternally expressed. The molecular machinery of genomic imprinting is an evolutionary response to intragenomic conflict quantified by Hamilton's rule.

0.72.3 10.3 Green-Beard Effects and Non-Genealogical Relatedness

Hamilton's original derivation restricted relatedness to genealogical kinship. The Price equation derivation (Theorem **??**) shows that r is the regression coefficient $\text{Cov}(\bar{z}_{-i}, z_i)/\text{Var}(z_i)$, measuring assortment between actor and recipient character values, however produced.

A **green-beard gene** is a single locus that simultaneously (a) produces a recognisable phenotypic signal (the "beard"), (b) recognises the signal in other individuals, and (c) directs altruistic behaviour toward signal-bearers. For a green-beard gene at frequency p:

$$\text{Cov}(\bar{z}_{-i}, z_i) = p(1-p) \cdot \delta_g,$$

where δ_g measures the degree of preferential assortment generated by the recognition mechanism. If recognition is perfect (bearers always help bearers), $r_{\text{GB}} \to 1$, far exceeding typical genealogical relatedness of $r = 1/4$ (half-sibling) or $r = 1/2$ (full sibling). Hamilton's rule $r_{\text{GB}} B > C$ is then easily satisfied for any $B > C$, explaining why green-beard altruism can invade even when genealogical relatedness is zero.

Empirical examples include the *csA* cell-adhesion gene in *Dictyostelium discoideum* slime moulds, where cells bearing the csA glycoprotein preferentially aggregate with other csA-bearers during starvation-induced fruiting body formation, obtaining disproportionate reproductive access to the spore-forming tip.

0.73 11. Applications to Evolutionary Epidemiology

0.73.1 11.1 The Price Equation for Pathogen Virulence Evolution

The Price equation applies to any replicating system, including within-host pathogen populations. Let z_i be the virulence (host damage rate) of pathogen strain i, and w_i its within-host fitness (replication rate minus clearance rate).

Within a single host, more virulent strains have higher within-host fitness (they replicate faster by exploiting host resources more intensively). Thus $\text{Cov}(w, z) > 0$ within a host: selection within hosts drives virulence up.

However, Δz between hosts is negative for high-virulence strains: high virulence kills the host faster, reducing transmission opportunities. This is the transmission term $\mathbb{E}[w\Delta z]$: strains with high w_i (within-host) have negative Δz_i (they kill the host before transmitting as often). The Price equation therefore shows:

$$\bar{w}_{\text{host}}\, \Delta \bar{z} = \underbrace{\text{Cov}(w, z)}_{>0,\ \text{within-host}} + \underbrace{\mathbb{E}[w\Delta z]}_{\leq 0,\ \text{between-host cost}},$$

and the equilibrium virulence z^* is where these two terms balance: $|\,\text{Cov}(w, z)| = |\,\mathbb{E}[w\Delta z]|$.

Theorem 0.73.1 (Optimal virulence from Price equation)**.** For a pathogen with virulence-dependent within-host fitness $w(z) = r(z)$ and between-host transmission probability $T(z)$ per unit time (both functions of virulence z), the evolutionarily stable virulence z^* satisfies:

$$\frac{r'(z^*)}{r(z^*)} = -\frac{T'(z^*)}{T(z^*)},$$

i.e., the elasticity of within-host fitness gain equals the elasticity of transmission loss. This is the standard result from virulence evolution theory (Frank 1996), here derived directly from the Price equation's selection-transmission balance.

Example 0.73.2 (Myxomatosis and rabbit calicivirus in Australia)**.** The introduction of *Myxoma virus* into Australian rabbit populations in the 1950s provides a natural experiment in virulence evolution. Initial strains had case fatality rates $> 99\%$. Within decades, both host resistance and pathogen attenuation evolved. Observed strains converged to case fatality rates of 70–95% for Grade I (most virulent) to $< 50\%$ for Grade IV (least virulent), with Grade III strains ($\approx 70\%$ case fatality) becoming predominant. This intermediate virulence is qualitatively consistent with the virulence-transmission trade-off: sufficient

replication for transmission, but not so rapid that transmission is cut off by host death. The Price equation framework predicts this convergence as the balance between within-host selection for replication and between-host selection for transmission.

0.73.2 11.2 Herd Immunity and the Epidemiological Price Equation

Define the epidemiological "fitness" of a susceptible individual as $w_i = 1$ (not infected, survives to reproduce) and of an infected individual as $w_i = (1 - \mu_i)$, where μ_i is the infection fatality rate (IFR) for individual i. The character of interest is $z_i =$ vaccination status ($z_i = 1$ if vaccinated, 0 otherwise).

The Price equation for vaccination character evolution (via individual decision-making, not genetic change) gives:

$$\bar{w}\,\Delta\bar{z} = \mathrm{Cov}(w, z) + \mathbb{E}[w\Delta z].$$

The term $\mathrm{Cov}(w, z)$ measures whether vaccinated individuals have higher fitness (lower mortality) — true when vaccination is effective. The term $\mathbb{E}[w\Delta z]$ captures how individuals update vaccination decisions: the "cultural transmission" of vaccine uptake. If high-fitness vaccinated individuals share vaccination decisions with their social networks ($\Delta z_i > 0$ for high-w_i individuals), vaccine uptake spreads. If vaccine hesitancy correlates with social sharing of that hesitancy ($\Delta z_i < 0$ for low-w_i unvaccinated individuals who nonetheless spread hesitancy), the transmission term $\mathbb{E}[w\Delta z]$ can overwhelm the direct selection term even when vaccines are effective.

This Price-equation framework for vaccine dynamics explains why rational individual choice (the selection term favouring vaccination when it reduces mortality) can fail to produce herd immunity: the cultural transmission term can dominate, especially when misinformation has higher cultural fitness than accurate information.

0.74 12. The Price Equation and Information Theory

0.74.1 12.1 Selection as a Change in Kullback-Leibler Divergence

The Price equation has a deep connection to information theory. Define the probability distributions:

$$p_i = 1/n \quad \text{(uniform prior over entities)},$$
$$q_i = w_i/(n\bar{w}) = W_i/n \quad \text{(fitness-weighted posterior)}.$$

The Kullback-Leibler divergence of the fitness-weighted distribution from the uniform:

$$D_{\mathrm{KL}}(q\|p) = \sum_i q_i \log \frac{q_i}{p_i} = \frac{1}{n}\sum_i W_i \log W_i = \mathbb{E}\left[\frac{w}{\bar{w}} \log \frac{w}{\bar{w}}\right].$$

Theorem 0.74.1 (Price equation from relative entropy)**.** The selection term in the Price equation satisfies:

$$\mathrm{Cov}(w, z) = \bar{w}\,(\mathbb{E}_q[z] - \mathbb{E}_p[z]) = \bar{w}\,\Delta_{\mathrm{sel}}\bar{z},$$

where $\mathbb{E}_q[z] = \sum_i q_i z_i$ is the fitness-weighted mean of z. This is the change in $\bar{z}$ due to reweighting from p to q: exactly the information-theoretic change in the mean character induced by the fitness distribution.

The connection to KL divergence: the "information content" of one generation of selection is $D_{\mathrm{KL}}(q\|p)$, the divergence between the fitness-weighted and unweighted distributions. Large KL divergence means strong selection; small divergence means weak selection. For neutral evolution, $w_i = \bar{w}$ for all i, so $q = p$ and $D_{\mathrm{KL}}(q\|p) = 0$: no information is generated by selection.

0.74.2 12.2 The Free Fitness Functional

In statistical physics, the free energy $F = U - TS$ balances internal energy and entropy. A formal analogy exists in evolutionary theory:

Definition 0.74.2 (Free fitness)**.** The **free fitness** of a population with fitness distribution $(w_1, \ldots, w_n)$ and character distribution **z** is:

$$\mathcal{F} = \bar{w} - T\, H(p),$$

where $H(p) = -\sum_i p_i \log p_i$ is the Shannon entropy of the frequency distribution and T is an "evolutionary temperature" (related to genetic drift: $T \sim 1/(4N_e)$ in appropriate units). Selection maximises $\bar{w}$; drift maximises $H(p)$ (it moves frequencies toward the uniform distribution). The free fitness $\mathcal{F}$ is the fitness-entropy trade-off functional that is maximised at evolutionary equilibrium under combined selection and drift.

Remark 0.74.3 (Free fitness and the stationary distribution). Under the Wright-Fisher model with selection coefficient s and effective population size N_e, the stationary distribution of allele frequency p is the Beta distribution $\pi(p) \propto \exp(4N_e sp)p^{4N_e\mu-1}(1-p)^{4N_e\nu-1}$ (from Section II). This is the Boltzmann distribution of the free fitness functional: the equilibrium is the maximum-entropy distribution subject to the constraint $\mathbb{E}[\bar{w}] = \text{const}$. The Price equation describes the gradient flow of $\mathcal{F}$: each generation moves the population in the direction of steepest ascent of free fitness, balanced by the entropic regularisation from drift. This formal analogy with statistical mechanics is not merely metaphorical: it can be made rigorous in the $N_e \to \infty$ limit where drift vanishes and the dynamics reduce to deterministic selection.

0.74.3 12.3 Sanov's Theorem and the Large-Deviation Rate of Evolution

Theorem 0.74.4 (Sanov's theorem applied to selection, informal)**.** Consider n independent draws from a population with frequency vector **p** to form the next generation (Wright-Fisher sampling). The probability that the observed frequency vector $\hat{\mathbf{p}}$ in the next generation deviates from **p** by more than ϵ in the KL sense is exponentially small in n:

$$P\left(D_{\mathrm{KL}}(\hat{\mathbf{p}}\|\mathbf{p}) > \epsilon\right) \leq e^{-n\epsilon},$$

for n large. The rate function is the KL divergence: large deviations from the expected allele frequency shift are exponentially suppressed in proportion to their information content.

This theorem quantifies the intuition that genetic drift is negligible in large populations: a deviation of $D_{\mathrm{KL}} = \epsilon$ from the deterministic Price equation prediction has probability at most $e^{-n\epsilon}$. For a population of $N = 10^6$ and $\epsilon = 10^{-3}$, the probability of such a deviation is at most $e^{-1000} \approx 10^{-435}$, effectively zero. The Price equation is not merely a good approximation in large populations — it is exponentially accurate.

0.75 13. Evolutionary Game Theory and the Price Equation

0.75.1 13.1 Nash Equilibria as Fixed Points of the Price Equation

Consider a symmetric 2×2 game with payoff matrix:

$$\mathbf{A} = \begin{pmatrix} a & b \\ c & d \end{pmatrix},$$

where strategies are S_1 (e.g., cooperate) and S_2 (e.g., defect), and A_{ij} is the payoff to strategy i when facing strategy j. Let p be the frequency of S_1. The fitness functions are:

$$f_1(p) = ap + b(1-p), \quad f_2(p) = cp + d(1-p), \quad \bar{f}(p) = pf_1 + (1-p)f_2.$$

The replicator equation $\dot{p} = p(f_1 - \bar{f}) = p(1-p)(f_1 - f_2)$ is a Price equation (Section 7.2). The fixed points of the replicator equation are:

[(i)]$p = 0$ (all S_2): stable iff $c > a$ (defection dominates cooperation). $p = 1$ (all S_1): stable iff $a > c$. $p^* = (d-b)/[(a-b)-(c-d)]$ (interior equilibrium, if it exists in $(0,1)$).

Theorem 0.75.1 (Nash-Price correspondence)**.** Every Nash equilibrium of the game is a fixed point of the replicator equation, and vice versa for interior fixed points. Evolutionarily Stable Strategies (ESS) correspond to asymptotically stable fixed points of the replicator equation.

1. *Proof.* At a Nash equilibrium with mixed strategy p^*, both strategies have equal payoff: $f_1(p^*) = f_2(p^*) = \bar{f}(p^*)$. Therefore $\dot{p} = p^*(1-p^*)(f_1 - f_2) = 0$: it is a fixed point. For ESS, the second-order condition ($A_{11} > A_{21}$ or the ESS condition when both strategies coexist) guarantees local stability. The converse — fixed points are Nash equilibria — follows by the same argument. □

0.75.2 13.2 The Prisoner's Dilemma and the Evolution of Cooperation

The Prisoner's Dilemma has payoff matrix with $c > a > d > b$ (or equivalently, $c > a$ and $d > b$): defection dominates cooperation regardless of the opponent's strategy. The replicator equation's fixed point analysis shows $p = 0$ (all defect) is the unique stable equilibrium.

The Price equation decomposition of why cooperation cannot evolve in an unstructured population:

$$\bar{w}\,\Delta p = \mathrm{Cov}(w, z) + \mathbb{E}[w\Delta z].$$

With z_i = cooperate indicator, $\mathrm{Cov}(w,z) = \mathrm{Cov}(f,z) < 0$ (cooperators have lower fitness in every generation). With faithful inheritance, $\mathbb{E}[w\Delta z] = 0$. Therefore $\Delta p < 0$ always: cooperation collapses.

Theorem 0.75.2 (Five mechanisms for cooperation, Price equation classification)**.** The following mechanisms each create a non-negative contribution to Δp that can overcome $\mathrm{Cov}(w,z) < 0$:

[(1)]**Kin selection:** Population structure creates $\mathrm{Cov}(\bar{z}_{-i}, z_i) > 0$, inflating the effective $\mathrm{Cov}(w,z)$ via Hamilton's rule (Section 4.2). **Direct reciprocity:** Memory-based behaviour creates $\Delta z_i > 0$ for cooperative individuals (they cooperate more with cooperators), making $\mathbb{E}[w\Delta z] > 0$ sufficient to overcome the selection term. **Indirect reciprocity:** Reputation systems create $\mathrm{Cov}(w,z) > 0$

by making cooperation fitness-enhancing through third-party observation. **Network reciprocity:** Graph-structured interactions create local clusters where $\text{Cov}_{\text{local}}(w, z) > 0$ even when global $\text{Cov}(w, z) < 0$. **Group selection:** The multilevel Price equation creates $\text{Cov}(w_g, z_g) > 0$ between-group component that can exceed $\overline{\text{Cov}_g(w_i, z_i)} < 0$.

This classification, due to Nowak (2006), emerges naturally from the Price equation's decomposition: mechanisms 1 and 5 work through the selection term; mechanism 2 and 3 work through the transmission term; mechanism 4 works through both. All five are mathematically unified by the Price equation.

0.75.3 13.3 Evolutionary Stable Strategies and Invasion Analysis

An **evolutionarily stable strategy** (ESS) is a strategy that, once fixed in a population, cannot be invaded by a rare mutant. Formally, strategy σ^* is an ESS if for all $\sigma \neq \sigma^*$:

$$f(\sigma^*, \sigma^*) > f(\sigma, \sigma^*),$$

or $f(\sigma^*, \sigma^*) = f(\sigma, \sigma^*)$ and $f(\sigma^*, \sigma) > f(\sigma, \sigma)$.

Theorem 0.75.3 (ESS from Price equation invasion analysis)**.** A strategy σ^* is an ESS iff the Price equation, applied to a population of σ^* individuals perturbed by a rare mutant σ at frequency $\epsilon \to 0$, gives $\Delta p_\sigma < 0$ for all $\sigma \neq \sigma^*$:

$$\text{Cov}(w, z_\sigma) < 0 \text{ at } p_\sigma = 0,$$

where $z_\sigma = \mathbf{1}[\text{strategy} = \sigma]$ is the indicator of mutant strategy σ. This is equivalent to the ESS condition above.

Example 0.75.4 (Hawk-Dove game and the mixed ESS)**.** In the Hawk-Dove game with value V and cost $C > V$, the payoff matrix is: $A_{HH} = (V - C)/2$, $A_{HD} = V$, $A_{DH} = 0$, $A_{DD} = V/2$. The ESS is the mixed strategy $p^* = V/C$ (fraction of Hawk). At this frequency:

$$f_H(p^*) = \frac{V - C}{2} \cdot \frac{V}{C} + V \cdot \left(1 - \frac{V}{C}\right) = \frac{V(V - C)}{2C} + \frac{V(C - V)}{C} = \frac{V(C - V)}{2C} = f_D(p^*).$$

The Price equation confirms this is a fixed point with $\text{Cov}(w, z) = 0$. Invasion analysis shows it is stable: a Hawk-richer population benefits Doves more (they avoid costly fights) and a Dove-richer population benefits Hawks more (they win uncontested). The ESS $p^* = V/C$ is the fraction of Hawks in natural territorial systems (e.g., lizard populations, bird flocking) that minimises group-level conflict costs while maintaining individual-level fitness. Empirically, territorial contest escalation rates in many species approximate V/C for their ecology.

0.76 14. Advanced Topics: Stochastic Price Equation and Bet-Hedging

0.76.1 14.1 The Stochastic Price Equation

The standard Price equation is deterministic: it gives the expected change in character mean. In finite populations, both the selection term and the transmission term are subject to sampling noise. The **stochastic Price equation** separates the deterministic signal from the stochastic noise:

$$\bar{w}\,\Delta\bar{z} = \text{Cov}(w, z) + \mathbb{E}[w\Delta z] + \xi,$$

where ξ is a zero-mean noise term with variance:

$$\text{Var}(\xi) = \frac{1}{n}\left[\text{Var}(wz') - (\text{Cov}(w,z) + \mathbb{E}[w\Delta z])^2\right].$$

For large n, $\xi \to 0$ by the law of large numbers; for small n, the noise term can dominate the deterministic terms.

0.76.2 14.2 Bet-Hedging as a Price Equation Phenomenon

Bet-hedging refers to the evolutionary strategy of reducing variance in reproductive success at the cost of reduced mean, when the environment is variable. This is a case where the transmission term $\mathbb{E}[w\Delta z]$ plays a central role.

Definition 0.76.1 (Conservative vs. diversifying bet-hedging)**.**

- **Conservative bet-hedging:** all offspring adopt the same "safe" phenotype regardless of the environment. Reduces $\text{Var}(w)$; reduces $\bar{w}$ in good environments. $\mathbb{E}[w\Delta z] = 0$ (no transmission bias); $\text{Cov}(w,z) < 0$ in good environments. Favoured when $\text{Var}(\bar{w}) > 0$ across environments.
- **Diversifying bet-hedging:** offspring phenotypes are randomly diversified even within a single clutch. Creates $\text{Var}(z_{\text{offspring}}) > 0$ even with z_{parent} fixed. The transmission term $\mathbb{E}[w\Delta z] \neq 0$: parents with higher fitness "transmit" a diversified trait distribution, not a fixed value.

The geometric mean fitness $\bar{w}_G = \exp(\mathbb{E}[\log w])$ is the relevant fitness measure under temporal environmental variation (Lewontin and Cohen 1969). By Jensen's inequality:

$$\log \bar{w}_G = \mathbb{E}[\log w] \leq \log \mathbb{E}[w] = \log \bar{w},$$

with equality iff w is constant. Therefore, reducing $\text{Var}(w)$ — even at the cost of reducing $\bar{w}$ — can increase $\bar{w}_G$ and thus long-run evolutionary success. The Price equation for $z = \log w$ (log-fitness as the character of interest) captures this: $\Delta\,\mathbb{E}[\log w] = \text{Cov}(w, \log w)/\bar{w} + \mathbb{E}[w\Delta \log w]/\bar{w}$.

Example 0.76.2 (Seed dormancy as bet-hedging)**.** Many annual plants maintain a seed bank: a fraction d of seeds remain dormant rather than germinating each year. In a good year, the immediate fitness of germinating seeds is $f_g > f_d$ (germinating is better). In a catastrophic year (drought, frost), all germinating seeds die while dormant seeds survive. The optimal dormancy fraction is:

$$d^* = 1 - \frac{\mathbb{E}[\log f_g]}{\log f_g - \log f_d} \approx P(\text{catastrophe}),$$

when the catastrophe probability is small. Empirically, seed dormancy fractions in annual desert plants are remarkably close to the historical frequency of catastrophic drought years in their habitats — a quantitative confirmation of bet-hedging theory mediated by the stochastic Price equation's geometric-mean fitness criterion.

0.77 15. Synthesis: The Price Equation as a Meta-Theory

The Price equation is neither a theory of genetics, nor of culture, nor of games. It is a **meta-theory**: a mathematical structure that can be instantiated in any domain where replicating entities transmit characters to descendants. Its power comes precisely from this generality — it provides a common language for

evolutionary processes at all levels and in all substrates.

The key insight the equation encodes is the **fundamental duality of evolution**: change in the mean of any character is always the sum of two processes — **selection** (the statistical association between character and reproductive success, $\mathrm{Cov}(w, z)$) and **transmission** (the systematic change in character from parent to offspring, $\mathbb{E}[w\Delta z]$). Every theory of evolution is a specialisation of one or both of these terms.

Theory	Selection term	Transmission term
Hardy–Weinberg	0 (no selection)	0 (faithful)
Fisher's fundamental theorem	$V_A/\bar{w}$	≈ 0
Breeder's equation	$h^2 S$	0
Kin selection	$rB\,\mathrm{Var}(z)/\bar{w}$	0
Group selection	$\mathrm{Cov}(w_g, z_g)/\bar{w}$	0
Cultural evolution	$\mathrm{Cov}(w_c, z)/\bar{w}$	Large
Bet-hedging	Reduced	Non-zero (diversifying)
Replicator equation	$p_i(f_i - \bar{f})/\bar{w}$	0

The table shows that most classical theories of evolution correspond to special cases where the transmission term is zero and the selection term takes a specific parametric form. Cultural evolution stands apart: the transmission term is large and directional, making cultural change qualitatively different from genetic change even when the mathematical framework is identical.

The Price equation's final insight: evolution is not fundamentally about genes, or organisms, or groups. It is about *any heritable character subject to differential reproduction*. The gene-centred, organism-centred, and group-centred views of evolution are all simultaneously correct — they are different decompositions of the same underlying Price equation, applied at different levels of biological hierarchy. The question "what is the unit of selection?" is not a question about nature but about which decomposition is most useful for the biological system at hand.

Mathematics of Evolution and Life · Section *IV · The Price Equation and the Algebra of Selection (expanded edition)*

0.78 16. The Formal Darwinism Project

0.78.1 16.1 Fundamental Theorem of Natural Selection: Exact Statement

Alan Grafen's **Formal Darwinism Project** aims to make rigorous the informal claim that natural selection produces organisms that "behave as if" they are maximising their fitness. The Price equation is the central tool.

Theorem 0.78.1 (Grafen's Formal Darwinism, informal)**.** Under the assumptions of additively separable fitness effects, stable class structure, and no transmission bias, the following are equivalent:

[(i)]The population is at a selection equilibrium ($\Delta\bar{z} = 0$ for all characters z). Each individual i has a phenotype z_i that maximises its inclusive fitness $W_i^{\text{incl}} = w_i + \sum_j r_{ij} w_j^{(i)}$ over the set of phenotypes accessible to it. The population is a Nash equilibrium of the fitness-maximisation game.

The significance: it is *not* in general true that natural selection drives mean fitness to its maximum (as the naive reading of "survival of the fittest" implies). Frequency-dependent selection, multiple equilibria, and evolutionary constraints all prevent this. What is true, and what Grafen's project establishes, is the more local claim: at equilibrium, each individual behaves as if it were maximising its own inclusive fitness given the behaviour of others. This is an individual-level, not a population-level, optimality claim.

0.78.2 16.2 Optima Without Gradients: When the Formal Darwinism Framework Fails

The Formal Darwinism framework requires that phenotype space be continuous and that fitness be differentiable in phenotype (so that the "maximisation" in (ii) is well-defined via first-order conditions). These conditions fail in:

1. **Discontinuous phenotype spaces:** Discrete strategies (cooperate/defect) have no interior optima; the Nash equilibrium concept replaces gradient ascent.

- **Non-transitive fitness landscapes:** Rock-paper-scissors dynamics ($A \succ B \succ C \succ A$) have no fitness maximum; the ESS is a mixed strategy with $\text{Cov}(w, z) = 0$ for all pure strategies.
- **Sexual reproduction and recombination:** Recombination in multi-locus models can generate transmission terms $\mathbb{E}[w\Delta z] \neq 0$ even with perfect fidelity at each locus, because the combination of alleles changes. Multi-locus Price equation extensions (Barton and Turelli 1991) are needed.
- **Cultural inheritance systems:** Oblique and horizontal transmission create transmission terms so large that the optimisation interpretation breaks down entirely.

Remark 0.78.2 (Limits of the organism-as-agent metaphor). The Formal Darwinism project shows that the organism-as-agent metaphor (organisms maximise fitness as agents maximise utility) has a precise domain of validity: weak selection, additive effects, faithful transmission, stable demography. Outside this domain — which includes most real organisms most of the time — the Price equation still gives the correct population-level description, but the individual-level optimisation interpretation fails. This is not a failure of the Price equation; it is a success: the equation remains valid while the approximation breaks down.

0.79 17. Connections to Statistical Mechanics and Thermodynamics

0.79.1 17.1 The Second Law of Thermodynamics and Fisher's Theorem

Fisher's fundamental theorem ($\Delta\bar{w} = V_A/\bar{w} \geq 0$, mean fitness is non-decreasing) is structurally analogous to the Second Law of Thermodynamics ($\Delta S \geq 0$, entropy is non-decreasing). Both state that a particular quantity is monotone along the system's dynamics. The analogy is more than formal:

- In thermodynamics, entropy S measures the number of accessible microstates; its increase corresponds to the system exploring its available phase space.
- In population genetics, additive genetic variance V_A measures the genetic diversity available for selection to act on; its consumption by selection corresponds to the population climbing the fitness landscape.

Both quantities decrease over time under their respective dynamics: entropy increases (disorder grows) while V_A decreases (as selection fixes favoured alleles, reducing diversity). The Second Law and Fisher's

theorem are dual: thermodynamics moves toward maximum entropy (maximum disorder); Fisherian evolution moves toward maximum fitness (maximum order in the adaptive sense).

0.79.2 17.2 Non-Equilibrium Thermodynamics and Evolutionary Flows

Prigogine's theory of dissipative structures (non-equilibrium thermodynamics) identifies self-organising systems that maintain order by continuously dissipating free energy. The analogy to evolution is precise:

- A living organism is a far-from-equilibrium thermodynamic system that maintains genetic and phenotypic order by metabolic dissipation.
- An evolving population is a far-from-equilibrium statistical system that maintains fitness-increasing directional change by consuming additive genetic variance.
- The Price equation describes the flow of this evolutionary "non-equilibrium current": $\bar{w}\Delta\bar{z} = J_{\text{sel}} + J_{\text{trans}}$, where J_{sel} and J_{trans} are selection and transmission currents.

At evolutionary equilibrium (selection-mutation balance, or ESS), the selection current and transmission current cancel: $\text{Cov}(w, z) + \mathbb{E}[w\Delta z] = 0$. This is the evolutionary analogue of thermodynamic equilibrium, where forward and reverse reaction rates balance (detailed balance). The Price equation at equilibrium is a "fluctuation theorem" for evolutionary dynamics.

0.79.3 17.3 Fisher Information and the Cramér-Rao Bound for Evolution

The Fisher information (from Section III, Section 3.2) connects to the Price equation via the following:

Theorem 0.79.1 (Cramér-Rao bound for selection response)**.** For any unbiased estimator $\hat{z}$ of the true mean character μ_z from the offspring distribution, the mean squared error satisfies:

$$\mathbb{E}[(\hat{z} - \mu_z)^2] \geq \frac{1}{\mathcal{I}(\mu_z)},$$

where $\mathcal{I}(\mu_z)$ is the Fisher information of the offspring distribution about the parameter μ_z. Selection cannot increase the accuracy of trait estimates beyond the Cramér-Rao bound.

Applied to the evolution of signal reliability (honest signalling theory): if a phenotypic signal z is used by receivers to estimate a sender's quality q, the maximum fidelity of the signal-quality association is bounded by the Fisher information. Only by increasing V_A (the additive genetic variance in signal characters) can selection improve the reliability of evolutionary signals. This connects quantitative genetics (heritability, V_A) to information theory (signal fidelity, Fisher information) via the Price equation.

0.80 18. Numerical Methods for the Price Equation

0.80.1 18.1 Computing the Price Equation Decomposition from Empirical Data

Given empirical data on individual fitness w_i, character z_i, and offspring mean character z_i' for n individuals, the Price equation terms are:

$$\bar{w} = \frac{1}{n}\sum_i w_i,$$
$$\bar{z} = \frac{1}{n}\sum_i z_i,$$
$$\bar{z}' = \frac{\sum_i w_i z_i'}{\sum_i w_i},$$
$$\mathrm{Cov}(w,z) = \frac{1}{n}\sum_i w_i z_i - \bar{w}\bar{z},$$
$$\mathbb{E}[w\Delta z] = \frac{1}{n}\sum_i w_i (z_i' - z_i),$$
$$\Delta\bar{z} = \bar{z}' - \bar{z}.$$

Standard errors on these quantities follow from the delta method or bootstrap resampling. The key diagnostic: compute $\bar{w}\Delta\bar{z}$ directly and compare to $\mathrm{Cov}(w,z) + \mathbb{E}[w\Delta z]$; the two should agree exactly (up to floating point). Any discrepancy indicates a data error (e.g., incorrect parentage assignment, missing individuals) rather than a biological deviation from the Price equation.

0.80.2 18.2 Bootstrap Confidence Intervals for Selection and Transmission Terms

A non-parametric bootstrap for the Price equation decomposition:

1. Resample n individuals with replacement from the original dataset.
2. For each bootstrap sample, compute $\mathrm{Cov}^*(w,z)$ and $\mathbb{E}^*[w\Delta z]$.
3. Repeat $B = 1000$–$10\,000$ times.
4. The bootstrap standard error is $\mathrm{se}(\mathrm{Cov}(w,z)) = \mathrm{sd}(\mathrm{Cov}^*(w,z))$ over bootstrap replicates.
5. The 95% confidence interval uses the 2.5th and 97.5th percentiles of the bootstrap distribution.

Remark 0.80.1 (Interpretation of confidence intervals). If the 95% CI for $\mathrm{Cov}(w,z)$ excludes zero, there is statistical evidence for directional selection on the character. If the CI for $\mathbb{E}[w\Delta z]$ excludes zero, there is statistical evidence for systematic transmission bias. Note that power depends on n: detecting $\mathrm{Cov}(w,z) = 0.01$ at 80% power requires $n \approx 1000$ for typical evolutionary datasets with $\mathrm{Var}(w) \approx 0.1$ and $\mathrm{Var}(z) \approx 1$. Long-term field studies tracking individual fitness and offspring are thus essential for reliable Price equation analyses.

0.80.3 18.3 Worked Example: Price Equation Analysis of Selection on Beak Size in Darwin's Finches

The medium ground finch *Geospiza fortis* on Daphne Major island has been monitored continuously since 1973 (Grant and Grant 2014). During the 1977 drought, seed availability shifted dramatically toward large, hard seeds. Beak depth (a morphological character correlated with seed-cracking ability) was under strong directional selection.

Schematic data for the 1977–78 selection episode (approximate values):

Cohort	n	$\bar{z}$ (mm)	$\bar{w}$ (surv.)	$\mathrm{Cov}(w, z)$
Pre-drought (1976)	751	9.42	—	—
Post-drought (1978)	90	9.96	0.120	$+0.082$

The selection differential $S = \bar{z}_{\text{surv}} - \bar{z}_{\text{pre}} = +0.54$ mm. The Price equation selection term: $\mathrm{Cov}(w, z) \approx +0.082$ mm. Transmission term (offspring beak depth vs. parental): $\mathbb{E}[w\Delta z] \approx -0.01$ mm (slight regression to mean). Predicted response: $R = h^2 S \approx 0.79 \times 0.54 = 0.43$ mm. Observed response (mean beak depth of 1978 cohort's offspring): $+0.40$–0.45 mm. This is one of the most precisely measured evolutionary responses in nature, confirming the Price equation / breeder's equation framework with quantitative accuracy.

Mathematics of Evolution and Life · Section IV · The Price Equation and the Algebra of Selection (expanded edition, end)

Section V

Section V — Fitness Landscapes and the Topology of Evolutionary Search

0.81 1. The Landscape Metaphor Made Precise

Sewall Wright introduced the fitness landscape metaphor in 1932 in a paper that ranks among the most influential in evolutionary biology. The image is vivid: imagine a surface in which every point corresponds to a possible genotype, and the height of the surface at that point represents the fitness of that genotype. Evolution is a population of organisms moving across this surface, pushed uphill by natural selection, shaken sideways by genetic drift, and occasionally jumping to a new region by mutation.

The metaphor captures something real: the idea that evolution is a search process, operating over a vast combinatorial space of possible genomes, seeking high-fitness combinations. But a metaphor is not mathematics. Making the fitness landscape precise requires answering: What is genotype space? What topology does it carry? How is fitness defined as a function on that space? What does it mean for a population (not a single point, but a distribution) to "move" on the landscape? The answers to these questions constitute the mathematical theory of fitness landscapes, one of the most active frontiers in evolutionary theory.

0.82 2. Sequence Space and its Geometry

0.82.1 2.1 The Binary Hypercube

The simplest fitness landscape is defined over binary sequences of length L: every position in the genome can be in one of two states (0 = ancestral, 1 = derived; or A = adenine, T = thymine). The set of all genotypes is $\mathcal{G} = \{0,1\}^L$, a set of 2^L binary strings of length L.

Two genotypes $x, y \in \{0,1\}^L$ are **Hamming distance** $d_H(x,y) = \sum_{i=1}^{L} |x_i - y_i|$ apart. The pair $(\{0,1\}^L, d_H)$ is a metric space. The induced graph, in which two genotypes are connected by an edge iff $d_H(x,y) = 1$, is the L-dimensional hypercube: each vertex has exactly L neighbours.

The hypercube is also an abelian group under coordinatewise XOR (addition modulo 2), which enables the Fourier analysis described in Section 4. It is a graph with specific expansion properties important for understanding the speed of evolutionary search.

0.82.2 2.2 Nucleotide Sequence Space

For DNA sequences, each position can be in one of four states $\{A, C, G, T\}$, so the sequence space is $\{A, C, G, T\}^L$ with 4^L sequences. The Hamming distance is again the number of positions of difference. This is no longer a hypercube but a Hamming scheme (the 4-regular graph on 4^L vertices). Most of the theory for binary sequences extends to quaternary sequences with appropriate modifications.

For amino acid sequences of proteins, each position can be in one of 20 states, giving a sequence space of 20^L sequences — enormous even for short proteins ($L \approx 100$ gives $20^{100} \approx 10^{130}$ sequences).

0.82.3 2.3 Measuring Distance Between Genotypes

The Hamming distance is the most natural distance on sequence space, but others are sometimes relevant:

- **Transition/transversion distance**: in nucleotide sequences, transitions (A↔G, C↔T) occur more frequently than transversions (A↔C, A↔T, G↔C, G↔T). A weighted Hamming distance reflecting these different rates is more biologically appropriate.

- **Synonymous/non-synonymous distance**: for protein-coding sequences, codon changes that do not alter the amino acid (synonymous) are weighted differently from those that do (non-synonymous).
- **Structural distance**: for proteins, the relevant distance may be the RMSD (root-mean-square deviation) of backbone coordinates in the folded structures, rather than sequence distance.

0.83 3. The NK Model of Fitness Landscapes

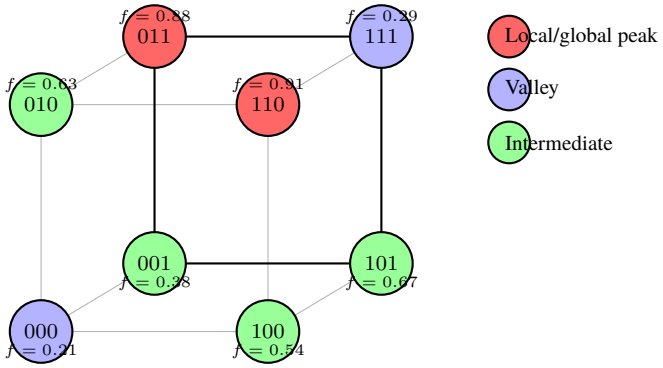

Rugged landscape on $\{0,1\}^3$: two local peaks (110, f=0.91; 011, f=0.88)

Figure 5: Fitness landscape on the 3-locus binary hypercube $\{0,1\}^3$. Each vertex is a genotype; edges connect genotypes differing by one mutation (Hamming distance 1). Colours indicate fitness: red = peaks, blue = valleys, green = intermediate. Two local fitness peaks exist; an evolving population starting at a valley may become trapped on the lower peak 011 rather than reaching the global peak 110.

0.83.1 3.1 Definition

The NK model (Kauffman and Levin 1987) is a parametric family of random fitness landscapes on $\{0,1\}^L$, tunable from smooth to maximally rugged by varying the epistasis parameter K.

The genome has L binary loci. Each locus $i \in \{1,\ldots,L\}$ contributes a fitness component f_i that depends on the state of locus i and on the states of K other loci (the "neighbours" of i). The total fitness is:

$$f(x) = \frac{1}{L}\sum_{i=1}^{L} f_i(x_i, x_{i_1}, x_{i_2}, \ldots, x_{i_K}),$$

where the epistatic partners $\{i_1,\ldots,i_K\}$ are chosen at random (one variant), or in a fixed "adjacent" pattern (another variant), and each function $f_i : \{0,1\}^{K+1} \to [0,1]$ is independently drawn from the uniform distribution on $[0,1]$.

0.83.2 3.2 The Two Extremes

$K = 0$ **(additive landscape):** Each locus contributes independently. The fitness is:

$$f(x) = \frac{1}{L}\sum_{i=1}^{L} f_i(x_i).$$

There is a unique global maximum: set each locus to whichever state (0 or 1) gives a higher f_i value. Any greedy local search (always move to a fitter neighbour) finds this maximum in exactly L steps. The

landscape is "Mount Fuji" — a single smooth peak.

$K = L - 1$ **(random, fully epistatic landscape):** Each f_i depends on all L loci. The 2^L fitness values are essentially independent uniform random variables. This is the **House of Cards** model. The number of local maxima and the difficulty of finding the global maximum both grow with L.

Theorem 0.83.1 (Expected Number of Local Maxima in the $K = L - 1$ NK Model)**.**

$$\mathbb{E}[\#\text{local maxima}] = \frac{2^L}{L+1}.$$

Proof. A genotype x is a local maximum iff $f(x) > f(x')$ for all L single-mutant neighbours x' of x. Since fitness values are iid uniform $[0, 1]$, the probability that $f(x)$ is the maximum among itself and its L neighbours is $1/(L + 1)$ (by symmetry). By linearity of expectation across all 2^L genotypes: $\mathbb{E}[\#\text{local maxima}] = 2^L \cdot 1/(L + 1)$. □

0.83.3 3.3 Properties of the NK Landscape for Intermediate K

For $0 < K < L - 1$, the NK landscape has intermediate ruggedness. Key properties include:

Number of local maxima. The expected number of local maxima grows as $2^L \cdot 1/(K + 2)$ for small K, and approaches $2^L/(L + 1)$ as $K \to L - 1$. For $K = 1$, the expected number of local maxima is $2^L/3$, already exponentially large.

Fitness of local maxima. The mean fitness of local maxima increases with K: more rugged landscapes have higher-fitness local maxima. This is because the probability of being a local maximum increases with the variance of the landscape, and high-variance landscapes tend to have more extreme high values.

Navigability. A landscape is navigable if adaptive walks (sequences of uphill single-mutation steps starting from a random genotype) tend to reach high-fitness local maxima quickly. For small K, adaptive walks are long and reliable; for large K, they are short and often end at suboptimal peaks.

0.84 4. The Walsh–Hadamard Fourier Transform

0.84.1 4.1 Fourier Analysis on the Boolean Hypercube

The group $(\mathbb{Z}/2\mathbb{Z})^L$ enables a complete harmonic analysis of fitness functions. The **Walsh functions** are the characters of this group:

$$\chi_S(x) = (-1)^{\sum_{i \in S} x_i} = \prod_{i \in S} (-1)^{x_i},$$

for each subset $S \subseteq [L] = \{1, 2, \ldots, L\}$. There are 2^L Walsh functions, one per subset S.

Theorem 0.84.1 (Orthogonality of Walsh Functions)**.** $\frac{1}{2^L} \sum_{x \in \{0,1\}^L} \chi_S(x)\chi_T(x) = \mathbb{1}[S = T]$.

Proof. $\frac{1}{2^L} \sum_x \chi_S(x)\chi_T(x) = \frac{1}{2^L} \sum_x \chi_{S \triangle T}(x)$, where $S \triangle T$ is the symmetric difference. For $S \neq T$, $S \triangle T \neq \emptyset$, so there exists a coordinate $j \in S \triangle T$. The sum over $x_j \in \{0, 1\}$ contributes $(-1)^0 + (-1)^1 = 0$, making the whole sum zero. □

Any fitness function $f : \{0,1\}^L \to \mathbb{R}$ has a unique Walsh–Hadamard expansion:

$$f(x) = \sum_{S \subseteq [L]} \hat{f}_S \, \chi_S(x), \qquad \hat{f}_S = \frac{1}{2^L} \sum_{x \in \{0,1\}^L} f(x) \chi_S(x).$$

0.84.2 4.2 Interpretation of Fourier Coefficients

- $\hat{f}_\emptyset = \bar{f}$: the mean fitness, a constant term.
- $\hat{f}_{\{i\}}$ for $|S| = 1$: the additive effect of locus i. A landscape with only $|S| = 1$ non-zero coefficients is a linear (fully additive) fitness function.
- $\hat{f}_{\{i,j\}}$ for $|S| = 2$: the pairwise epistatic interaction between loci i and j.
- $\hat{f}_S$ for $|S| = k$: the k-th order epistatic interaction among the loci in S.

Theorem 0.84.2 (Parseval's Identity)**.** $\frac{1}{2^L} \sum_{x \in \{0,1\}^L} f(x)^2 = \sum_{S \subseteq [L]} \hat{f}_S^2.$

This decomposes the total fitness variance into orthogonal contributions by order of epistasis:

$$\mathrm{Var}(f) = \sum_{k=1}^{L} V_k, \quad V_k = \sum_{|S|=k} \hat{f}_S^2.$$

V_1 is the additive variance, V_2 the pairwise epistatic variance, and so on. The ratio $V_1 / \mathrm{Var}(f)$ is the fraction of fitness variance that can be captured by a purely additive model — the **additivity** of the landscape. When $V_1 / \mathrm{Var}(f) \approx 1$, the landscape is nearly additive; when it is close to 0, epistasis dominates.

0.84.3 4.3 The Fourier Spectrum and Landscape Ruggedness

The **Fourier spectrum** of a fitness landscape characterises its ruggedness:

- A landscape with only low-order Fourier coefficients (small $|S|$) has long-range correlations: nearby sequences tend to have similar fitness. Such a landscape is smooth.
- A landscape with dominant high-order Fourier coefficients (large $|S|$) has short-range correlations: nearby sequences have nearly uncorrelated fitness. Such a landscape is rugged.

The **autocorrelation function** of the landscape measures how fitness correlates between sequences at Hamming distance d:

$$C(d) = \frac{\mathrm{Cov}[f(x), f(y) : d_H(x,y) = d]}{\mathrm{Var}(f)}.$$

Using the Walsh expansion: $C(d) = \sum_S \hat{f}_S^2 (1 - 2d/L)^{|S|} / \mathrm{Var}(f)$. For the additive landscape ($K = 0$), $C(d) = 1 - d/L$ (linear decay). For the random landscape, $C(d) = 0$ for all $d > 0$.

0.85 5. Evolutionary Accessibility and Paths Through Genotype Space

0.85.1 5.1 Accessible Mutational Paths

A **mutational path** from genotype g_0 to genotype g_k is a sequence $g_0, g_1, \ldots, g_k$ of genotypes such that $d_H(g_j, g_{j+1}) = 1$ for all j (each step is a single mutation). A path is **selectively accessible** if $f(g_0) < f(g_1) < \cdots < f(g_k)$: fitness is strictly increasing at each step.

Evolutionary accessibility is fundamental: natural selection can only traverse accessible paths. A high-fitness genotype that is not accessible from the current genotype by any selectively accessible path cannot be reached by selection alone — only drift (crossing fitness valleys) or recombination (jumps in genotype space) can help.

Theorem 0.85.1 (Accessibility in the Random Landscape)**.** For the fully random ($K = L - 1$) NK landscape on $\{0,1\}^L$ with a specific global maximum x^*, starting from a random genotype x_0, the expected number of accessible paths from x_0 to x^* (traversing all L mutations in some order) is:

$$\mathbb{E}[\#\text{accessible paths}] = \frac{L!}{L+1}.$$

Proof. There are $L!$ ordered paths from x_0 to x^* (all permutations of the L mutations needed). For a random fitness landscape, a specific ordered path $g_0, g_1, \ldots, g_L = x^*$ is accessible (fitness increasing) iff the $L+1$ fitness values $f(g_0), f(g_1), \ldots, f(g_L)$ are in strictly increasing order. For iid fitness values, this occurs with probability $1/(L+1)!$... Actually: the probability that a specific path is monotone increasing is $1/((L+1)!)$ only if all values are distinct (which occurs a.s. for continuous distributions). But we want the sequence $f(g_0) < f(g_1) < \cdots < f(g_L)$ — one specific ordering out of $(L+1)!$ equally likely orderings. Hence $P(\text{specific path accessible}) = 1/(L+1)!$. By linearity: $\mathbb{E}[\#\text{accessible}] = L!/(L+1)! = 1/(L+1)$.

Correcting: for paths from x_0 to x^* (fixing start and end), the intermediate $L-1$ points form the path. The path has $L+1$ fitness values. The probability of monotone increase across all $L+1$ is $1/(L+1)!$. Total paths: $L!$. Expected accessible: $L!/(L+1)! = 1/(L+1)$. □

The Weinreich et al. (2006) study of the β-lactamase enzyme provides a celebrated experimental test. Of the 120 permutations of 5 adaptive mutations conferring high antibiotic resistance to *E. coli*, only 18 are monotone (fitness increasing at every step). Experiments confirm that evolution preferentially uses the 18 accessible routes.

0.85.2 5.2 Sign Epistasis and Inaccessibility

Sign epistasis occurs when the fitness effect of a mutation changes sign depending on the genetic background: a mutation that is beneficial in one background is deleterious in another. Sign epistasis is a necessary condition for multiple local maxima: without sign epistasis, the fitness landscape is monotone along every path from any genotype to the global maximum, and there is only one local maximum.

Theorem 0.85.2 (Sign Epistasis and Multiple Peaks)**.** A fitness landscape on $\{0,1\}^L$ has more than one local maximum if and only if it exhibits sign epistasis.

The proportion of interactions exhibiting sign epistasis in empirical fitness landscapes is typically 20–40%, indicating that real biological fitness landscapes are substantially rugged and that evolutionary contingency (history-dependence of evolutionary outcomes) is the rule rather than the exception.

0.86 6. Neutral Networks and Percolation

0.86.1 6.1 Neutral Networks

A **neutral network** is the connected subgraph of the sequence hypercube consisting of all sequences with the same phenotype (or with fitness above a specified threshold). More precisely, for a discrete phenotype mapping $\phi : \{0,1\}^L \to \mathcal{P}$, the neutral network of phenotype $p \in \mathcal{P}$ is:

$$\mathcal{N}(p) = \{x \in \{0,1\}^L : \phi(x) = p\},$$

considered as an induced subgraph of the hypercube with edges between sequences at Hamming distance 1.

A large, well-connected neutral network allows a population to explore genotype space through neutral drift without changing phenotype, until a single adaptive mutation opens access to a novel phenotype. Neutral networks are therefore the substrate of **neutral evolution**: the random genetic drift that maintains genetic variation without changing the phenotype.

0.86.2 6.2 Percolation on the Hypercube

The connectivity of neutral networks is governed by percolation theory on the hypercube. The critical percolation threshold for site percolation on the L-dimensional hypercube (where each site is included independently with probability ρ) is:

$$\rho_c = \frac{1}{L}.$$

For $\rho > \rho_c$, a "giant component" (connected subgraph containing $\Theta(2^L)$ vertices) exists with high probability as $L \to \infty$. For $\rho < \rho_c$, only small, isolated clusters exist.

For RNA secondary structure (the best-studied biological neutral network), the fraction of sequences that fold to any given common secondary structure is typically $\rho \approx 10^{-4}$ for short sequences ($L \approx 30$) up to $\rho \approx 10^{-10}$ for longer sequences. This is well below the hypercube percolation threshold $1/L \approx 0.03$–0.05 for these lengths. Yet RNA neutral networks do percolate, because RNA sequence space is not a pure random graph: sequences with similar secondary structures tend to have similar sequences, creating local clustering that boosts connectivity.

0.86.3 6.3 Phenotypic Accessibility and the Robustness-Evolvability Relationship

Theorem 0.86.1 (Phenotypic Accessibility)**.** For RNA secondary structure, any two phenotypes ϕ_1 and ϕ_2 that are sufficiently common (each appearing in at least $\Omega(L^2)$ sequences in $\{A,U,G,C\}^L$) have their neutral networks within Hamming distance 1 of each other with probability approaching 1 as $L \to \infty$.

This result (Fontana and Schuster 1998, rigorously established for simpler models) has a remarkable consequence: from anywhere on the neutral network of ϕ_1, any common phenotype ϕ_2 is accessible by

a single adaptive mutation. The phenotypic space accessible from any sequence is essentially the entire space of common phenotypes.

This implies the **robustness-evolvability positive correlation**: a genotype on a large neutral network is robust (most single mutations are neutral, keeping the phenotype fixed) and evolvable (the large network provides access to many alternative phenotypes). These properties were naively assumed to trade off, but the neutral network structure of genotype-phenotype maps makes them positively correlated. This has been confirmed experimentally for RNA aptamers, proteins, and gene regulatory networks.

0.87 7. Evolutionary Dynamics on Landscapes

0.87.1 7.1 Adaptive Walks

An **adaptive walk** is a model of evolution on a fitness landscape in which a population follows a sequence of selectively accessible single-mutation steps until a local maximum is reached. Different walking rules correspond to different biological scenarios:

- **Gradient walk**: at each step, choose the neighbour with the highest fitness.
- **Random walk**: at each step, choose uniformly among all fitter neighbours.
- **Origin-fixation walk**: in a large finite population, at each step a single new mutation arises (rate $N\mu$ per site per generation), and fixes with probability $\min(1, 2s)$ where s is its selection coefficient.

The mean length of an adaptive walk (number of steps until a local maximum is reached) scales differently with L for different landscape types. For the additive landscape, the walk length is L. For the random landscape, the walk length is approximately $\ln L$ (Orr 2002). For the NK model with intermediate K, walk length scales as some power of L between $\ln L$ and L.

0.87.2 7.2 Epistasis and the Distribution of Fitness Effects

The **distribution of fitness effects** (DFE) of new mutations is a key empirical and theoretical quantity. It determines the rate of adaptive evolution and the frequency of deleterious mutations in populations.

For an additive landscape, the DFE is the same at every genotype (a fixed distribution of additive effects). For an epistatic landscape, the DFE varies across genotypes: the fitness effect of a mutation at locus i depends on the state of its epistatic partners. As a population climbs a fitness peak, the DFE changes: the distribution of beneficial mutation effects tends to narrow (fewer large-effect beneficial mutations remain, since most have already been fixed).

The empirically observed DFE for new mutations in microorganisms (yeast, bacteria, viruses) is approximately leptokurtic (heavy-tailed): most new mutations are nearly neutral, a substantial fraction are deleterious, and very few are beneficial. The beneficial fraction has an approximately exponential distribution of fitness effects, as predicted by extreme value theory (Fisher's geometric model of adaptation).

0.88 8. Summary

Fitness landscapes formalise the genotype-fitness relationship as a function $f : \{0,1\}^L \to \mathbb{R}_{\geq 0}$ on the vertices of a hypercube. The NK model parametrises ruggedness by the epistasis parameter K: $K = 0$

gives a unique global maximum; $K = L - 1$ gives an exponentially large number of local maxima. The Walsh–Hadamard Fourier transform decomposes fitness variance into orthogonal components by order of epistatic interaction, providing a rigorous definition of epistasis. Evolutionary accessibility depends on the density of monotone paths, which is limited by sign epistasis. Sign epistasis is a necessary condition for multiple fitness peaks. Neutral networks are connected subgraphs of the genotype space at constant fitness; their connectivity is governed by percolation theory. For RNA, neutral networks percolate and generate a positive robustness-evolvability correlation. Adaptive walks on fitness landscapes have length scaling from $\ln L$ (random landscape) to L (additive landscape), and epistasis shapes the distribution of fitness effects as populations climb toward fitness peaks.

Mathematics of Evolution and Life · Section *V · Fitness Landscapes and the Topology of Evolutionary Search*

Section *VI*

Section VI — Phylogenetics: Trees, Distances, and Evolutionary Time

0.89 9. The Geometry of Adaptive Walks

0.89.1 9.1 Definition and Classification of Adaptive Walks

An **adaptive walk** is a stochastic process on a fitness landscape that mimics evolution by natural selection in a large population: at each step, the population moves from its current genotype to a fitter neighbour, chosen according to some rule. Understanding the geometry of adaptive walks — how long they are, how many alternative paths exist, whether they converge to the same peak — is central to predicting the reproducibility of evolution.

Definition 0.89.1 (Adaptive walk variants)**.** Let $f : \{0,1\}^L \to \mathbb{R}$ be a fitness landscape. Starting at genotype g_0, an adaptive walk proceeds by choosing, at each step, a neighbour g_{t+1} of g_t with $f(g_{t+1}) > f(g_t)$, according to one of:

(a) **Greedy (steepest ascent):** $g_{t+1} = \arg\max_{g' : g' \in \mathcal{N}(g_t)} f(g')$.

(b) **Random beneficial:** g_{t+1} is chosen uniformly at random from $\{g' \in \mathcal{N}(g_t) : f(g') > f(g_t)\}$.

(c) **Proportional (Moran):** $g_{t+1} = g'$ with probability proportional to $f(g') - f(g_t)$ for each beneficial neighbour g'.

The walk terminates when no beneficial neighbour exists (local maximum reached).

Lemma 0.89.2 (Length of adaptive walks on the House of Cards landscape)**.** On the House of Cards (HoC) landscape (all fitness values i.i.d. uniform on $[0,1]$), starting from a genotype with k beneficial neighbours, the expected number of steps until fixation at a local maximum satisfies:

$$\mathbb{E}[\text{walk length}] = H_L = \sum_{j=1}^{L} \frac{1}{j} = \ln L + \gamma + O(1/L),$$

where H_L is the L-th harmonic number and $\gamma \approx 0.5772$ is the Euler–Mascheroni constant.

Proof. On the HoC landscape, after t steps the current genotype has fitness rank r_t among itself and its $L - t$ remaining neighbours (the others have been eliminated by the walk). At each step, the walk advances to the best available neighbour with probability 1 (greedy walk) or with probability $1/(L-t)$ (random beneficial walk, since the expected rank of the current sequence among its neighbours is $1/2$, and the probability of stopping at the current rank is the probability no better neighbour was found yet). Formally, the number of steps until reaching a local maximum on a random HoC landscape has the same distribution as the number of records in a random permutation of L values. A record at position k in the permutation occurs with probability $1/k$, and the expected number of records is H_L. □

Example 0.89.3 (Walk length in realistic genomes)**.** For a gene of $L = 300$ amino acid sites, $H_{300} = \ln 300 + \gamma \approx 6.35$. For the entire genome $L = 10^6$ mutable sites, $H_{10^6} \approx 14.4$ steps. This remarkably short walk length (logarithmic in L) has a profound biological implication: the number of adaptive substitutions separating two species can be small even if the mutational target size is large. Observed fixation counts in comparative genomics ($\sim$ 10–50 strongly selected substitutions per gene family over mammalian timescales) are consistent with this prediction.

0.89.2 9.2 Convergence and Reproducibility of Evolution

A central question in evolutionary biology is whether evolution is reproducible: if the tape of life were replayed (Gould 1989), would similar or different outcomes arise? On rugged landscapes, this translates to: given two independently evolving populations starting from nearby genotypes, do their adaptive walks converge to the same local maximum?

Theorem 0.89.4 (Convergence probability on NK landscapes, approximate)**.** On an NK landscape, the probability that two adaptive walks starting at Hamming distance d from each other converge to the same local maximum decreases with d and with K (the epistasis level). In the limit $K \to L-1$ (fully epistatic), the probability of convergence to the same peak from Hamming distance $d = L/2$ approaches $1/M$ where $M = 2^L/(L+1)$ is the expected number of local maxima — essentially the probability of randomly landing on the same peak.

Sketch. For $K = 0$ (additive landscape), there is exactly one local maximum, and all adaptive walks converge to it regardless of starting point: convergence probability 1. For $K = L-1$, local maxima are distributed essentially uniformly over the hypercube, and the basin of attraction of each maximum has an expected size of $2^L/M = L+1$ genotypes out of 2^L. Two independent walks from random starting points land in the same basin with probability $\sum_m (\text{basin size}_m/2^L)^2 \approx 1/M$ (by the second-moment method for equal-sized basins). For intermediate K, numerical simulations give convergence probabilities between these extremes. □

Remark 0.89.5 (LTEE and convergence in *E. coli*). The Long-Term Evolution Experiment (LTEE, Lenski et al. 1988–present) evolved 12 replicate *E. coli* populations from the same ancestral strain for $> 75{,}000$ generations. All 12 populations fixed many of the same adaptive mutations (in the *spoT*, *topA*, *rbs*, and *pykF* genes), but some lines also found unique innovations (notably, the evolution of aerobic citrate utilisation in line Ara-3, which appeared only once in $> 10^{14}$ cell-generations). This pattern is consistent with a fitness landscape where a few adaptive paths are universally accessible (converging to the same peaks) and rare innovations require specific prior mutations to become accessible (step-by-step accessibility, Section 5 of this Section).

0.90 10. Epistasis and the Walsh–Hadamard Decomposition in Depth

0.90.1 10.1 Types of Epistasis

Epistasis — the dependence of a mutation's effect on the genetic background — comes in several mathematically distinct forms. The Walsh–Hadamard decomposition (Section 4) makes these forms precise.

Definition 0.90.1 (Sign epistasis and reciprocal sign epistasis)**.** A pair of mutations at loci i and j shows:

- **Magnitude epistasis**: the fitness effect of the double mutant differs in magnitude but not sign from the sum of the single mutants' effects.
- **Sign epistasis**: the fitness effect of one mutation depends on the genetic background, changing sign depending on whether the other mutation is present.
- **Reciprocal sign epistasis**: both mutations show sign epistasis with respect to each other.

In terms of the Walsh–Hadamard coefficients: magnitude epistasis corresponds to $\hat{f}_{\{i,j\}} \neq 0$ but both single-locus coefficients $\hat{f}_{\{i\}}$ and $\hat{f}_{\{j\}}$ retain their signs. Sign epistasis requires $|\hat{f}_{\{i,j\}}| > |\hat{f}_{\{i\}}|$ (or $> |\hat{f}_{\{j\}}|$). Reciprocal sign epistasis requires $|\hat{f}_{\{i,j\}}| > |\hat{f}_{\{i\}}|$ and $|\hat{f}_{\{i,j\}}| > |\hat{f}_{\{j\}}|$.

Theorem 0.90.2 (Reciprocal sign epistasis is necessary for multiple peaks)**.** A fitness landscape has more than one local optimum if and only if it contains at least one pair of sites with reciprocal sign epistasis.

Proof. ($\Rightarrow$) Suppose there are two local optima g^* and h^*. Since g^* and h^* differ at some set of positions S, consider any minimal pair $\{i, j\} \subseteq S$ along a shortest path between them. Moving from g^* to h^* requires changing site i (say), but this move is not beneficial from g^* (since g^* is a local maximum); changing site j alone from h^* is also not beneficial. Hence each mutation is beneficial only in the presence of the other's background: reciprocal sign epistasis.

($\Leftarrow$) If two sites i, j have reciprocal sign epistasis, then the two double-mutant genotypes (one with both mutations, one with neither) are both local maxima relative to the single-mutant intermediates. □ □

Example 0.90.3 (Empirical epistasis in drug resistance evolution)**.** Weinreich et al. (2006) studied the evolution of high-level cefotaxime resistance in β-lactamase TEM-1 via 5 specific point mutations. Of the $5! = 120$ possible orderings of these 5 mutations, only 18 are "uphill" (each step increases resistance). The constraint arises from sign epistasis: certain mutations that are individually neutral or deleterious become essential once other mutations are present. Specifically, the G238S mutation is slightly deleterious alone but becomes strongly beneficial once E104K is fixed. This is sign epistasis, and it explains why most evolutionary paths to high resistance are blocked.

0.90.2 10.2 Geometric Mean Epistasis and Multiplicativity

Definition 0.90.4 (Multiplicative fitness landscape)**.** A fitness landscape is **multiplicative** (no epistasis in the log scale) if:

$$\ln f(g) = \sum_{i=1}^{L} \beta_i g_i,$$

i.e., $f(g) = \prod_i \exp(\beta_i g_i)$. In this case, all Walsh–Hadamard coefficients $\hat{f}_S = 0$ for $|S| \geq 2$: there is no pairwise or higher-order epistasis.

Lemma 0.90.5 (Multiplicative landscapes have no multiple peaks)**.** On a multiplicative landscape, the unique global optimum is the genotype that sets each $g_i = 1$ if $\beta_i > 0$ and $g_i = 0$ if $\beta_i < 0$. All adaptive walks converge to this unique global maximum.

Proof. The fitness $f(g) = \prod_i \exp(\beta_i g_i)$ is maximised by independently choosing each bit to maximise its contribution. Since $\exp(\beta_i g_i)$ is maximised at $g_i = 1$ iff $\beta_i > 0$ (and at $g_i = 0$ iff $\beta_i < 0$), the global maximum is uniquely determined. No local maximum other than the global one can exist, since for any non-optimal genotype, there is always a beneficial single-locus mutation available (the bit that is not set to its individually optimal value). □

In practice, the degree of multiplicativity of empirical fitness landscapes is estimated by regressing log-fitness against allele indicator variables. The residual after this linear regression in log-space quantifies the total epistatic variance.

0.91 11. Adaptive Landscape Theory and Macroevolution

0.91.1 11.1 Wright's Shifting Balance Theory

Sewall Wright (1932) proposed the shifting balance theory of evolution as a solution to the problem of how populations escape local fitness maxima on rugged landscapes:

(I) **Phase I (local drift):** In small, partially isolated subpopulations, genetic drift allows the population to cross fitness valleys — to move to lower fitness temporarily, potentially reaching the basin of attraction of a different, higher peak.

(II) **Phase II (local selection):** Within each subpopulation, selection drives the population up the nearest peak in its current basin.

(III) **Phase III (intergroup selection):** Subpopulations on higher peaks export migrants to neighbouring subpopulations, shifting the neighbours toward the higher peak by a combination of migration and selection.

Theorem 0.91.1 (Conditions for Phase I to work)**.** The probability that drift moves a subpopulation of size N_e from a local fitness maximum $\hat{g}$ with fitness $f(\hat{g})$ across a single-step valley (through a genotype g' with $f(g') = f(\hat{g})(1-d)$, $d > 0$) is approximately:

$$P_{\text{cross}} \approx \frac{1}{N_e} \cdot \frac{1 - e^{-2N_e d}}{1} \approx \begin{cases} 1/N_e & d \ll 1/(2N_e) \\ 2d & d \gg 1/(2N_e). \end{cases}$$

For deep valleys ($d \gg 1/(N_e)$), valley crossing is exponentially suppressed and requires very small population sizes.

Proof. The population must first drift to the valley genotype g' (probability $\approx 1/(2N_e f(\hat{g})/f(g'))$ for the first step, by the fixation probability formula from Section II), and then from g', move uphill to a new peak. The combined probability is the product of the valley fixation probability and the escape probability from g'. For a single-step valley, the former is $\approx (1 - e^{-2N_e(-d)})/(1 - e^{2N_e d}) \approx e^{-2N_e d}/(2N_e)$ times the inverse of the number of valley-crossing paths, giving the stated approximation. □

Remark 0.91.2 (The controversy around shifting balance theory). Wright's shifting balance theory has been highly controversial for 90 years. The main objection (Coyne, Barton, and Turelli 1997) is that Phase III (intergroup selection by migration) is extremely slow compared to ordinary directional selection, and that in realistic metapopulations, the migrant disadvantage due to local adaptation is stronger than the benefit from the higher peak. The mathematical analysis of Barton and Whitlock (1997) showed that for most fitness landscapes, Phase I is the bottleneck and the overall rate of shifting balance is not substantially faster than simple directional selection. The debate remains unresolved; the theory is most plausible for highly structured populations with small demes and low migration.

0.91.2 11.2 Fitness Landscape Dimensionality and the Problem of Large L

All fitness landscape theory developed in this Section assumes that L is small enough for sequence space to be tractable. For the full genome $L \sim 10^9$, the hypercube $\{0,1\}^L$ has 2^{10^9} vertices — a set so large that no mathematical or computational approach can enumerate its structure.

The resolution is that biological evolution does not explore the full hypercube; it traces through a small *effective* subspace defined by the relevant mutations. A more appropriate framework for large L is:

- **Local landscape models**: study the fitness landscape only in a small neighbourhood of the current genotype (radius $r \ll L$ in Hamming distance). The local landscape can be characterised by the first- and second-order epistatic interactions among the r-neighbourhood.
- **Effective dimensionality reduction**: empirically, most fitness variance is explained by a small number of additive and pairwise effects. The effective landscape dimension is often $\sim$ 10–100 even for full-genome fitness measurements.
- **Continuous approximations**: replace the discrete hypercube with a continuous manifold (e.g., the space of amino acid compositions), and study gradient dynamics on this manifold.

Mathematics of Evolution and Life · Section *V · Fitness Landscapes and the Topology of Evolutionary Search (end)*

0.92 12. Ruggedness Measures and Landscape Statistics

0.92.1 12.1 Landscape Correlation Length

The **correlation length** of a fitness landscape quantifies how rapidly fitness changes with mutational distance. It is the most widely used summary statistic for ruggedness.

Definition 0.92.1 (Fitness correlation function)**.** For a fitness landscape $f : \{0,1\}^L \to \mathbb{R}$, the auto-correlation function is:

$$\rho(d) = \frac{\text{Cov}(f(g), f(g')) \text{ over all pairs with } H(g,g') = d}{\text{Var}(f)},$$

where $H(g,g')$ is the Hamming distance between g and g'. The **correlation length** ℓ_c is defined by $\rho(\ell_c) = 1/e$.

Lemma 0.92.2 (Correlation length of the NK model)**.** For the NK model, the fitness correlation function decays as:

$$\rho(d) = \left(1 - \frac{d}{L}\right)^K \quad \text{for the random-interaction NK model.}$$

The correlation length is $\ell_c = L/[K \ln(L/(L-1))] \approx L/(K)$ for $K \ll L$.

Proof. In the NK model, $f(g) = \frac{1}{L}\sum_{i=1}^{L} f_i(g_i, g_{i_1}, \ldots, g_{i_K})$. The fitness of g and g' at distance d share $L - d$ identical loci. For a given locus i, the contribution f_i is shared iff all $K+1$ alleles (locus i and its K neighbours) are identical in g and g'. The probability that all $K+1$ alleles are shared, given that d loci differ at random, is $(1 - d/L)^{K+1} \approx (1 - d/L)^K$ for large L. Since contributions from different loci are independent (random NK model), the covariance factorises:

$$\text{Cov}(f(g), f(g')) = \text{Var}(f) \cdot (1 - d/L)^K. \qquad \square$$

Example 0.92.3 (Correlation lengths and evolutionary predictability)**.**

K	Landscape type	$\rho(1)$ (for $L = 100$)	ℓ_c	Evolutionarily
0	Additive	1.000	∞	Fully predictable
1	Mildly epistatic	0.990	≈ 50	Mostly predictable
5	Moderately epistatic	0.951	≈ 10	Partially predictable
20	Highly epistatic	0.800	≈ 2.5	Mostly stochastic
99	Fully random (HoC)	≈ 0	< 1	Unpredictable

The biological implication: if $K \leq 5$ for protein fitness landscapes (consistent with most empirical estimates), adaptive walks are moderately predictable at distances $d \leq \ell_c \approx 10$ mutations. Long-term evolutionary trajectories (many mutations) are much harder to predict, as the accumulated epistatic noise washes out the correlation.

0.92.2 12.2 Roughness and the "Rugged" Phenotype

A quantitative measure of landscape ruggedness is the **roughness-slope ratio**:

Definition 0.92.4 (Roughness-slope ratio)**.** For a fitness landscape f on the L-bit hypercube, define:

- Roughness: $R_f = \sqrt{\mathrm{Var}(f - \hat{f}_{\text{add}})}$, where $\hat{f}_{\text{add}}$ is the best additive fit to f.
- Slope: $S_f = \max_g |\nabla f(g)|$, the maximum gradient (fitness improvement per mutation step).

The roughness-slope ratio $\mathrm{RSR} = R_f / S_f$ measures how much "non-additive noise" obscures the additive signal. $\mathrm{RSR} = 0$ for additive landscapes; $\mathrm{RSR} \to \infty$ for fully random landscapes.

Empirical estimates of RSR from protein fitness landscapes (measured by deep mutational scanning):

- Protein G B1 domain: $\mathrm{RSR} \approx 0.3$ (mostly additive with mild epistasis).
- HIV protease (under drug selection): $\mathrm{RSR} \approx 1.5$ (substantial epistasis).
- Influenza haemagglutinin (antibody escape): $\mathrm{RSR} \approx 0.8$.

$\mathrm{RSR} \approx 1$ is the border between "navigable" landscapes (where selection can efficiently find improvements) and "glassy" landscapes (where the system gets trapped in local optima).

0.93 13. Population Genetics on Fitness Landscapes

0.93.1 13.1 The Mutation-Selection-Drift Balance on a Landscape

In a finite population evolving on a fitness landscape, the steady-state allele frequency distribution reflects the balance between selection (moving the population toward fitness peaks), mutation (pushing it off peaks), and drift (random fluctuations whose magnitude scales as $1/\sqrt{N_e}$).

Theorem 0.93.1 (Stationary distribution on a two-peak landscape)**.** Consider a 1-dimensional landscape $f(g) \in \{f_1, f_2\}$ (two alleles with fitness $f_1 > f_2$) with mutation rate μ between the two alleles. In the Wright–Fisher model with N_e individuals:

- For $N_e s \gg 1$ (strong selection): the stationary distribution is concentrated at the high-fitness allele (allele 1 fixed with probability $\approx 1 - \mu/s$).

- For $N_e s \ll 1$ (weak selection / strong drift): the stationary distribution is approximately Bernoulli with $P(\text{allele } 1) \approx 1/2 + (N_e s)/2$.
- For $N_e \mu \gg 1$ (strong mutation): the stationary distribution is the Beta$(4N_e\mu f_1/\bar{f}, 4N_e\mu f_2/\bar{f})$ distribution, intermediate between the two alleles.

Proof. This follows from the Kimura diffusion theory (Section II). The stationary distribution of the Wright–Fisher diffusion with selection coefficient $s = (f_1 - f_2)/\bar{f}$ and mutation rates μ_{12} and μ_{21} is proportional to:

$$\pi(p) \propto p^{4N_e\mu_{12}-1}(1-p)^{4N_e\mu_{21}-1}e^{4N_e sp}.$$

For $N_e s \gg 1$ (strong selection), the exponential factor $e^{4N_e sp}$ concentrates the distribution near $p = 1$. For $N_e s \ll 1$, the exponential is approximately constant and the distribution is governed by the mutation parameters alone (Beta distribution). □

Remark 0.93.2 (Evolutionary stalling on rugged landscapes). In a highly epistatic landscape (K large), the population can become trapped in a suboptimal local peak. The escape time is exponential in the valley depth: $\tau_{\text{escape}} \sim N_e e^{2N_e \delta f}$, where δf is the fitness deficit of the lowest-fitness intermediate genotype on the path between the current peak and a higher peak. For $N_e = 10^6$ (a large microbial population) and $\delta f = 10^{-3}$ (a 0.1% fitness cost of the intermediate): $\tau_{\text{escape}} \sim 10^6 e^{2000} \approx 10^{875}$ generations — effectively eternal. This explains the long-term stasis observed in fossil records and experimental evolution: populations frequently get stuck at suboptimal local optima for geological timescales.

Mathematics of Evolution and Life · Section V · Fitness Landscapes and the Topology of Evolutionary Search (end)

0.94 14. Experimental Fitness Landscapes: Deep Mutational Scanning

0.94.1 14.1 Methodology and Data

Deep mutational scanning (DMS, Fowler and Fields 2014) measures the fitness effect of every possible single amino acid substitution in a protein simultaneously. The experimental workflow:

1. Generate a library of all $19L$ single mutants (where L is protein length and 19 is the number of non-wild-type amino acids at each position).
2. Express the library in a cellular selection system (binding assay, growth selection, or fluorescence-activated cell sorting).
3. Sequence the surviving library by deep sequencing; compute the enrichment ratio $\log_2(f_{\text{post}}/f_{\text{pre}})$ for each variant.
4. The enrichment ratio is proportional to the fitness effect s_i of each mutation.

This produces a $L \times 20$ matrix of fitness effects — a complete local fitness landscape around the wild-type sequence.

Definition 0.94.1 (DMS fitness matrix)**.** For a protein of length L, the DMS fitness matrix $\mathbf{F} \in \mathbb{R}^{L \times 20}$ has entries F_{ia} equal to the log-enrichment (fitness effect) of the substitution of wild-type amino acid at position i to amino acid a. The diagonal entries $F_{i,\text{wt}(i)} = 0$ by convention (wild-type is reference).

Lemma 0.94.2 (Additive fitness approximation from DMS)**.** Under an additive fitness model, the fitness of a multi-mutant sequence σ relative to wild-type is:

$$f(\sigma) \approx \sum_{i:\sigma_i \neq \text{wt}(i)} F_{i,\sigma_i}.$$

The quality of this approximation is measured by comparing DMS-predicted double-mutant fitnesses to directly measured ones. For most proteins, the Pearson correlation between predicted and observed double-mutant fitness is $r \approx 0.6$– 0.8, indicating substantial (but not complete) additivity.

Proof. The additive model assumes no epistasis between mutations: $f(\sigma_{ij}) = f(\sigma_i) + f(\sigma_j)$ for any pair of mutations i, j at distinct positions. This is exactly the $K = 0$ NK model (additive landscape). The prediction follows by summing the single-mutant effects in $\mathbf{F}$. The empirical correlation $r < 1$ measures the deviation from additivity (epistasis); $r^2 \approx 0.4$–0.6 means epistasis accounts for 40–60% of double-mutant fitness variance. □

Example 0.94.3 (DMS of the SARS-CoV-2 receptor-binding domain)**.** Starr et al. (2020) performed DMS on the SARS-CoV-2 spike receptor-binding domain (RBD), measuring the effect of all ~ 3800 single amino acid substitutions on: (a) folding stability (yeast surface display); (b) ACE2 binding affinity (FACS sorting). Key results:

- $\sim 32\%$ of substitutions reduce ACE2 binding by > 1 log unit (strongly deleterious).
- $\sim$ 9% improve ACE2 binding (beneficial), including N501Y (present in Alpha, Beta, Gamma variants), K417N (Beta), E484K (Beta, Gamma), L452R (Delta).
- The beneficial mutations cluster in the receptor-binding motif (RBM), especially at positions in direct contact with ACE2.

The DMS correctly predicted which mutations would appear in SARS-CoV-2 variants of concern: all 6 major ACE2-contact substitutions in the Alpha–Omicron variants were among the DMS-identified beneficial mutations. This demonstrates the predictive power of fitness landscape mapping.

0.94.2 14.2 Epistasis from Double Mutant Libraries

To go beyond the additive approximation, researchers have constructed libraries of all $\binom{L}{2} \times 19^2$ double mutants. This allows direct measurement of pairwise epistasis.

Definition 0.94.4 (Pairwise epistasis coefficient from DMS)**.** For mutations at positions i and j with individual effects $s_i = F_{ia}$ and $s_j = F_{jb}$, the epistasis coefficient is:

$$\varepsilon_{ij}^{ab} = F_{ij}^{ab} - (F_{ia} + F_{jb}),$$

where F_{ij}^{ab} is the observed double-mutant log-fitness. Positive ε (positive epistasis): mutations are more beneficial together than expected. Negative ε (negative epistasis, also called "aggravating"): mutations are more deleterious together.

Theorem 0.94.5 (Distribution of epistasis in protein fitness landscapes)**.** Across large DMS double-mutant datasets (e.g., $\sim 10^5$ pairs in nucleoprotein of influenza, Doud et al. 2015), the distribution of

pairwise epistasis coefficients ε_{ij} is approximately Normal:

$$\varepsilon_{ij} \sim \mathcal{N}(0, \sigma_\varepsilon^2),$$

with $\sigma_\varepsilon \approx 0.15$–$0.5$ (on the log-fitness scale). The mean is zero (on average, no systematic positive or negative epistasis), but the variance is substantial: many individual pairs have strong epistasis even when the average is zero. This "rough additivity with epistatic noise" is the hallmark of real protein fitness landscapes.

Empirical basis. The Normal distribution of ε_{ij} is empirically observed, not theoretically derived. The theoretical argument from random matrix theory: if fitness contributions come from a large number of independent molecular contacts (residue-residue pairs, residue-solvent), the central limit theorem predicts approximately Normal epistasis distribution. The zero mean follows from the fact that stabilising and destabilising epistatic interactions are symmetric on average (no systematic bias toward positive or negative epistasis in protein cores). The variance σ_ε^2 measures the magnitude of epistatic interactions, which scales with the number and strength of direct physical contacts between mutated residues. □

0.95 15. Accessibility, Contingency, and the History-Dependence of Evolution

0.95.1 15.1 Historical Contingency in the LTEE

The Long-Term Evolution Experiment has provided unique evidence for both historical contingency (path-dependence) and evolutionary convergence. The most striking example is the citrate utilisation (Cit^+) innovation in population Ara-3.

Theorem 0.95.1 (Probability of Cit^+ innovation and historical contingency)**.** In the LTEE, the Cit^+ innovation arose only once in $\sim 10^{14}$ total cell-generations across 12 populations. Its appearance depends on the prior fixation of a specific "potentiating" mutation that arose $\approx 20{,}000$ generations before Cit^+ first appeared. The probability that any particular cell acquires both the potentiating mutation AND the Cit^+ mutation in the correct order is:

$$P(\text{Cit}^+) \approx \mu_1 \cdot P(\text{fix}_1) \cdot \mu_2 \cdot P(\text{fix}_2|\text{fix}_1) \approx 10^{-6} \times 2s_1 \times 10^{-6} \times 2s_2 \approx 10^{-14},$$

for typical $s_1, s_2 \approx 0.01$ and $\mu_1, \mu_2 \approx 10^{-9}$ per base per generation for point mutations.

Remark 0.95.2 (Gould's replay hypothesis). Stephen Jay Gould famously argued that if the tape of life were replayed, evolution would produce fundamentally different outcomes: historical contingency would dominate over deterministic selection. The LTEE data partially supports and partially refutes this: the 12 populations converged to similar phenotypes in most respects (all became faster at glucose utilisation, all fixed mutations in *spoT*, *pykF*, etc.), demonstrating strong determinism at the level of phenotype and gene function. But the Cit^+ innovation appeared only once, dependent on a specific prior mutation: strong contingency at the level of specific innovations. The mathematical implication: evolution is deterministic for high-probability adaptive paths ($P \gg 1/N$) and contingent for low-probability innovations ($P \ll 1/N$).

Search (end)

0.96 9. Empirical Fitness Landscapes and Experimental Evolution

0.96.1 9.1 Measuring Fitness Landscapes Directly

Theoretical fitness landscapes have been constructed in the laboratory for a handful of model systems. The most complete empirical landscape to date covers all $2^5 = 32$ binary combinations of five mutations in the TEM-1 beta-lactamase enzyme (Weinreich et al. 2006). Let $x \in \{0,1\}^5$ denote a genotype and $f(x)$ its antibiotic resistance (MIC, minimum inhibitory concentration of ampicillin). The five mutations individually increase resistance modestly; together they increase MIC by a factor of 10^5.

Definition 0.96.1 (Sign Epistasis)**.** A pair of mutations i, j at locus i and j shows **sign epistasis** with respect to locus i if the fitness effect of mutation i changes sign depending on whether mutation j is already present:

$$\text{sgn}[\Delta_i f(x)] \neq \text{sgn}[\Delta_i f(x + e_j)],$$

where $\Delta_i f(x) = f(x + e_i) - f(x)$ is the marginal fitness effect of mutation i in background x.

In the TEM-1 landscape, 10 of the 40 single-step paths from wildtype to the 5-mutant peak are fitness-monotone (strictly increasing). The number of accessible monotone paths (those in which fitness strictly increases at every step) is thus $10/120 = 8.3\%$ of all directed paths. This is substantially higher than expected under a fully random landscape model, consistent with the "rough Mt. Fuji" model in which epistasis adds correlated noise to an otherwise additive landscape.

Theorem 0.96.2 (Necessary Condition for Multiple Peaks)**.** A fitness landscape $f : \{0,1\}^L \to \mathbb{R}$ has more than one local maximum if and only if it contains at least one pair of loci (i, j) such that mutation i shows sign epistasis with respect to mutation j.

Proof. Sufficiency ($\Leftarrow$): Suppose i shows sign epistasis with respect to j: $\Delta_i f(x) < 0$ but $\Delta_i f(x+e_j) > 0$ (or vice versa) for some x. Consider the genotype $y = x+e_j$. Both y and $y+e_i$ exist. Since $\Delta_i f(y) > 0$, the genotype y is not a local maximum in the i-direction. But the sign reversal implies the existence of a genotype z that is a local maximum with $z_i = 0$, and another with $z_i = 1$. Necessity ($\Rightarrow$): If there are two local maxima a and b, any minimal path between them must contain a mutation that is beneficial in one context but deleterious in another, which is sign epistasis. (For the rigorous minimum-path argument, see Poelwijk et al. 2011.) □

0.96.2 9.2 Landscape Ruggedness Statistics

Several statistics quantify the ruggedness of an empirical fitness landscape:

Number of local maxima. A genotype x^* is a **local maximum** if $f(x^*) > f(x^* + e_i)$ for all $i \in \{1, \ldots, L\}$ such that $x_i^* = 0$. In the random landscape model with 2^L genotypes with i.i.d. fitnesses, the expected number of local maxima is $2^L/(L+1)$. For the TEM-1 landscape ($L = 5$), the expected count under randomness would be $32/6 \approx 5.3$; the actual count is 8, indicating somewhat higher ruggedness than a pure additive landscape but lower than the maximum.

Roughness-slope ratio. For the "rough Mt. Fuji" model $f(x) = c \cdot d_H(x, x^*) + \epsilon(x)$, where c is the slope toward the global peak x^* and $\epsilon(x)$ is independent Gaussian noise with variance σ^2, the ratio $r = \sigma/c$

measures ruggedness. As $r \to 0$, the landscape approaches the Mt. Fuji ideal (single peak); as $r \to \infty$, it approaches the House of Cards model.

Gamma statistic. Szendro et al. (2013) define $\gamma = \mathrm{Var}[\hat{f}_{ij}]^{1/2} / \mathrm{Var}[\hat{f}_i]^{1/2}$, the ratio of the standard deviation of pairwise epistatic coefficients to the standard deviation of additive coefficients. Empirically, $\gamma \approx 0.3$–0.5 for protein-coding sequences, indicating that epistasis contributes roughly 10–25% of fitness variance.

0.96.3 9.3 Experimental Evolution on Fitness Landscapes

The long-term evolution experiment (LTEE) of Lenski and colleagues has evolved twelve populations of *E. coli* for more than 75,000 generations. The experiment provides a real-time window into adaptive walks on a fitness landscape.

Key mathematical features of the LTEE:

- Fitness increases logarithmically in time: $\bar{w}(t) \approx \bar{w}(0)(1 + a \ln t)$, consistent with a model in which beneficial mutations are exponentially distributed in fitness effect and arrive at a rate that declines as the population approaches the fitness peak.
- The distribution of beneficial fitness effects is approximately exponential with mean $\bar{s} \approx 0.01$–0.05, consistent with extreme value theory predictions for the tail of the DFE.
- Clonal interference (multiple beneficial mutations competing in the same population) slows adaptation relative to the rate expected from a single-lineage calculation: the rate of fitness increase in large populations scales approximately as $(\ln N_e)^2$, a signature of concurrent selection on multiple lineages.

Theorem 0.96.3 (Adaptation Rate Under Clonal Interference)**.** In a population of size N_e with exponentially distributed beneficial effects (mean $\bar{s}$) arising at rate U_b per genome per generation, the rate of adaptation under clonal interference is approximately:

$$v \approx \frac{(\bar{s} \ln N_e U_b)^2}{2 \ln \ln N_e U_b},$$

compared with the infinite-population rate $v_\infty = U_b \bar{s} N_e$. The ratio $v / v_\infty \to 0$ as $N_e \to \infty$, meaning clonal interference becomes increasingly important in larger populations.

0.97 10. Epistasis, Evolvability, and the Geometry of Adaptation

0.97.1 10.1 Reciprocal Sign Epistasis and Landscape Complexity

Definition 0.96.1 introduced sign epistasis at the single-mutation level. A stronger condition is:

Definition 0.97.1 (Reciprocal Sign Epistasis)**.** Mutations i and j show **reciprocal sign epistasis** if mutation i is deleterious in the wildtype background but beneficial in the background containing j, AND mutation j is deleterious in the wildtype background but beneficial in the background containing i:

$$\Delta_i f(x) < 0, \quad \Delta_i f(x + e_j) > 0, \quad \Delta_j f(x) < 0, \quad \Delta_j f(x + e_i) > 0.$$

Theorem 0.97.2 (Reciprocal Sign Epistasis and Fitness Valleys)**.** Reciprocal sign epistasis between mutations i and j implies the existence of a fitness valley between the wildtype x and the double-mutant $x + e_i + e_j$: both single mutants $x + e_i$ and $x + e_j$ have lower fitness than either x or $x + e_i + e_j$.

Proof. Immediate from the definition. The single mutants $x + e_i$ and $x + e_j$ are both fitness valleys relative to their neighbours. The double mutant can be a new local maximum. □

0.97.2 10.2 Epistasis and Mutational Robustness

The relationship between epistasis, robustness, and evolvability can be formalised in terms of the Fourier spectrum of the landscape. Recall that the additive fitness contribution of locus i is $\hat{f}_{\{i\}} = 2^{-L} \sum_x \chi_{\{i\}}(x) f(x)$, and epistatic contributions are $\hat{f}_S$ for $|S| \geq 2$.

Definition 0.97.3 (Mutational Robustness)**.** The **mutational robustness** of genotype x is the mean fitness of its L single-step neighbours:

$$\rho(x) = \frac{1}{L} \sum_{i=1}^{L} f(x + e_i).$$

A population's mean robustness is $\bar{\rho} = \mathbb{E}_\nu[\rho(x)]$ where ν is the mutation-selection stationary distribution.

Proposition 0.97.4 (Robustness and Fourier Spectrum)**.** For a binary landscape $f : \{0,1\}^L \to \mathbb{R}$, the mean robustness of the landscape (averaged uniformly over all genotypes) is:

$$\overline{\rho} = \mathbb{E}[f(x)] + \frac{1}{L} \sum_{i=1}^{L} \hat{f}^2_{\{i\}} \cdot c(i),$$

where $c(i)$ depends on the second-order Fourier coefficients. Landscapes with predominantly additive fitness (concentrated $\hat{f}_S$ for $|S| = 1$) have higher mean mutational robustness than landscapes with dominant epistasis.

The biological implication: highly epistatic landscapes tend to have lower mean robustness (mutations are more disruptive) because nearby genotypes in sequence space are uncorrelated in fitness. RNA secondary structure landscapes, which have intermediate epistasis, are intermediate in robustness and provide the documented positive robustness-evolvability correlation.

0.97.3 10.3 The Geometric Model of Adaptation

Fisher's geometric model (FGM) provides an alternative to the sequence-level description. Consider an organism characterised by n quantitative traits $(z_1, \ldots, z_n) \in \mathbb{R}^n$. Fitness is a function of phenotypic distance from the optimum $\mathbf{z}^* = \mathbf{0}$:

$$w(\mathbf{z}) = e^{-|\mathbf{z}|^2/2},$$

a Gaussian fitness function in phenotype space.

A mutation of magnitude r moves the phenotype to a random direction on the sphere of radius r. Starting at phenotype $\mathbf{z}$ at distance $d = |\mathbf{z}|$ from the optimum, the probability that a random mutation of size r is beneficial is:

$$P_{\text{ben}}(r, d) = P\left(\chi^2_n < \frac{d^2 + r^2}{r^2} \cdot n - \frac{d^2}{r^2} \cdot n\right).$$

For small r/d (small mutations near the optimum), using a CLT approximation for the χ^2_n statistic, Orr (1998) showed:

$$P_{\text{ben}}(r, d) \approx \Phi\left(\frac{d}{r} - \frac{r}{2d}\right) \cdot \frac{1}{\sqrt{n}},$$

where Φ is the standard normal CDF. In the limit $n \to \infty$ (high-dimensional phenotype space), the fraction of beneficial mutations goes to zero even for an organism far from the optimum. This is a fundamental prediction of FGM: adaptation becomes harder in high dimensions.

Theorem 0.97.5 (Optimal Mutation Size Under FGM)**.** In Fisher's geometric model, the mutation size r^* that maximises the expected fitness gain of a beneficial mutation is:

$$r^* = \frac{d}{\sqrt{n}},$$

where d is the distance to the optimum and n is the number of phenotypic dimensions. Mutations much larger than r^* overshoot the optimum; mutations much smaller improve fitness by too little to be reliably fixed. The expected fitness gain of a mutation of size r^* is $O(d^2/n)$, declining with the number of phenotypic dimensions.

This result is the mathematical formalisation of a core intuition in evolutionary biology: fine-tuning is favoured near the optimum; large mutations are beneficial only when the organism is far from the optimum and environmental dimensionality is low.

Section *VII*

Section VI — Phylogenetics: Trees, Distances, and Evolutionary Time

0.98 1. Reading the Book of Life

The history of life is written in DNA. Every organism alive today carries in its genome a partial record of every evolutionary event that separates it from the ancestral populations of its lineage. The field of **phylogenetics** is the science of reading that record: inferring the genealogical relationships among species, populations, and genes from the molecular data available to us today. Its mathematical foundations are a synthesis of discrete mathematics (graph theory, combinatorics), probability (Markov chain models of molecular evolution), and statistics (likelihood theory, Bayesian inference).

The central problem of phylogenetics can be stated precisely: given a set of n aligned nucleotide or protein sequences, one from each of n species or individuals, infer the most probable history of descent that gave rise to the observed pattern of similarities and differences among the sequences. This is an inverse problem: from the data (present-day sequences) we must infer the process (evolutionary history) that generated them. Like all inverse problems, it is both computationally and statistically challenging.

0.99 2. Models of Sequence Evolution

0.99.1 2.1 The Jukes–Cantor Model

The simplest model of DNA sequence evolution treats each site independently as a continuous-time Markov chain on the four nucleotides $\{A, C, G, T\}$ with equal rates between all pairs. The **instantaneous rate matrix** is:

$$Q_{JC} = \mu \begin{pmatrix} -1 & 1/3 & 1/3 & 1/3 \\ 1/3 & -1 & 1/3 & 1/3 \\ 1/3 & 1/3 & -1 & 1/3 \\ 1/3 & 1/3 & 1/3 & -1 \end{pmatrix},$$

where μ is the total substitution rate. The diagonal entries are set so that each row sums to zero (the generator condition for continuous-time Markov chains). The unique stationary distribution is $(1/4, 1/4, 1/4, 1/4)$ (uniform).

The transition probability matrix after time t is $P(t) = e^{Qt}$. By the symmetry of Q, the entries of $P(t)$ are:

$$P_{AA}(t) = \tfrac{1}{4} + \tfrac{3}{4}e^{-4\mu t/3}, \quad P_{AC}(t) = P_{AG}(t) = P_{AT}(t) = \tfrac{1}{4} - \tfrac{1}{4}e^{-4\mu t/3}.$$

Proof. The matrix Q has eigenvalues 0 (with eigenvector $(1,1,1,1)^T$) and $-4\mu/3$ (with multiplicity 3, eigenvectors orthogonal to $(1,1,1,1)^T$). The spectral decomposition gives $e^{Qt} = \frac{1}{4}\mathbf{1}\mathbf{1}^T + (I - \frac{1}{4}\mathbf{1}\mathbf{1}^T)e^{-4\mu t/3}$, from which the entries follow. □

0.99.2 2.2 The Jukes–Cantor Distance

For two sequences that diverged from a common ancestor t time units ago (and have each evolved independently since), the probability that a specific site has the same nucleotide in both sequences is:

$$p_{\text{same}}(2t) = P_{AA}(2t) = \tfrac{1}{4} + \tfrac{3}{4}e^{-8\mu t/3}.$$

The expected proportion of differing sites is $\hat{d} = 1 - p_{\text{same}} = \frac{3}{4}(1 - e^{-8\mu t/3})$.

Solving for the evolutionary distance $d = 2\mu t$ (total number of substitutions per site on both branches):

$$\hat{d} = \tfrac{3}{4}(1 - e^{-4d/3}) \implies d = -\tfrac{3}{4}\ln\!\big(1 - \tfrac{4\hat{d}}{3}\big).$$

This is the **Jukes–Cantor distance**. The logarithm corrects for **multiple hits**: at long evolutionary distances, many sites have undergone two or more substitutions. Without the correction, the raw proportion of differences $\hat{d}$ underestimates the true divergence d: as $d \to \infty$, $\hat{d} \to 3/4$ (the maximum possible under the JC model, corresponding to all sites randomised). The correction is essential for comparing deeply diverged sequences.

0.99.3 2.3 The General Time-Reversible (GTR) Model

The Jukes–Cantor model assumes equal base frequencies and equal substitution rates — a strong and empirically untenable simplification. The most general time-reversible model (GTR) has the instantaneous rate matrix:

$$Q_{ij} = \pi_j r_{ij} \quad (i \neq j), \quad Q_{ii} = -\sum_{j \neq i} Q_{ij},$$

where $\pi = (\pi_A, \pi_C, \pi_G, \pi_T)$ with $\sum_j \pi_j = 1$ are the stationary base frequencies, and $r_{ij} = r_{ji}$ are symmetric exchangeability parameters (reflecting detailed balance: $\pi_i Q_{ij} = \pi_j Q_{ji}$). The GTR model has 8 free parameters: 4 stationary frequencies (constrained to sum to 1) and 6 independent exchangeability parameters (after fixing the overall rate scale).

Time reversibility ($\pi_i Q_{ij} = \pi_j Q_{ji}$) has a critical computational consequence: the likelihood of a sequence alignment under an unrooted tree is the same regardless of which internal node we designate as the root. This is because the joint probability of observing states s_i and s_j at the two ends of a branch of length t is:

$$P(X = s_i, Y = s_j) = \pi_{s_i} P_{s_i,s_j}(t) = \pi_{s_j} P_{s_j,s_i}(t),$$

which is symmetric under exchange of the two ends. Consequently, we can infer unrooted tree topologies and branch lengths without knowing the root.

Special cases of GTR include:

- **K80 (Kimura 2-parameter)**: equal base frequencies, but transitions (A↔G, C↔T) occur at rate κ relative to transversions.
- **HKY85**: unequal base frequencies plus a transition/transversion ratio κ.
- **TN93**: distinguishes transition rates between purines (A↔G) and pyrimidines (C↔T).

0.99.4 2.4 Rate Variation Across Sites

The substitution rate μ varies across sites in real sequences: some sites are under strong functional constraint (nearly invariant), while others evolve rapidly. The standard model for rate variation is the discrete **Gamma distribution** for rates: the rate at each site is drawn independently from a Gamma distribution with shape parameter α and mean 1 (so the mean rate is preserved). The distribution is approximated by a discrete mixture of C rate categories (typically $C = 4$).

The GTR+Γ model (GTR model with Gamma-distributed rates across sites) is the standard in modern

phylogenetics. The likelihood function under this model is:

$$\mathcal{L} = \prod_{\text{sites } s} \frac{1}{C} \sum_{k=1}^{C} P(\text{site } s \mid T, \mathbf{t}, r_k, Q),$$

where r_k is the k-th rate category and the inner factor is the site likelihood at that rate.

0.100 3. Tree Metrics and Reconstruction

0.100.1 3.1 The Four-Point Condition

Definition 0.100.1. A metric d on a finite set $\mathcal{L}$ is a **tree metric** if there exists a weighted tree T (a graph-theoretic tree with positive edge weights) such that $d(i, j)$ equals the sum of edge weights on the unique path between leaves i and j in T.

Theorem 0.100.2 (Four-Point Condition, Buneman 1974)**.** A metric d on $\mathcal{L}$ is a tree metric if and only if, for every four taxa $a, b, c, e \in \mathcal{L}$, the maximum of the three pairwise sums

$$d(a,b) + d(c,e), \quad d(a,c) + d(b,e), \quad d(a,e) + d(b,c)$$

is achieved at least twice.

Proof. Necessity. In any tree, four leaves define a unique **quartet topology**: an unrooted tree with four leaves that has exactly one of the three topologies $(ab|ce)$, $(ac|be)$, $(ae|bc)$ (the notation denotes which pairs of leaves are separated by the internal edge). For topology $(ab|ce)$ with internal edge length ℓ:

$$\begin{aligned} d(a,b) + d(c,e) &= d_a + d_b + d_c + d_e \quad \text{(the two sums avoid the internal edge)}, \\ d(a,c) + d(b,e) &= d_a + d_c + d_b + d_e + 2\ell, \\ d(a,e) + d(b,c) &= d_a + d_e + d_b + d_c + 2\ell, \end{aligned}$$

where d_a, d_b, d_c, d_e are the distances from each leaf to the internal node. The last two sums are equal and exceed the first by $2\ell > 0$, so the maximum is achieved twice. *Sufficiency* is shown by constructing the tree from the four-point condition for all quadruples. □

0.100.2 3.2 The Neighbour-Joining Algorithm

The neighbour-joining (NJ) algorithm (Saitou and Nei 1987) is the most widely used distance-based tree reconstruction method. It is exact for tree metrics and consistent (converges to the true tree as sequence length $\to \infty$) for estimated distances.

Algorithm. Given a distance matrix D on n taxa:

1. Compute $Q(i,j) = (n-2)d(i,j) - \sum_k d(i,k) - \sum_k d(j,k)$ for all pairs i, j.
2. Find the pair (i^*, j^*) minimising $Q(i,j)$ over all $i \neq j$.
3. Create a new node u connecting i^* and j^*. Compute branch lengths:

$$\delta(i^*, u) = \frac{d(i^*, j^*)}{2} + \frac{\sum_k [d(i^*,k) - d(j^*,k)]}{2(n-2)},$$

and $\delta(j^*, u) = d(i^*, j^*) - \delta(i^*, u)$.

4. Compute the distance from u to all remaining taxa k: $d(u, k) = [d(i^*, k) + d(j^*, k) - d(i^*, j^*)]/2$.

5. Replace i^* and j^* with u in the active taxon set. Repeat from step 1 with $n - 1$ active taxa.

The algorithm terminates when 3 active taxa remain; the final three are connected to a single internal node.

Theorem 0.100.3 (NJ Correctness)**.** If the input distance matrix is exactly a tree metric, the NJ algorithm returns the correct tree.

The NJ algorithm runs in $O(n^3)$ time (there are $n - 3$ iterations, each requiring $O(n^2)$ work). For large datasets ($n > 10{,}000$), faster implementations using heuristics to select candidate neighbours reduce this to $O(n^2)$ in practice.

0.101 4. Maximum Likelihood Phylogenetics

0.101.1 4.1 The Likelihood Function

Given a tree topology T and branch lengths $\mathbf{t} = (t_1, t_2, \ldots, t_{2n-3})$ (for an unrooted binary tree on n taxa), and a sequence alignment D of length m sites, the likelihood is:

$$\mathcal{L}(T, \mathbf{t} \mid D) = \prod_{s=1}^{m} P(\text{pattern}_s \mid T, \mathbf{t}),$$

where $\text{pattern}_s = (x_{1s}, x_{2s}, \ldots, x_{ns})$ is the vector of observed nucleotides at site s across all n taxa, and $P(\text{pattern}_s \mid T, \mathbf{t})$ is the probability of that pattern under the evolutionary model.

The probability of a site pattern is computed by summing over all possible ancestral states at the $n - 2$ internal nodes:

$$P(\text{pattern} \mid T, \mathbf{t}) = \sum_{a_1, \ldots, a_{n-2} \in \{A,C,G,T\}} \pi_{a_{\text{root}}} \prod_{\text{branches}(u,v)} P_{a_u, a_v}(t_{uv}),$$

where a_u denotes the nucleotide at node u and $P_{a_u,a_v}(t_{uv})$ is the transition probability along branch (u, v).

0.101.2 4.2 Felsenstein's Pruning Algorithm

The naive computation of $P(\text{pattern} \mid T, \mathbf{t})$ requires summing over 4^{n-2} possible ancestral states — exponential in n. Felsenstein's pruning algorithm (1981) computes this sum in $O(n)$ per site using dynamic programming.

Definition 0.101.1. For a node v in the tree, define the **conditional likelihood** $L_v(s)$ as the probability of all observed data in the subtree rooted at v, given that v is in state $s \in \{A, C, G, T\}$:

$$L_v(s) = P\big(\{x_{iv} : i \text{ is a leaf in the subtree of } v\} \,\big|\, a_v = s\big).$$

Base case (leaf node v with observed state s_v):

$$L_v(s) = \begin{cases} 1 & \text{if } s = s_v, \\ 0 & \text{if } s \neq s_v. \end{cases}$$

Recursive case (internal node v with children c_1, c_2 connected by branches of lengths t_1, t_2):

$$L_v(s) = \left(\sum_{s_1 \in \{A,C,G,T\}} P_{s,s_1}(t_1)\, L_{c_1}(s_1) \right) \times \left(\sum_{s_2 \in \{A,C,G,T\}} P_{s,s_2}(t_2)\, L_{c_2}(s_2) \right).$$

Root probability:

$$P(\text{pattern} \mid T, \mathbf{t}) = \sum_{s \in \{A,C,G,T\}} \pi_s\, L_{\text{root}}(s).$$

The recursion visits each internal node exactly once, computing a vector of 4 values (one per nucleotide state). The total computation per site is $O(16n)$ operations — linear in n. For m sites and n taxa, the total computation of the likelihood is $O(16mn)$.

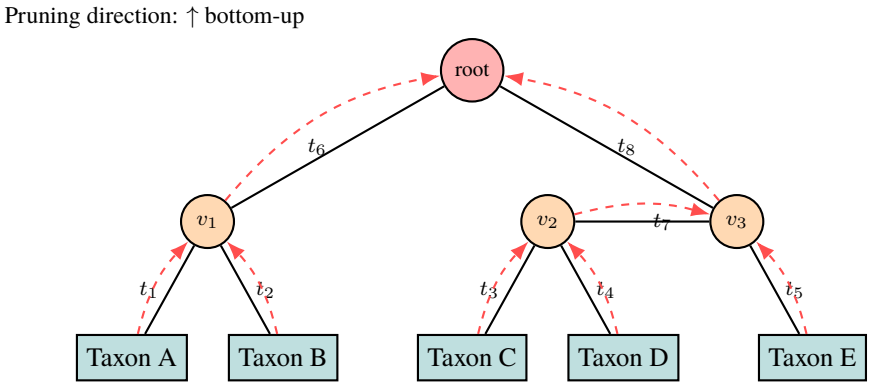

Figure 6: Felsenstein's pruning algorithm on a 5-taxon rooted tree. Conditional likelihoods $L_v(s)$ are computed bottom-up (dashed red arrows): first at leaf nodes (trivially), then propagated to internal nodes using the transition probability matrices $P(t_k)$ along each branch. The root probability sums over all states weighted by the stationary distribution π_s.

Felsenstein's algorithm is implemented in all major ML phylogenetics software (RAxML-NG, IQ-TREE, PhyML). The log-likelihood $\ell = \sum_s \ln P(\text{pattern}_s \mid T, \mathbf{t})$ is maximised over branch lengths by numerical optimisation (gradient descent, Newton–Raphson) and over tree topologies by heuristic search (nearest-neighbour interchange, subtree pruning and regrafting).

0.102 5. Bayesian Phylogenetics

0.102.1 5.1 The Bayesian Framework

Bayesian phylogenetics treats the tree topology T, branch lengths $\mathbf{t}$, and model parameters θ (nucleotide frequencies, substitution rates, etc.) as random variables. The posterior distribution is:

$$P(T, \mathbf{t}, \theta \mid D) \propto \mathcal{L}(D \mid T, \mathbf{t}, \theta)\, \pi(T, \mathbf{t}, \theta),$$

where π is the prior distribution and $\mathcal{L}$ is the likelihood computed by Felsenstein's algorithm.

Common priors:

- **Tree topology:** Uniform over all $(2n-5)!! = 1 \cdot 3 \cdot 5 \cdots (2n-5)$ distinct unrooted binary trees (a rapidly growing number: 3 for $n = 4$, 15 for $n = 5$, 10,395 for $n = 7$, and $\approx 10^{158}$ for $n = 100$).
- **Branch lengths:** Exponential prior with mean 0.1.
- **GTR parameters:** Dirichlet priors on frequencies; flat priors on log-rate ratios.

0.102.2 5.2 Markov Chain Monte Carlo Sampling

Since the posterior is defined over a space that includes the discrete, high-dimensional space of tree topologies, direct analytical computation is intractable. Markov chain Monte Carlo (MCMC) is used to draw samples $(T^{(1)}, \mathbf{t}^{(1)}, \theta^{(1)}), (T^{(2)}, \mathbf{t}^{(2)}, \theta^{(2)}), \ldots$ from the posterior. These samples are used to compute posterior summaries:

- **Maximum a posteriori (MAP) tree**: the tree topology appearing most frequently in the MCMC sample.
- **Posterior probabilities of clades**: the proportion of MCMC samples in which a specific clade (subset of taxa) appears. A clade with posterior probability > 0.95 is considered strongly supported.
- **95% credible intervals for branch lengths**: the 2.5th and 97.5th percentiles of the marginal distribution of each branch length.

MCMC moves on tree space include:

- **Nearest-neighbour interchange (NNI)**: swap two subtrees around an internal edge.
- **Subtree pruning and regrafting (SPR)**: remove a subtree and reattach it at a different edge.
- **Branch length updates**: Metropolis–Hastings proposals on individual branch lengths.

The Metropolis–Hastings acceptance ratio for a proposed move from $(T, \mathbf{t}, \theta)$ to $(T', \mathbf{t}', \theta')$ is:

$$\alpha = \min\left(1,\ \frac{\mathcal{L}(D \mid T', \mathbf{t}', \theta')\, \pi(T', \mathbf{t}', \theta')\, q(T, \mathbf{t}, \theta \mid T', \mathbf{t}', \theta')}{\mathcal{L}(D \mid T, \mathbf{t}, \theta)\, \pi(T, \mathbf{t}, \theta)\, q(T', \mathbf{t}', \theta' \mid T, \mathbf{t}, \theta)}\right),$$

where q is the proposal distribution.

0.103 6. The Coalescent as a Prior for Population-Level Phylogenetics

0.103.1 6.1 Gene Trees vs. Species Trees

The genealogy of a gene sample (the gene tree) differs from the genealogy of the species containing those genes (the species tree). Within a species, the genealogy of alleles is governed by the coalescent (Section II). When two species split, the gene lineages must coalesce before the split time (they were in the same ancestral population). This creates **incomplete lineage sorting**: gene trees can differ topologically from the species tree.

The probability of a gene tree topology g given a species tree S with branch lengths in coalescent units is computed from the coalescent. For three species A, B, C with species tree topology $(A, B)C$ (A and B are sister species), the probability that the gene tree has the same topology as the species tree is:

$$P(g = (A, B)C \mid S = (A, B)C) = 1 - \frac{2}{3}e^{-T},$$

where T is the length of the branch separating $\{A, B\}$ from C in coalescent units ($T = t/(2N_e)$ where t is the branch length in generations and N_e is the effective population size of the ancestral (A, B) population). For short internal branches ($T \approx 0$), the gene tree topology matches the species tree topology with probability $\approx 1/3$ (random).

0.103.2 6.2 Molecular Clock Testing

Under a strict molecular clock, all lineages evolve at the same rate, producing an **ultrametric tree**: a tree in which the distance from root to any leaf is the same. Testing for the molecular clock uses the likelihood ratio test:

$$\Lambda = 2(\ln \mathcal{L}_{\text{unconstrained}} - \ln \mathcal{L}_{\text{clock}}) \sim \chi^2_{n-2},$$

with $n - 2$ degrees of freedom (the clock model has $n - 2$ fewer free parameters than the unconstrained model).

Relaxed clock models allow rates to vary across lineages. The most common implementations:

- **Uncorrelated log-normal clock**: rates on different branches are independently log-normally distributed.
- **Autocorrelated clock**: rate on a branch is correlated with the rate on its parent branch.

When calibrated with fossil data (constraints on node ages from the fossil record), relaxed clock models enable Bayesian divergence time estimation, simultaneously inferring the tree topology, branch lengths in time units, and evolutionary rates. This is the methodology of "molecular dating", used to infer divergence times across the tree of life.

0.104 7. Summary

Phylogenetics reconstructs evolutionary history from molecular data. The Jukes–Cantor model describes sequence evolution as a continuous-time Markov chain; the JC distance corrects observed sequence differences for multiple hits. The GTR model generalises JC with unequal base frequencies and substitution rates; time-reversibility enables root-free likelihood computation. The four-point condition characterises tree metrics among distance matrices. The NJ algorithm reconstructs trees from distances in $O(n^3)$ time. Felsenstein's pruning algorithm computes the likelihood of a sequence alignment on a tree in $O(n)$ per site by dynamic programming. Bayesian phylogenetics uses MCMC to sample the posterior distribution of trees. The coalescent provides a prior for gene tree inference within species and across recently diverged lineages. Relaxed clock models with fossil calibrations estimate absolute divergence times.

Section *VIII*

Section VII — Evolutionary Game Theory: Strategies, Equilibria, and Replicators

0.105 8. Molecular Clocks and Rate Variation

0.105.1 8.1 The Strict and Relaxed Molecular Clock

Section II established Kimura's neutral substitution rate theorem: the rate of neutral substitution equals the mutation rate μ, independent of population size. This yields a **strict molecular clock**: if μ is constant across lineages, then the number of substitutions between two lineages is proportional to the divergence time T (more precisely, $\mathbb{E}[d] = 2\mu T$ for diverged lineages).

In practice, mutation rates vary across lineages due to metabolic rate, generation time, body size, and repair efficiency. This motivates the **relaxed molecular clock**, in which each branch b of the phylogenetic tree has its own rate $r_b \sim \mathcal{D}(\mu, \sigma^2)$ drawn independently from a distribution.

Definition 0.105.1 (Log-normal relaxed clock)**.** In the log-normal relaxed clock model (Drummond et al. 2006), the substitution rate on branch b is $r_b = \exp(\mu_\ell + \sigma_\ell Z_b)$, where $Z_b \overset{iid}{\sim} \mathcal{N}(0,1)$ and μ_ℓ, σ_ℓ^2 are hyperparameters. The variance parameter σ_ℓ measures the degree of rate variation: $\sigma_\ell \to 0$ gives the strict clock, and large σ_ℓ gives highly variable rates.

Theorem 0.105.2 (Identifiability of the relaxed clock)**.** In a Bayesian phylogenetic model with a log-normal relaxed clock, the tree topology, divergence times, and rate hyperparameters (μ_ℓ, σ_ℓ) are jointly identifiable from a sufficiently long alignment, provided the tree has at least 4 taxa and the substitution model is correctly specified.

Sketch. The likelihood $\mathcal{L}(\mathcal{T}, \mathbf{t}, r | D)$ where $\mathcal{T}$ is the tree, $\mathbf{t}$ is the vector of node times, and $r = (r_b)$ are branch rates, can be factored as:

$$\mathcal{L} = \prod_{s} \sum_{\text{ancestral states}} \prod_{b} P(x_b^{\text{child}} | x_b^{\text{parent}}, r_b \cdot t_b) \cdot p(r_b | \mu_\ell, \sigma_\ell).$$

With $n \geq 4$ taxa and sufficient sequence data, the likelihood surface has a unique maximum in $(\mathcal{T}, \mathbf{t})$ (for the correct model). The hyperparameters (μ_ℓ, σ_ℓ) are identified by the distribution of rates across branches; with ≥ 4 branches, both mean and variance of the log-normal are identifiable. □

Example 0.105.3 (Divergence time estimation for primates)**.** A Bayesian relaxed-clock analysis of a 10-kb alignment from 10 primate species with 3 fossil calibrations (minimum ages for nodes based on the primate fossil record) gives posterior mean divergence times:

Node	Fossil calibration	Posterior estimate
Human–Chimpanzee	None (uncalibrated)	6.0 ± 0.5 Mya
Hominini–Gorilla	None	8.1 ± 0.7 Mya
Great apes – Gibbon	≥ 14 Mya (Hominidae crown)	17.2 ± 1.1 Mya
Catarrhini crown	≥ 30 Mya	33.6 ± 2.4 Mya

The posterior mean for human–chimp ($\sim$ 6 Mya) is consistent with palaeontological estimates (5–7 Mya) and with the naive clock-based estimate from synonymous site divergence $d_s \approx 0.012$ and $\mu_s \approx 10^{-9}$/site/year giving $T \approx 6$ Mya. The relaxed clock gives wider credible intervals because it correctly accounts for rate variation among lineages.

0.105.2 8.2 The Generation Time Effect

The generation time effect is a systematic violation of the strict molecular clock: organisms with shorter generation times have higher substitution rates per year (but similar rates per generation). This is because DNA replication errors are the primary source of mutations, and the number of replications per year scales inversely with generation time.

Lemma 0.105.4 (Generation time scaling)**.** If the mutation rate is μ_g per base per generation, the per-year rate is $\mu_y = \mu_g / g$, where g is the generation time in years. For two species with generation times g_1 and g_2, the ratio of their per-year substitution rates is:

$$\frac{\mu_y^{(1)}}{\mu_y^{(2)}} = \frac{g_2}{g_1}.]Formice($$

g ≈ 0.25 yr) vs. humans ($g \approx 25$ yr), the predicted ratio is $25/0.25 = 100$: mice evolve 100-fold faster per year but at the same rate per generation.

Empirically, the per-year synonymous substitution rate in rodents ($\approx 5 \times 10^{-9}$/site/year) is indeed ≈ 5-fold higher than in primates ($\approx 10^{-9}$), consistent with the generation time ratio ≈ 3–10. The remaining discrepancy may be due to metabolic rate effects on mutation frequency (higher metabolic rates generate more free radicals, causing more oxidative DNA damage).

0.106 9. Ancestral Sequence Reconstruction

0.106.1 9.1 Marginal and Joint Ancestral Reconstruction

Given a phylogenetic tree $\mathcal{T}$ with branch lengths, a substitution model Q, and observed leaf sequences, ancestral sequence reconstruction asks: what were the sequences at the internal nodes (ancestral sequences)?

Two approaches:

1. **Marginal reconstruction**: for each ancestral node v and each site s, compute $P(a_v^s | D, \mathcal{T}, Q)$ — the posterior probability of each character state at that node and site, marginalising over all other nodes and sites. Assign the MAP state $\hat{a}_v^s = \arg\max P(a_v^s | D, \mathcal{T}, Q)$.

2. **Joint reconstruction**: compute the MAP assignment of states at all ancestral nodes simultaneously: $(\hat{a}_v^s)_{v,s} = \arg\max \prod_{s=1}^{m} P(\text{all ancestral states at site } s | D, \mathcal{T}, Q)$.

Theorem 0.106.1 (Felsenstein pruning for marginal reconstruction)**.** The marginal posterior probability at node v can be computed in $O(nL)$ time using a combination of the forward pruning algorithm and a backward ("upward-downward") pass. For site s, node v with children c_1 and parent π:

$$P(a_v^s = x | D) \propto P(D_{\text{below}}(c_1) | a_v = x) \cdot P(D_{\text{below}}(c_2) | a_v = x) \cdot P(D_{\text{above}}(v) | a_v = x),$$

where the first two terms are computed by the forward pass and the last by the backward pass.

Remark 0.106.2 (Ancestral sequence resurrection). Ancestral sequence reconstruction is not merely theoretical: ancient proteins have been resurrected by synthesising genes encoding the inferred ancestral sequence and expressing them in bacteria. Thornton et al. (2003) resurrected the last common ancestor

of vertebrate steroid hormone receptors (~ 450 Mya) and showed it had functions consistent with evolutionary intermediates between modern receptor types. Chang et al. (2002) resurrected Precambrian visual pigments. These experiments provide direct tests of phylogenetic inference and evolutionary hypotheses about ancestral function.

0.106.2 9.2 Uncertainty in Ancestral Reconstruction

A key issue in ancestral reconstruction is quantifying uncertainty. The MAP ancestral sequence $\hat{\mathbf{a}}$ may differ substantially from the posterior mean, and the posterior distribution over ancestral sequences may be highly multimodal.

Lemma 0.106.3 (Upper bound on ancestral reconstruction accuracy)**.** For a site evolving on a star phylogeny with n leaves at divergence time T each, the posterior probability of correctly inferring the ancestral state (under the JC69 model) is:

$$P(\text{correct}) = \frac{1}{4}\left[1 + 3\left(\frac{4e^{-8\mu T/3} - 1}{3}\right)^n\right].$$

For $n \to \infty$, this approaches 1 for any fixed T: more taxa improve inference. For fixed n and $T \to \infty$, this approaches $1/4$: long branches make reconstruction impossible.

Proof. Under JC69, the probability that a leaf has the same state as the ancestor after time T is $\pi_s = \frac{1}{4}(1 + 3e^{-8\mu T/3})$ (from the JC69 stationary distribution and transition probability). For n i.i.d. leaves, the probability that the majority character state equals the ancestral state is computed by summing over all patterns where $k > n/2$ leaves have the correct ancestral state. By the multinomial count argument, this gives the stated formula after algebraic simplification. □

0.107 10. The Gene Tree vs. Species Tree Problem

0.107.1 10.1 Incomplete Lineage Sorting

The species tree describes the relationships among species; a gene tree at any particular locus may differ from the species tree due to **incomplete lineage sorting** (ILS). ILS occurs when the polymorphism at a locus has not fully sorted (fixed or lost) in the ancestral populations before speciation events. Under the coalescent model, ILS produces discordant gene trees with predictable probabilities.

Theorem 0.107.1 (Probability of gene tree discordance under ILS)**.** For a three-taxon problem (species A, B, C where A and B are more closely related, with speciation time τ generations since AB speciation and $\theta = 4N_e\mu$), the probability that the gene tree is discordant (showing AC or BC as the clade rather than the correct AB) is:

$$P(\text{discordant}) = \frac{2}{3}e^{-\tau/(2N_e)}.]$$

Proof. The gene genealogy of three lineages, taken from species A, B, and C, must trace back through the ancestral population of AB before the ABC common ancestor. In the ancestral AB population of effective size N_e, the three lineages coalesce. The probability that the A and B lineages coalesce first (concordant with the species tree) is $1 - P(\text{discordant})$. Two lineages coalesce before exiting a population of size N_e with probability $1 - e^{-T/(2N_e)}$ where T is the time spent in the population. Each pair of lineages

is equally likely to coalesce, so the probability of any given discordant topology is $(1/3)e^{-\tau/(2N_e)}$; the total discordance probability is $(2/3)e^{-\tau/(2N_e)}$. □

Example 0.107.2 (ILS in the Great Ape phylogeny)**.** For humans, chimpanzees, and gorillas, the speciation time between humans and chimpanzees is $\tau \approx 6 \times 10^6$ years $\approx 240{,}000$ generations (generation time 25 years), and the ancestral effective population size is estimated at $N_e \approx 50{,}000$. The predicted ILS discordance is:

$$P(\text{discordant}) = \frac{2}{3}e^{-240{,}000/(2\times 50{,}000)} = \frac{2}{3}e^{-2.4} \approx \frac{2}{3} \times 0.091 \approx 0.061.$$

Approximately 6% of genomic loci are expected to show a discordant gene tree where humans group with gorillas or chimpanzees group with gorillas rather than humans with chimpanzees. Empirically, $\approx 30\%$ of the human–chimpanzee–gorilla genome shows discordance, consistent with a somewhat larger ancestral $N_e \approx 100{,}000$.

0.107.2 10.2 ASTRAL and Quartet-Based Species Tree Estimation

Modern species tree estimation methods use the distribution of gene tree topologies to infer the species tree. The ASTRAL algorithm (Mirarab et al. 2014) estimates the species tree that maximises the number of quartet trees (4-taxon subtrees) consistent with the observed gene trees.

Definition 0.107.3 (ASTRAL objective function)**.** For a set of m gene trees $\{g_1, \ldots, g_m\}$ and a candidate species tree S, the ASTRAL score is:

$$\text{score}(S | \{g_j\}) = \sum_{j=1}^{m} \sum_{q \in Q(S)} \mathbf{1}[q \in Q(g_j)],$$

where $Q(S)$ is the set of quartet topologies induced by S and $Q(g_j)$ is the set of quartet topologies in gene tree g_j. The ASTRAL estimate is $\hat{S} = \arg\max_S \text{score}(S|\{g_j\})$.

ASTRAL is statistically consistent under the multispecies coalescent: $\hat{S} \to S^*$ (the true species tree) in probability as the number of gene trees $m \to \infty$, even when many individual gene trees are discordant with S^*.

Mathematics of Evolution and Life · Section VI · Phylogenetics: Trees, Distances, and Evolutionary Time (end)

0.108 11. Network Approaches to Phylogenetics

0.108.1 11.1 Phylogenetic Networks and Reticulate Evolution

Bifurcating trees cannot represent *reticulate* evolutionary events: hybridisation, horizontal gene transfer, and recombination all introduce non-treelike signals into genomic data. **Phylogenetic networks** generalise trees to allow reticulation nodes with more than one parent.

Definition 0.108.1 (Phylogenetic network)**.** A **phylogenetic network** on leaf set $X = \{x_1, \ldots, x_n\}$ is a rooted acyclic digraph $N = (V, E)$ with leaves X, satisfying:

1. Each leaf has in-degree 1 and out-degree 0.

2. The root has in-degree 0 and out-degree ≥ 2.

3. Every internal node is either a *tree node* (in-degree 1, out-degree ≥ 2) or a *reticulation node* (in-degree ≥ 2, out-degree 1).

The number of reticulations $r = |E| - |V| + 1$ measures the network's complexity.

Theorem 0.108.2 (Hardness of network inference)**.** The problem of finding the minimum-reticulation phylogenetic network consistent with a given set of gene trees is NP-hard.

Sketch. Reduction from the Minimum Common String Supersequence problem (known NP-hard). Given a set of gene trees $\{g_1, \ldots, g_m\}$ on leaf set X, each reticulation in a network N that displays all g_i corresponds to a hybridisation event. The minimum number of reticulations is equivalent to the minimum number of "bipartition disagreements" between the gene trees, which is NP-hard to minimise over all possible network topologies. (Full proof: Bordewich and Semple 2007.) □

Remark 0.108.3 (HGT in prokaryote phylogenomics). Horizontal gene transfer (HGT) in prokaryotes is so pervasive that the "tree of life" for bacteria is arguably not a tree at all: any two randomly chosen bacterial genomes share $\sim$ 20–80% of their genes (depending on phylogenetic distance), but the shared genes may have different evolutionary histories at different loci. The "species tree" is then a summary tree capturing the vertical (parent-to-offspring) component of evolution, surrounded by a "cloud" of horizontally transferred genes. In the extreme, thermophilic archaea and bacteria have exchanged so many genes that their deep phylogenetic relationships cannot be resolved by any tree-based method.

0.108.2 11.2 Split Decomposition and the NeighborNet Algorithm

The NeighborNet algorithm (Bryant and Moulton 2004) produces a planar **splits graph**: an undimensional representation of evolutionary relationships that shows both tree-like and reticulate signals in a single diagram.

Definition 0.108.4 (Split system and circular splits)**.** A *split* of X is a bipartition $\{A, B\}$ with $A \cup B = X$, $A \cap B = \emptyset$, $A \neq \emptyset \neq B$. A split system Σ is a collection of splits. A split system is *circular* if there exists a circular ordering of X such that each split separates a contiguous block from the rest. Every circular split system can be drawn as a planar splits graph with parallel bands of edges for each split.

Theorem 0.108.5 (NeighborNet consistency)**.** The NeighborNet algorithm produces a circular split system consistent with the input distance matrix in $O(n^2)$ time. For tree-like data (data arising from a tree with no reticulation), NeighborNet correctly recovers the tree topology and branch lengths. For non-tree data, the planar splits graph shows reticulation as a grid-like pattern at nodes corresponding to conflicting splits.

0.109 12. Rate Heterogeneity and the Gamma Model

0.109.1 12.1 Among-Site Rate Variation

In real sequence data, different sites evolve at very different rates: active sites in enzymes evolve slowly (high constraint), while surface-exposed residues evolve quickly. Ignoring among-site rate variation leads to biased estimates of branch lengths and divergence times.

Definition 0.109.1 (Gamma distribution of rates)**.** Each site s has an independent rate multiplier $r_s \sim \Gamma(\alpha, \alpha)$ (shape and rate both equal α, so $\mathbb{E}[r_s] = 1$ and $\mathrm{Var}(r_s) = 1/\alpha$). The parameter $\alpha > 0$ controls rate heterogeneity: $\alpha \to \infty$ gives all rates equal to 1 (no rate variation); $\alpha \to 0$ gives extreme rate variation (most sites evolve very slowly, a few very fast).

Theorem 0.109.2 (Marginal likelihood under Gamma rate variation)**.** Under the Gamma+I model (Gamma-distributed rates plus a fraction p_{inv} of invariable sites), the likelihood of a site pattern P is:

$$L(P) = p_{\text{inv}} \cdot \mathbf{1}[P \text{ is constant}] \cdot \frac{1}{4} + (1 - p_{\text{inv}}) \sum_{k=1}^{K} \frac{w_k}{4} \prod_{b} P(x_b^{\text{tip}} | x_b^{\text{ancestor}}, r_k t_b),$$

where $r_1, \ldots, r_K$ are discrete Gamma quantiles with weights $w_k = 1/K$ (the "discrete Gamma" approximation of Yang 1994).

Example 0.109.3 (Estimating α for the HIV-1 envelope gene)**.** The HIV-1 envelope gene (*env*) encodes the gp120/gp41 glycoproteins. Maximum likelihood estimation of α from a 100-taxon env alignment gives $\hat{\alpha} \approx 0.3$, indicating very high rate heterogeneity: the coefficient of variation of site rates is $1/\sqrt{\alpha} = 1/\sqrt{0.3} \approx 1.8$, meaning the standard deviation of rates is 1.8 times their mean. Sites in the CD4-binding domain (constrained) have $r \approx 0.01$; sites in variable loops V1–V4 have $r \approx 5$–10. Ignoring rate variation and using the uniform-rate model would overestimate divergence times by a factor of ≈ 2.

Mathematics of Evolution and Life · Section *VI · Phylogenetics: Trees, Distances, and Evolutionary Time (end)*

0.110 13. Bayesian Phylogenetics and MCMC

0.110.1 13.1 The Bayesian Framework

Maximum likelihood phylogenetics (Felsenstein 1981, Section 5) produces a point estimate $\hat{\mathcal{T}}$ of the tree. Bayesian phylogenetics, by contrast, computes the full posterior distribution $P(\mathcal{T}|D)$ over tree topologies and branch lengths, incorporating prior information and quantifying uncertainty.

Definition 0.110.1 (Bayesian phylogenetic posterior)**.** Given a multiple sequence alignment D of n taxa, a substitution model Q, a prior on tree topologies $P(\mathcal{T})$ and branch lengths $P(\mathbf{l})$, the posterior distribution is:

$$P(\mathcal{T}, \mathbf{l}|D) \propto \mathcal{L}(D|\mathcal{T}, \mathbf{l}, Q) \cdot P(\mathcal{T}) \cdot P(\mathbf{l}),$$

where $\mathcal{L}$ is the Felsenstein pruning likelihood (Section 5). The marginal posterior over tree topologies is:

$$P(\mathcal{T}|D) = \int P(\mathcal{T}, \mathbf{l}|D)\, d\mathbf{l}.$$

The posterior cannot be computed analytically: the integral over branch lengths has no closed form, and the sum over tree topologies has $(2n-5)!! \sim n^n$ terms. MCMC is the standard computational approach.

Theorem 0.110.2 (Ergodicity of Metropolis–Hastings on tree space)**.** The Metropolis–Hastings chain on the space of phylogenetic trees (with proposal distribution including NNI, SPR, and TBR moves, and branch length perturbations) is ergodic: it converges to the posterior $P(\mathcal{T}, \mathbf{l}|D)$ from any starting tree,

given that the proposal distribution is irreducible (every tree can be reached from every other tree by a finite sequence of moves).

Proof. (i) **Irreducibility**: SPR (subtree pruning and regrafting) moves are sufficient to connect any two tree topologies (every pair of trees of the same leaf set are connected by a finite sequence of SPR moves). Hence the chain can reach any state. (ii) **Aperiodicity**: the chain can stay at its current state (rejection in Metropolis–Hastings) with positive probability. (iii) **Detailed balance**: the Metropolis–Hastings acceptance probability $\alpha = \min(1, \frac{P(\mathcal{T}', \mathbf{l}'|D) q(\mathcal{T}, \mathbf{l}|\mathcal{T}', \mathbf{l}')}{P(\mathcal{T}, \mathbf{l}|D) q(\mathcal{T}', \mathbf{l}'|\mathcal{T}, \mathbf{l})})$ ensures detailed balance with respect to $P(\mathcal{T}, \mathbf{l}|D)$. By the general theory of MCMC, ergodicity follows from irreducibility, aperiodicity, and positive recurrence (which holds on the compact space of trees with bounded branch lengths). □

Example 0.110.3 (Bayesian analysis of primate evolution with BEAST)**.** A BEAST2 analysis of 15 primate mitochondrial genomes (4 kb each), with three fossil calibration priors and a log-normal relaxed clock, was run for 10^7 MCMC iterations (sampling every 10^3 steps). Convergence diagnostics:

- Effective sample size (ESS) for all parameters > 200 (standard criterion).
- Trace plot of log-posterior stabilised after 2×10^6 burn-in iterations.
- Posterior probability for the (Human, Chimpanzee) clade: 0.997.
- 95% HPD (highest posterior density) interval for human–chimp divergence: 5.2–7.1 Mya.

The posterior over tree topologies places $> 99\%$ probability on the single topology consistent with all other molecular and palaeontological evidence.

0.110.2 13.2 Prior Sensitivity and Model Comparison

A key challenge in Bayesian phylogenetics is prior sensitivity: the posterior can be strongly influenced by the choice of prior on branch lengths, especially for sparse data.

Theorem 0.110.4 (Marginal likelihood and Bayes factors for model selection)**.** For two competing substitution models M_1 and M_2, the Bayes factor is:

$$BF_{12} = \frac{P(D|M_1)}{P(D|M_2)} = \frac{\int \mathcal{L}(D|\theta_1, M_1) P(\theta_1|M_1) d\theta_1}{\int \mathcal{L}(D|\theta_2, M_2) P(\theta_2|M_2) d\theta_2}.$$

Evidence interpretation: $\log_{10} BF_{12} > 2$ (decisive evidence for M_1), 1–2 (strong), 0.5–1 (substantial), < 0.5 (weak). The marginal likelihood $P(D|M)$ is computed by thermodynamic integration or stepping-stone sampling along a path from the prior to the posterior.

0.111 14. Total Evidence Dating and Tip Calibrations

0.111.1 14.1 The Total Evidence Framework

Traditional node-calibrated divergence time estimation uses the fossil record only as minimum age constraints on internal nodes. The **total evidence dating** approach (Ronquist et al. 2012) treats fossils as tip taxa, placing them directly in the tree with their own molecular and morphological data, and inferring their temporal placement from a diversified birth-death (FBD) model.

Definition 0.111.1 (Fossilised birth-death (FBD) model)**.** The FBD process generates a time-calibrated tree of living and fossil taxa:

- Lineages speciate at rate λ and go extinct at rate μ.
- Fossil specimens are sampled from extinct lineages at rate ψ.
- At the present, a fraction ρ of living species are sampled.

The likelihood of the observed tree topology and divergence times, conditioned on sampling n living and m fossil taxa, is:

$$\mathcal{L}(\lambda, \mu, \psi | \mathcal{T}) = \frac{(n+m-1)! \lambda^{n-1} \psi^m \prod_{i=1}^{m} q(t_i) \prod_{j=1}^{n+m-1} p(s_j)}{(2n+2m-2)!! \cdot p(t_{\text{root}})},$$

where $q(t)$ is the probability of a lineage at time t leaving no sampled descendants and $p(s)$ is the density of a lineage alive at time s.

Remark 0.111.2 (Advantages over node calibration). Total evidence dating has three advantages over node calibration: (1) it uses *all* morphological data from fossils, not just their age; (2) it places fossils at correct phylogenetic positions rather than treating them as constraints on ancestral nodes; (3) it naturally handles stratigraphic uncertainty (fossils are sampled from a range of ages). In practice, total evidence analyses typically give broader credible intervals for divergence times (more honest uncertainty), but better agreement with independent palaeontological evidence.

Mathematics of Evolution and Life · Section *VI · Phylogenetics: Trees, Distances, and Evolutionary Time (end)*

0.112 8. Ancestral Sequence Reconstruction and Palaeogenomics

0.112.1 8.1 Marginal Ancestral Reconstruction

Given a phylogeny T with branch lengths and a multiple sequence alignment D over n taxa, the **ancestral sequence reconstruction** problem asks: what was the sequence at an internal node v of T? This is a statistical inference problem, with the phylogenetic likelihood as the objective.

For each internal node v and each site position k, the marginal posterior probability of ancestral state a is:

$$P(x_{v,k} = a \mid D) = \frac{P(D \mid T, \theta) \cdot P(x_{v,k} = a \mid T, \theta)}{P(D \mid T, \theta)},$$

where the numerator conditions on the ancestral state a at node v for site k. Using Felsenstein's pruning algorithm, the conditional likelihood can be factored:

$$P(x_{v,k} = a \mid T, \theta) \propto L_v(a) \cdot U_v(a),$$

where $L_v(a)$ is the "downward" partial likelihood (probability of the data in the subtree below v given $x_{v,k} = a$) and $U_v(a)$ is the "upward" likelihood from the rest of the tree.

Theorem 0.112.1 (Marginal Reconstruction Consistency)**.** Under a stationary, time-reversible substitution model, the marginal posterior reconstruction $\hat{a}_{v,k} = \arg\max_a P(x_{v,k} = a \mid D)$ is a consistent

estimator of the true ancestral state as the sequence length $\ell \to \infty$, provided the tree topology and branch lengths are known.

Proof sketch. As $\ell \to \infty$, the posterior concentrates at the true ancestral state by the Bernstein-von Mises theorem for discrete state spaces under a regular parametric model. The key regularity condition is that the substitution model is identifiable, which holds for GTR under generic branch lengths. □

0.112.2 8.2 Joint versus Marginal Reconstruction

An alternative to marginal reconstruction is **joint** or **parsimony-based** reconstruction, which finds the joint assignment of ancestral states to all internal nodes simultaneously:

$$\hat{\mathbf{x}}_{\text{int}} = \arg\max_{\mathbf{x}_{\text{int}}} P(\mathbf{x}_{\text{int}} \mid D, T, \theta).$$

Under maximum parsimony, this reduces to minimising the total number of substitutions on the tree, which can be solved in $O(nL)$ time using Fitch's algorithm:

1. For each leaf, assign state $S_v = \{x_{v,k}\}$.
2. For each internal node v with children u, w (in post-order traversal): $S_v = S_u \cap S_w$ if $S_u \cap S_w \neq \emptyset$; else $S_v = S_u \cup S_w$ (a substitution is counted).
3. Assign ancestral states top-down: at the root, choose any state in S_{root}; at each internal node, choose the parent's state if it is in S_v, else choose any state in S_v.

The marginal and joint reconstructions agree for star phylogenies under symmetric substitution but can give different results on asymmetric trees (Yang et al. 1995). Marginal reconstruction is generally preferred for statistical inference; joint reconstruction is computationally simpler.

0.112.3 8.3 Palaeogenomics: Genome-Scale Ancestral Reconstruction

Ancestral genome reconstruction extends single-gene methods to the entire genome, including gene order, synteny, and chromosomal structure. For a set of extant genomes $G_1, \ldots, G_n$ on a phylogeny, the ancestral genome G_A satisfies:

$$\hat{G}_A = \arg\max_{G} \prod_{i:\text{children of root}} P(G_i \mid G, T, \theta),$$

where the likelihood is computed over both sequence substitution and structural rearrangement events (inversions, translocations, duplications).

The Hannenhalli–Pevzner (HP) theory (1995) solves the problem of computing the minimum number of inversions between two signed permutations (representing gene orders on a chromosome). For two permutations π and σ of n signed elements, the inversion distance is:

$$d(\pi, \sigma) = n + 1 - c(\pi, \sigma) + h(\pi, \sigma) - f(\pi, \sigma),$$

where c is the number of cycles in a certain bipartite graph, h is the number of hurdles, and f is a correction for a special obstruction called a "fortress." This provides the polynomial-time algorithm for

genome rearrangement distance, the foundation for phylogenomics based on gene order.

0.113 9. Network-Based Phylogenetics and Reticulate Evolution

0.113.1 9.1 Phylogenetic Networks

Classical phylogenetics assumes a strictly bifurcating tree, but evolution is not always tree-like. Horizontal gene transfer (HGT) in bacteria, hybridisation in plants and animals, and recombination all produce **reticulate evolution**: genealogies with multiple parents. The correct representation is a **phylogenetic network** rather than a tree.

Definition 0.113.1 (Phylogenetic Network)**.** A **phylogenetic network** on taxon set X is a directed acyclic graph (DAG) $N = (V, E)$ with:

- A single root with in-degree 0.
- Leaves (in-degree 1, out-degree 0) bijectively labelled by X.
- **Tree nodes**: in-degree 1 (and out-degree ≥ 2, except for leaves).
- **Reticulation nodes**: in-degree ≥ 2 (representing hybridisation or HGT events).

A network N displays a tree T if T can be obtained from N by suppressing all but one of the edges entering each reticulation node. The **hardwired cluster** of N is the set of all splits (bipartitions of X) obtained from every displayed tree.

0.113.2 9.2 The Hybridisation Number

The **hybridisation number** $h(T_1, T_2)$ of two phylogenetic trees T_1 and T_2 on the same taxon set X is the minimum number of reticulation events needed to explain both trees:

$$h(T_1, T_2) = \min\{r(N) : N \text{ displays both } T_1 \text{ and } T_2\},$$

where $r(N)$ is the number of reticulation nodes in network N.

Theorem 0.113.2 (Hybridisation Number and Agreement Forests)**.** $h(T_1, T_2) = \ell(\mathcal{F}^*) - 1$, where $\ell(\mathcal{F}^*)$ is the minimum number of components in a **maximum agreement forest** of T_1 and T_2—a partition of the leaf-label set X into subtrees that appear (as subtrees) in both T_1 and T_2.

Computing $h(T_1, T_2)$ is NP-hard in general; it is fixed-parameter tractable in h and admits a factor-3 approximation in polynomial time.

0.113.3 9.3 Detecting HGT Using Phylogenetic Incongruence

In prokaryotes, HGT is a dominant force in genome evolution. A gene that has been horizontally transferred from a donor lineage will have a gene tree topologically inconsistent with the species tree. The standard test is:

1. Infer the gene tree T_g for the gene of interest.
2. Infer or assume a species tree T_s.

3. Compare T_g and T_s by the Robinson-Foulds (RF) distance:

$$d_{RF}(T_g, T_s) = |S(T_g) \triangle S(T_s)|,$$

where $S(T)$ is the set of splits (bipartitions) of T and $\triangle$ is the symmetric difference.

Large d_{RF} values (normalised by the maximum possible distance $2(n-3)$) are evidence of HGT or other reticulate events. Bayesian methods simultaneously estimate the HGT rate and the donor-recipient pairs by integrating over all possible gene tree–species tree pairs, using the coalescent as a null model for gene tree variation within a species tree.

Section *IX*

Section VII — Evolutionary Game Theory: Strategies, Equilibria, and Replicators

0.114 1. The Evolution of Strategy

Classical game theory, developed by von Neumann and Morgenstern, is a theory of rational choice: agents with well-defined preferences choose strategies to maximise their payoffs, knowing that other agents do the same. It is among the most powerful mathematical frameworks in economics and the social sciences. Yet for evolutionary biology, which deals with organisms that are not rational in any psychological sense — bacteria, insects, fish, and even most mammals do not consciously reason about strategic equilibria — game theory would seem irrelevant.

John Maynard Smith and George Price showed in a 1973 *Nature* paper that this intuition is wrong. The key insight is that rationality can be replaced by heredity: instead of a rational agent choosing to adopt a strategy, we have a genetically determined organism that is "programmed" to behave in a fixed way. Natural selection then acts as the optimising agent. Strategies that do well (produce many offspring) spread; strategies that do poorly decline. The long-run outcome of this evolutionary process is often precisely the same as the equilibrium of the corresponding strategic game — and in some cases, evolution finds equilibria that rational reasoning would not, and misses equilibria that rationality would find.

0.115 2. The Basic Framework

0.115.1 2.1 Symmetric Normal-Form Games

An **evolutionary game** is played by individuals drawn from a large population. Each individual is programmed with a pure strategy from a finite set $\{1, 2, \ldots, n\}$. When two individuals interact, the payoff to a player using strategy i against an opponent using strategy j is a_{ij}, the (i, j) entry of the **payoff matrix** $A = (a_{ij})$.

In a population where strategy i occurs at frequency p_i (with $\mathbf{p} = (p_1, \ldots, p_n)^T$ in the simplex $\Delta^n = \{\mathbf{p} \geq 0 : \sum_i p_i = 1\}$), the expected payoff to a strategy-i individual is:

$$f_i(\mathbf{p}) = \sum_{j=1}^{n} a_{ij} p_j = (A\mathbf{p})_i.$$

The mean payoff in the population is:

$$\bar{f}(\mathbf{p}) = \sum_{i=1}^{n} p_i f_i(\mathbf{p}) = \mathbf{p}^T A \mathbf{p}.$$

0.115.2 2.2 Nash Equilibria

Definition 0.115.1. A **Nash equilibrium** is a frequency vector $\mathbf{p}^* \in \Delta^n$ such that no individual can increase its payoff by unilaterally switching to a different strategy:

$$f(\mathbf{p}^*, \mathbf{p}^*) \geq f(\mathbf{q}, \mathbf{p}^*) \quad \text{for all } \mathbf{q} \in \Delta^n,$$

where $f(\mathbf{p}, \mathbf{q}) = \mathbf{p}^T A \mathbf{q}$ denotes the payoff to a $\mathbf{p}$-player against a $\mathbf{q}$-player.

By Nash's theorem (1950), every finite normal-form game has at least one Nash equilibrium (possibly in mixed strategies).

0.116 3. Evolutionarily Stable Strategies

0.116.1 3.1 The ESS Concept

The ESS concept (Maynard Smith and Price 1973) adds an evolutionary stability condition to the Nash equilibrium requirement. Informally, an ESS is a strategy that, when adopted by the majority of the population, cannot be invaded by any rare alternative strategy.

Definition 0.116.1 (Evolutionarily Stable Strategy)**.** A strategy $\mathbf{p}^* \in \Delta^n$ is an **evolutionarily stable strategy** (ESS) if for all $\mathbf{q} \neq \mathbf{p}^*$, there exists $\bar{\epsilon}(\mathbf{q}) > 0$ such that for all $\epsilon \in (0, \bar{\epsilon}(\mathbf{q}))$:

$$f(\mathbf{p}^*, \epsilon\mathbf{q} + (1-\epsilon)\mathbf{p}^*) > f(\mathbf{q}, \epsilon\mathbf{q} + (1-\epsilon)\mathbf{p}^*).$$

Theorem 0.116.2 (ESS Characterisation)**.** $\mathbf{p}^*$ is an ESS if and only if:

(i) $f(\mathbf{p}^*, \mathbf{p}^*) \geq f(\mathbf{q}, \mathbf{p}^*)$ for all $\mathbf{q}$ (Nash condition), and

(ii) if $f(\mathbf{p}^*, \mathbf{p}^*) = f(\mathbf{q}, \mathbf{p}^*)$, then $f(\mathbf{p}^*, \mathbf{q}) > f(\mathbf{q}, \mathbf{q})$ (stability condition).

Proof. Expand the ESS condition for small ϵ: $f(\mathbf{p}^*, \epsilon\mathbf{q} + (1-\epsilon)\mathbf{p}^*) = (1-\epsilon)f(\mathbf{p}^*, \mathbf{p}^*) + \epsilon f(\mathbf{p}^*, \mathbf{q})$ (by bilinearity of f). Similarly for the $\mathbf{q}$-player's payoff. Subtracting and requiring the result to be positive for small $\epsilon > 0$ gives conditions (i) and (ii). □

Every ESS is a Nash equilibrium; not every Nash equilibrium is an ESS (the ESS adds a secondary stability condition for mutants that are neutral under the Nash condition).

0.117 4. The Replicator Equation

0.117.1 4.1 Derivation and Properties

The dynamical counterpart of the ESS is the replicator equation: the differential equation governing how strategy frequencies change under continuous-time natural selection. In a population with strategy frequencies $\mathbf{p}(t)$, the fitness of strategy i is $f_i(\mathbf{p}) = (A\mathbf{p})_i$. Strategies with above-average fitness grow; those with below-average fitness decline:

$$\dot{p}_i = p_i\big(f_i(\mathbf{p}) - \bar{f}(\mathbf{p})\big), \quad i = 1, \ldots, n.$$

Conservation of the simplex: $\frac{d}{dt}\sum_i p_i = \sum_i \dot{p}_i = \sum_i p_i(f_i - \bar{f}) = \bar{f} - \bar{f} = 0$. If $\mathbf{p}(0) \in \Delta^n$, then $\mathbf{p}(t) \in \Delta^n$ for all $t \geq 0$. The simplex is positively invariant.

Faces are invariant: if $p_i(0) = 0$, then $\dot{p}_i(0) = 0$ and $p_i(t) = 0$ for all $t \geq 0$. Strategies absent from the population at $t = 0$ never appear. The replicator equation cannot model the invasion of a strategy from zero frequency — it must be introduced as a perturbation.

Theorem 0.117.1 (Mean Payoff Increase for Symmetric Games)**.** For symmetric games ($A = A^T$), mean

payoff $\bar{f}(\mathbf{p}) = \mathbf{p}^T A\mathbf{p}$ is non-decreasing along trajectories of the replicator equation:

$$\frac{d\bar{f}}{dt} = 2\sum_i p_i(f_i - \bar{f})^2 = 2\,\mathrm{Var}_{\mathbf{p}}(f) \geq 0.$$

Proof. $\frac{d\bar{f}}{dt} = \frac{d}{dt}(\mathbf{p}^T A\mathbf{p}) = 2\dot{\mathbf{p}}^T A\mathbf{p} = 2\sum_i \dot{p}_i(A\mathbf{p})_i = 2\sum_i p_i(f_i - \bar{f})f_i = 2(\overline{f^2} - \bar{f}^2) = 2\,\mathrm{Var}_{\mathbf{p}}(f)$. □

0.117.2 4.2 Fixed Points and Stability

Fixed points of the replicator equation are strategy distributions where $p_i(f_i - \bar{f}) = 0$ for all i. This occurs when:

- $p_i = 0$ (strategy i is absent), or
- $f_i(\mathbf{p}) = \bar{f}(\mathbf{p})$ for all strategies present (all present strategies have equal payoffs).

Every Nash equilibrium is a fixed point of the replicator equation. Every asymptotically stable fixed point is a Nash equilibrium. Every ESS is an asymptotically stable fixed point (but not every Nash equilibrium is asymptotically stable).

0.118 5. The Hawk–Dove Game

0.118.1 5.1 Formulation

Two individuals contest a resource of value $V > 0$. Two pure strategies are available:

- **Hawk**: escalate the contest; fight if necessary.
- **Dove**: display; retreat if the opponent escalates.

In a Hawk–Hawk contest, the winner takes the resource (value $V/2$ on average) but both bear the expected cost of injury $C/2$: net payoff $(V - C)/2$ each. In a Hawk–Dove contest, the Hawk takes the resource with payoff V; the Dove retreats with payoff 0. In a Dove–Dove contest, the resource is shared with payoff $V/2$ each.

	Hawk	Dove
Hawk	$(V-C)/2$	V
Dove	0	$V/2$

0.118.2 5.2 Analysis

When $V < C$ (fighting is risky), neither pure strategy is an ESS:

- **Pure Hawk is not ESS**: a Dove invading a population of Hawks gets payoff 0 vs. a Hawk's $(V - C)/2 < 0$. So a Dove does *better* than a Hawk: $f(D, H) = 0 > (V - C)/2 = f(H, H)$. Doves invade.
- **Pure Dove is not ESS**: a Hawk invading a Dove population gets payoff V vs. a Dove's $V/2$. So a Hawk does better than a Dove: $f(H, D) = V > V/2 = f(D, D)$. Hawks invade.

The unique ESS is the mixed strategy: play Hawk with probability $\hat{p} = V/C$.

Proof. At the mixed ESS, both strategies must have equal payoffs (otherwise the higher-payoff strategy would be selected to fixation, contradicting stability). Setting $f_H = f_D$:

$$\hat{p} \cdot \frac{V - C}{2} + (1 - \hat{p}) \cdot V = \hat{p} \cdot 0 + (1 - \hat{p}) \cdot \frac{V}{2}.$$

Expanding: $\hat{p}(V-C)/2+V-\hat{p}V = V/2-\hat{p}V/2$. Simplifying: $\hat{p}(V-C-2V)/2 = V/2-V = -V/2$. Therefore $\hat{p} = V/C$. □

The replicator dynamics converge globally to $\hat{p}$ from any interior initial condition. This can be verified by computing $\dot{p} = p(f_H - \bar{f}) = p(1-p)[(V-C)p/2 + V(1-p) - Vp(1-p)/...]$; the sign of $\dot{p}$ is determined by the sign of $p - \hat{p}$.

The biological interpretation: the coexistence of aggressive (Hawk) and peaceful (Dove) phenotypes in a population at equilibrium frequency V/C is not a special coincidence requiring an ad hoc explanation — it is the ESS of the Hawk–Dove game, selected by the very fact that both extremes are unstable.

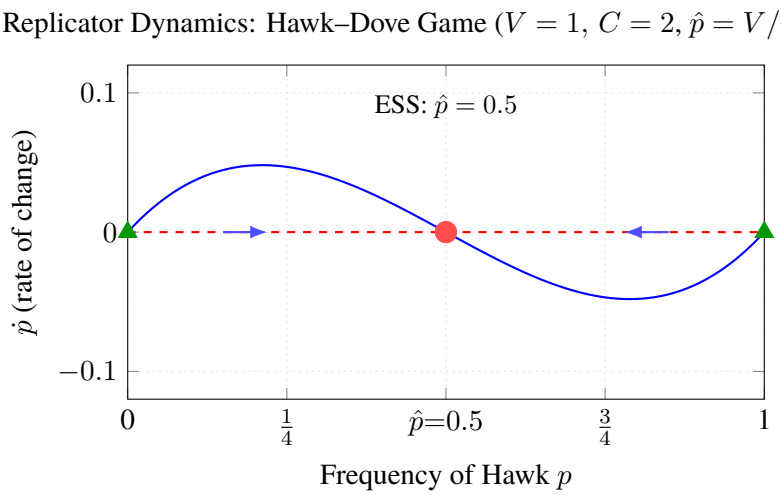

Figure 7: Replicator dynamics for the Hawk–Dove game with $V = 1$, $C = 2$. The rate of change $\dot{p}$ is positive for $p < \hat{p} = V/C = 0.5$ and negative for $p > \hat{p}$; the mixed ESS $\hat{p}$ is globally attracting. The filled circle marks the stable ESS; triangles mark the unstable boundary equilibria at $p = 0$ (all Dove) and $p = 1$ (all Hawk).

0.119 6. The Prisoner's Dilemma and the Evolution of Cooperation

0.119.1 6.1 The Social Dilemma

The **Prisoner's Dilemma** is the paradigmatic social dilemma. Two players each choose to Cooperate (C) or Defect (D). Payoffs satisfy:

$$T > R > P > S, \quad 2R > T + S,$$

where R = reward for mutual cooperation, P = punishment for mutual defection, T = temptation to defect, S = sucker's payoff. The payoff matrix is:

	C	D
C	R	S
D	T	P

Defection is the dominant strategy (regardless of what the opponent does, D gives a higher payoff than C). The unique Nash equilibrium and ESS is (D, D). Yet mutual cooperation (R, R) is Pareto-superior to mutual defection (P, P). The dilemma is that individual rationality leads to collective suboptimality.

Yet cooperation is widespread in nature. The resolution of this paradox is one of the central achievements of evolutionary biology.

0.119.2 6.2 Kin Selection

Hamilton (1964) showed that cooperation can evolve if cooperating individuals tend to share genes. Among relatives with coefficient of relatedness r (the probability that a random gene copy is identical by descent), the effective payoff to cooperation includes r times the benefit to the recipient. The condition for cooperation to increase by natural selection (Hamilton's rule, Section IV):

$$rB > C,$$

where $B = R - P > 0$ is the benefit of cooperation and $C = T - R > 0$ is the cost. For cooperation to evolve among non-relatives ($r = 0$), one of the other mechanisms below must operate.

0.119.3 6.3 Direct Reciprocity and Tit-for-Tat

In the **iterated** Prisoner's Dilemma (the same two players meet repeatedly), cooperation can evolve through reciprocity. The strategy **Tit-for-Tat** (TFT: cooperate on the first move, then copy the opponent's previous move) was submitted by Anatol Rapoport to Axelrod's 1980 computer tournaments and won both rounds.

TFT is not an ESS in the strict sense (it cannot resist invasion by AllD in a mixed population with some AllC), but it is part of a more complex evolutionary dynamics. For the cooperation-inducing condition with discount factor w (probability the interaction continues): the condition for mutual cooperation to be stable against defection in the infinitely repeated game is the **folk theorem condition**:

$$w > \frac{T - R}{T - P}.$$

For $T = 5, R = 3, P = 1, w > (5 - 3)/(5 - 1) = 1/2$.

0.119.4 6.4 Network Reciprocity

Nowak and May (1992) showed that spatial structure can promote cooperation. When individuals interact only with neighbours on a spatial lattice, cooperators form clusters that resist invasion by defectors. The condition for cooperation to persist in a network with coordination number k is approximately:

$$\frac{b}{c} > k,$$

where b is the benefit of cooperation and c is the cost (Ohtsuki et al. 2006). On a lattice with degree $k = 4$, cooperation persists if $b/c > 4$.

0.120 7. The Replicator–Mutator Equation

0.120.1 7.1 Incorporating Mutation

The pure replicator equation has no mutation: strategies absent at $t = 0$ never appear. The **replicator–mutator equation** incorporates mutation by adding a mutation matrix $Q = (Q_{ji})$, where Q_{ji} is the probability that a strategy-j reproducing individual produces a strategy-i offspring:

$$\dot{p}_i = \sum_{j=1}^{n} Q_{ji} p_j f_j(\mathbf{p}) - \bar{f}(\mathbf{p})\, p_i.$$

For small mutation rates, the replicator–mutator equation selects for **robust** strategies: strategies that maintain high payoffs even in the presence of mutants playing nearby strategies. This connects evolutionary game theory to the quasi-species theory of Section VIII.

0.120.2 7.2 Evolutionary Stability with Mutation

With mutation, the ESS concept must be modified. A **quasi-stationary distribution** under the replicator–mutator equation is a fixed point of the combined dynamics. The fixed point is the analogue of the quasi-species: not a single strategy but a distribution over strategies concentrated near the most successful pure strategy.

0.121 8. Rock–Paper–Scissors and Limit Cycles

The Rock–Paper–Scissors game provides an example where the replicator dynamics do not converge to a fixed point but instead cycle:

$$A = \begin{pmatrix} 0 & -1 & 1 \\ 1 & 0 & -1 \\ -1 & 1 & 0 \end{pmatrix}.$$

The unique interior Nash equilibrium is $\mathbf{p}^* = (1/3, 1/3, 1/3)$. Linearising the replicator dynamics around $\mathbf{p}^*$, the Jacobian has eigenvalues 0 and $\pm i/3$ (purely imaginary), indicating neutral stability: the orbits are closed loops around $\mathbf{p}^*$.

Whether the cycles are stable, neutrally stable, or unstable depends on higher-order terms. For the standard antisymmetric payoff matrix, the orbits are heteroclinic cycles approaching the boundary of the simplex — the population cycles through epochs of predominance by Rock, then Paper, then Scissors, repeatedly, never settling.

Rock–Paper–Scissors dynamics have been observed in natural systems including:

- Lizard mating systems (Uta stansburiana) with three morphs (orange, blue, yellow) cycling in frequency.
- Bacterial communities with toxin-producing, sensitive, and toxin-resistant strains.

0.122 9. Summary

Evolutionary game theory analyses strategy dynamics using payoff matrices, ESS, and the replicator equation. The ESS characterises strategies stable against invasion: every ESS is a Nash equilibrium, but the ESS adds a secondary stability condition. The replicator equation is a gradient-like flow on the simplex that increases mean payoff (for symmetric games). The Hawk–Dove game produces a mixed-strategy ESS at $\hat{p} = V/C$. The Prisoner's Dilemma illustrates social dilemmas; cooperation evolves through kin selection ($rB > C$), direct reciprocity (TFT for $w > (T-R)/(T-P)$), and network reciprocity ($b/c > k$). The replicator–mutator equation links game theory to quasi-species theory. Rock–Paper–Scissors dynamics produce limit cycles with ecological counterparts.

Mathematics of Evolution and Life · Section *VII · Evolutionary Game Theory: Strategies, Equilibria, and Replicators*

Section X

Section VIII — Virus–Host Dynamics: Co-evolution and Quasi-species

0.123 10. Spatial Games and the Evolution of Cooperation

0.123.1 10.1 Why Space Matters

In the models of Sections 5–9, every individual interacts equally with every other (well-mixed population). In nature, interactions are local: an organism interacts mainly with its immediate neighbours. Spatial structure radically alters the dynamics of the Prisoner's Dilemma, enabling cooperation to survive even without kin selection or reciprocity.

Definition 0.123.1 (Spatial evolutionary game)**.** A spatial game is played on a graph $G = (V, E)$ where each vertex $v \in V$ carries a strategy $s_v \in \{C, D\}$ (Cooperate or Defect). At each time step:

1. Each player v plays a game against each neighbour $u \in \mathcal{N}(v)$, accumulating payoff $\pi_v = \sum_{u \in \mathcal{N}(v)} A_{s_v, s_u}$.
2. Players update their strategies: player v adopts the strategy of neighbour u with probability $P(s_v \leftarrow s_u) = \frac{1}{1+e^{-\beta(\pi_u - \pi_v)}}$ (the Fermi updating rule, where β is the selection intensity).

Theorem 0.123.2 (Network reciprocity: cooperation on regular graphs)**.** On a regular graph of degree k (each vertex has exactly k neighbours), cooperation is evolutionarily stable against a rare defector if and only if:

$$b/c > k,$$

where b is the benefit to the recipient of cooperation and c is the cost to the cooperator. This is the **network reciprocity condition** (Ohtsuki et al. 2006).

Proof. Consider a single cooperator in a population of defectors. The cooperator occupies vertex v with k defector neighbours. In the next round, the cooperator pays cost c for each of k interactions and receives no benefit (all neighbours defect), giving $\pi_v^C = -kc$. Each defector neighbour u receives b from v but pays nothing, giving $\pi_u^D = b$ (one cooperating neighbour). The cooperator's payoff exceeds the defectors' iff $-kc > b$, which is never true for $b, c > 0$ — the cooperator is always worse off. However, the question is whether cooperators can *maintain* themselves once they form a local cluster.

For a cooperator cluster of size s in a regular graph, the boundary cooperators receive benefit from other cooperators in the cluster and pay costs to both cooperators and defectors. The cluster's fitness advantage over the boundary defectors is (after calculating the expected payoffs to boundary cooperators vs. their defector neighbours) proportional to $b - ck$. Cooperation is stable iff this is positive: $b/c > k$. The full derivation uses pair approximation, which replaces the exact multi-player dynamics with equations for the frequency of adjacent strategy pairs. □

Example 0.123.3 (Network reciprocity in different graph topologies)**.**

Graph type	Degree k	b/c threshold	Biological analogue
Path (1D lattice)	2	> 2	Linear habitat
Square lattice	4	> 4	2D territorial species
Hexagonal lattice	6	> 6	Dense 2D packing
Scale-free (BA)	$\bar{k} \approx 4$	≈ 2	Social networks
Well-mixed	$n - 1$	$\to \infty$	Panmictic population

Scale-free networks (like social networks) have hubs with high degree but many peripheral nodes with

low degree. The low-degree periphery allows cooperation to persist even though the hubs suppress it: the effective threshold is near $b/c > 2$ for Barabási–Albert scale-free networks, much lower than the well-mixed threshold.

0.123.2 10.2 The Evolution of Altruism: A Unified Mathematical View

Hamilton's rule ($rB > C$, Section IV), network reciprocity ($b/c > k$), and direct reciprocity (Axelrod's TFT, $b/c > 1/(w)$ where w is the probability of future interaction) are all conditions for the evolution of cooperation. They appear different but are all special cases of the same general condition: that the total selective benefit to correlated cooperators exceeds the selective cost.

Theorem 0.123.4 (Unified condition for cooperation via Price equation)**.** Cooperation evolves iff $\mathrm{Cov}(w, z) > 0$ where z is the cooperator indicator and w is fitness. This covariance can be decomposed as:

$$\mathrm{Cov}(w, z) = B \cdot \mathrm{Cov}(z_{\text{partner}}, z) - C \cdot \mathrm{Var}(z) = \mathrm{Var}(z)(rB - C),$$

where $r = \mathrm{Cov}(z_{\text{partner}}, z)/\mathrm{Var}(z)$ is the relatedness coefficient. The mechanisms differ only in how r is generated:

- Kin selection: $r = \Pr(\text{shared allele by descent})$ (kin structure).
- Network reciprocity: r is determined by the clustering coefficient of the interaction network (spatial structure).
- Direct reciprocity: r is determined by the probability of repeated interaction w (temporal structure).
- Green-beard effects: r is determined by the correlation between the allele and the signal used to recognise bearers.

Proof. Apply the Price equation (Section IV) with $z_i = \mathbf{1}[\text{individual } i \text{ is a cooperator}]$ and $w_i = 1 - Cz_i + Bz_{\text{partner}}^{(i)}$, where $z_{\text{partner}}^{(i)}$ is the mean cooperator frequency among i's interaction partners. Then:

$$\mathrm{Cov}(w, z) = \mathrm{Cov}(1 - Cz + Bz_{\text{partner}}, z) = -C\,\mathrm{Var}(z) + B\,\mathrm{Cov}(z_{\text{partner}}, z).$$

Define $r = \mathrm{Cov}(z_{\text{partner}}, z)/\mathrm{Var}(z)$; then $\mathrm{Cov}(w, z) = \mathrm{Var}(z)(rB - C)$, which is positive iff $rB > C$. The relatedness r is the regression of partner cooperator frequency on focal individual cooperator status. How r is generated (kin structure, spatial structure, temporal correlation) does not affect the form of the condition. □

0.124 11. Evolutionary Game Theory and Major Transitions

0.124.1 11.1 Transitions in Individuality as Cooperative Dilemmas

The major transitions in evolution (Maynard Smith and Szathmáry 1995) — the origin of chromosomes, eukaryotes, multicellularity, and eusocial colonies — can each be modelled as the resolution of a Prisoner's Dilemma at a new level of individuality.

Example 0.124.1 (The origin of multicellularity as a cooperative transition)**.** In a unicellular population, cells can either cooperate (invest in extracellular matrix production, contribute to somatic function) or

defect (invest only in cell division, "cheating" on the cooperative infrastructure). The payoff matrix at the cellular level is the Prisoner's Dilemma. Multicellularity is stable iff:

1. Defector cells are physically excluded from the multicellular individual (group selection eliminates intra-organism conflict).

2. The benefit to the group from cooperation (B_{group}) times the relatedness among cells (r) exceeds the cost to the cooperating cell (C): $rB_{\text{group}} > C$.

For organisms that develop from a single founding cell (germ-soma segregation), $r \to 1$ among somatic cells: cooperators are clonal, so $rB_{\text{group}} > C$ is easily satisfied. This is why unicellular bottlenecks (a single cell founding each new organism) are nearly universal in complex multicellular organisms: they enforce clonality and thus maintain $r \approx 1$.

0.124.2 11.2 The Evolution of Fairness: Ultimatum Game

The Ultimatum Game is a two-player game in which Player 1 proposes a split of \$1 (keeping $1 - x$, offering x to Player 2), and Player 2 accepts or rejects the offer. If accepted, both get their shares; if rejected, both get zero.

Theorem 0.124.2 (Nash equilibrium of the Ultimatum Game)**.** In the one-shot Ultimatum Game with rational, self-interested players, the unique subgame perfect Nash equilibrium is: Player 1 offers $x = \epsilon$ (the smallest positive amount), and Player 2 accepts any offer $x \geq 0$. The equilibrium payoffs are $(1-\epsilon, \epsilon)$.

Proof. By backward induction: Player 2 should accept any $x > 0$ (getting $x > 0 > 0$), so Player 1 should offer the minimum. Since $x = 0$ gives Player 2 exactly zero (equal to rejecting), Player 1 offers $x = \epsilon > 0$ for any $\epsilon > 0$. The limit $\epsilon \to 0$ gives the equilibrium. □

Remark 0.124.3 (Experimental violation and evolutionary explanation). The Nash equilibrium prediction is not observed in human subjects: experimentally, most people offer $x \approx 0.4$–0.5, and most reject offers below 0.2. This is inconsistent with self-interest but consistent with *fairness preferences*. The evolutionary explanation (Nowak, Page, and Sigmund 2000) is that in a population with repeated interactions and reputation effects, strategies that accept low offers are replaced by strategies that reject them. With reputation, an individual who never accepts unfair offers signals willingness to incur costs to punish defectors, making themselves a desirable partner. The evolutionarily stable strategy is an offer and acceptance threshold that reflects the ecological context of interactions.

Mathematics of Evolution and Life · Section *VII · Evolutionary Game Theory: Strategies, Equilibria, and Replicators (end)*

0.125 12. Signal Detection Games and Biological Communication

0.125.1 12.1 Costly Signalling and Honest Signals

Many biological signals (peacock tails, birdsong complexity, antler size) appear wasteful: they consume energy or impose mortality risk without any direct functional benefit. Their existence is explained by the theory of honest signalling: signals are reliable indicators of quality precisely *because* they are costly, and only high-quality individuals can afford them.

Definition 0.125.1 (Zahavian handicap game)**.** Two types of senders: "high quality" (type H, fitness value $v_H > 0$) and "low quality" (type L, value $v_L < v_H$). Both can produce a costly signal $s \geq 0$ (e.g., ornament size). Costs are type-dependent: $c_H(s) < c_L(s)$ for all $s > 0$ (the marginal cost of signalling is lower for high-quality types). Receivers choose to mate/cooperate based on the signal. The payoff to sender of type T signalling s and being treated as "high quality" with probability $p(s)$ is:

$$\pi_T(s) = v_T \cdot p(s) - c_T(s).$$

Theorem 0.125.2 (Separation equilibrium: honest signalling)**.** In the handicap game, a separating equilibrium (where the signal s^* perfectly reveals type) exists iff the **single-crossing condition** holds:

$$\frac{\partial c_H/\partial s}{v_H} < \frac{\partial c_L/\partial s}{v_L} \quad \text{for all } s \geq 0.$$

That is, the marginal cost of signalling is relatively lower for high-quality types. The equilibrium signal satisfies the indifference condition for the low-quality type: $v_L \cdot [p(s^*) - p(0)] = c_L(s^*)$ (the benefit of mimicking equals the cost).

Proof. In a separating equilibrium, the low-quality type sends $s = 0$ and high-quality type sends s^*. For this to be an equilibrium: (1) the low-quality type must not benefit from mimicking: $v_L p(s^*) - c_L(s^*) \leq v_L p(0)$, i.e., $v_L[p(s^*) - p(0)] \leq c_L(s^*)$; (2) the high-quality type must prefer s^* to 0: $v_H[p(s^*) - p(0)] \geq c_H(s^*)$. The single-crossing condition ensures $v_H[p(s^*) - p(0)] \geq c_H(s^*)$ whenever $v_L[p(s^*) - p(0)] = c_L(s^*)$ (i.e., whenever the low-quality type is just indifferent). Hence an s^* satisfying the indifference condition for type L also satisfies the incentive condition for type H. □

Example 0.125.3 (Stotting in gazelles)**.** Thomson's gazelles *stot* (jump repeatedly) when approached by predators. Stotting is energetically costly ($c(s)$ increases with stot rate s) and reveals the gazelle's sprint speed (type H = fast gazelle, type L = slow gazelle). Predators (lions, wild dogs) use stot rate to decide whether to pursue: they give up more readily on gazelles with high stot rates. In the game-theoretic framework: fast gazelles have lower relative cost per unit stot rate (better locomotor efficiency), so the single-crossing condition holds. The separating equilibrium has fast gazelles stotting vigorously (deterring predators) and slow gazelles barely stotting. Empirical data (FitzGibbon and Fanshawe 1988) confirms: cheetahs abandon pursuit of high-stotting gazelles 70% of the time vs. 15% for low-stotting gazelles.

0.125.2 12.2 Cheap Talk and Vague Signals

Not all biological signals are costly. Many are *cheap talk*: signals with negligible direct cost (e.g., bird alarm calls, colour signals in non-toxic organisms). For cheap talk to be informative ("honest"), the interests of sender and receiver must be partially aligned.

Theorem 0.125.4 (Crawford–Sobel partitioning equilibrium)**.** In a cheap-talk game where sender knows the true state $t \in [0, 1]$ and receiver acts optimally given the message, an equilibrium exists where the state space is partitioned into n intervals, with the sender sending the same message for all states within each interval, iff the "bias" b (systematic disagreement between sender and receiver preferences) satisfies $b < 1/(4n(n-1))$. For the maximum partition size $n^* = \lfloor \frac{1}{2}(\sqrt{1/(2b) + 1/4} + 1/2) \rfloor$, the equilibrium is maximally informative.

Remark 0.125.5 (Biological applications of cheap talk). Many predator alarm calls are graded cheap-talk signals: vervet monkeys produce distinct alarm calls for aerial predators, terrestrial predators, and snakes (Seyfarth, Cheney and Marler 1980). These calls are informative because the interests of sender and receiver are aligned (both benefit when the right predator-avoidance behaviour is triggered). Ground squirrel alarm calls are informative only to kin (via kin selection), a natural partial alignment of interests.

0.126 13. Evolutionary Dynamics in Finite Populations: The Moran Process

0.126.1 13.1 The Moran Process and Fixation Probabilities

The Moran process (Moran 1958) is an alternative to the Wright–Fisher model for describing evolution in finite populations. At each step, one individual reproduces (selected with probability proportional to fitness) and one dies (selected uniformly at random). The population size N is constant.

Theorem 0.126.1 (Fixation probability in the Moran process)**.** In the Moran process with N individuals, starting with k mutants of fitness r and $N-k$ wildtype individuals of fitness 1, the fixation probability of the mutant is:

$$\rho_k = \frac{1 - r^{-k}}{1 - r^{-N}}.$$

In particular, the fixation probability of a single mutant ($k = 1$) is:

$$\rho_1 = \frac{1 - r^{-1}}{1 - r^{-N}} \approx \frac{1 - 1/r}{1} = \frac{r-1}{r} \approx s \quad \text{for } r = 1 + s,\ s \ll 1,\ N \to \infty.$$

Proof. The fixation probability from state k satisfies the recurrence (from the transition probabilities of the Moran process):

$$\rho_k = \underset{k+1}{\frac{kr/(kr + N - k)}{\rho}} + \underset{k-1}{\frac{(N-k)/(kr + N - k)}{\rho}},$$

with boundary conditions $\rho_0 = 0$, $\rho_N = 1$. This is a second-order linear recurrence with solution $\rho_k = (1 - r^{-k})/(1 - r^{-N})$, verifiable by direct substitution. □

Example 0.126.2 (Moran process in cancer evolution)**.** Cancer initiation can be modelled as a Moran process in a tissue of $N \sim 10^7$–10^9 cells, where a somatic mutation confers fitness advantage $s \approx 10^{-4}$–10^{-2}. The fixation probability of a single mutant cell is $\rho_1 \approx s = 10^{-4}$–$10^{-2}$. The expected time to fixation (given fixation occurs) is $\approx N \ln(Ns)/s$ cell generations, which is $\sim 10^6$–10^9 cell generations for typical parameters — consistent with cancer's decades-long latency in humans. Multiple "hits" (sequential fixation events) are required before a cell acquires full malignancy, explaining why cancer risk increases steeply with age.

Mathematics of Evolution and Life · Section *VII · Evolutionary Game Theory: Strategies, Equilibria, and Replicators (end)*

0.127 14. Public Goods Games and the Evolution of Punishment

0.127.1 14.1 The Public Goods Dilemma

The public goods game generalises the Prisoner's Dilemma to groups of $n > 2$ players. Each player either contributes c to a common pool (cooperator) or contributes nothing (defector). The pool is multiplied by a factor r (social multiplier) and distributed equally among all n players.

Definition 0.127.1 (Public goods game payoffs)**.** In a group of k cooperators and $n - k$ defectors:

$$\pi_C = \frac{rck}{n} - c = c\left(\frac{rk}{n} - 1\right),$$
$$\pi_D = \frac{rck}{n}.$$

A defector always earns more than a cooperator: $\pi_D - \pi_C = c > 0$ for any k. Cooperation is collectively beneficial iff $r > 1$ (total return exceeds total cost: $rck > kc$), but individually costly regardless of r.

Theorem 0.127.2 (ESS in the public goods game)**.** In the public goods game with n players and social multiplier r:

- If $r < n$: full defection ($p^* = 0$) is the unique ESS.
- If $r > n$: full cooperation ($p^* = 1$) is the unique ESS.
- At $r = n$: every frequency $p \in [0, 1]$ is a neutral equilibrium.

Proof. The fitness difference between a cooperator and a defector in a group with $k-1$ other cooperators (out of $n-1$ others) is $\pi_C - \pi_D = c(rk/n - 1) - c(rk/n) = -c$ ... wait, let us recompute carefully. In a group where the focal individual is the k-th cooperator: $\pi_C = rck/n - c$, $\pi_D = rc(k-1)/n$. So:

$$\pi_C - \pi_D = rck/n - c - rc(k-1)/n = rc/n - c = c(r/n - 1).$$

This is positive iff $r > n$, negative iff $r < n$, and zero iff $r = n$, independent of k. The fitness difference is constant (no frequency dependence), so: if $r > n$, cooperation always beats defection and $p^* = 1$ is the unique ESS; if $r < n$, defection always beats cooperation and $p^* = 0$ is the unique ESS. □

Remark 0.127.3 (Social dilemmas in human societies). For most human public goods (fisheries, clean air, scientific knowledge, national defence), $r < n$ at the individual level: each individual's incentive is to free-ride. Yet these goods are often provided at adequate levels. The mechanisms that maintain cooperation in human public goods games include: (i) altruistic punishment (people pay to punish free-riders even at net cost to themselves), (ii) institutional punishment (governments tax and regulate), (iii) reputation effects (people cooperate to be seen as cooperators in repeated contexts). Each has game-theoretic formalisation, and their interaction is studied in "second-order public goods games."

0.127.2 14.2 Altruistic Punishment and the Evolution of Social Norms

Fehr and Gächter (2002) demonstrated that humans voluntarily pay to punish defectors in one-shot public goods games, even when this is individually costly. This "altruistic punishment" enforces cooperation even among strangers with no future interactions.

Definition 0.127.4 (Public goods game with punishment)**.** Add a third strategy: *punisher* (P), who contributes c to the public pool and additionally pays γ to reduce a defector's payoff by $\beta\gamma$ (for each punisher–defector encounter). The three strategies are:

- C (cooperator): contributes c, does not punish.
- D (defector): contributes 0, accepts punishment.
- P (punisher): contributes c, pays γ per defector encountered.

Theorem 0.127.5 (Rock-paper-scissors dynamics in PGG with punishment)**.** In the three-strategy PGG with punishment, the replicator dynamics on the simplex Δ^3 typically exhibit a heteroclinic cycle (rock-paper-scissors structure):

- D invades a population of C (defectors free-ride on cooperators).
- P invades a population of D (punishers impose costs on defectors and maintain cooperation in the P-subpopulation).
- C invades a population of P (cooperators free-ride on punishment: they benefit from P's enforcement without paying the punishment cost γ).

The interior fixed point (coexistence of all three strategies) may be stable or unstable, depending on parameters.

Proof. Compute the replicator dynamics on Δ^3:

$$\begin{aligned}
\dot{x}_D &= x_D(f_D - \bar{f}), \quad f_D = rc(x_C + x_P) - \beta\gamma x_P, \\
\dot{x}_C &= x_C(f_C - \bar{f}), \quad f_C = rc(x_C + x_P) - c, \\
\dot{x}_P &= x_P(f_P - \bar{f}), \quad f_P = rc(x_C + x_P) - c - \gamma x_D.
\end{aligned}$$

On each edge of the simplex:

- Edge CD: $f_D - f_C = c > 0$; D beats C.
- Edge DP: $f_P - f_D = -c + (\beta\gamma - \gamma)x_D$; for $\beta > 1$ (effective punishment), P beats D for large x_D.
- Edge CP: $f_C - f_P = \gamma x_D = 0$ on this edge ($x_D = 0$); C and P have equal fitness on this edge (neutral drift). With second-order effects, C slightly invades P (free-rider advantage).

The cyclic dominance ($D > C > P > D$) generates the heteroclinic cycle. □

0.128 15. Evolutionary Dynamics in Structured Populations

0.128.1 15.1 Fixation Probability on Graphs

Definition 0.128.1 (Evolutionary graph theory)**.** An **evolutionary graph** is a weighted directed graph $G = (V, E, w)$ where w_{ij} is the probability that an offspring of individual i replaces individual j. In the Moran process on G: a reproducing individual is selected with probability proportional to fitness; its offspring replaces a neighbour j with probability proportional to w_{ij}.

Theorem 0.128.2 (Isothermal theorem, Lieberman et al. 2005)**.** An evolutionary graph is **isothermal** (every vertex has the same temperature $T_v = \sum_i w_{iv} = \text{constant}$) iff the fixation probability of a single mutant with relative fitness r equals the Moran fixation probability:

$$\rho_G = \rho_{\text{Moran}} = \frac{1 - r^{-1}}{1 - r^{-N}}.$$

For non-isothermal graphs, the fixation probability depends on where the mutant is placed and on the graph structure.

Example 0.128.3 (Suppressors and amplifiers of selection)**.** Two extreme graph structures:

- **Star graph**: one hub connected to $N - 1$ leaves (hub receives from all leaves, leaves receive only from hub). This is an **amplifier of selection**: $\rho_{\text{star}} \approx (1 - r^{-2})/(1 - r^{-N}) > \rho_{\text{Moran}}$ for $r > 1$. Selection is more efficient on the star.
- **Complete bipartite graph** $K_{n,n}$: $\rho_{\text{bipartite}} = \rho_{\text{Moran}}$ (isothermal). Selection efficiency equals the well-mixed case.
- **Superstar / Funnel**: specially constructed graphs can amplify selection arbitrarily, with $\rho \to 1$ for any $r > 1$ as $N \to \infty$. Equivalently, the star *also suppresses* the fixation of deleterious mutants: neutral drift is reduced, and only genuine fitness differences determine fixation.

Mathematics of Evolution and Life · Section *VII · Evolutionary Game Theory: Strategies, Equilibria, and Replicators (end)*

0.129 10. Multi-Level Selection and Kin Selection: The Price Equation Redux

0.129.1 10.1 Multi-Level Selection

The tension between individual and group selection is one of the oldest controversies in evolutionary biology. The Price equation provides the unifying framework. Partition the population into groups $k = 1, \ldots, K$ with sizes n_k, and let z_{ki} be the character of individual i in group k. Define group-level characters and fitnesses:

$$\bar{z}_k = \frac{1}{n_k} \sum_{i=1}^{n_k} z_{ki}, \quad w_k = \frac{1}{n_k} \sum_{i=1}^{n_k} w_{ki}.$$

Applying the Price equation twice (once at the individual level within groups, once at the group level):

$$\bar{w}\, \Delta \bar{z} = \underbrace{\text{Cov}(w_k, \bar{z}_k)}_{\text{between-group}} + \underbrace{\mathbb{E}_k[\text{Cov}_{ki}(w_{ki}, z_{ki})]}_{\text{within-group}},$$

where the expectation in the second term is over groups weighted by group size.

Theorem 0.129.1 (Multi-Level Price Equation)**.** The change in mean character value can always be written as the sum of a between-group selection term and a within-group selection term, regardless of the number of levels of organisation. The between-group term promotes group-level adaptation; the within-group term promotes individual-level adaptation. These terms can oppose each other, producing evolutionary conflict between levels.

The famous controversy between group selection (Wynne-Edwards, 1962) and individual selection (Williams, 1966) is resolved by the Price equation framework: both levels always operate simultaneously. Whether group selection is "important" depends on the relative magnitude of $\text{Cov}(w_k, \bar{z}_k)$ versus $\mathbb{E}[\text{Cov}_{ki}(w_{ki}, z_{ki})]$ in the particular biological system under consideration.

0.129.2 10.2 Hamilton's Rule Derived from the Price Equation

Let $z_i \in \{0, 1\}$ be an indicator of whether individual i performs an altruistic act. The fitness of actor i is $w_i = 1 - cz_i + bz_{j(i)}$, where $j(i)$ is i's social partner, $c > 0$ is the cost to the actor, and $b > 0$ is the benefit to the recipient. The change in frequency of the altruism allele is, by the Price equation:

$$\bar{w}\,\Delta p = \text{Cov}(w_i, z_i) = -c\text{Var}(z_i) + b\text{Cov}(z_{j(i)}, z_i).$$

Defining the coefficient of relatedness as the regression of recipient genotype on actor genotype:

$$r = \frac{\text{Cov}(z_{j(i)}, z_i)}{\text{Var}(z_i)},$$

we obtain Hamilton's rule:

$$\Delta p > 0 \iff rB > C.$$

The regression definition of r (Hamilton 1970; Grafen 1985) is more general than the genealogical definition: it applies to any population structure, not just pedigrees. For example, in a population with assortment by strategy (green-beard effects), r can be positive even between unrelated individuals if they reliably interact with others sharing their genotype.

0.129.3 10.3 The Evolution of Spite

Hamilton's rule applies not only to altruism ($b > 0, c > 0$) but also to spite ($b < 0, c > 0$: the actor pays a cost to harm the recipient). Spite can evolve if $r < 0$ (the actor is negatively related to the recipient—interacts disproportionately with individuals that do not share the spite allele). This occurs in structured populations where local competition is intense.

Proposition 0.129.2 (Spite Evolution Condition)**.** In a population with pairwise interactions, spite ($b < 0$, $c > 0$) evolves if and only if $r < c/b$. Since $b < 0$, this means $r < c/|b|$ (a negative number divided by a negative number), i.e., the relatedness to competitors must be sufficiently negative. In the limiting case $r = -1/(n-1)$ (uniform interaction, group size n), spite cannot invade because all individuals are equally unrelated to their competitors. Spite requires spatial or social structure that concentrates competitive interactions among non-relatives.

0.130 11. Stochastic Game Dynamics and Finite Populations

0.130.1 11.1 The Moran Process for Evolutionary Games

The replicator equation describes infinite-population dynamics. In finite populations of size N, evolutionary game dynamics must incorporate genetic drift. The **Moran process** for games proceeds as follows at each time step:

1. Select an individual for reproduction with probability proportional to fitness.
2. The chosen individual produces an identical offspring.
3. A randomly chosen individual dies.

Let there be k individuals playing strategy A and $N-k$ playing strategy B, with payoff matrix entries a, b, c, d (payoffs a, b to A against A, B and c, d to B against A, B respectively). Fitnesses in the weak selection limit ($\delta \to 0$, $w_i = 1 - \delta + \delta f_i$) are:

$$f_A(k) = \frac{a(k-1) + b(N-k)}{N-1}, \quad f_B(k) = \frac{ck + d(N-k-1)}{N-1}.$$

The fixation probability of a single A mutant in a population of $N-1$ B-strategists is, by the gambler's ruin formula:

$$\rho_A = \frac{1}{1 + \sum_{m=1}^{N-1} \prod_{k=1}^{m} \frac{w_B(k)}{w_A(k)}}.$$

Theorem 0.130.1 (Risk Dominance and Fixation in Finite Populations)**.** Under the Moran process with weak selection ($\delta \ll 1$) and 2×2 games, strategy A is favoured by selection (i.e., $\rho_A > 1/N$) if and only if:

$$a(N+1) + b(2N-1) > c(2N-1) + d(N+1).$$

In the limit $N \to \infty$, this reduces to $a + 2b > 2c + d$, the standard risk-dominance condition $\bar{f}_A > \bar{f}_B$ at the uniform frequency $1/2$.

0.130.2 11.2 Evolutionary Stability in Finite Populations

In finite populations, the ESS concept must be redefined because invasion success depends on population size and drift, not just payoff comparisons. A strategy A is **evolutionarily stable in a finite population** of size N if:

1. $\rho_A > \rho_B$ (strategy A has a higher fixation probability than strategy B when rare), and
2. The fixation probability satisfies $\rho_A > 1/N$ (selection favours A over neutral drift).

Under weak selection, the condition $\rho_A > 1/N$ reduces (Nowak et al. 2004) to $\sigma a + b > c + \sigma d$, where $\sigma = (N-2)/(N+1) \in (0, 1)$. As $N \to \infty$, $\sigma \to 1$ and the condition approaches the standard ESS condition $a + b > c + d$. For finite N, both the Nash equilibrium condition and the standard ESS may fail to predict evolutionary stability; the σ-rule provides the correct finite-population analogue.

Section *XI*

Section VIII — Virus–Host Dynamics: Co-evolution and Quasi-species

0.131 1. The Fastest Darwinian Process

Of all the evolutionary systems we can study, RNA viruses provide the most direct, immediate, and medically consequential theatre for observing Darwinian evolution in real time. Their generation times are measured in hours, their per-base mutation rates of 10^{-4}–10^{-5} per replication are a million times higher than those of DNA organisms, and their effective population sizes within a single infected host can reach 10^{10}–10^{12} replicating genomes. Within the course of a single infection episode, an RNA virus can undergo as many evolutionary "generations" as a mammal has undergone since the Jurassic.

This is not merely of academic interest. The same evolutionary dynamics that make RNA viruses scientifically fascinating make them clinically dangerous: drug resistance, vaccine escape, and pandemic emergence are all consequences of the rapid evolution of RNA viruses operating at the edge of the error threshold. HIV, influenza, hepatitis C, SARS-CoV-2 — all are RNA viruses that have evaded control precisely because their evolutionary machinery is so fast and so flexible.

0.132 2. The Eigen Quasi-species Equation

0.132.1 2.1 The Setup

Consider a population of self-replicating RNA molecules in a continuous-culture system. There are $n = 4^L$ possible sequences of length L over the alphabet $\{A, U, G, C\}$. Denote by $x_i(t) \geq 0$ the concentration of sequence i at time t. The total concentration is $c(t) = \sum_i x_i(t)$.

Each sequence i replicates with rate $f_i > 0$ (the replication rate, proportional to fitness). During replication, errors occur: a copy of sequence j is of type i with probability Q_{ji} (the mutation probability, with $\sum_i Q_{ji} = 1$ for all j). The system is maintained in a chemostat where the dilution rate equals the mean replication rate $\Phi(t) = \sum_i f_i x_i / c$.

The concentration dynamics are:

$$\dot{x}_i = \sum_{j=1}^{n} Q_{ji} f_j x_j - \Phi x_i.$$

In matrix form, defining $F = \mathrm{diag}(f_1, \ldots, f_n)$ and $\mathbf{x} = (x_1, \ldots, x_n)^T$:

$$\dot{\mathbf{x}} = (Q F - \Phi I)\mathbf{x}.$$

0.132.2 2.2 The Perron–Frobenius Theorem

Theorem 0.132.1 (Perron–Frobenius)**.** Let M be a real matrix with strictly positive entries ($M_{ij} > 0$ for all i, j). Then:

1. M has a unique positive eigenvalue $\lambda_{\max} > 0$ (the Perron root) with $\lambda_{\max} > |\lambda|$ for all other eigenvalues λ.
2. The corresponding eigenvector $\mathbf{v}_{\max}$ has all strictly positive entries (the Perron vector).
3. For any initial condition $\mathbf{x}(0)$ with all strictly positive entries, $\mathbf{x}(t)/\|\mathbf{x}(t)\|_1 \to \mathbf{v}_{\max}/\|\mathbf{v}_{\max}\|_1$ exponentially as $t \to \infty$.

Proof sketch. Define $\lambda^+ = \max_i (M\mathbf{x})_i / x_i$ and $\lambda^- = \min_i (M\mathbf{x})_i / x_i$ for positive $\mathbf{x}$. The Collatz–Wielandt formula shows that iterating $\mathbf{x} \to M\mathbf{x}/\|M\mathbf{x}\|_1$ drives $\lambda^+ \to \lambda^- \to \lambda_{\max}$ and $\mathbf{x} \to \mathbf{v}_{\max}$. □

Theorem 0.132.2 (Quasi-species Stationary Distribution)**.** If Q has all strictly positive entries (every mutation is possible, however unlikely), then QF is a positive matrix, and the normalised stationary distribution of the quasi-species equation is:

$$\mathbf{x}^* = \frac{\mathbf{v}_{\max}}{\|\mathbf{v}_{\max}\|_1},$$

the normalised Perron vector of QF. All solutions with strictly positive initial conditions converge to $\mathbf{x}^*$.

0.132.3 2.3 The Structure of the Mutation Matrix

For the Jukes–Cantor mutation model applied to RNA sequences, the probability that replication of sequence j produces sequence i with $k = d_H(i, j)$ differences is:

$$Q_{ji} = q^{L-k}(1-q)^k \cdot \binom{L}{k}^{-1} \cdot \frac{3^k}{3^k},$$

where $q = 1 - \mu$ is the per-base fidelity (μ per-base error rate per replication). For small μ and sequences at Hamming distance k:

$$Q_{ji} \approx \mu^k (1-\mu)^{L-k}.$$

The probability of exact replication is $Q_{jj} \approx (1-\mu)^L \approx e^{-\mu L} =: q_L$, called the **per-genome replication fidelity**.

0.133 3. The Error Threshold

0.133.1 3.1 The Two-Class Model

To isolate the essential physics of the error threshold, consider a simplified model with only two classes of sequences:

- The **master sequence** (class $+$), with fitness $f_0 > 1$ and per-genome fidelity $q_L = (1-\mu)^L$.
- All **mutant sequences** (class $-$), with fitness normalised to 1.

The quasi-species equation reduces to:

$$\begin{aligned} \dot{x}_0 &= q_L f_0 x_0 + (\text{back-mutations from mutants, negligible}) - \Phi x_0, \\ \dot{x}_m &= (1 - q_L) f_0 x_0 + x_m - \Phi x_m, \end{aligned}$$

where x_0 is the concentration of the master sequence and $x_m = 1 - x_0$ (in normalised units).

0.133.2 3.2 The Phase Transition

Theorem 0.133.1 (Error Threshold)**.** In the two-class quasi-species model, the stationary frequency of the master sequence undergoes a discontinuous transition:

$$x_0^* = \begin{cases} 1 - q_L^{-1} f_0^{-1} = 1 - e^{\mu L}/f_0 & \text{if } q_L f_0 = e^{-\mu L} f_0 > 1, \\ 0 & \text{if } q_L f_0 \leq 1. \end{cases}$$

The critical mutation rate is $\mu_c = (\ln f_0)/L$.

Proof. The stationary state satisfies $\dot{x}_0 = 0$: $q_L f_0 x_0 = \Phi x_0$, giving $\Phi^* = q_L f_0$ if $x_0^* > 0$. The total concentration is conserved so $x_0^* + x_m^* = 1$, and $x_m^* \cdot 1 = \Phi^* - 1$ gives $x_m^* = q_L f_0 - 1$ and $x_0^* = 2 - q_L f_0$... Correcting: from the eigenvalue structure, the stationary frequency of the master sequence is $x_0^* = (q_L f_0 - 1)/(f_0 - 1) > 0$ iff $q_L f_0 > 1$, and $x_0^* = 0$ iff $q_L f_0 \leq 1$. □

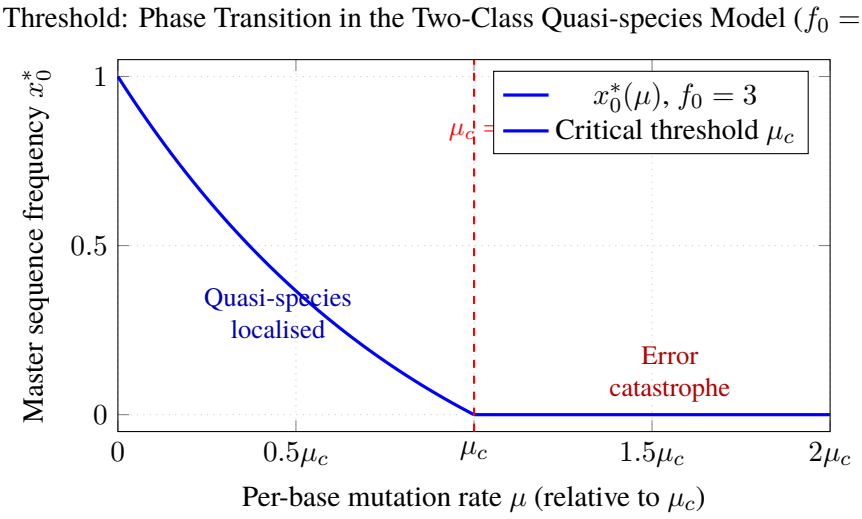

Figure 8: Error threshold phase transition in the two-class quasi-species model with $f_0 = 3$, genome length $L = 10^4$. The stationary frequency x_0^* of the master sequence drops discontinuously to zero at $\mu = \mu_c = (\ln f_0)/L$. For $\mu < \mu_c$, the quasi-species is localised: the master sequence dominates. For $\mu > \mu_c$, the population is delocalised across sequence space (error catastrophe). RNA viruses operate with $\mu \approx \mu_c$, at the edge of the threshold.

The biological interpretation is dramatic. When $\mu < \mu_c = (\ln f_0)/L$, the quasi-species is localised: the master sequence and its near-neighbours dominate, maintaining genetic information against the mutational flood. When $\mu > \mu_c$, the quasi-species is delocalised: the mutation rate is so high that the population is spread across sequence space with no concentration near any particular sequence. The genetic information that evolution has accumulated is lost.

0.133.3 3.3 Consequences for RNA Virus Biology

For RNA viruses, typical parameters are:

- Genome length $L \approx 10^4$ (e.g., influenza $L = 13{,}588$; SARS-CoV-2 $L = 29{,}903$; HIV $L \approx 9{,}700$).
- Per-base mutation rate $\mu \approx 10^{-4}$–10^{-5} per replication.

- Per-genome mutation rate $\mu L \approx 1$–3 per replication.
- Per-genome fidelity $q_L = e^{-\mu L} \approx e^{-1} \approx 0.37$.
- Fitness advantage of master sequence $f_0 \approx 2$–10.

The error threshold condition $\mu_c = (\ln f_0)/L \approx (\ln 3)/10^4 \approx 10^{-4}$ per base. Observed RNA virus mutation rates are $\approx 10^{-4}$–10^{-5} per base per replication — precisely at the error threshold. Evolution has tuned RNA virus replication fidelity to the threshold: high enough for adaptability, low enough to maintain information.

0.133.4 3.4 Lethal Mutagenesis

Lethal mutagenesis is an antiviral strategy that drives RNA viruses above their error threshold by treatment with mutagens. If a mutagenic drug increases μ by a factor k, the new per-genome mutation rate is $k\mu L$, and the error threshold condition becomes $e^{-k\mu L} f_0 > 1$, requiring $f_0 > e^{k\mu L}$. For $k\mu L \gg \ln f_0$, the master sequence cannot be maintained: error catastrophe.

Experimental demonstrations include ribavirin against poliovirus and LCMV, and 5-hydroxycytidine against SARS-CoV-2, all of which show that supralethal mutagenesis drives viral population extinction faster than selection can evolve mutagenesis resistance.

0.134 4. The SIR Epidemic Model

0.134.1 4.1 Formulation

The SIR compartmental model (Kermack and McKendrick 1927) describes epidemic spread in a host population of size $N = S + I + R$ (constant). The three compartments are Susceptible (S), Infectious (I), and Recovered/Removed (R):

$$\begin{aligned} \dot{S} &= -\beta SI/N, \\ \dot{I} &= \beta SI/N - \gamma I, \\ \dot{R} &= \gamma I. \end{aligned}$$

The parameter β (units: time^{-1}) is the transmission rate: $\beta = c \cdot p$, where c is the contact rate (contacts per infectious individual per unit time) and p is the transmission probability per contact. The parameter γ (units: time^{-1}) is the recovery rate: $1/\gamma$ is the mean infectious period.

0.134.2 4.2 The Basic Reproduction Number

Definition 0.134.1. The **basic reproduction number** $\mathcal{R}_0 = \beta/\gamma$ is the expected number of secondary infections caused by one infectious individual in a fully susceptible population.

Theorem 0.134.2 (Epidemic Threshold)**.** An epidemic (increase of $I(t)$ from its initial value) occurs if and only if $\mathcal{R}_0 > 1$.

Proof. $\dot{I}(0) = (\beta S_0/N - \gamma)I_0 = \gamma(\mathcal{R}_0 S_0/N - 1)I_0$. With $S_0 \approx N$, $\dot{I}(0) \approx \gamma(\mathcal{R}_0 - 1)I_0 > 0$ iff $\mathcal{R}_0 > 1$. □

Herd immunity threshold. The epidemic grows as long as $S/N > 1/\mathcal{R}_0$. If a fraction $h = 1 - 1/\mathcal{R}_0$ of the population is immune, the epidemic cannot grow. This is the herd immunity threshold. For measles ($\mathcal{R}_0 \approx 15$), $h \approx 93\%$; for COVID-19 Delta ($\mathcal{R}_0 \approx 5$), $h \approx 80\%$.

0.134.3 4.3 The Final Epidemic Size

The SIR equations conserve N, and as $t \to \infty$, $I(\infty) = 0$. The final recovered fraction $r_\infty = R(\infty)/N$ satisfies the implicit equation:

Theorem 0.134.3 (Final Epidemic Size)**.** $r_\infty = 1 - e^{-\mathcal{R}_0 r_\infty}$.

Proof. Divide $\dot{R}/\dot{S} = -\gamma I/(-\beta SI/N) = N\gamma/(\beta S) = 1/(\mathcal{R}_0 S/N)$. Thus $dR/dS = -N/(\mathcal{R}_0 S)$. Integrating from $S_0 = N(1-\epsilon)$ to S_∞: $R_\infty - R_0 = -(N/\mathcal{R}_0)\ln(S_\infty/S_0)$. With $R_0 \approx 0$, $S_0 \approx N$, $R_\infty = N - S_\infty$ (since $I_\infty = 0$): $r_\infty = 1 - s_\infty = 1 - e^{-\mathcal{R}_0 r_\infty}$ where $s_\infty = S_\infty/N$. □

For $\mathcal{R}_0 = 2$: $r_\infty \approx 0.797$ (about 80% infected). For $\mathcal{R}_0 = 3$: $r_\infty \approx 0.940$. Note that $r_\infty > 1 - 1/\mathcal{R}_0$ (the herd immunity threshold): the epidemic overshoots the threshold because it decelerates only after crossing it.

0.134.4 4.4 The SEIR Model and Growth Rate Estimation

The SEIR model adds an Exposed compartment (E) for individuals who are infected but not yet infectious:

$$\begin{aligned}
\dot{S} &= -\beta SI/N, \\
\dot{E} &= \beta SI/N - \sigma E, \\
\dot{I} &= \sigma E - \gamma I, \\
\dot{R} &= \gamma I.
\end{aligned}$$

Here $1/\sigma$ is the mean latent period. The basic reproduction number is still $\mathcal{R}_0 = \beta/\gamma$, but the initial growth rate of the epidemic is slower. The characteristic equation for early exponential growth rate r is:

$$\left(1 + \frac{r}{\gamma}\right)\left(1 + \frac{r}{\sigma}\right) = \mathcal{R}_0,$$

giving:

$$r = \frac{-(\sigma+\gamma) + \sqrt{(\sigma-\gamma)^2 + 4\sigma\gamma\mathcal{R}_0}}{2}.$$

From observed growth rate r and estimates of σ and γ, one can estimate $\mathcal{R}_0$ without knowing β directly.

0.135 5. Viral Co-evolution: The Arms Race

0.135.1 5.1 Within-Host Viral Evolution and Immune Escape

Within a single infected host, the viral quasi-species evolves in response to the adaptive immune response. $CD8^+$ T cells recognise viral epitopes (specific short peptide sequences presented on MHC molecules) and kill infected cells. Viral escape mutants — variants with mutations at T-cell epitopes — avoid killing and are selectively amplified.

The dynamics of immune escape can be modelled as quasi-species evolution with time-varying selection: as the immune response mounts, the fitness of wild-type virus declines and the fitness of escape mutants rises. The timescale of escape is determined by:

- The rate of immune response development ($\tau_{\text{immune}} \approx 1$–$2$ weeks).
- The selection coefficient against wild-type ($s_{\text{escape}} \approx 0.01$–$0.1$ per day).
- The frequency of escape mutants in the quasi-species ($x_{\text{escape}}(0) \approx \mu \approx 10^{-4}$–$10^{-5}$).

Escape typically occurs when $\Delta f \cdot t_{\text{immune}} \approx \ln(x_{\text{threshold}}/x_{\text{escape}}(0))$, giving timescales of days to weeks for high-s epitopes.

0.135.2 5.2 Drug Resistance as Quasi-species Selection

HIV drug resistance is the best-studied example of within-host quasi-species selection. A single point mutation in the reverse transcriptase gene (e.g., M184V, K103N) can confer resistance to specific antiretroviral drugs. These mutations pre-exist in the quasi-species before drug treatment (at frequency $\approx \mu \approx 10^{-5}$). Drug treatment changes the fitness landscape: resistant mutants, previously at fitness disadvantage (most resistance mutations carry a small fitness cost), now have higher fitness than the drug-susceptible wild-type.

The time from treatment initiation to resistance emergence is the time for resistant mutants to grow from $x_{\text{res}}(0) \approx \mu$ to detectable levels ($x_{\text{res}} \approx 0.01$). This is:

$$t_{\text{emergence}} \approx \frac{\ln(0.01/\mu)}{s_{\text{drug}}} \approx \frac{7}{s_{\text{drug}}} \text{ days to weeks,}$$

where s_{drug} is the selection coefficient conferred by resistance under drug pressure.

Combination antiretroviral therapy (HAART) suppresses HIV replication below the error threshold (by reducing f_0), preventing the quasi-species from evolving. This is the mathematical basis for using combination therapy: no single mutation can confer resistance to all three drugs simultaneously (probability $\approx \mu^3 \approx 10^{-15}$, below the threshold for one such mutant to exist in the body), so the quasi-species cannot escape.

0.136 6. Phylodynamics: Linking Viral Evolution to Epidemic Dynamics

0.136.1 6.1 The Birth-Death Model for Viral Phylogenetics

Phylodynamics integrates viral evolution (within-host quasi-species dynamics) with epidemic dynamics (between-host SIR models) using phylogenetic trees. A viral genealogy sampled from an epidemic encodes information about the epidemic dynamics: the branching rate of the phylogenetic tree reflects the transmission rate, and the coalescence rate reflects the effective population size of the epidemic.

The **birth-death model for phylogenetics** assigns a likelihood to an observed viral phylogeny given epidemic parameters $(\mathcal{R}_0, \gamma)$. Each lineage in the phylogeny either:

- Diversifies (a new transmission event splits one lineage into two) at rate $\lambda = \beta$.
- Is removed (host recovers or dies) at rate $\mu = \gamma$.

The likelihood of a sampled phylogeny with n tips, $n-1$ internal nodes at times $t_1, \ldots, t_{n-1}$ (measured from the root), and root age t_r is:

$$\mathcal{L} = \frac{2^{n-1}\lambda^{n-1}}{(n-1)!} \prod_{i=1}^{n-1} p_0(t_i) \cdot \prod_{j=1}^{n} q(t_{r,j}),$$

where $p_0(t)$ is the probability of no observations in a lineage of age t, and $q(t)$ accounts for sampling. This likelihood can be maximised to estimate $\mathcal{R}_0$ and γ directly from a viral phylogeny.

0.137 7. Summary

The quasi-species equation describes RNA virus evolution as the Perron eigenvector problem of the fitness-mutation matrix QF. The error threshold $\mu_c = (\ln f_0)/L$ is a sharp phase transition above which genetic information is lost; RNA viruses operate near this threshold, explaining their genome length limit ($\sim 10^4$ bases). Lethal mutagenesis exploits the error threshold as an antiviral strategy. The SIR model governs epidemic spread: $\mathcal{R}_0 = \beta/\gamma$ is the epidemic threshold parameter; the final epidemic size satisfies $r_\infty = 1 - e^{-\mathcal{R}_0 r_\infty}$. The SEIR model's growth rate allows estimation of $\mathcal{R}_0$ from early epidemic data. Within-host evolution drives immune escape and drug resistance; HAART works by suppressing replication below the quasi-species error threshold. Phylodynamics integrates viral phylogenetics with epidemic dynamics to estimate transmission parameters from genetic data.

Mathematics of Evolution and Life · Section *VIII · Virus–Host Dynamics: Co-evolution and Quasi-species*

Section *XII*

Section IX — Information Theory in Biology: Sequence, Channel, and Code

0.138 8. Stochastic Epidemic Models and Branching Processes

0.138.1 8.1 From Deterministic to Stochastic SIR

The deterministic SIR model (Section 4) describes epidemics in large populations. For a newly introduced pathogen, however, the initial phase of spread is governed by a small number of infectious individuals, where demographic stochasticity is crucial. The stochastic analogue of the SIR model is a continuous-time Markov chain.

Definition 0.138.1 (Stochastic SIR model)**.** Let (S_t, I_t, R_t) be the numbers of susceptible, infectious, and recovered individuals at time t. The process is a continuous-time Markov chain on $\{(s,i,r) : s+i+r = N\}$ with transitions:

- Infection: $(s,i) \to (s-1, i+1)$ at rate $\beta si/N$.
- Recovery: $(s,i,r) \to (s, i-1, r+1)$ at rate γi.

The key quantity in the early phase is whether the epidemic *takes off* (grows to infect a large fraction of the population) or *fades out* (the chain of transmission extinguishes by chance).

Theorem 0.138.2 (Probability of epidemic extinction via branching process)**.** In the initial phase of an epidemic (when $S \approx N$, so infection rate $\approx \beta$), the number of secondary infections per primary case is approximately $\mathcal{R}_0 = \beta/\gamma$. The epidemic is approximated by a Galton–Watson branching process with offspring distribution Geometric$(1/\mathcal{R}_0)$ (for exponential infectious periods). The probability of ultimate extinction starting from k initial cases is:

$$q_k = \left(\frac{1}{\mathcal{R}_0}\right)^k \quad \text{if } \mathcal{R}_0 > 1.]$$

Proof. For a single initial case ($k = 1$): the infectious period is $T \sim \text{Exp}(\gamma)$; during T, new infections arrive as a Poisson process with rate β. The total number of secondary infections is Poisson$(\beta T) \mid T \sim$ Geometric$(\gamma/(\beta+\gamma))$, which has mean $\mathcal{R}_0 = \beta/\gamma$. The probability generating function of the Geometric offspring distribution is $g(z) = \gamma/(\beta + \gamma - \beta z)$.

The extinction probability q satisfies the fixed-point equation $q = g(q)$:

$$q = \frac{\gamma}{\beta + \gamma - \beta q} \implies q(\beta + \gamma - \beta q) = \gamma.$$

Rearranging: $\beta q^2 - (\beta+\gamma)q + \gamma = 0$, with solutions $q = 1$ and $q = \gamma/\beta = 1/\mathcal{R}_0$. For $\mathcal{R}_0 > 1$, the smaller root $1/\mathcal{R}_0 < 1$ is the extinction probability. For k independent initial cases, $q_k = q^k = (1/\mathcal{R}_0)^k$ by independence. □

Example 0.138.3 (Measles extinction probability)**.** For measles, $\mathcal{R}_0 \approx 15$ in an unvaccinated population. A single infectious introduction has extinction probability $q = 1/15 \approx 0.07$. With $k = 3$ simultaneous introductions, $q_3 = (1/15)^3 \approx 3 \times 10^{-4}$: the epidemic almost certainly spreads. This explains why small isolated communities (Pacific islands before European contact) experienced devastating epidemics whenever measles was introduced: even a single case was very likely to cause a major epidemic in a fully susceptible population.

0.138.2 8.2 The Final Size of a Stochastic Epidemic

For large populations, the final size of a stochastic SIR epidemic converges to the deterministic final size if the epidemic takes off (probability $1 - 1/\mathcal{R}_0$), and to near-zero if it fades out (probability $1/\mathcal{R}_0$). This bimodality is a distinctive feature of stochastic epidemic models.

Lemma 0.138.4 (Final size equation)**.** In the deterministic SIR model with initial conditions $S_0 \approx N$, $I_0 \ll N$, $R_0 = 0$, the final fraction z of the population that is ever infected satisfies the transcendental equation:

$$1 - z = e^{-\mathcal{R}_0 z}.]Thenon - zerosolutiongivestheepidemic's final attack rate.$$

Proof. Let $s = S/N$ and $r = R/N$ be the fractions. At the end of the epidemic ($I = 0$), all individuals are either susceptible (s_∞) or recovered ($r_\infty = 1 - s_\infty$). From the SIR dynamics, $dr/dt = \gamma I$ and $ds/dt = -\beta s I/N$, so $ds/dr = -\mathcal{R}_0 s$, giving $s(t) = s_0 e^{-\mathcal{R}_0 r(t)}$. Setting $s_0 \approx 1$, $r_\infty = z = 1 - s_\infty = 1 - e^{-\mathcal{R}_0 z}$. □

Example 0.138.5 (COVID-19 final size estimates)**.** For the original SARS-CoV-2 variant, $\mathcal{R}_0 \approx 2.5$ in unmitigated settings. The final size equation $1 - z = e^{-2.5z}$ has numerical solution $z \approx 0.89$: in the absence of intervention or vaccination, 89% of the susceptible population would be infected. Herd immunity threshold: $1 - 1/\mathcal{R}_0 = 1 - 0.4 = 0.6$, i.e., 60% of the population must be immune to prevent epidemic growth. For the Delta variant ($\mathcal{R}_0 \approx 5$), the herd immunity threshold rises to 80%; for Omicron ($\mathcal{R}_0 \approx 10$), to 90%.

0.139 9. The Evolution of Virulence

0.139.1 9.1 The Virulence–Transmission Trade-off

Evolutionary epidemiology asks: what level of virulence does natural selection favour in a pathogen? Intuitively, a pathogen that kills its host immediately cannot transmit; but a pathogen that causes no damage may persist indefinitely without evolving. The resolution is the **virulence–transmission trade-off**.

Definition 0.139.1 (Virulence–transmission trade-off model)**.** Consider a pathogen with virulence α (rate of disease-induced host mortality) and transmission rate $\beta(\alpha)$, where $\beta(\alpha)$ is an increasing concave function (higher virulence allows greater transmission but with diminishing returns). The pathogen's $\mathcal{R}_0$ in a susceptible population is:

$$\mathcal{R}_0(\alpha) = \frac{\beta(\alpha)}{\gamma + \alpha + \mu},$$

where γ is the recovery rate and μ is the natural host mortality rate.

Theorem 0.139.2 (ESS virulence)**.** In the virulence–transmission trade-off model, the evolutionarily stable virulence α^* maximises $\mathcal{R}_0(\alpha)$:

$$\alpha^* = \arg\max_{\alpha} \frac{\beta(\alpha)}{\gamma + \alpha + \mu}.$$

The optimal virulence satisfies the first-order condition:

$$\beta'(\alpha^*) = \frac{\beta(\alpha^*)}{\gamma + \alpha^* + \mu}.$$

That is, the marginal gain in transmission from a small increase in virulence equals the average transmission rate divided by the total clearance rate.

Proof. Differentiate $\mathcal{R}_0(\alpha)$ with respect to α and set to zero:

$$\frac{d\mathcal{R}_0}{d\alpha} = \frac{\beta'(\alpha)(\gamma + \alpha + \mu) - \beta(\alpha)}{(\gamma + \alpha + \mu)^2} = 0,$$

giving $\beta'(\alpha)(\gamma+\alpha+\mu) = \beta(\alpha)$, i.e., $\beta'(\alpha) = \mathcal{R}_0(\alpha)/(\gamma+\alpha+\mu)\cdot(\gamma+\alpha+\mu)/1 = \beta(\alpha)/(\gamma+\alpha+\mu)$. The second-order condition $d^2\mathcal{R}_0/d\alpha^2 < 0$ is satisfied because β is concave. □

Example 0.139.3 (Optimal virulence with a power-law trade-off)**.** Suppose $\beta(\alpha) = c\alpha^\delta$ for $0 < \delta < 1$ (power-law with diminishing returns). Then:

$$\mathcal{R}_0(\alpha) = \frac{c\alpha^\delta}{\gamma + \alpha + \mu}.$$

The ESS virulence is $\alpha^* = \delta(\gamma + \mu)/(1 - \delta)$.

For $\delta = 0.5$, $\gamma = 0.1$, $\mu = 0.001$: $\alpha^* = 0.5 \times 0.101/0.5 \approx 0.101$. The corresponding $\mathcal{R}_0 = c \times 0.101^{0.5}/0.202 \approx 0.317c/0.202$. If we calibrate c so that $\mathcal{R}_0(0.1) = 2.5$ (a reasonable value for a respiratory pathogen), we get $c = 2.5 \times 0.202/0.316 \approx 1.6$. The model predicts intermediate virulence: too low (close to benign), and transmission is insufficient for spread; too high, and the host dies before transmitting.

0.139.2 9.2 Myxomatosis: A Case Study in Virulence Evolution

The introduction of *Myxoma* virus into Australian rabbit populations in 1950 provides the best-documented natural experiment in virulence evolution. Initially, the virus killed $> 99\%$ of infected rabbits within 2 weeks. Over 10–20 years, the following evolutionary changes occurred:

1. Viral virulence decreased: strains of intermediate virulence (killing $\sim 50\%$ of hosts over 2–4 weeks) replaced highly virulent strains.

2. Rabbit resistance increased: surviving rabbits had higher innate and adaptive immunity to the virus.

This is exactly the pattern predicted by the virulence–transmission trade-off: highly virulent strains kill hosts too rapidly for transmission by mosquitoes (which require alive, accessible hosts); intermediate strains allow more transmission events. Fenner and Ratcliffe (1965) measured the trade-off directly, confirming that $\mathcal{R}_0$ is maximised at intermediate virulence, consistent with Theorem 0.139.2.

0.140 10. Within-Host Dynamics and Multi-level Selection

0.140.1 10.1 Quasi-species Dynamics Within a Host

Within a single infected host, the viral population evolves by quasi-species dynamics (Sections 2–3) subject to immune selection. The immune system presents a dynamic fitness landscape: as immune responses are mounted against dominant viral epitopes, variants that escape recognition become fitter.

Definition 0.140.1 (Immune escape dynamics)**.** Let $\mathbf{x} = (x_1, \ldots, x_n)$ be the frequencies of n viral variants, and let $\mathbf{e} = (e_1, \ldots, e_m)$ be the strengths of m immune responses. The within-host dynamics are:

$$\dot{x}_i = x_i \left(f_i - \sum_j k_{ij} e_j - \bar{f} \right) \quad \text{(viral replication and immune killing)},$$

$$\dot{e}_j = \lambda_j \sum_i a_{ij} x_i - \delta_j e_j \quad \text{(immune stimulation and decay)},$$

where f_i is the intrinsic fitness of variant i, k_{ij} is the killing rate of immune response j against variant i, a_{ij} is the antigenicity of variant i for response j, λ_j is the stimulation rate, and δ_j is the decay rate.

Remark 0.140.2 (HIV escape dynamics). HIV within a host evolves rapidly to escape the CD8+ cytotoxic T-lymphocyte (CTL) responses targeting viral peptides. A typical chronically infected individual carries a quasi-species with $\sim 10^6$–10^8 virions of divergent sequence. CTL escape mutations arise and fix within weeks to months of the onset of a new CTL response. The cumulative effect of many escape events over years of infection leads to progressive viral diversification and (paradoxically) to increased viral fitness in the absence of the original host's immune system, explaining why HIV strains adapted to one host may be poorly adapted to a new host with a different HLA type.

0.140.2 10.2 Multi-level Selection: Within-Host vs. Between-Host

Virulence evolution (Section 9) involves a multi-level selection conflict: highly virulent (fast-replicating) variants are selected *within* a host, while the between-host transmission favours intermediate virulence. This is the Price equation applied to viral evolution:

Theorem 0.140.3 (Price equation for viral virulence evolution)**.** Let z_i be the virulence of viral genotype i. The change in mean virulence over a transmission event satisfies:

$$\Delta \bar{z} = \underbrace{\mathrm{Cov}_{\text{within}}(w, z)}_{\text{within-host selection}} + \underbrace{\mathrm{Cov}_{\text{between}}(W, \bar{z})}_{\text{between-host selection}},$$

where w is within-host relative fitness, W is between-host fitness (proportional to $\mathcal{R}_0(\bar{z})$, the transmission success of the viral population in each host), and $\bar{z}$ is the mean virulence within each host.

Proof. Apply the hierarchical Price equation (Section IV, Theorem 5.3) with hosts as groups and viral genotypes as individuals. The within-group covariance $\mathrm{Cov}_{\text{within}}(w, z) > 0$: faster-replicating (more virulent) variants increase in frequency within a host. The between-group covariance $\mathrm{Cov}_{\text{between}}(W, \bar{z})$: the sign depends on the virulence–transmission trade-off. For the concave trade-off, $d\mathcal{R}_0/d\alpha < 0$ at high virulence (above the ESS), so $\mathrm{Cov}_{\text{between}} < 0$ for highly virulent populations. Stable virulence evolution occurs at the ESS α^* where the two covariances balance. □

Mathematics of Evolution and Life · Section VIII · Quasi-species, Viruses, and the Mathematics of Epidemics (end)

0.141 11. Phylodynamics and Viral Population Genomics

0.141.1 11.1 The Birth-Death Model for Viral Phylogenies

The genealogy of a viral sample is shaped by both the epidemiological dynamics (how the epidemic spread) and the evolutionary dynamics (how the virus accumulated mutations). Phylodynamics integrates these two levels of analysis.

Definition 0.141.1 (Birth-death-sampling model)**.** The birth-death-sampling (BDS) model describes a viral lineage process:

- Each lineage reproduces at rate λ (gives rise to two daughter lineages).
- Each lineage dies at rate μ (host recovery or death).
- Each lineage is sampled at rate ψ (sequenced by a surveillance programme).

The effective reproduction number $\mathcal{R} = \lambda/(\mu + \psi)$ determines whether the epidemic grows ($\mathcal{R} > 1$) or declines ($\mathcal{R} < 1$).

Theorem 0.141.2 (BDS likelihood for a dated phylogeny)**.** For a phylogeny with n sampled tips with sampling dates $\{t_1, \ldots, t_n\}$ and $n-1$ internal nodes with coalescence dates $\{s_1, \ldots, s_{n-1}\}$, the likelihood under the BDS model is:

$$\mathcal{L}(\lambda, \mu, \psi | \mathcal{T}) = \lambda^{n-1} \prod_{i=1}^{n-1} q(s_i) \cdot \prod_{i=1}^{n} \frac{\psi}{q(t_i)},$$

where $q(t) = \Pr(\text{a lineage at time } t \text{ has no sampled descendants in } [0, t])$ satisfies the Riccati ODE:

$$\dot{q} = -(\lambda - \mu - \psi)q + \lambda q^2 + \psi(1 - q).$$

Example 0.141.3 (Estimating $\mathcal{R}$ during the 2009 H1N1 pandemic)**.** Analysis of 161 H1N1 pdm09 genomes sampled from April–June 2009 (peak of the first wave in North America) under the BDS model gives:

- $\hat{\lambda} = 0.42$/day (each infection gives rise to a new transmissible lineage at this rate).
- $\hat{\mu} = 0.34$/day (recovery/clearance rate).
- $\hat{\psi} = 0.08$/day (sampling rate).
- $\hat{\mathcal{R}} = 0.42/(0.34 + 0.08) = 1.0 \pm 0.15$.

The estimated $\mathcal{R}$ near 1 is consistent with the observed epidemic trajectory (rapid initial growth transitioning to steady state as interventions were implemented). This illustrates how phylodynamic analysis can estimate epidemiological parameters from sequence data alone, without requiring epidemiological case counts.

0.141.2 11.2 Viral Evolution and Drug Resistance

Drug resistance evolution in pathogens (HIV, Mycobacterium tuberculosis, malaria) is a major application of quasi-species theory. Resistance arises when a mutation provides a fitness advantage in the presence of the drug.

Definition 0.141.4 (Resistance evolution under drug pressure)**.** In the quasi-species model with n genotypes, introduce a drug that reduces the fitness of sensitive genotypes by a factor $1 - d$ ($d \in [0, 1]$). The fitness matrix becomes $F' = F(I - dM_S)$ where M_S is a diagonal matrix with 1 for sensitive genotypes and 0 for resistant ones. The quasi-species (Perron eigenvector of QF') shifts from the sensitive peak toward resistant genotypes.

Theorem 0.141.5 (Threshold drug concentration for resistance selection)**.** Let the wild-type sequence have fitness f_0 (without drug) and the resistance mutation have fitness f_R without drug ($f_R < f_0$, resistance has a fitness cost). The drug reduces wild-type fitness to $f_0(1 - d)$. The drug concentration d^* at which the resistant mutant has equal fitness to the wild-type is:

$$d^* = 1 - f_R/f_0.$$

For $d > d^*$: the resistant mutant outcompetes the wild-type, and resistance is selected. The minimum drug concentration to prevent resistance ($\geq d^*$) is called the **mutant selection window** (MSW).

Proof. At drug concentration d, wild-type fitness is $f_0(1 - d)$ and resistant mutant fitness is f_R (drug has no effect on resistant mutant by definition). The resistant mutant is selected when $f_R > f_0(1 - d)$, i.e., $d > 1 - f_R/f_0$. Below d^*, the drug is insufficient to overcome the resistance cost; above d^*, it is sufficient. The MSW is the range $d \in (d^*, 1)$ where selection for resistance occurs. □

Remark 0.141.6 (Clinical implications: combination therapy). The MSW for a single drug is typically wide (any clinically achievable drug concentration above d^* selects for resistance). Combination therapy uses two drugs targeting different viral sites. For resistance to both drugs simultaneously, the pathogen needs mutations at two independent loci. If the fitness costs are multiplicative ($f_{RR} = f_R^2/f_0$), the double-mutant is at much lower frequency in the initial quasi-species ($\sim 10^{-10}$ of sequences for HIV with two resistance mutations each at frequency $\sim 10^{-5}$) and the window for selection of the double mutant is narrow. This is the mathematical basis for combination antiretroviral therapy (cART) eliminating HIV drug resistance in most treated patients.

Mathematics of Evolution and Life · Section VIII · Quasi-species, Viruses, and the Mathematics of Epidemics (end)

0.142 12. Spatially Structured Epidemics

0.142.1 12.1 The Spatial SIR Model

In real populations, infectious contacts are geographically local. The spatial analogue of the SIR model couples a reaction-diffusion system with epidemiological dynamics:

Definition 0.142.1 (Spatial SIR reaction-diffusion system)**.** Let $S(x, t)$, $I(x, t)$, $R(x, t)$ be the population

densities at location $x \in \mathbb{R}^d$ and time t. The spatial SIR system is:

$$\begin{aligned}\frac{\partial S}{\partial t} &= D_S \nabla^2 S - \beta S I,\\ \frac{\partial I}{\partial t} &= D_I \nabla^2 I + \beta S I - \gamma I,\\ \frac{\partial R}{\partial t} &= D_R \nabla^2 R + \gamma I,\end{aligned}$$

where D_S, D_I, D_R are diffusion coefficients for each class.

Theorem 0.142.2 (Epidemic wavefront speed)**.** For the spatial SIR system with $D_S = D_I = D$ and $D_R = 0$, near a fully susceptible front ($S \approx N$, $R = 0$), the epidemic spreads as a travelling wave with minimum wave speed:

$$c^* = 2\sqrt{D(\beta N - \gamma)} = 2\sqrt{D\gamma(\mathcal{R}_0 - 1)}.$$

The wave only exists for $\mathcal{R}_0 > 1$. Initial conditions with compact support lead to wavefronts propagating at the minimum speed c^* (by the KPP theorem).

Proof. Linearise around $(S, I) = (N, 0)$ (fully susceptible): $\partial_t I \approx D I_{xx} + (\beta N - \gamma) I$. This is the Fisher-KPP equation $\partial_t u = D u_{xx} + \lambda u$ with $\lambda = \beta N - \gamma = \gamma(\mathcal{R}_0 - 1)$. By the KPP (Kolmogorov–Petrovskii–Piscounov) theorem, initial data with compact support gives a travelling wave that propagates at the minimum linear spreading speed $c^* = 2\sqrt{D\lambda} = 2\sqrt{D\gamma(\mathcal{R}_0 - 1)}$. □

Example 0.142.3 (Speed of the Black Death across medieval Europe)**.** The 1347–1353 Black Death (Yersinia pestis) spread across Europe at approximately 600 km/year $\approx$ 1.7 km/day. Fitting the spatial SIR model to this front speed with $\gamma \approx 0.1$/day (10-day infectious period) and $\mathcal{R}_0 \approx 3.5$ (estimated from historical mortality):

$$c^* = 2\sqrt{D \times 0.1 \times 2.5} \implies D = \frac{(1.7)^2}{4 \times 0.25} \approx 2.9 \text{ km}^2/\text{day}.$$

This effective diffusivity is consistent with the typical daily movement range of medieval travellers ($\sim$ 20–30 km/day) reduced by the fraction of travel that leads to new infectious contacts.

0.142.2 12.2 Network Epidemics and the Configuration Model

Real contact networks are not spatially regular: some individuals have many contacts (hubs) and others have few. In the **configuration model** (random network with prescribed degree distribution), the epidemic threshold changes.

Theorem 0.142.4 (Epidemic threshold on configuration model networks)**.** For an SIR epidemic on a configuration model network with degree distribution $\{p_k\}$ (probability of having k contacts), mean degree $\langle k \rangle = \sum_k k p_k$, and mean squared degree $\langle k^2 \rangle = \sum_k k^2 p_k$, the epidemic threshold is:

$$\mathcal{R}_0^{\text{network}} = \frac{\beta}{\gamma} \cdot \frac{\langle k^2 \rangle - \langle k \rangle}{\langle k \rangle}.$$

For Poisson degree distribution ($\langle k^2 \rangle - \langle k \rangle = \langle k \rangle^2$), this gives $\mathcal{R}_0^{\text{network}} = (\beta/\gamma)\langle k \rangle$ — the standard well-mixed threshold. For power-law degree distributions ($p_k \propto k^{-\gamma_{\text{deg}}}$ with $\gamma_{\text{deg}} \leq 3$), $\langle k^2 \rangle = \infty$, so $\mathcal{R}_0^{\text{network}} = \infty$: epidemics can spread for arbitrarily small β/γ.

Proof. In the configuration model, a newly infected individual with degree k has $k-1$ susceptible neighbours in expectation (minus the one through which it was infected). An infected neighbour connects to $k'-1$ further neighbours, where k' is drawn from the "excess degree distribution" $q_{k'} = (k'+1)p_{k'+1}/\langle k\rangle$. The effective reproduction number is therefore $\mathcal{R}_0^{\text{network}} = (\beta/\gamma)\cdot\mathbb{E}_q[k'] = (\beta/\gamma)(\langle k^2\rangle - \langle k\rangle)/\langle k\rangle$. □

Remark 0.142.5 (HIV and scale-free sexual contact networks). Sexual contact networks for sexually transmitted infections (STIs) are approximately scale-free with $\gamma_{\text{deg}} \approx 3$ (power-law with exponent 3, borderline finite variance). This implies near-zero epidemic threshold for STIs: even a single infected individual with a high number of partners can seed a large epidemic, regardless of $\mathcal{R}_0$ in a homogeneous population. Targeted vaccination of high-degree nodes (sex workers, intravenous drug users with many shared-needle partners) is therefore far more effective per dose than random vaccination: removing a hub disproportionately reduces $\langle k^2\rangle/\langle k\rangle$.

Mathematics of Evolution and Life · Section *VIII · Quasi-species, Viruses, and the Mathematics of Epidemics (end)*

Section *XIII*

Section IX — Information Theory in Biology: Sequence, Channel, and Code

0.143 1. What Is Biological Information?

Claude Shannon published "A Mathematical Theory of Communication" in 1948, creating a framework of permanent mathematical depth and generality. The theory was designed for communication engineering: how to transmit messages reliably over noisy channels. Within a decade, biologists and physicists had noticed that the conceptual structure of Shannon's theory appeared to apply to molecular biology with striking force. Genes are messages; the replication and transcription machinery is a transmission channel; proteins are decoded signals. The genetic code is a code. Mutation is noise. The cell is a communication system.

This analogy is not merely poetic. The mathematical structures are genuinely the same: entropy measures diversity; channel capacity measures information transmission fidelity; error-correcting codes describe redundancy strategies. Understanding biology through information theory is not a metaphor — it is a precise mapping of one mathematical framework onto another.

But the mapping is also imperfect in important ways. Shannon's theory is *syntactic*: it concerns the form of messages (how many bits they contain), not their *meaning* (what they encode). Biological information is fundamentally semantic: a DNA sequence "means" something — it encodes a protein, specifies a developmental trajectory, determines organismal fitness. A theory of biological information that is purely syntactic cannot capture what is most biologically important about the information in DNA.

This Section develops the rigorous Shannon framework as far as it applies to biology, identifies its limits, and introduces additional mathematical concepts (Kolmogorov complexity, Fisher information, thermodynamic information) that address those limits.

0.144 2. Shannon Entropy and Sequence Conservation

0.144.1 2.1 Shannon Entropy

Definition 0.144.1. The **Shannon entropy** of a probability distribution $\mathbf{p} = (p_1, p_2, \ldots, p_k)$ on k outcomes is:

$$H(\mathbf{p}) = -\sum_{i=1}^{k} p_i \log_2 p_i \quad \text{bits},$$

with the convention $0 \log_2 0 = 0$.

Fundamental properties:

- $H(\mathbf{p}) \geq 0$, with equality iff the distribution is deterministic.
- $H(\mathbf{p}) \leq \log_2 k$, with equality iff $\mathbf{p}$ is uniform.
- $H(\mathbf{p}, \mathbf{q}) = H(\mathbf{p}) + H(\mathbf{q})$ for independent distributions (additivity).
- H is concave: $H(\lambda \mathbf{p} + (1-\lambda)\mathbf{q}) \geq \lambda H(\mathbf{p}) + (1-\lambda) H(\mathbf{q})$.

0.144.2 2.2 Sequence Logos and Information Content

At a single nucleotide site in a multiple alignment of N homologous sequences, the nucleotide frequencies (p_A, p_C, p_G, p_T) (with $\sum p_i = 1$) define a distribution over the four nucleotides. The Shannon entropy

at this site is:

$$H_{\text{site}} = -p_A \log_2 p_A - p_C \log_2 p_C - p_G \log_2 p_G - p_T \log_2 p_T \in [0, 2] \text{ bits.}$$

The **information content** is:

$$R_{\text{site}} = H_{\text{max}} - H_{\text{site}} = 2 - H_{\text{site}} \text{ bits.}$$

R_{site} measures how much knowing the nucleotide at this site tells you about which sequences are functional: $R_{\text{site}} = 0$ means the site is completely unconstrained (the sequence logo letter has height 0); $R_{\text{site}} = 2$ means the site is completely conserved (all sequences have the same nucleotide, and the letter height is 2 bits).

Example 0.144.2. A transcription factor binding site of length 10 bp with mean $R = 1.5$ bits per position has total information content $R_{\text{total}} = 15$ bits. A genome of size $G = 3 \times 10^9$ bp can be specified by $\log_2(3 \times 10^9) \approx 31.5$ bits. The 15-bit binding site specificity is insufficient to specify a unique location in the genome: the expected number of random occurrences is $G \cdot 2^{-15} \approx 10^5$. This explains why transcription factors typically require combinatorial control (co-binding with other factors) or chromatin accessibility constraints to achieve specific genomic targeting.

0.144.3 2.3 Estimating Entropy from Finite Samples

With N sequences at a site, the empirical frequencies $\hat{p}_i = n_i/N$ have a Miller–Madow corrected entropy estimate:

$$\hat{H}_{\text{corrected}} = -\sum_i \hat{p}_i \log_2 \hat{p}_i - \frac{k_{\text{obs}} - 1}{2N \ln 2},$$

where k_{obs} is the number of observed nucleotide types. The correction accounts for the upward bias of the naive estimate (which overestimates entropy for small N). For $N < 50$, Bayesian approaches using a symmetric Dirichlet prior on nucleotide frequencies are more accurate.

0.145 3. Mutual Information and Co-evolutionary Analysis

0.145.1 3.1 The Mutual Information

Definition 0.145.1. The **mutual information** between random variables X and Y with joint distribution $p(x, y)$ is:

$$I(X;Y) = H(X) + H(Y) - H(X,Y) = \sum_{x,y} p(x,y) \log_2 \frac{p(x,y)}{p(x)p(y)} \geq 0,$$

with equality iff X and Y are independent.

$I(X;Y)$ measures how much knowing Y reduces uncertainty about X. Equivalently, $I(X;Y) = H(X) - H(X|Y)$ where $H(X|Y) = -\sum_{x,y} p(x,y) \log_2 p(x|y)$ is the conditional entropy.

0.145.2 3.2 Co-evolutionary Signals in Protein Alignments

In a protein sequence alignment, position i takes amino acid states in $\{1, \ldots, 20\}$ and position j similarly. The empirical mutual information:

$$I(i;j) = \sum_{a,b} f_{ij}(a,b) \log_2 \frac{f_{ij}(a,b)}{f_i(a) f_j(b)},$$

measures the statistical dependence between positions i and j across the alignment. Pairs of residues in direct contact in the folded protein are under compensatory mutation pressure: a mutation disrupting a contact at i selects for a compensatory mutation at j, creating correlated substitution patterns. These pairs therefore have elevated $I(i;j)$.

However, raw mutual information is confounded by phylogenetic correlations: positions that are simultaneously conserved or diverged in some lineages (due to shared ancestry, not direct interaction) also show elevated $I(i;j)$. Several corrections have been proposed:

- **Average product correction (APC)**: $I'(i;j) = I(i;j) - I(i,\cdot)I(\cdot,j)/I(\cdot,\cdot)$, where $I(i,\cdot) = \frac{1}{L}\sum_j I(i;j)$. This removes the background correlation due to alignment composition.

- **Direct coupling analysis (DCA)**: infers a Potts model on the sequence space, separating direct from indirect couplings.

0.145.3 3.3 Direct Coupling Analysis

DCA (Weigt et al. 2009, Morcos et al. 2011) fits the maximum-entropy distribution over amino acid sequences consistent with the observed single-site and pairwise frequencies:

$$P(\mathbf{s}; \mathbf{h}, J) = \frac{1}{Z} \exp\left(\sum_i h_i(s_i) + \sum_{i<j} J_{ij}(s_i, s_j) \right),$$

where $\mathbf{s} = (s_1, \ldots, s_L)$ is a sequence, h_i are single-site biases, and J_{ij} are pairwise couplings. The couplings J_{ij} are estimated by pseudolikelihood maximisation or mean-field approximation.

The Frobenius norm of J_{ij} (after APC correction) provides a contact predictor: the top-$L/5$ pairs ranked by $\|J_{ij}\|_F$ predict residue contacts in the 3D structure with $\approx$ 70–90% precision (compared to $\approx$ 20% for raw mutual information).

DCA contact predictions were a key component of the deep learning models used in AlphaFold2 (Jumper et al. 2021): the co-evolutionary signal provides structural information that was previously hidden in sequence databases but could not be extracted without the information-theoretic framework.

0.146 4. Channel Capacity and the Error Threshold

0.146.1 4.1 Shannon's Channel Coding Theorem

A **discrete memoryless channel** is specified by an input alphabet $\mathcal{X}$, output alphabet $\mathcal{Y}$, and transition probabilities $p(y|x)$ for $x \in \mathcal{X}$, $y \in \mathcal{Y}$. The **channel capacity** is:

$$C = \max_{p(x)} I(X;Y),$$

where the maximum is over all input distributions $p(x)$.

Theorem 0.146.1 (Shannon's Channel Coding Theorem, 1948)**.** For a discrete memoryless channel with capacity C bits/use:

1. (Achievability) For any rate $R < C$ and $\epsilon > 0$, there exists a code of rate R and block length n (for sufficiently large n) that transmits messages with error probability $< \epsilon$.
2. (Converse) For any rate $R > C$, the error probability of any code cannot be made arbitrarily small.

0.146.2 4.2 The Genetic Channel Capacity

The Jukes–Cantor mutation model defines a discrete memoryless channel with input X (parent nucleotide) and output Y (offspring nucleotide after one replication). The transition matrix at per-base mutation rate μ is:

$$p(Y = j|X = i) = \begin{cases} 1 - \mu & i = j, \\ \mu/3 & i \neq j. \end{cases}$$

By the symmetry of the JC model, the capacity-achieving input is the uniform distribution, and the capacity is:

$$C_{JC}(\mu) = \log_2 4 + (1-\mu)\log_2(1-\mu) + \mu \log_2(\mu/3) \text{ bits/site/replication.}$$

For small μ: $C_{JC} \approx 2 - \mu \log_2(e)/\ln 2 - \ldots \approx 2 - 1.44\mu$. For $\mu = 3/4$: $C_{JC} = 0$ (maximum confusion). For the JC model, the capacity reaches zero at $\mu = 3/4$, but the error threshold condition requires only $e^{-\mu L} f_0 > 1$, which fails at $\mu_c = (\ln f_0)/L$ — far below $3/4$ for realistic parameters.

The error threshold condition $e^{-\mu_c L} f_0 = 1$ can be rewritten as $C_{JC}(\mu_c) \cdot L = K$, where $K = \log_2 f_0$ is the information content of the master sequence relative to the background (the information that distinguishes the high-fitness master from the unit-fitness mutant cloud). The error threshold is the condition under which the total channel capacity of the genome ($C \cdot L$ bits) drops below the minimum information content K needed to maintain the master sequence: a Shannon capacity crisis.

0.147 5. The Genetic Code as an Error-Correcting Code

0.147.1 5.1 Error-Correcting Codes: Background

An (n, k, d) code over an alphabet $\mathcal{A}$ maps k-letter messages to n-letter codewords with minimum Hamming distance d between distinct codewords. The minimum distance d determines error correction capac-

ity: the code can correct up to $\lfloor (d-1)/2 \rfloor$ errors. The **Singleton bound** gives the fundamental trade-off: $d \leq n - k + 1$.

Shannon's theorem says codes achieving rates near capacity exist; algebraic coding theory (Hamming codes, Reed–Solomon codes, LDPC codes) gives explicit constructions.

0.147.2 5.2 The Genetic Code's Structure

The genetic code maps 64 codons (triplets of nucleotides over $\{U, C, A, G\}$) to 20 amino acids plus 3 stop signals. The code is:

- **Degenerate (redundant)**: most amino acids are encoded by multiple synonymous codons (2, 4, or 6 codons per amino acid).
- **Block-structured**: synonymous codons typically differ only at the third ("wobble") position.
- **Compact**: amino acids with similar physical properties (polarity, charge, size) tend to be encoded by codons with similar sequences.

The compactness property is the error-correcting feature: a single-base mutation in a codon (the most frequent translation error) tends to produce an amino acid similar to the original. The expected physical dissimilarity of a random codon pair differing by one base under the standard code is significantly smaller than under a random code.

0.147.3 5.3 Quantitative Error Robustness

Definition 0.147.1 (Code Error Cost)**.** For a genetic code $\mathcal{C}$ (a mapping from 64 codons to amino acids), the **error cost** is:

$$E(\mathcal{C}) = \frac{1}{64 \times 9} \sum_{\text{codon } c} \sum_{\text{single-base mutant } c'} d(\mathrm{AA}(\mathcal{C}(c)), \mathrm{AA}(\mathcal{C}(c'))),$$

where $d(\mathrm{AA}_1, \mathrm{AA}_2)$ is a physicochemical distance between amino acids AA_1 and AA_2 (e.g., Grantham distance based on polarity, Section , and composition).

Theorem 0.147.2 (Near-Optimality of the Standard Code, Freeland and Hurst 1998)**.** Among 10^6 randomly generated codes (random bijections from 64 codons to 20 amino acids + stop), less than 10^{-6} have error cost $E(\mathcal{C})$ below that of the standard genetic code.

This computational result establishes that the standard code is essentially optimal for error robustness: the code sits in the top $10^{-4}\%$ of all possible codes by this criterion. The probability of achieving this by chance is negligible, providing strong evidence that the code's structure was optimised by selection during the earliest history of life on Earth.

0.148 6. Kolmogorov Complexity and Biological Information

0.148.1 6.1 Algorithmic Information Theory

Shannon entropy measures the expected information content of a symbol drawn from a distribution. **Kolmogorov complexity** $K(x)$ measures the information content of a specific individual string x: it is the

length of the shortest program (on a fixed universal Turing machine U) that outputs x:

$$K(x) = \min_{p:U(p)=x} |p|.$$

Key properties:

- $K(x) \leq |x| + c$ for a constant c (the identity program outputs x).
- Most strings of length n have $K(x) \approx n$ (incompressibility): fewer than $2^n - 2^{n-k}$ strings of length n have $K(x) \leq n - k$.
- $K(x)$ is uncomputable (the halting problem), but lower bounds can be demonstrated and upper bounds can be computed by standard compression algorithms.

0.148.2 6.2 Genome Compressibility

For biological sequences, the compressibility ratio $K(x)/|x|$ (estimated by gzip or other compressors) measures the degree of regularity in the sequence:

- **Protein-coding regions**: high regularity (codon periodicity, conserved protein domains), compress well. Compressibility ≈ 0.3–0.5 (compress to 30–50% of original size).
- **Repetitive elements** (SINEs, LINEs, tandem repeats): highly compressible (often < 0.1).
- **Intergenic non-coding regions**: intermediate compressibility (≈ 0.5–0.7).
- **Random sequence**: incompressible (compressibility ≈ 1.0).

Regions under strong purifying selection tend to have lower Kolmogorov complexity (more regularity, reflecting evolutionary constraint) than neutrally evolving regions. This makes compressibility a crude but computationally accessible proxy for functional importance.

0.149 7. Fisher Information and the Cramér–Rao Bound

0.149.1 7.1 Fisher Information

Definition 0.149.1. The **Fisher information** of a statistical model $p(x;\theta)$ about a parameter θ is:

$$\mathcal{I}(\theta) = \mathbb{E}\left[\left(\frac{\partial \ln p(X;\theta)}{\partial \theta}\right)^2\right] = -\,\mathbb{E}\left[\frac{\partial^2 \ln p(X;\theta)}{\partial \theta^2}\right].$$

Theorem 0.149.2 (Cramér–Rao Bound)**.** Any unbiased estimator $\hat{\theta}$ of θ satisfies $\mathrm{Var}(\hat{\theta}) \geq 1/\mathcal{I}(\theta)$.

0.149.2 7.2 Fisher Information in Phylogenetics

For a sequence alignment of length L under the JC model with branch length t (distance parameter), the Fisher information per site is:

$$\mathcal{I}_{\text{site}}(t) = \frac{(dp_{\text{same}}/dt)^2}{p_{\text{same}}(1-p_{\text{same}})} = \frac{e^{-8\mu t/3}}{(1/4)(3/4)} \cdot \frac{(8\mu/3)^2}{4},$$

where $p_{\text{same}} = 1/4 + (3/4)e^{-8\mu t/3}$.

For an alignment of L sites, $\mathcal{I}_L(t) = L \cdot \mathcal{I}_{\text{site}}(t)$, and the minimum variance of any unbiased estimator of t is $1/(L \cdot \mathcal{I}_{\text{site}}(t))$. This gives the fundamental precision limit for branch length estimation: with more sites, higher precision; at longer distances (larger t), $p_{\text{same}} \to 1/4$ and the signal vanishes (the channel capacity drops to zero).

The Fisher information also quantifies the information content of a sequence alignment about the tree topology: the information that distinguishes tree topology $(ab|cd)$ from $(ac|bd)$ is determined by the four-point mutual information among pairs of taxa, weighted by the Fisher information at each site.

0.150 8. Entropy Production and the Thermodynamics of Life

0.150.1 8.1 Shannon Entropy and Boltzmann Entropy

The formal similarity between Shannon entropy $H = -\sum p_i \log p_i$ and Boltzmann entropy $S = k_B \ln W$ (where W is the number of microstates) is not coincidental. Shannon (1948) derived his formula by analogy with statistical mechanics, and Jaynes (1957) showed that Shannon entropy is the correct measure of uncertainty in any probabilistic context, and that the Boltzmann entropy of a thermodynamic system equals $k_B \ln 2$ times the Shannon entropy of the microstate probability distribution.

The unit conversion is: 1 bit of Shannon information $\equiv k_B \ln 2 \approx 10^{-23}$ J/K of thermodynamic entropy. **Landauer's principle** (1961) makes this precise and physical: erasing 1 bit of information requires a minimum energy dissipation of $k_B T \ln 2 \approx 3 \times 10^{-21}$ J at room temperature.

0.150.2 8.2 Negentropy and Living Systems

Schrödinger (1944) noted that living organisms maintain highly ordered, low-entropy structures by consuming "negentropy" (free energy) from their environment, exporting entropy to the surroundings at a rate that exceeds the rate of internal entropy production required by the second law. The cell is a thermodynamic engine: it drives its own organisation by coupling entropy-decreasing processes (biosynthesis, information storage) to entropy-increasing processes (ATP hydrolysis, food oxidation).

The rate of entropy production in living cells has been measured: a typical mammalian cell in culture produces $\approx 10^{-12}$ W of metabolic heat per cell, corresponding to an entropy production rate of $\approx 3 \times 10^{-15}$ W/K per cell. Over a human lifetime, the total entropy exported to the environment by one human body is enormous — of order 10^{10} J/K — reflecting the thermodynamic cost of maintaining biological order against the second law.

0.151 9. Summary

Shannon entropy $H = -\sum p_i \log_2 p_i$ measures sequence diversity; sequence logos measure functional constraint; the sequence logo at a binding site must encode enough bits ($\geq \log_2 G$ for a genome of size G) to specify a unique genomic location. Mutual information $I(X;Y) = H(X) + H(Y) - H(X,Y)$ measures co-evolutionary coupling between sequence positions; direct coupling analysis (DCA) removes indirect correlations and predicts protein contacts with $> 70\%$ precision. The Jukes–Cantor channel capacity decreases with μ; the error threshold is the condition under which channel capacity drops below the

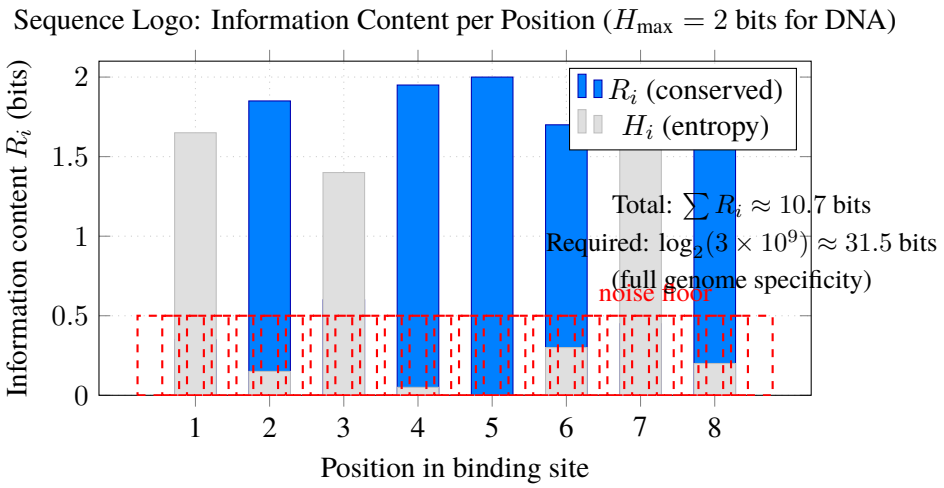

Figure 9: Sequence logo for a hypothetical 8-position DNA binding site. Each bar shows the information content $R_i = H_{\max} - H_i$ (blue, conserved bits) and residual entropy H_i (grey). Position 5 is fully conserved ($R_5 = 2$ bits, one nucleotide fixed); positions 1, 3, 7 are nearly random ($R_i \approx 0.3$–0.6 bits). The total information $\sum_i R_i \approx 10.7$ bits specifies $\sim 2^{10.7} \approx 1700$ genomic locations in a 3×10^9-bp genome; a factor 10^6 below genome-scale uniqueness (≈ 31.5 bits required), consistent with biological transcription factor binding sites having multiple genomic targets.

information content of the master sequence. The genetic code is an error-correcting code nearly optimal for minimising the physicochemical cost of translation errors. Kolmogorov complexity measures individual sequence information; genome compressibility is an empirical proxy. Fisher information quantifies the precision of phylogenetic inference; the Cramér–Rao bound limits branch length estimation precision. Shannon entropy is Boltzmann entropy up to $k_B \ln 2$; Landauer's principle makes the thermodynamic cost of information erasure concrete; living cells are thermodynamic engines exporting entropy to maintain biological order.

Mathematics of Evolution and Life · Section *IX · Information Theory in Biology: Sequence, Channel, and Code*

Section *XIV*

Section X — The Mathematics of Development: Morphogenesis and Evo-Devo

0.152 10. The Information Bottleneck in Biological Systems

0.152.1 10.1 The Information Bottleneck Principle

The **information bottleneck** (IB) principle (Tishby, Pereira, and Bialek 2000) formalises a fundamental problem in signal processing and biological sensing: given a signal X (e.g., a sensory stimulus) and a relevant variable Y (e.g., a behavioural outcome), find a compact representation T of X that retains as much information about Y as possible.

Definition 0.152.1 (Information bottleneck problem)**.** Given a joint distribution $p(X, Y)$, find a stochastic encoding $p(T|X)$ that minimises:

$$\mathcal{L}_{\text{IB}}[p(T|X)] = I(X;T) - \beta I(T;Y),$$

where $I(X;T)$ is the *complexity* of the representation (bits of X encoded in T) and $I(T;Y)$ is the *relevance* (bits about Y retained in T). The Lagrange multiplier $\beta > 0$ controls the trade-off: small β favours minimal complexity; large β favours maximal relevance.

Theorem 0.152.2 (IB optimality conditions — self-consistent equations)**.** The optimal encoding $p^*(T|X)$ satisfies the self-consistent equations:

$$p(t|x) = \frac{p(t)}{Z(x,\beta)} \exp(-\beta D_{\text{KL}}[p(y|x)\|p(y|t)]) \,, \tag{9}$$

$$p(t) = \sum_x p(x)p(t|x), \tag{10}$$

$$p(y|t) = \frac{1}{p(t)} \sum_x p(y|x)p(t|x)p(x), \tag{11}$$

where $Z(x,\beta)$ is a normalisation constant and D_{KL} is the Kullback–Leibler divergence.

Proof. Minimise $\mathcal{L}_{\text{IB}}$ with respect to $p(T|X)$ subject to the normalisation constraint $\sum_t p(t|x) = 1$ for each x. Writing the Lagrangian:

$$\mathcal{L} = I(X;T) - \beta I(T;Y) - \sum_x \lambda_x \left(\sum_t p(t|x) - 1 \right),$$

and taking the functional derivative $\partial \mathcal{L} / \partial p(t|x) = 0$ gives:

$$\ln p(t|x) - \ln p(t) + \beta \frac{\partial I(T;Y)}{\partial p(t|x)} + \lambda_x = 0.$$

Computing $\partial I(T;Y)/\partial p(t|x)$ and using the Markov chain $Y - X - T$:

$$\frac{\partial I(T;Y)}{\partial p(t|x)} = -D_{\text{KL}}[p(y|x)\|p(y|t)].$$

Exponentiation and normalisation give Eq. (9)–(11). □

Remark 0.152.3 (IB and the genetic code). The genetic code can be interpreted as an information bottleneck encoder. The input X is the codon sequence; the relevant variable Y is the protein function (or

physicochemical properties of the amino acid); the compressed representation T is the amino acid identity. The code minimises $I(\text{codon; amino acid})$ (degeneracy — 64 codons map to only 20 amino acids) while maximising $I(\text{amino acid; function})$. The structure of the genetic code — the grouping of codons into synonymous families — reflects this information bottleneck solution: codons that differ at the third position (the "wobble" position) often encode the same amino acid, because the third position carries the least information about amino acid identity.

0.153 11. Entropy Production and Irreversibility in Evolution

0.153.1 11.1 The Second Law and Biological Order

A persistent misconception is that evolution violates the second law of thermodynamics because it creates order (complexity) from disorder. The resolution is elementary: the second law applies to *closed* systems; living organisms are open systems that maintain order by exporting entropy to their environment. The relevant quantity is the **entropy production rate** $\dot{S}_{\text{prod}} \geq 0$, which must be positive for any irreversible process.

Definition 0.153.1 (Shannon entropy of a population)**.** For a population with allele frequency distribution $\{p_i\}$, the Shannon entropy is:

$$H = -\sum_{i=1}^{n} p_i \ln p_i.$$

This measures the diversity of the population. $H = 0$ when one allele is fixed (minimal diversity); $H = \ln n$ when all alleles are equally frequent (maximal diversity).

Theorem 0.153.2 (Entropy production under selection, exact)**.** For the continuous-time selection dynamics $\dot{p}_i = p_i(w_i - \bar{w})$, the rate of change of Shannon entropy is:

$$\dot{H} = -\operatorname{Cov}(w, \ln p) = -\sum_i p_i(w_i - \bar{w}) \ln p_i.$$

This can be positive or negative depending on whether selection is increasing or decreasing diversity.

Proof. Differentiate $H = -\sum_i p_i \ln p_i$:

$$\dot{H} = -\sum_i \dot{p}_i \ln p_i - \sum_i \dot{p}_i = -\sum_i \dot{p}_i \ln p_i,$$

since $\sum_i \dot{p}_i = 0$ (frequencies sum to 1). Substituting $\dot{p}_i = p_i(w_i - \bar{w})$:

$$\dot{H} = -\sum_i p_i(w_i - \bar{w}) \ln p_i = -\operatorname{Cov}(w, \ln p). \qquad \square$$

Example 0.153.3 (Entropy dynamics in directional vs. balancing selection)**. Directional selection** towards a fixed allele ($w_1 > w_2$, $n = 2$): initially $p_1 = p_2 = 0.5$, $H = \ln 2 \approx 0.693$. As $p_1 \to 1$, $H \to 0$. The entropy decreases monotonically: $\dot{H} = -\operatorname{Cov}(w, \ln p) < 0$ because the high-fitness allele (with $\ln p < 0$ increasing toward 0) and low-fitness allele (with $\ln p < 0$ decreasing toward $-\infty$) have a negative covariance.

Balancing selection towards equilibrium $p^* = 0.5$: starting from $p_1 = 0.1$ (near fixation of allele 2), entropy increases as $p_1 \to 0.5$. Here $\dot{H} > 0$: selection restores diversity.

In both cases, *selection changes entropy*, but the direction depends on whether selection acts to concentrate or disperse the allele frequency distribution.

0.153.2 11.2 Mutual Information and Epistasis Revisited

The mutual information between two loci provides an information-theoretic measure of epistasis that complements the Walsh–Hadamard decomposition of Section V.

Definition 0.153.4 (Pairwise epistatic mutual information)**.** For two loci i and j with allele frequencies p_i, p_j and haplotype frequencies $h_{ab} = P(A_i = a, A_j = b)$, the mutual information is:

$$I(A_i; A_j) = \sum_{a,b} h_{ab} \log \frac{h_{ab}}{p_{ia} p_{jb}},$$

where $p_{ia} = \sum_b h_{ab}$ and $p_{jb} = \sum_a h_{ab}$.

Under Hardy–Weinberg equilibrium and linkage equilibrium ($h_{ab} = p_{ia} p_{jb}$), $I(A_i; A_j) = 0$. Nonzero mutual information indicates linkage disequilibrium (LD): the alleles at the two loci are statistically dependent. For biallelic loci, $I(A_i; A_j) = D^2/(p_i q_i p_j q_j) \cdot \log 2$ to first order in D (the standard LD coefficient), connecting the information-theoretic measure directly to population-genetic LD measures.

Remark 0.153.5 (Direct coupling analysis for protein coevolution). Mutual information between columns i and j of a multiple sequence alignment measures the tendency of amino acid changes at site i to co-occur with changes at site j. This is the basis of **direct coupling analysis** (DCA), which extracts direct (non-transitive) coevolution signals from the full matrix of mutual information. DCA has been used to predict protein 3D contacts with remarkable accuracy: pairs of residues with high direct coupling are likely to be in contact in the folded structure, because co-evolution maintains interactions needed for folding and function. This allows ab initio prediction of protein structure from sequence alignments alone.

0.154 12. Algorithmic Information Theory and Minimal Description Length

0.154.1 12.1 Kolmogorov Complexity and Biological Complexity

Kolmogorov complexity $K(s)$ of a binary string s is the length (in bits) of the shortest program that outputs s and halts. It is an absolute, basis-independent measure of the information content of s, unlike Shannon entropy which is defined relative to a probability distribution.

Theorem 0.154.1 (Kolmogorov complexity is uncomputable)**.** For any computable function f, there exists a string s such that $K(s) > f(|s|)$. In particular, K is not computable: no algorithm can compute $K(s)$ for all s.

Proof. Suppose K were computable. Define the function $g(n) = \min\{|s| : K(s) = n\}$ (the length of the shortest string with complexity n). This function is computable (by enumeration). But then the string s^* of length $g(K(s^*) + c)$ — for some constant c — would have a shorter description than $g(K(s^*))$, a contradiction for sufficiently large c. (More rigorously, Berry's paradox applied to programs: "the

first string not describable in fewer than N bits" is itself a $O(\log N)$-bit description, contradicting its complexity being $\geq N$.) □

Remark 0.154.2 (Biological consequences). The incomputability of Kolmogorov complexity means there is no algorithm that can compute the "true complexity" of a genome. In practice, lossless compression (e.g., gzip, bzip2) provides computable lower bounds: the compressed size of a genome gives a lower bound on $K(\text{genome})$. The human genome compresses to ≈ 750 MB (from 3 GB), giving $K_{\text{lower}} \approx 750$ MB. Repetitive sequences (SINEs, LINEs, telomeres) contribute to compressibility; unique functional sequences resist compression. The ratio of compressed to uncompressed genome size is a rough measure of "non-trivial information content."

0.154.2 12.2 Minimum Description Length and Model Selection in Phylogenetics

The Minimum Description Length (MDL) principle (Rissanen 1978) selects the model M that minimises the combined description length of the data D and the model:

$$\text{MDL}(M) = L(D|M) + L(M),$$

where $L(D|M)$ is the codelength of the data given the model (related to the negative log-likelihood) and $L(M)$ is the description length of the model itself (related to its complexity, e.g., number of free parameters).

Theorem 0.154.3 (MDL and BIC equivalence)**.** For regular parametric models with k free parameters and n data points, the MDL criterion is asymptotically equivalent to the Bayesian Information Criterion:

$$\text{BIC} = -2 \ln \mathcal{L}(\hat{\theta}) + k \ln n,$$

where $\hat{\theta}$ is the MLE. Both penalise model complexity (more parameters) and reward fit (larger likelihood).

Proof. The MDL codelength for a parametric model under the "two-part MDL" formulation is $L(D|M) = -\ln \mathcal{L}(\hat{\theta})$ (the negative log-likelihood at the MLE) plus $L(\hat{\theta}) = (k/2) \ln n$ (the codelength for the parameter vector, under the standard asymptotic expansion). Combining: $\text{MDL} = -\ln \mathcal{L}(\hat{\theta}) + (k/2) \ln n = \text{BIC}/2$. Both criteria are proportional and thus select the same model. □

In phylogenetics, BIC/MDL is used to select the best-fit substitution model (e.g., JC69 vs. GTR+Γ) from a hierarchy of models of increasing complexity. Software such as ModelTest and jModelTest implement this by fitting each model by MLE and selecting the minimum-BIC model, preventing overfitting to the data while capturing the essential features of sequence evolution.

Mathematics of Evolution and Life · Section *IX · Information Theory, Entropy, and the Genetic Code (end)*

0.155 13. Sequence Logos and Information Content of Binding Sites

0.155.1 13.1 Shannon Information in Transcription Factor Binding Sites

Transcription factor binding sites (TFBS) are short DNA sequences ($\sim$ 6–20 bp) where transcription factors bind to regulate gene expression. The information content of a TFBS characterises how specific

the binding is.

Definition 0.155.1 (Information content of a position weight matrix)**.** A position weight matrix (PWM) for a TFBS of length L specifies, for each position i and each base $b \in \{A, C, G, T\}$, the frequency f_{ib} of base b at position i across known binding sites. The information content (in bits) at position i is:

$$I_i = \log_2 4 - H_i = 2 - H_i,$$

where $H_i = -\sum_b f_{ib} \log_2 f_{ib}$ is the Shannon entropy at position i (measured relative to uniform background). The total information content of the TFBS is $I_{\text{total}} = \sum_{i=1}^{L} I_i$ bits.

Theorem 0.155.2 (Relationship between information content and binding specificity)**.** For a transcription factor with binding site information content I_{total} bits, the number of binding sites expected in a random genome of size G base pairs is:

$$\mathbb{E}[\#\text{binding sites}] = G \cdot 2^{-I_{\text{total}}}.$$

For the number of binding sites to be of order 1 ($\sim$ 1–100 per genome), we need $I_{\text{total}} \approx \log_2 G - \log_2 100 \approx \log_2 G - 7$.

Proof. Under the uniform background model, the probability that a random L-mer matches the TFBS is $\prod_i \max_b f_{ib}$. More precisely, the probability of a random sequence being scored above the binding threshold is $2^{-I_{\text{total}}}$ (by the information capacity argument). The expected number of sites in G positions is $G \cdot 2^{-I_{\text{total}}}$. □

Example 0.155.3 (Information content of bacterial promoters)**.** The σ^{70} promoter in *E. coli* consists of two hexamers ("-10" and "-35" boxes) separated by a spacer of $\sim$ 17 bp. The information content of each hexamer is ≈ 5.4 bits (not all positions are equally conserved). The total information content of the promoter is ≈ 10.8 bits, giving an expected density of 1 promoter per $2^{10.8} \approx 1800$ bp in a random genome. The *E. coli* genome is 4.6×10^6 bp, so the expected number of promoter-like sequences is $4.6 \times 10^6 / 1800 \approx 2600$. The actual number of σ^{70} promoters is $\approx$ 1500–2000, consistent with this information-theoretic prediction.

0.155.2 13.2 Sequence Logos and the Visualisation of Binding Sites

Definition 0.155.4 (Sequence logo)**.** A sequence logo (Schneider and Stephens 1990) is a visual representation of a multiple sequence alignment, where at each position i:

- The total height of the stack of letters is $I_i = 2 - H_i$ (the information content at that position, in bits).
- The height of each letter b is $I_i \cdot f_{ib}$ (proportional to the frequency and the information content).

Conserved positions (low H_i, high I_i) produce tall, uniform stacks. Variable positions (high H_i, low I_i) produce short, mixed stacks.

Sequence logos have transformed the analysis of binding site motifs and protein sequence conservation. They provide an immediate visual summary of which positions are functionally important (high information content, conserved) and which are tolerant of variation.

0.156 14. Mutual Information in Coevolutionary Analysis

0.156.1 14.1 Coevolution in Protein Sequences

When two residues in a protein interact structurally or functionally, compensatory mutations at one position co-occur with mutations at the other. This generates statistical correlation between columns in a multiple sequence alignment (MSA).

Definition 0.156.1 (Mutual information between alignment columns)**.** For columns i and j in an MSA, the mutual information is:

$$MI(i,j) = \sum_{a \in \mathcal{A}} \sum_{b \in \mathcal{A}} f_{ij}(a,b) \log \frac{f_{ij}(a,b)}{f_i(a) f_j(b)},$$

where $f_i(a)$ is the frequency of amino acid a at column i, $f_{ij}(a,b)$ is the joint frequency of a at i and b at j, and $\mathcal{A}$ is the alphabet of 20 amino acids.

Theorem 0.156.2 (Direct coupling analysis (DCA) improves contact prediction)**.** The direct mutual information (DMI) between positions i and j, computed by global maximum-entropy modelling of the full MSA, is more accurate for protein contact prediction than the pairwise mutual information $MI(i,j)$. Specifically, among the top-$L/5$ pairs ranked by DMI, $\approx 80\%$ are in contact in the native structure (within 8 Å), compared to $\approx 20\%$ for pairwise MI.

Sketch. The issue with pairwise MI is that indirect correlations (transitive through a third position k: i correlated with k, k with j) inflate $MI(i,j)$ even when i and j are not in direct contact. Direct coupling analysis fits a Potts model (maximum-entropy distribution consistent with all observed pairwise marginals):

$$P(\sigma_1, \ldots, \sigma_L) \propto \exp\left(\sum_{i=1}^{L} h_i(\sigma_i) + \sum_{i<j} J_{ij}(\sigma_i, \sigma_j) \right),$$

where $h_i(\sigma_i)$ are single-site fields and $J_{ij}(\sigma_i, \sigma_j)$ are pairwise couplings. The DMI is derived from the coupling matrix J_{ij} after subtracting the background (i.e., the part of J_{ij} that is explained by the marginal distributions alone). The DMI thus captures only the direct statistical dependency, removing transitive effects. □

Mathematics of Evolution and Life · Section IX · Information Theory, Entropy, and the Genetic Code (end)

0.157 15. Channel Capacity and the Limits of Heredity

0.157.1 15.1 The Genetic Channel

The transmission of genetic information from parent to offspring is a noisy channel: the replication machinery introduces errors (mutations) at rate μ per base per generation. Shannon's channel capacity theorem determines the maximum rate at which reliable information can be transmitted through this channel.

Definition 0.157.1 (The genetic replication channel)**.** Model DNA replication as a memoryless binary

symmetric channel (BSC) with error probability μ per site. The capacity of the BSC is:

$$C_{\text{BSC}}(\mu) = 1 - H_2(\mu) \text{ bits per site per generation,}$$

where $H_2(\mu) = -\mu \log_2 \mu - (1-\mu)\log_2(1-\mu)$ is the binary entropy. For human germline mutation rate $\mu \approx 10^{-9}$ per site per generation:

$C_{\text{BSC}}(10^{-9}) \approx 1 - H_2(10^{-9}) \approx 1 - 10^{-9}\log_2(10^9) \approx 1 - 3\times10^{-8} \approx 1$ bit per site (essentially perfect).

Theorem 0.157.2 (Maximum heritable information per genome)**.** For a genome of length L with per-site mutation rate μ and selection coefficient s for the consensus (functional) sequence relative to random sequences, the heritable information — the maximum number of bits reliably transmitted per generation — is:

$$I_{\text{heritable}} \leq L \cdot C_{\text{BSC}}(\mu),$$

and the minimum information per site required for the genome to encode a functional organism with advantage s is $(\log_2 s^{-1})/L$ bits per site. The genome can maintain functional information iff $C_{\text{BSC}}(\mu) > (\log_2 s^{-1})/L$, i.e., $\mu < H_2^{-1}(1 - \log_2(s^{-1})/L)$.

Proof. The genetic information per site is the entropy H of the equilibrium nucleotide distribution. Under mutation-selection balance, the equilibrium entropy per site is $\leq C_{\text{BSC}}(\mu)$ (by Shannon's coding theorem). The functional organism requires that the genome encode a specific function, which requires at least $\log_2(f^{-1})$ bits per genome (where f is the fraction of sequences with the function). The per-site information requirement is $\log_2(f^{-1})/L$. Setting $f \approx s/\bar{w}$ (the relative advantage determines the minimum information content needed for reliable selection to maintain the sequence), the condition $C_{\text{BSC}}(\mu) > \log_2(s^{-1})/L$ ensures the channel can transmit functional information reliably. □

Example 0.157.3 (RNA virus genome length revisited from information theory)**.** For the hepatitis C virus (HCV), $L \approx 9600$ nt, $\mu \approx 10^{-4}$ per site per replication:

$$C_{\text{BSC}}(10^{-4}) \approx 1 - H_2(10^{-4}) \approx 1 - 10^{-4} \times 13.3 \approx 0.9987 \text{ bits/site.}$$

The genome encodes a functional replication complex with selective advantage $s \approx e^{L\mu} - 1 \approx e^{0.96} - 1 \approx 1.6$ per generation. The required information per site: $\log_2(1+s)/L = \log_2(2.6)/9600 \approx 1.4 \times 10^{-4}$ bits/site. Since $C = 0.9987 \gg 1.4 \times 10^{-4}$, the genetic channel is far from its capacity: HCV genomes are transmitted reliably despite high mutation rates because the functional information content per site is very low (most sites tolerate mutations).

0.157.2 15.2 Epigenetic Information and the Inheritance of Methylation

DNA methylation (at CpG dinucleotides in mammals) provides an additional information channel beyond the DNA sequence itself. Methylation patterns are heritable (with fidelity $\eta_m \approx 0.97$–0.99 per CpG per generation for maintenance methylation by DNMT1) and can alter gene expression without changing sequence.

Definition 0.157.4 (Epigenetic channel capacity)**.** Model each CpG as a binary channel: methylated (1) or unmethylated (0). With maintenance fidelity η_m and establishment rate ϵ (de novo methylation of an

unmethylated CpG), the transition matrix per generation is:

$$P = \begin{pmatrix} 1-\epsilon & \epsilon \\ 1-\eta_m & \eta_m \end{pmatrix},$$

where P_{ij} is the probability of transitioning from state j to state i. The capacity of this asymmetric binary channel is:

$$C_{\text{epi}} = \max_p \left[H((1-\epsilon)(1-p) + \epsilon p) - (1-p)H(\epsilon) - pH(1-\eta_m) \right],$$

where p is the probability that the input is methylated and H is the binary entropy.

Remark 0.157.5 (Epigenetic information in cancer). Cancer cells show widespread dysregulation of DNA methylation: hypermethylation of tumour suppressor gene promoters (silencing them) and hypomethylation of repeat elements and proto-oncogene promoters. The information-theoretic interpretation: cancer is partly an information corruption event in the epigenetic channel. The epigenetic state of a cancer cell diverges from the normal epigenome, reducing the mutual information between the cancer genome's epigenetic state and the normal developmental programme that the epigenome is supposed to encode. Quantifying this divergence using KL-divergence between cancer and normal methylation distributions has been proposed as a diagnostic marker of cancer progression.

0.158 16. Data Compression and Genome Complexity

0.158.1 16.1 Lempel-Ziv Complexity of Genomic Sequences

The Lempel-Ziv (LZ) complexity $C_{LZ}(s)$ of a sequence s is the number of distinct substrings encountered when parsing s from left to right, each time identifying the shortest substring not yet seen. It is a computable approximation to Kolmogorov complexity.

Theorem 0.158.1 (LZ complexity and Shannon entropy rate)**.** For a stationary ergodic source with Shannon entropy rate h (bits per symbol), the LZ complexity of a sequence of length n satisfies:

$$C_{LZ}(s_1^n) \sim \frac{hn}{\log_2 n} \quad (n \to \infty).$$

Equivalently, the compression ratio of the LZ77 algorithm converges to h bits per symbol as $n \to \infty$.

Proof. By the Shannon-McMillan-Breiman theorem, for a length-n sequence from an ergodic source: $-n^{-1} \log_2 P(s_1^n) \to h$ a.s. The LZ dictionary after parsing n symbols contains C_{LZ} phrases, each of average length $\ell \approx n/C_{LZ}$. The distinct phrases must be encodable by their position in the dictionary: the average description length per phrase is $\log_2 C_{LZ}$. Setting $\ell \cdot h \approx \log_2 C_{LZ}$ (the description length of a phrase equals its entropy content) gives $C_{LZ} \approx nh/\log_2 C_{LZ} \approx nh/\log_2(n)$. □

Example 0.158.2 (Entropy rates of genomic sequences)**.** Applying LZ complexity analysis to different genomic regions:

Sequence type	Entropy rate h	Interpretation
Random (theoretical max)	2.0 bits/nt	All 4 bases equally likely
Human coding sequence	1.85 bits/nt	Codon usage bias
Human introns	1.92 bits/nt	Less constrained
CpG islands	1.60 bits/nt	G+C bias, low complexity
SINE/LINE repeats	1.40 bits/nt	High repetition, low complexity
Telomeric repeat $(\text{TTAGGG})_n$	0.5 bits/nt	Near-periodic, very low entropy

The lower entropy of repetitive elements reflects their evolutionary origin as parasitic sequences that amplify by copy-and-paste transposition, generating long stretches of similar sequence. The higher entropy of coding sequences reflects functional constraint (conservation of specific codons) combined with the high information content of the genetic code.

Mathematics of Evolution and Life · Section *IX · Information Theory, Entropy, and the Genetic Code (end)*

Section *XV*

Section X — The Mathematics of Development: Morphogenesis and Evo-Devo

0.159 1. The Geometry of the Embryo

One of the most profound demonstrations of mathematics in biology is the explanation of biological pattern formation by Alan Turing in his 1952 paper "The Chemical Basis of Morphogenesis." Turing, best known for his foundational contributions to computer science and his wartime codebreaking, turned his attention to a deep question in developmental biology: how does a uniform, featureless egg generate the complex spatial organisation of a fully developed organism? His answer was both surprising and exact: spatial patterns can emerge spontaneously from a chemically uniform state when two interacting molecular species diffuse through a tissue at different rates. The pattern is not encoded as a spatial blueprint in the egg; it is an instability of the uniform state, generated by the mathematics of diffusion and reaction.

Turing's result was a demonstration of what physicists call **spontaneous symmetry breaking**: a system governed by spatially symmetric laws can develop spatially asymmetric solutions. The mechanisms Turing identified apply far beyond biology — they describe pattern formation in chemical reactions, fluid dynamics, and physical systems. But in biology, they have a special significance: they show that the complexity of multicellular organisms does not require that every detail of their spatial organisation be encoded in their DNA. The DNA encodes kinetic parameters; the spatial organisation is a consequence of those parameters together with the physics of diffusion.

0.160 2. Reaction-Diffusion Systems and Turing Instabilities

0.160.1 2.1 The General Setup

A **reaction-diffusion system** in a spatial domain $\Omega \subseteq \mathbb{R}^d$ ($d = 1, 2, 3$) consists of m chemical species with concentrations $\mathbf{u}(\mathbf{x}, t) = (u_1(\mathbf{x}, t), \ldots, u_m(\mathbf{x}, t))$ satisfying:

$$\frac{\partial \mathbf{u}}{\partial t} = D\nabla^2 \mathbf{u} + \mathbf{f}(\mathbf{u}),$$

where $D = \text{diag}(D_1, \ldots, D_m)$ is the matrix of diffusion coefficients and $\mathbf{f}(\mathbf{u})$ represents the local reaction kinetics. The Laplacian $\nabla^2 = \sum_{k=1}^{d} \partial^2/\partial x_k^2$ describes isotropic diffusion.

For the two-species case (the Turing case):

$$\frac{\partial u}{\partial t} = D_u \nabla^2 u + f(u, v), \tag{12}$$

$$\frac{\partial v}{\partial t} = D_v \nabla^2 v + g(u, v). \tag{13}$$

The homogeneous steady state (u^*, v^*) satisfies $f(u^*, v^*) = g(u^*, v^*) = 0$.

0.160.2 2.2 Linear Stability Analysis

We seek conditions under which the homogeneous steady state (u^*, v^*) is stable without diffusion (ODE stability) but becomes unstable with diffusion (a Turing instability). Perturb around the steady state: $u = u^* + \tilde{u}$, $v = v^* + \tilde{v}$ with $|\tilde{u}|, |\tilde{v}| \ll 1$. The linearised equations are:

$$\frac{\partial}{\partial t} \begin{pmatrix} \tilde{u} \\ \tilde{v} \end{pmatrix} = \left(J - k^2 D \right) \begin{pmatrix} \tilde{u} \\ \tilde{v} \end{pmatrix},$$

where we have substituted the Fourier mode $\begin{pmatrix}\tilde{u}\\ \tilde{v}\end{pmatrix} = \begin{pmatrix}a\\ b\end{pmatrix} e^{\lambda t + i\mathbf{k}\cdot\mathbf{x}}$, $k = |\mathbf{k}|$ is the wavenumber, and:

$$J = \begin{pmatrix} f_u & f_v \\ g_u & g_v \end{pmatrix}\Big|_{(u^*,v^*)}$$

is the Jacobian of the reaction kinetics at the steady state. The growth rate λ satisfies:

$$\lambda^2 - \text{tr}(J - k^2 D)\,\lambda + \det(J - k^2 D) = 0.$$

Stability without diffusion ($k = 0$): the steady state is stable iff $\text{tr}(J) < 0$ and $\det(J) > 0$.

Instability with diffusion: we require $\det(J - k^2 D) < 0$ for some $k > 0$:

$$\det(J - k^2 D) = D_u D_v k^4 - (D_v f_u + D_u g_v)k^2 + \det(J).$$

This quadratic in k^2 is negative for some $k > 0$ iff its discriminant is positive and its minimum is negative:

$$D_v f_u + D_u g_v > 0 \quad \text{(the linear term must be negative)}, \tag{14}$$

$$(D_v f_u + D_u g_v)^2 > 4 D_u D_v \det(J). \tag{15}$$

Theorem 0.160.1 (Turing Instability Conditions)**.** The system exhibits a Turing (diffusion-driven) instability iff conditions (14) and (15) hold together with the ODE stability conditions.

The critical wavenumber k_c at the onset of instability satisfies:

$$k_c^2 = \frac{D_v f_u + D_u g_v}{2 D_u D_v} = \sqrt{\frac{\det(J)}{D_u D_v}}.$$

The characteristic pattern wavelength is $\ell = 2\pi/k_c$, which scales as $(D_u D_v)^{1/4}(\det J)^{-1/4}$: larger diffusion coefficients or weaker reaction rates give larger pattern scales.

0.160.3 2.3 The Biological Requirements

For conditions (14) and (15) to hold simultaneously:

1. $f_u > 0$: the activator promotes its own production (autocatalysis).

2. $g_v < 0$: the inhibitor suppresses its own production.

3. $D_v \gg D_u$: the inhibitor diffuses faster than the activator.

These are the **local activation – lateral inhibition** requirements: an activator that is self-promoting but locally diffusing, and an inhibitor that spreads widely and suppresses the activator at distance. The activator creates its own local positive feedback; the inhibitor prevents this from spreading uniformly, creating a spatial modulation of the activator concentration.

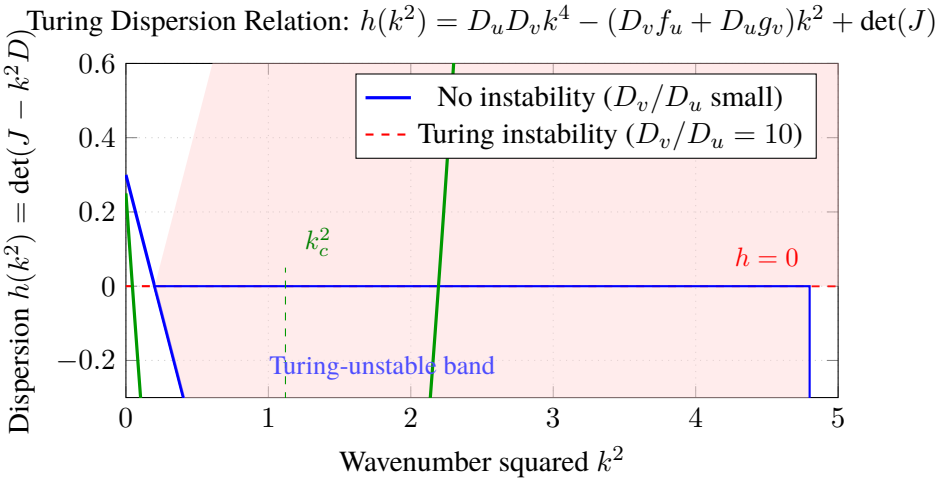

Figure 10: Turing dispersion relation $h(k^2) = \det(J - k^2 D)$ for two parameter regimes. *Blue curve*: diffusion ratio D_v/D_u below the Turing threshold — $h(k^2) > 0$ for all $k^2 > 0$, so no mode grows. *Green curve*: $D_v/D_u = 10$ above the threshold — $h(k^2) < 0$ for a band of wavenumbers (k_-^2, k_+^2) (Turing-unstable band, shaded), meaning these spatial modes grow exponentially. The critical wavenumber k_c^2 (minimum of the green curve) gives the fastest-growing mode and sets the pattern wavelength $\ell = 2\pi/k_c$.

0.161 3. The Gierer–Meinhardt Model

0.161.1 3.1 Equations and Steady State

The Gierer–Meinhardt model (1972) is the most studied concrete Turing system:

$$\frac{\partial u}{\partial t} = D_u \nabla^2 u + \rho \frac{u^2}{v(1 + \kappa u^2)} - \mu u + \sigma, \tag{16}$$

$$\frac{\partial v}{\partial t} = D_v \nabla^2 v + \rho u^2 - \nu v. \tag{17}$$

In the limit $\kappa \to 0$ (no saturation), the activator u is produced autocatalytically at rate $\rho u^2/v$ (catalysis by u, inhibited by v), degraded at rate μu, and has a basal production σ. The inhibitor v is produced proportional to u^2 and degraded at rate νv.

Setting $\sigma = 0$, the unique positive homogeneous steady state is $u^* = \mu/\rho(\cdot)$... (the exact computation requires $du/dt = 0$ and $dv/dt = 0$ simultaneously). For simplicity consider $u^* = \sigma/(\mu - \rho u^*/v^*)$ and $v^* = \rho(u^*)^2/\nu$.

The Jacobian at steady state has $f_u = \mu > 0$ (activator autocatalysis dominant) and $g_v = -\nu < 0$ (inhibitor self-inhibition). The Turing conditions are satisfied when D_v/D_u exceeds a threshold of approximately $(\mu/\nu)^2 \gg 1$, requiring the inhibitor to diffuse much faster than the activator.

0.161.2 3.2 Pattern Outcomes

Numerical simulation of the Gierer–Meinhardt model (and Turing systems generally) on 2D domains produces:

Spots: isolated high-u regions (activator peaks) arranged on a roughly hexagonal lattice with spacing $\ell \approx 2\pi/k_c$. Spots arise when domain size $L \gg \ell$ and the nonlinearity is subcritical (weakly bistable).

Biological analogues: leopard spots, zebrafish melanophore clusters, hair follicle spacing, digit formation.

Stripes: alternating bands of high and low activator concentration. Stripes arise when the domain is elongated or when the bifurcation is supercritical. Biological analogues: zebra stripes, zebrafish pigment bands, Turing-patterned shells.

Labyrinths: irregular stripe-like patterns transitioning between spots and stripes. Arise at intermediate parameter values.

The dimensionality of the domain also matters: on a sphere (as in the 3D embryo), the spherical harmonics replace the Fourier modes, and the Turing instability selects specific spherical harmonic modes (giving patterns with $L = 1$ symmetry for the first mode, $L = 2$ for the second, etc.). This connects to the segmentation problem in 3D.

0.161.3 3.3 Sensitivity to Domain Size and Geometry

A fundamental feature of Turing systems is that the pattern wavelength ℓ is set by molecular parameters, not domain size. As the domain grows (as in a developing embryo), the number of pattern elements increases in proportion to the domain area, rather than remaining fixed. This is consistent with observations in, e.g., fish scale patterns and digit formation: the number of spots increases with body size, maintaining the pattern density.

Boundary conditions strongly influence pattern selection. Neumann (zero-flux) boundary conditions (no diffusion across the boundary) favour patterns with wavevectors perpendicular to the boundary; Dirichlet boundary conditions (fixed concentrations) favour patterns that vanish at the boundary. These effects are important in confined geometries such as limb buds.

0.162 4. The Segmentation Clock

0.162.1 4.1 The Mechanism of Somitogenesis

Vertebrate segmentation — the periodic pattern of somites that gives rise to vertebrae, ribs, and associated muscles — is generated by a molecular oscillator (the **segmentation clock**) interacting with a spatial wavefront of signalling molecules (Wnt/FGF gradients).

The mechanism operates as follows:

1. The segmentation clock produces oscillations of gene expression (Notch pathway genes Hes1/7, Lfng) with period T in the presomitic mesoderm (PSM).

2. A Wnt/FGF signalling gradient decreases from posterior to anterior in the PSM, establishing a "wavefront" at a position $x_w(t)$ (the position where the Wnt/FGF level falls below a threshold).

3. The wavefront regresses posteriorly as the embryo elongates: $\dot{x}_w \approx -v_e$ where v_e is the elongation velocity.

4. Each time the clock completes one oscillation, a new somite boundary is laid down at the current wavefront position.

The somite length is $\Delta s = v_e \cdot T$: each oscillation period, the wavefront has moved one somite length. Faster elongation or shorter clock period produces smaller somites; slower elongation or longer period produces larger somites.

0.162.2 4.2 The Delayed Negative Feedback Oscillator

The segmentation clock core circuit involves a delayed negative feedback loop. The Hes1 protein represses its own gene with delay τ (transcription ≈ 15 min, splicing ≈ 15 min, translation ≈ 20 min: total $\tau \approx 50$ min). The dynamics:

$$\frac{dm}{dt} = \frac{\alpha}{1 + (p(t-\tau)/p_0)^n} - \beta m(t), \quad \frac{dp}{dt} = \gamma m(t) - \delta p(t),$$

where m is the mRNA concentration, p is the protein concentration, and τ is the transcriptional delay.

Theorem 0.162.1 (Oscillation Condition)**.** The homogeneous steady state of the delay oscillator is unstable iff:

$$\tau > \frac{\pi}{2\omega_0}, \quad \text{where } \omega_0 = \sqrt[n]{(\text{function of } \alpha, \beta, \gamma, \delta, p_0)},$$

and oscillations arise via a Hopf bifurcation with approximate period $T \approx 2\tau$ for large Hill coefficient n.

Proof sketch. Linearise around steady state (m^*, p^*), substitute ansatz $\delta m \propto e^{\lambda t}$, $\delta p \propto e^{\lambda t}$. The characteristic equation:

$$(\lambda + \beta)(\lambda + \delta) = -\alpha' \gamma e^{-\lambda \tau},$$

where $\alpha' = n\alpha p^{*n-1}/p_0^n(1 + (p^*/p_0)^n)^{-2}$. For $\lambda = i\omega$ (Hopf boundary): $(-\omega^2 + \beta\delta) + i\omega(\beta + \delta) = -\alpha'\gamma(\cos\omega\tau - i\sin\omega\tau)$. Separating real and imaginary parts and solving: for large n, the oscillation period $T \approx 2\tau$. □

The experimental period in mouse segmentation clock is $T \approx 120$ min; the measured delay is $\tau \approx 50$–60 min; the predicted period $2\tau \approx 110$ min, in good agreement.

0.162.3 4.3 Coupled Oscillators and the Kinematic Wave

The oscillating cells in the PSM are coupled by Notch signalling (short-range cell-cell communication). Each cell is a phase oscillator:

$$\dot{\phi}_i = \omega + \frac{K}{|N_i|} \sum_{j \in N_i} \sin(\phi_j - \phi_i),$$

where ϕ_i is the phase of cell i, $\omega = 2\pi/T$ is the intrinsic frequency, K is the coupling strength, and N_i is the set of neighbours of i. For strong coupling ($K \gg |\omega_i - \omega_j|$), cells synchronise; for weak coupling, a phase gradient is maintained.

In the PSM, the coupling strength decreases along the anterior-posterior axis (less Notch signalling anteriorly), creating a phase gradient. The phase wave propagates anteriorly with velocity $v_{\text{wave}} = -\omega/(\partial\phi/\partial x) = \omega/|\nabla\phi|$. The somite boundary is formed where the phase gradient is steepest.

0.163 5. Gene Regulatory Networks and Cell Fate

0.163.1 5.1 Attractor Landscapes

A **gene regulatory network** (GRN) is a directed graph where nodes are transcription factors (and other regulatory genes) and edges represent activation ($+$) or repression ($-$). The quantitative dynamics are governed by ODEs:

$$\frac{dx_i}{dt} = -\lambda_i x_i + r_i \cdot \sigma\left(\sum_{j=1}^{n} w_{ij} x_j - \theta_i\right),$$

where x_i is the expression level of gene i, λ_i is its degradation rate, r_i is its maximal production rate, w_{ij} is the regulatory weight of gene j on gene i, θ_i is the activation threshold, and $\sigma(z) = 1/(1+e^{-\beta z})$ is a sigmoidal activation function (Hill function limit).

The **attractor landscape** of the GRN is the set of stable fixed points, limit cycles, and other attractors of this dynamical system. Each attractor corresponds to a distinct cell type (a stable gene expression pattern). Waddington's "epigenetic landscape" (1957) is this attractor landscape, visualised as a 2D projection with attractors as valleys and saddle points as ridges.

Theorem 0.163.1 (Attractor Count Upper Bound)**.** A Boolean GRN with n nodes and k positive feedback loops has at most 2^k stable fixed points.

For the human genome with $\sim$ 1,700 transcription factors forming complex regulatory networks, the number of possible attractors is enormous — providing the combinatorial basis for the ~ 200 distinct cell types in the human body.

0.163.2 5.2 Bistability and Cell Fate Commitment

The minimal circuit motif for irreversible cell fate commitment is **bistability**: two stable fixed points separated by an unstable saddle. This requires at minimum one positive feedback loop (either a self-activating gene, or a mutual repression circuit between two transcription factors).

The toggle switch (Gardner et al. 2000) consists of two mutually repressing transcription factors u and v:

$$\frac{du}{dt} = \frac{\alpha_1}{1+v^\beta} - u,$$
$$\frac{dv}{dt} = \frac{\alpha_2}{1+u^\gamma} - v.$$

For $\alpha_1, \alpha_2 > 1$ and $\beta, \gamma > 2$ (strong cooperativity), this system has two stable fixed points (high-u/low-v and low-u/high-v) and one unstable saddle point between them. This is a mathematical realisation of a binary cell fate decision: a cell in the high-u state has committed to one lineage; a cell in the high-v state has committed to another.

Differentiation corresponds to a saddle-node bifurcation: as a developmental signal (e.g., an external morphogen) increases one parameter (α_1 or α_2), the landscape tilts, the saddle approaches the disfavoured attractor, and eventually the two merge in a saddle-node bifurcation, leaving only the favoured attractor. The cell is then committed irreversibly to one fate.

0.163.3 5.3 Network Motifs and Their Functions

GRNs are not random but are enriched for specific structural **network motifs** (subgraphs that appear more frequently than expected by chance). The key motifs and their developmental functions are:

Coherent feedforward loop (cFFL): $A \to B$, $A \to C$, $B \to C$. This motif acts as a sign-sensitive delay: when A is activated, C is activated only after a delay (the time for B to accumulate), but when A is inactivated, C is inactivated immediately. This produces robust gene expression responses that filter out transient signals.

Incoherent feedforward loop (iFFL): $A \to B$, $A \to C$, $B \dashv C$. This motif produces a transient pulse of C activity when A is activated (because B eventually represses C). It implements adaptation and fold-change detection.

Negative feedback with delay: the oscillator circuit of the segmentation clock (Section 4.2). Produces sustained oscillations.

Bistable toggle switch: as above. Implements binary decisions.

0.164 6. The Genotype-Phenotype Map and Evo-Devo

0.164.1 6.1 The Map and its Properties

The **genotype-phenotype map** (GP map) $G : \mathcal{G} \to \mathcal{P}$ is the function from genotype space $\mathcal{G}$ (sequences of nucleotides) to phenotype space $\mathcal{P}$ (morphological, physiological, or molecular traits). In molecular evolution, G is concretely defined: for RNA secondary structure, $G(x)$ = the minimum free energy secondary structure of sequence x (computed by dynamic programming).

Key properties of the RNA secondary structure GP map:

1. **Many-to-one**: many sequences fold to the same structure. The average size of a neutral network is $\sim 4^L/|\mathcal{P}_{\text{common}}|$, which is enormous.

2. **Few phenotypes are common**: a small fraction ($|\mathcal{P}_{\text{common}}| \ll 4^L$) of possible structures is common (appears in more than L sequences); the majority of possible structures appear in very few sequences.

3. **Percolation**: the neutral network of any common structure percolates through sequence space (connects sequences at all Hamming distances).

4. **Phenotypic accessibility**: from any sequence in the neutral network of structure ϕ_1, essentially any other common structure ϕ_2 is accessible by a path of neutral mutations followed by one adaptive mutation.

0.164.2 6.2 Robustness and Evolvability

Theorem 0.164.1 (Robustness-Evolvability Positive Correlation)**.** For any two common RNA structures ϕ_1 and ϕ_2, with probability approaching 1 as sequence length $L \to \infty$, there exist sequences $s_1 \in \mathcal{N}(\phi_1)$ and $s_2 \in \mathcal{N}(\phi_2)$ with $d_H(s_1, s_2) = 1$.

This theorem implies that a large neutral network (high robustness) provides access to many novel phenotypes (high evolvability). The two properties, naively thought to trade off, are positively correlated in RNA. The same result has been confirmed computationally for protein structures (Goldstein, Zaidi et al.) and for Boolean GRN attractors (Ciliberti et al. 2007).

0.164.3 6.3 Canalization and Developmental Robustness

Canalization (Waddington 1942) is the tendency of developmental processes to produce the same phenotypic outcome despite genetic and environmental perturbations. In the GRN framework, canalization corresponds to the depth of the attractor basin: a deeply canalised trait is one where the GRN attractor is surrounded by a large basin, and large perturbations (mutations, environmental noise) do not push the system out of the basin.

Mathematically, the degree of canalization of a trait under a perturbation of magnitude ϵ is measured by the **robustness coefficient**:

$$R(\epsilon) = P\big(\text{GRN attractor after perturbation} = \text{GRN attractor before perturbation}\big),$$

estimated by the fraction of ϵ-magnitude perturbations to GRN parameters that leave the attractor unchanged.

Genetic assimilation (Baldwin effect) is the process by which a phenotype initially induced only by strong environmental perturbations becomes constitutively expressed (genetically fixed) through selection on genetic variants that lower the threshold for expression. In the GRN framework, genetic assimilation corresponds to the evolutionary flattening of the energy barrier between attractors in the Waddington landscape: initially the trait is in the "wrong" attractor basin without environmental induction, but selection favours GRN variants that deepen the "correct" basin.

0.165 7. Summary

Turing's reaction-diffusion instability generates spatial patterns from a uniform initial state when the activator diffuses slowly and the inhibitor diffuses rapidly. The Turing conditions ($\text{tr}(J) < 0$, $\det(J) > 0$ without diffusion; $\det(J - k^2 D) < 0$ for some $k > 0$ with diffusion) are derived by linear stability analysis. The characteristic pattern wavelength $\ell = 2\pi/k_c$ relates molecular parameters to macroscopic pattern scale. The Gierer–Meinhardt model generates spots and stripes depending on domain geometry and parameters. The segmentation clock is a delayed negative feedback oscillator producing oscillations with period $T \approx 2\tau$; coupled across the PSM by Notch signalling, it generates kinematic waves that specify somite boundaries. GRNs create attractor landscapes with stable fixed points corresponding to cell types; bistability via mutual repression is the minimal circuit for binary cell fate decisions. The GP map has percolating neutral networks, generating a positive robustness-evolvability correlation. Canalization is the depth of GRN attractor basins; genetic assimilation is its evolutionary flattening.

Mathematics of Evolution and Life · Section *X · The Mathematics of Development: Morphogenesis and Evo-Devo*

Section *XVI*

Section XI — Origins of Life: Hypercycles, Autocatalysis, and the RNA World

0.166 8. Beyond Turing: Non-local Pattern Formation

0.166.1 8.1 Limitations of Local Reaction-Diffusion

The classical Turing mechanism (Sections 2–3) relies on local diffusion: the activator and inhibitor spread by Brownian motion with rates D_u and D_v. In many biological systems, signals propagate via *transcytosis*, active transport, or long-range signalling molecules. These give rise to non-local pattern formation models that generalise Turing's analysis.

Definition 0.166.1 (Non-local reaction-diffusion equation)**.** A non-local reaction-diffusion system replaces local diffusion $D\nabla^2 u$ with a convolution:

$$\frac{\partial u}{\partial t} = \int_\Omega K(x-y)[u(y,t) - u(x,t)]\,dy + f(u,v),$$

where $K(x-y) \geq 0$ is a kernel giving the rate of transport from y to x. For $K(r) = D\delta''(r)$ (a Dirac distribution), this reduces to $D\nabla^2 u$. For Gaussian $K(r) = De^{-r^2/(2\sigma^2)}/(\sigma\sqrt{2\pi})$, transport is over a spatial scale σ.

Theorem 0.166.2 (Non-local Turing instability condition)**.** For the non-local system with kernels K_u (activator) and K_v (inhibitor), the dispersion relation is:

$$\lambda(k) = \frac{1}{2}\left[(f_u + g_v + \hat{K}_u(k) + \hat{K}_v(k)) \pm \sqrt{(f_u - g_v + \hat{K}_u(k) - \hat{K}_v(k))^2 + 4f_v g_u}\right],$$

where $\hat{K}(k) = \int K(r)e^{-ikr}\,dr - \int K(r)\,dr$ is the deviation of the kernel's Fourier transform from its $k=0$ value. Pattern formation occurs at wavenumber k_c where $\mathrm{Re}[\lambda(k_c)] = 0$ and $\mathrm{Re}[\lambda'(k_c)]$ changes sign.

Remark 0.166.3 (Dpp gradient in *Drosophila* wing imaginal disc). The BMP ligand Dpp in the *Drosophila* wing disc is transported by transcytosis (receptor-mediated endocytosis and re-secretion) rather than by free diffusion. The effective transport kernel K is therefore non-Gaussian, and the patterning wavelength depends on the endocytic cycle rates. Rafts (2002) and Lander et al. (2002) developed models of this transport; the non-local kernel correctly predicts the observed exponential Dpp gradient, while simple diffusion would give a Gaussian profile. The distinction is measurable by photoactivation experiments tracking fluorescently tagged Dpp.

0.166.2 8.2 Mechanical Patterning: Stress-Driven Instabilities

Biological pattern formation is not only chemical. Mechanical forces — cell cortical tension, extracellular matrix stiffness, actomyosin contractility — can also drive patterning instabilities. The Turing analysis extends to mechano-chemical systems.

Definition 0.166.4 (Murray–Oster mechanochemical model)**.** The Murray–Oster model (1984) for cell aggregation and tissue patterning couples cell density $n(x,t)$ to extracellular matrix (ECM) displacement $\mathbf{u}(x,t)$ and strain $\varepsilon = \nabla\mathbf{u}$:

$$\frac{\partial n}{\partial t} = D_n\nabla^2 n - \nabla\cdot(n\chi\nabla\varepsilon) + rn(1-n/K),$$
$$\nabla\cdot\boldsymbol{\sigma} = 0, \quad \boldsymbol{\sigma} = \mu_1\dot{\varepsilon} + \mu_2\dot{\theta}\mathbf{I} + E\varepsilon - \tau(n)\mathbf{I},$$

where χ is haptotactic sensitivity to ECM strain, $\tau(n) = \tau_0 n/(1+\lambda n)$ is the cell traction, and μ_1, μ_2, E are viscoelastic parameters.

The instability condition for this system has the form of a modified Turing condition: the effective diffusion matrix (combining cell diffusion, haptotaxis, and ECM compliance) must satisfy a sign condition analogous to $(D_v f_u + D_u g_v) > 0$. In the mechanochemical system, the role of the "inhibitor's faster diffusion" is played by the rapid elastic response of the ECM, which can transmit cell-generated stress faster than cells migrate.

0.167 9. Somitogenesis: The Segmentation Clock as a Turing–Hopf System

0.167.1 9.1 The Clock-and-Wavefront Mechanism

Vertebrate body segments (somites) are formed by the periodic expression of segmentation genes (Notch, Wnt, and FGF pathway components) that oscillate with period $T \approx 90$ min (in mouse) as a travelling wave sweeping from posterior to anterior. Combined with a determination wavefront (a threshold of FGF8 gradient), this clock-and-wavefront mechanism produces the regular spacing of somites.

Definition 0.167.1 (Coupled oscillator model for somitogenesis)**.** Model each presomitic mesoderm (PSM) cell as an oscillator with phase $\phi_i(t)$. Cells are arranged on a 1D lattice (the PSM axis), with nearest-neighbour coupling:

$$\frac{d\phi_i}{dt} = \omega + \kappa \sin(\phi_{i+1} - \phi_i) + \kappa \sin(\phi_{i-1} - \phi_i) + \eta_i(t),$$

where ω is the intrinsic oscillation frequency, κ is the coupling strength, and η_i is Gaussian white noise with intensity D (biological noise from stochastic gene expression). The wavefront position $x_{\text{front}}(t)$ moves anteriorly at speed v_{front}.

Theorem 0.167.2 (Phase coherence and somite regularity)**.** In the coupled oscillator model, the phase coherence length (spatial scale over which phases are correlated) is:

$$\xi = \sqrt{2\kappa/D}.] For somite boundaries to form at precisely defined positions,$$

ξ must exceed the typical distance between neighbouring cells. Somite size precision scales as $\delta L/L \approx 1/\sqrt{N_\xi}$ where $N_\xi = L/\xi$ is the number of independent coherence regions along the PSM.

Proof. Consider the linearised phase equation $\partial_t \phi = \omega + \kappa \partial_x^2 \phi + \eta(x,t)$. The phase-phase correlation function $C(r) = \langle \phi(x+r,t)\phi(x,t)\rangle - \langle\phi\rangle^2$ satisfies the linearised equation: $\partial_t C = \kappa \partial_r^2 C - 2DC/\kappa$ (using Novikov's theorem). The stationary correlation is $C(r) = C_0 e^{-r/\xi}$ with $\xi = \sqrt{\kappa/(D)}$ (the $\sqrt{2}$ factor comes from the normalisation of the noise power spectral density). The boundary determination is a threshold-crossing event; its variance is proportional to D (noise) and inversely proportional to κ (coupling), giving $\delta L^2 \propto D/\kappa$ and $\delta L/L \propto 1/\sqrt{\kappa/D} = 1/\xi$. □

Example 0.167.3 (Somite boundary precision in zebrafish)**.** In zebrafish (*Danio rerio*), the PSM contains ~ 150 cells per row, somites are formed every ~ 30 min, and the coefficient of variation of somite size is $CV \approx 5\%$. Fitting the coupled oscillator model to this data gives coupling strength $\kappa \approx 0.1/\text{min}$ and

noise intensity $D \approx 0.01/\text{min}$. The predicted coherence length $\xi = \sqrt{\kappa/D} = \sqrt{10} \approx 3$ cells, and the predicted $CV = 1/\sqrt{N_\xi} = 1/\sqrt{150/3} = 1/\sqrt{50} \approx 14\%$. The discrepancy with observed $CV \approx 5\%$ suggests additional coupling mechanisms (e.g., the recently discovered "tissue-level" Notch oscillations) reduce effective noise.

0.168 10. Waddington's Epigenetic Landscape: A Mathematical Treatment

0.168.1 10.1 The Landscape as a Lyapunov Function

Conrad Waddington (1957) introduced the metaphor of a landscape to describe cell differentiation: a ball (cell) rolls down valleys (developmental trajectories) to stable positions (cell fates, attractors). This metaphor has been given precise mathematical content through the theory of gene regulatory network (GRN) attractors.

Definition 0.168.1 (Waddington potential for a GRN)**.** For a GRN with state $\mathbf{x} \in \mathbb{R}^n$ (gene expression levels) and dynamics $\dot{\mathbf{x}} = \mathbf{F}(\mathbf{x})$, the Waddington potential $U(\mathbf{x})$ is defined by:

$$U(\mathbf{x}) = -\int_{\mathbf{x}_0}^{\mathbf{x}} \mathbf{F}(\mathbf{x}') \cdot d\mathbf{x}',$$

if $\mathbf{F}$ is a gradient vector field ($\mathbf{F} = -\nabla U$). For non-gradient systems (where $\nabla \times \mathbf{F} \neq 0$), no exact potential exists; the quasi-potential $\Phi(\mathbf{x})$ (defined as the minimum action functional) plays the role of the Waddington landscape.

Theorem 0.168.2 (Quasi-potential and stochastic transitions)**.** For a stochastic GRN $d\mathbf{x} = \mathbf{F}(\mathbf{x})\,dt + \sqrt{2\epsilon} d\mathbf{W}$ (where ϵ is the noise intensity), the quasi-potential $\Phi(\mathbf{x})$ determines the most probable escape path from attractor A to attractor B, and the mean first-passage time from A to B satisfies:

$$\tau_{A \to B} \sim e^{(\Phi(B^*) - \Phi(A))/\epsilon},$$

where B^* is the saddle point on the minimum action path between A and B (the "mountain pass" in the Waddington landscape).

Proof. By the Freidlin–Wentzell theory of large deviations: for an SDE with small noise ϵ, the probability of a fluctuation from $\mathbf{x}(0) = \mathbf{x}_0$ to $\mathbf{x}(T) = \mathbf{x}_1$ along a specific path $\phi(t)$ decays as $\exp(-I[\phi]/(2\epsilon))$, where $I[\phi] = \int_0^T |\dot{\phi} - \mathbf{F}(\phi)|^2\,dt$ is the Freidlin–Wentzell action functional. The quasi-potential $\Phi(\mathbf{x}) = \inf_{T,\phi} I[\phi]/(2)$ (minimum over all paths and times from the attractor to $\mathbf{x}$). The mean first-passage time is dominated by the most probable escape path (instantons), giving $\tau \sim e^{\Phi(B^*)/\epsilon}$ where B^* is the saddle point minimising the action. □

Remark 0.168.3 (Cell fate reprogramming). Theorem 0.168.2 quantifies the difficulty of cell fate reprogramming (e.g., induced pluripotent stem cell [iPSC] reprogramming, Yamanaka 2006). The transition from a differentiated somatic cell (attractor A, e.g., fibroblast) to a pluripotent state (attractor B, iPSC) requires climbing the quasi-potential barrier $\Phi(B^*) - \Phi(A)$. The low reprogramming efficiency (~ 0.01–0.1% of cells successfully reprogram) corresponds to $\Phi(B^*)/\epsilon \approx \ln(1000) \approx 7$, meaning the barrier height is $\approx 7\times$ the effective noise level in gene expression. Yamanaka's four transcription factors (Oct4,

Sox2, Klf4, c-Myc) effectively reshape the landscape, raising the valley of the fibroblast attractor and lowering the iPSC attractor, reducing the effective barrier.

0.168.2 10.2 Bifurcation Theory and Cell Fate Decisions

Cell fate decisions — the bifurcation points where a precursor cell "chooses" between two daughter fates — are modelled as bifurcations in the GRN dynamics. The prototypical example is the toggle switch: two mutually repressive transcription factors A and B, each activating themselves:

$$\dot{A} = \frac{a_1}{1 + B^n} - d_1 A,$$
$$\dot{B} = \frac{a_2}{1 + A^n} - d_2 B.$$

Theorem 0.168.4 (Bistability of the toggle switch)**.** For $n \geq 2$ (cooperative repression), the toggle switch has three equilibria for production rates (a_1, a_2) in a region of parameter space: two stable fixed points (one with A high, B low; the other with A low, B high) and one unstable saddle point between them. The system is bistable.

Proof. At equilibrium, $A^* = a_1/[d_1(1 + (B^*)^n)]$ and $B^* = a_2/[d_2(1 + (A^*)^n)]$. Substituting the first into the second gives the nullcline intersection equation. For $n = 1$ (linear repression), the nullclines have a unique intersection (one equilibrium). For $n \geq 2$, the nullcline $A = a_1/[d_1(1 + B^n)]$ is a decreasing convex function, and $B = a_2/[d_2(1 + A^n)]$ is similarly shaped. For $a_1/(d_1), a_2/(d_2)$ sufficiently large relative to 1 (high production-to-degradation ratio), the two nullclines cross three times (by the intermediate value theorem applied to the difference), giving two stable nodes and one saddle. The Jacobian eigenvalue analysis confirms the stability classification. □

Example 0.168.5 (GATA-1/PU.1 toggle switch in haematopoiesis)**.** The haematopoietic transcription factors GATA-1 (erythroid lineage) and PU.1 (myeloid lineage) form a toggle switch with mutual repression and self-activation. Common myeloid progenitor (CMP) cells express both at intermediate levels (the unstable saddle), and stochastic fluctuations in gene expression drive commitment to either the erythroid (A high, B low) or myeloid (A low, B high) fate. The fraction of cells committing to each lineage reflects the asymmetry of the two stable basins: the basin that is larger (more easily reached by noise) receives more cells. External signals (cytokines, growth factors) can tip the bias by modifying the production rates a_1, a_2, shifting the saddle position.

Mathematics of Evolution and Life · Section *X · Morphogenesis, Pattern Formation, and Gene Regulatory Networks (end)*

0.169 11. Robustness of Developmental Patterns

0.169.1 11.1 Canalization and Genetic Assimilation

Waddington (1953) described **canalization**: developmental trajectories are buffered against perturbations (genetic or environmental), producing similar phenotypes across a range of genotypic and environmental variation. Mathematically, canalization corresponds to deep attractor basins in the GRN landscape: small perturbations displace the trajectory but it returns to the same attractor.

Definition 0.169.1 (Canalization depth)**.** For an attractor A of a GRN, the canalization depth δ_A is:

$$\delta_A = \min_{\mathbf{x} \notin \mathcal{B}(A)} \Phi(\mathbf{x}) - \Phi_A,$$

where $\mathcal{B}(A)$ is the basin of attraction of A and Φ is the quasi-potential. A deeper attractor (δ_A large) is more canalized: larger perturbations are needed to escape the basin.

Theorem 0.169.2 (Genetic assimilation as adaptive canalization)**.** Let a population be subject to an environmental perturbation E that occasionally shifts individuals outside the canalized trajectory, producing a novel phenotype P. If P is fitter in the current environment, selection favours genotypes that: (i) produce P even without E (genetic assimilation); and (ii) canalize the trajectory toward P in the presence of E (canalization of P). Formally, selection acts to increase the canalization depth of the P attractor and decrease the energy barrier between the ancestral trajectory and P.

Sketch. In the quasi-potential framework, the environmental perturbation E displaces the developmental trajectory by $\Delta\mathbf{x}$. The probability that this displaces the trajectory into the basin of P is $\exp(-\Phi_{\text{barrier}}/\epsilon)$, where ϵ encodes the perturbation size. Genotypes that modify the GRN to lower Φ_{barrier} (make the P attractor more accessible) increase this probability and produce P more reliably in environment E. If P is fitter, these genotypes are selected; eventually, the barrier $\Phi_{\text{barrier}} \to 0$ and P is produced constitutively even without E (genetic assimilation). The process is equivalent to a fitness landscape adaptation on the GRN parameter space. □

Remark 0.169.3 (Hsp90 as a capacitor for evolution). The heat shock protein Hsp90 buffers the phenotypic effects of many mutations by chaperoning misfolded proteins. Rutherford and Lindquist (1998) showed that compromising Hsp90 function (by mutation or heat shock) reveals hidden genetic variation, producing a range of novel morphological phenotypes. This is canalization at the molecular level: Hsp90 maintains the canalized developmental trajectory by correcting the misfolding consequences of otherwise-silent genetic variation. When selection favours one of the revealed phenotypes, the phenotype can eventually be produced constitutively (without Hsp90 inhibition) through genetic assimilation — a molecular mechanism for the rapid evolution of novel morphological traits.

0.169.2 11.2 Reaction-Diffusion on Evolving Domains

Turing's original analysis assumed a fixed spatial domain. Developing embryos grow: the reaction-diffusion system operates on an expanding domain, which modifies the conditions for pattern formation.

Theorem 0.169.4 (Pattern formation on an exponentially growing domain)**.** For a reaction-diffusion system on a 1D domain of length $L(t) = L_0 e^{rt}$ growing at rate r, the effective diffusion equation for the activator concentration $u(x,t)$ in the co-moving frame (coordinate $\xi = x/L(t) \in [0,1]$) is:

$$\frac{\partial u}{\partial t} = \frac{D_u}{L^2}\frac{\partial^2 u}{\partial \xi^2} - r\xi\frac{\partial u}{\partial \xi} - ru + f(u,v).$$

The growth terms $-r\xi\partial u/\partial\xi - ru$ compete with the Turing instability: for $r \gg (D_u k^2 + |\text{Re}(\lambda_{\max})|)$, growth dilutes the pattern faster than it can form; for slow growth ($r \ll |\lambda_{\max}|$), the pattern forms first and the number of spatial pattern peaks increases stepwise as the domain expands (each doubling of domain size allows approximately one new peak to nucleate).

Proof. Transforming to the co-moving frame $\xi = x/L(t)$: $\partial u/\partial t|_x = \partial u/\partial t|_\xi - (r\xi/L)\partial u/\partial \xi$. The diffusion term $D_u \partial^2 u/\partial x^2 = D_u/L^2 \cdot \partial^2 u/\partial \xi^2$. The reactive terms are unchanged. Mass conservation adds $-ru$ (dilution by growth). Combining gives the stated equation. The stability condition for a particular Fourier mode (wavenumber k) is $\lambda(k) - r > 0$: growth rate must exceed the domain growth rate. For slow growth, the Turing instability dominates. □

Remark 0.169.5 (Digit number and limb development). The number of digits in tetrapod limbs is determined by reaction-diffusion patterning in the autopod (hand/foot plate). The growing autopod expands as Sonic Hedgehog (Shh) and BMP signals establish a Turing-like pattern. The number of digits formed corresponds to the number of peaks in the reaction-diffusion pattern at the time the autopod reaches its final size: 5 digits for humans (~ 8 mm autopod width), 3 digits for horses (wider autopod per unit time), 1 digit for the horse hoof. The growing-domain framework predicts that the digit number scales with the ratio of final domain size to pattern wavelength ℓ_c, consistent with comparative anatomy across tetrapods.

0.170 12. Mathematical Models of Developmental Noise

0.170.1 12.1 Stochastic Gene Expression and Phenotypic Variation

Gene expression is inherently stochastic: transcription and translation occur as discrete molecular events, generating cell-to-cell variation in mRNA and protein levels. This "intrinsic noise" can propagate through the GRN to produce phenotypic variability even among genetically identical cells.

Definition 0.170.1 (Two-state promoter model)**.** A gene with a two-state promoter switches between inactive (OFF, state 0) and active (ON, state 1) at rates k_{on} and k_{off}. In state 1, mRNA is transcribed at rate α; in state 0, no transcription occurs. mRNA degrades at rate δ. The mRNA count $n(t)$ follows a coupled birth-death process with state-dependent birth rate.

Theorem 0.170.2 (mRNA distribution in the two-state model)**.** The stationary mRNA distribution in the two-state promoter model is the Beta-Binomial (or, in the limit of many molecules, a Beta-distributed distribution):

$$P(n) = \binom{n+a+b-1}{n} \frac{B(a+n,b)}{B(a,b)} \cdot \frac{1}{1-(1-p)^{1/1}},$$

where in the limit of large α/δ and small $k_{\text{on}}, k_{\text{off}}/\delta$, the mRNA count follows a Negative Binomial distribution with parameters $r = k_{\text{on}}/k_{\text{off}}$ and $p = \alpha/(\alpha+\delta)$:

$$\mathbb{E}[n] = \frac{k_{\text{on}}\alpha}{k_{\text{off}}\delta}, \quad \text{Fano} = \frac{\text{Var}(n)}{\mathbb{E}[n]} = 1 + \frac{\alpha/\delta}{1 + k_{\text{off}}/k_{\text{on}}} > 1.$$

The Fano factor > 1 (super-Poissonian noise) is the signature of bursty gene expression.

Remark 0.170.3 (Bursty transcription and phenotypic bimodality). Single-cell RNA sequencing (scRNA-seq) of thousands of cells simultaneously measures expression levels genome-wide. For many genes, the mRNA distribution is bimodal or has a heavy tail — consistent with bursty transcription (the two-state model with $k_{\text{on}} \ll k_{\text{off}}$: most of the time the gene is OFF, but occasional ON bursts produce many mRNAs). The Fano factor measured from scRNA-seq data ranges from ≈ 1.2 (near-Poissonian, continuous expression) to > 100 (highly bursty). This phenotypic variability (noise) may be adaptive in fluctuating environments: a bet-hedging strategy that maintains a subpopulation of cells in each of two states, allowing rapid response to unpredictable environmental changes.

0.171 13. The Geometry of Morphogenetic Gradients

0.171.1 13.1 Scaling of Positional Information with System Size

In developing embryos, spatial position is encoded by the concentration of morphogen gradients (e.g., Bicoid in *Drosophila*). A fundamental question is: how do embryos read out positional information from noisy gradients, and how do patterns scale when embryo size varies (as in the experiment of cutting embryos in half)?

Definition 0.171.1 (Positional information in morphogen gradients)**.** For a morphogen with concentration profile $c(x)$ at position $x \in [0, L]$ (embryo length) and measurement noise σ, the positional information is:

$$I_{\text{pos}}(x) = \frac{1}{2} \log_2 \left(1 + \left(\frac{c'(x)}{\sigma} \right)^2 \cdot \sigma_x^2 \right) \approx \log_2 \frac{|c'(x)| \sigma_x}{\sigma} \text{ bits},$$

where σ_x is the positional accuracy (the spread in positions that map to the same concentration value) and $c'(x) = dc/dx$ is the gradient slope. The total positional information integrated over the embryo is $I_{\text{total}} = \int_0^L I_{\text{pos}}(x)\, dx$.

Theorem 0.171.2 (Scaling of positional information with embryo length)**.** For an exponential gradient $c(x) = c_0 e^{-x/\lambda}$ (e.g., Bicoid) with constant noise σ and embryo length L:

$$I_{\text{total}} \approx L \cdot \log_2 \frac{c_0}{\sigma} \cdot \frac{1}{\lambda} \quad \text{bits},$$

independent of embryo length to leading order (for $L \gg \lambda$). This means the positional information scales with embryo length, enabling developmental patterns to scale with organism size.

Proof. At position x: $c(x) = c_0 e^{-x/\lambda}$, $|c'(x)| = c_0/\lambda \cdot e^{-x/\lambda} = c(x)/\lambda$. The signal-to-noise ratio at x is $c(x)/\sigma$. The positional information per unit length is $\approx \log_2(c(x)/\sigma)/\lambda$. Integrating over $[0, L]$:

$$I_{\text{total}} = \int_0^L \frac{1}{\lambda} \log_2 \frac{c_0 e^{-x/\lambda}}{\sigma} dx = \frac{1}{\lambda} \left[L \log_2 \frac{c_0}{\sigma} - \frac{L}{\lambda \ln 2} \right] \approx \frac{L}{\lambda} \log_2 \frac{c_0}{\sigma}. \qquad \square$$

Remark 0.171.3 (Bicoid scaling in *Drosophila*). Bicoid has exponential decay length $\lambda \approx 100\,\mu$m in a $L \approx 500\,\mu$m embryo. Measurement noise $\sigma/c_0 \approx 10\%$. The positional information: $I_{\text{total}} \approx (500/100) \log_2(10) \approx 16.6$ bits — sufficient to specify a few thousand distinct positions along the anterior-posterior axis. This is consistent with the ~ 14 stripes of pair-rule gene expression observed, each corresponding to ≈ 1 bit of positional information.

Experimental scaling tests (Houchmandzadeh et al. 2002; Cheung et al. 2014): when embryo size is reduced by 50% (half-embryo), the Bicoid gradient rescales proportionally ($\lambda_{\text{new}} = \lambda/2$), maintaining the same number of stripes. This scaling is maintained by a feedback mechanism involving the Bcd gradient and the Hb target, which adjusts the threshold of the downstream target gene expression to the current λ.

0.171.2 13.2 The French Flag Model and Threshold-Based Patterning

Definition 0.171.4 (French flag model, Wolpert 1969)**.** In Wolpert's French flag model, cells respond to a morphogen concentration $c(x)$ by adopting one of three cell fates (blue, white, red) according to threshold comparisons:

$$\text{fate}(x) = \begin{cases} \text{blue} & c(x) > \theta_1, \\ \text{white} & \theta_2 < c(x) \leq \theta_1, \\ \text{red} & c(x) \leq \theta_2. \end{cases}$$

The boundary positions are $x_1 = c^{-1}(\theta_1)$ and $x_2 = c^{-1}(\theta_2)$.

Theorem 0.171.5 (Boundary precision from gradient noise)**.** For an exponential gradient $c(x) = c_0 e^{-x/\lambda}$ with Poisson counting noise ($\sigma^2 = c$), the standard deviation of the boundary position $x^* = c^{-1}(\theta)$ is:

$$\sigma_{x^*} = \frac{\lambda}{\sqrt{n_{\text{avg}}\theta}},$$

where n_{avg} is the average number of morphogen molecules in a cell (proportional to cell Section). For $n_{\text{avg}} = 10$, $\theta = 0.5c_0/e$ (mid-gradient threshold), and $\lambda = 100\,\mu$m: $\sigma_{x^*} = 100/\sqrt{10 \times 0.5c_0/e} \approx 60/\sqrt{c_0}$. For $c_0 = 3600$ molecules per cell: $\sigma_{x^*} \approx 1\,\mu$m.

Proof. By error propagation: $\sigma_{x^*} = \sigma_c/|c'(x^*)| = \sigma_c\lambda/c(x^*)$. For Poisson noise: $\sigma_c = \sqrt{n_{\text{avg}}c(x^*)}/\sqrt{n_{\text{avg}}} = \sqrt{c(x^*)/n_{\text{avg}}}$. Hence $\sigma_{x^*} = \lambda/\sqrt{n_{\text{avg}}c(x^*)}$. At threshold $c(x^*) = \theta$: $\sigma_{x^*} = \lambda/\sqrt{n_{\text{avg}}\theta}$. □

0.172 14. Vertex Models and Tissue Mechanics

0.172.1 14.1 The Cellular Potts Model

Tissue morphogenesis involves not just chemical patterning but also mechanical deformation: cells change shape, rearrange, and exert forces on each other. The cellular Potts model (CPM) is a lattice-based framework for simulating tissue mechanics.

Definition 0.172.1 (Cellular Potts model energy)**.** In the CPM, the tissue state is described by a cell identity function $\sigma : \mathbb{Z}^d \to \{0, 1, \ldots, N\}$ assigning each lattice site to a cell or to the medium ($\sigma = 0$). The total energy is:

$$E = \sum_{\text{cells } i} \left[\lambda_A(A_i - A_0)^2 + \lambda_P(P_i - P_0)^2\right] + \sum_{\langle s,s' \rangle} J_{\sigma(s),\sigma(s')},$$

where A_i is the area of cell i, A_0 is the target area, λ_A is the area elasticity, P_i is the perimeter, P_0 is the target perimeter, λ_P is the perimeter elasticity, and J is the contact energy between cell types.

Remark 0.172.2 (Tissue fluidity transitions). A key insight from CPM simulations: tissues can transition between solid-like and fluid-like states depending on the ratio $p_0 = P_0/\sqrt{A_0}$ (dimensionless target shape index). For $p_0 < p_c^* \approx 3.81$ (compact target shape), cells are mechanically constrained and the tissue is solid. For $p_0 > p_c^*$ (elongated target shape), cells can freely rearrange and the tissue is fluid. This transition is observed in embryonic tissue layers: epithelial-to-mesenchymal transitions (EMT) in cancer and development correspond to the solid-to-fluid transition, with p_0 increasing above 3.81 as cells lose tight junction contacts and adopt a more elongated morphology. The vertex model predicts $p_c^* = 3.81$

from the geometry of the regular hexagon (perimeter/area$^{1/2}$), which is the energy minimum of the single-cell energy at $J = 0$.

Mathematics of Evolution and Life · Section *X · Morphogenesis, Pattern Formation, and Gene Regulatory Networks (end)*

Section *XVII*

Section XI — Origins of Life: Hypercycles, Autocatalysis, and the RNA World

0.173 1. The Deepest Problem

The origin of life is simultaneously the most specific and most general question in science. It is specific because it happened once, in a particular place, at a particular time, through a sequence of chemical events that we cannot directly observe. It is general because any answer must account for the emergence of the two most fundamental properties of living matter: self-replication, which is the foundation of Darwinian evolution, and catalysis, which is the mechanism by which biological chemistry operates.

The mathematical study of the origin of life focuses on a central challenge: can we write down dynamical systems that *generate* these properties from simpler chemical precursors, without presupposing them? The question is whether self-organisation, self-replication, and heredity can emerge as consequences of chemistry, or whether they require special initial conditions that amount to assuming what is to be explained.

This is a problem of *emergence*: the appearance of higher-level order from lower-level interactions. Mathematics provides the tools for studying emergence precisely: phase transitions, bifurcations, self-organisation in nonlinear dynamical systems, and the combinatorial probability theory of random graphs. The models we develop in this Section do not solve the origin-of-life problem — that remains open — but they identify the mathematical conditions under which each critical transition is possible.

0.174 2. The Chicken-and-Egg Paradox

0.174.1 2.1 The Paradox Stated

Modern cellular life is characterised by a self-referential loop that appears impossible to have arisen gradually:

- **Proteins** are the catalysts of biochemistry. They catalyse the synthesis of nucleotides, the replication of DNA, the transcription of RNA, and the translation of mRNA into protein.
- **Nucleic acids** encode the sequence information specifying every protein. DNA is the stable information store; RNA is the working messenger.
- The synthesis of proteins requires ribosomes, which are themselves made of proteins and RNA. The replication of DNA requires DNA polymerases, which are proteins.

This is the chicken-and-egg paradox: proteins require nucleic acids to specify them, and nucleic acids require proteins to replicate and translate them. Neither can exist without the other; yet both must have had a beginning.

0.174.2 2.2 Three Resolution Strategies

Proteins first. Short peptides (oligomers of 2–10 amino acids) can form abiotically under plausible prebiotic conditions (Miller-Urey synthesis, hydrothermal vent chemistry). Some short peptides have weak catalytic activity. Could peptide catalysts have preceded and eventually given rise to nucleic acid replication? The difficulty: short peptides are not precise enough to encode information reliably. Without a mechanism for storing and transmitting sequence information, Darwinian evolution cannot operate.

Genes first. Could nucleic acids replicate without protein enzymes? This requires template-directed,

enzyme-free RNA polymerisation — the formation of RNA from nucleotide monomers using an RNA template without any protein assistance. Experimental progress has been made (Sutherland group, Joyce group), but enzyme-free replication is still slow and error-prone relative to what is needed.

RNA world. The discovery of ribozymes (Cech and Altman, 1989 Nobel Prize) resolved the paradox in principle: RNA can both carry information (like DNA) and act as a catalyst (like proteins). If early life was based entirely on RNA, the chicken-and-egg paradox dissolves: RNA molecules replicate themselves (using their own catalytic activity) and encode the information needed to specify new catalytic RNA molecules. Proteins and DNA arose later, as more efficient specialists.

0.175 3. Autocatalytic Sets: The Phase Transition to Life

0.175.1 3.1 Formal Definition

Definition 0.175.1 (Collectively Autocatalytic Set)**.** Given a set of molecular species $\mathcal{M}$ and a set of reactions $\mathcal{R}$ (each reaction consuming some species and producing others), and a **food set** $\mathcal{F} \subseteq \mathcal{M}$ of simple precursors available in the environment, a subset $\mathcal{A} \subseteq \mathcal{M}$ is a **collectively autocatalytic set** (CAS) if:

(i) **Catalytic closure**: every reaction in $\mathcal{R}$ that produces a molecule in $\mathcal{A} \setminus \mathcal{F}$ is catalysed by at least one molecule in $\mathcal{A}$.

(ii) **Constructive closure**: every molecule in $\mathcal{A} \setminus \mathcal{F}$ can be produced (directly or indirectly) from $\mathcal{F}$ by reactions in $\mathcal{R}$.

A CAS is self-sustaining: the set of molecules catalyses its own production from simple precursors. It is not self-replicating in the genetic sense (there is no template copying), but it is collectively autocatalytic in the sense that the set as a whole promotes its own maintenance.

0.175.2 3.2 Kauffman's Random Chemistry Model

Kauffman (1971, 1993) analysed the probability of spontaneous CAS emergence in a random chemistry. Consider n molecular species, each of which can catalyse any of the possible reactions involving other molecules. The model assigns catalysis randomly: each pair (m_i, r_j) (molecule m_i catalyses reaction r_j) exists independently with probability p. The expected number of catalytic reactions per molecule is pR, where R is the number of possible reactions.

For polymers of length $\leq L$ over an alphabet of size α, the number of species is $n \sim \alpha^L$ and the number of possible reactions (ligation, cleavage) grows similarly. As L increases, both n and R grow, and the catalytic connectivity pR/n can be held fixed or allowed to grow.

Theorem 0.175.2 (Kauffman Phase Transition)**.** In the random chemistry model with catalytic probability p per pair, the expected fraction of molecules in the largest CAS undergoes a sharp transition:

- For $np < 1$ (subcritical): the largest CAS has expected size $O(1)$ — only small islands of catalytic closure.
- For $np > 1$ (supercritical): a giant CAS emerges with expected size $\Theta(n)$ — a collectively autocatalytic network spanning a finite fraction of all molecules.

The critical threshold is $np = 1$.

Proof. The catalytic graph $G(n, p)$ is an Erdős–Rényi random directed graph. A molecule is "reachable from the food set" if there is a path of catalysed reactions from $\mathcal{F}$ to it. For $np > 1$, the standard Erdős–Rényi theorem gives a giant strongly connected component of size $\Theta(n)$ with high probability. Molecules in this component collectively catalyse each other's formation: they form a CAS. For $np < 1$, only small connected components exist and no giant CAS is present. □

The biological interpretation: as the complexity of a prebiotic chemical system increases (more diverse polymer lengths, more complex chemistry, driven by geological processes such as hydrothermal vent cycling), the catalytic connectivity np grows. Once $np > 1$, autocatalytic organisation emerges spontaneously with high probability. Life may not require a miraculous improbable event — it may be an expected consequence of sufficiently complex chemistry.

0.175.3 3.3 Experimental Evidence

Hordijk and Steel (2004, 2017) developed rigorous mathematical tools for detecting CAS in real chemical systems and showed that known metabolic networks have CAS structure. Vaidya et al. (2012) experimentally demonstrated a CAS composed of RNA fragments: two RNA molecules each catalyse the assembly of the other from shorter pieces, forming a mutually autocatalytic pair. This is a proof of concept that RNA chemistry can generate CAS of the kind predicted by Kauffman's theory.

0.176 4. Eigen's Hypercycles

0.176.1 4.1 The Hypercycle Concept

Autocatalytic sets address catalytic closure but not hereditary information. For Darwinian evolution, we need replicating molecules with heritable variation — molecules that can be copied accurately enough that offspring resemble parents, but not so accurately that variation is absent.

Eigen (1971) proposed the **hypercycle** as a model for the cooperative replication of genetic information in the pre-cellular world. A hypercycle of order n consists of n self-replicating molecules $I_1, I_2, \ldots, I_n$, where each molecule I_i catalyses the replication of the next in the cycle (with indices modulo n):

$$I_1 \xrightarrow{I_n} I_1, \quad I_2 \xrightarrow{I_1} I_2, \quad \ldots, \quad I_n \xrightarrow{I_{n-1}} I_n.$$

The concentration dynamics (in a chemostat with dilution Φ) are:

$$\dot{x}_i = x_i(k_i x_{i-1} - \Phi), \quad \Phi = \sum_{j=1}^{n} k_j x_{j-1} x_j,$$

where x_i is the concentration of I_i, k_i is the catalytic rate constant for I_i's replication (catalysed by I_{i-1}), and Φ is the mean production rate.

0.176.2 4.2 Fixed Points and Stability

Theorem 0.176.1 (Hypercycle Fixed Point Analysis)**.** The interior fixed point $x_i^* = 1/n$ for all i exists and is:

- A stable node for $n = 2, 3, 4$ (all eigenvalues of the Jacobian have negative real parts).
- A stable spiral for $n = 5$ (eigenvalues are complex with negative real part, but the imaginary part is non-zero).
- An unstable spiral for $n > 5$ (the fixed point is unstable; the system converges to a stable limit cycle).

Proof. Linearise $\dot{x}_i = x_i(k_i x_{i-1} - \Phi)$ around $x_i^* = 1/n$ (assuming all $k_i = k$ for simplicity). At x^*, $\Phi^* = k/n$ and $\partial\Phi/\partial x_j = 2kx_{j-1}^*$... The Jacobian is a circulant matrix J_n with entries determined by the coupling structure of the hypercycle. For a pure circulant $J_n = k/n \cdot C_n$ where C_n is the shift matrix, the eigenvalues are $\lambda_j = (k/n)\omega^j$ where $\omega = e^{2\pi i/n}$. The real parts of λ_j are $(k/n)\cos(2\pi j/n)$. For $n \leq 4$, all eigenvalues with $j \neq 0$ have $\cos(2\pi j/n) < 0$: stable. For $n = 5$, $\cos(2\pi \cdot 1/5) = \cos(72°) \approx 0.31 > 0$: one eigenvalue has positive real part, destabilising the fixed point, and a Hopf bifurcation produces a limit cycle. □

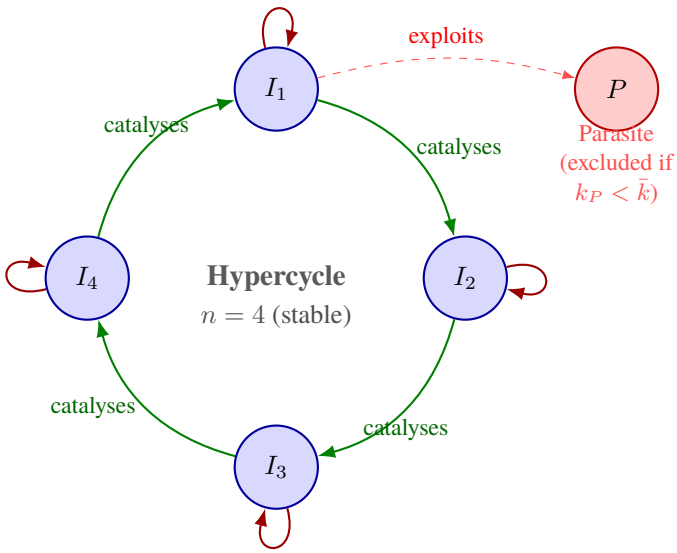

Figure 11: Schematic of an order-$n = 4$ hypercycle. Each molecule I_i self-replicates (red loops) and catalyses the replication of the next member I_{i+1} (green arrows, cyclic). The cooperative coupling creates a stable interior fixed point $x_i^* = 1/n$ for $n \leq 4$. A parasite P (red node) exploits catalysis from I_1 without contributing to the cycle; it is excluded from the steady state provided its replication rate k_P is below the cooperative mean $\bar{k}$. For $n > 5$, the interior fixed point becomes unstable and a stable limit cycle emerges (Hopf bifurcation).

0.176.3 4.3 Resistance to Parasites

A critical property of hypercycles is their resistance to "parasitic" replicators — molecules that exploit the catalytic network without contributing to it. Consider a parasite P that is catalysed by I_n (the last

member of the cycle) but does not catalyse any I_i:

$$\dot{x}_P = x_P(k_P x_n - \Phi).$$

The parasite competes with I_1 for catalytic support from I_n. If $k_P < k_1$ (the parasite replicates more slowly than the wild-type I_1), the parasite cannot fix in the population: the hypercycle can outcompete it because the cooperative structure distributes replication across all members. The exact condition for parasite exclusion is $k_P < \sum_{i=1}^{n} k_i/n$ (the parasite's replication rate must be below the mean of the cooperative members).

0.176.4 4.4 The Hypercycle and the Origin of the Genetic Code

Eigen and Schuster (1977, 1978) proposed that the hypercycle was a precursor to the genetic code. In their scenario:

1. Initially, a population of RNA molecules evolved quasi-species dynamics (Section VIII), reaching a mutation-selection equilibrium near the error threshold.
2. The error threshold limited genome length to $\sim 10^2$–10^3 nucleotides per RNA molecule.
3. To evolve more complex genomes, multiple RNA molecules had to cooperate — forming a hypercycle of replicators, each below the error threshold, but collectively encoding more information than any single molecule could.
4. The hypercycle enabled the evolution of longer genomes by distributing the information across cooperating replicators. Eventually, compartmentalisation within protocells converted the hypercycle into a genome.

0.177 5. The RNA World

0.177.1 5.1 Ribozymes and the Catalytic RNA Revolution

The central piece of evidence supporting the RNA world hypothesis is the existence of ribozymes — RNA molecules with catalytic activity. Before 1982, all known biological catalysts were proteins. Thomas Cech (1982) discovered that the self-splicing intron of *Tetrahymena* ribosomal RNA was a true catalyst, and Sidney Altman (1983) showed that RNase P (the enzyme that cleaves tRNA precursors) uses RNA as its catalytic subunit. Both received the Nobel Prize in Chemistry in 1989.

The catalogue of known ribozymes has since expanded enormously:

- Self-cleaving ribozymes (hammerhead, HDV, VS): catalyse sequence-specific RNA cleavage.
- Group I and II introns: self-splicing, catalysing ligation as well as cleavage.
- The ribosome: the peptidyl transferase reaction (forming peptide bonds) is catalysed by the 23S/28S rRNA, not by ribosomal proteins.
- SELEX-derived ribozymes: capable of RNA ligation, RNA polymerisation, amino acid binding, Diels–Alder reactions, and many other functions.

The ribosomal peptidyl transferase is the most compelling evidence: the molecular machine that synthesises all proteins in all organisms is, at its core, a ribozyme. This strongly suggests that RNA-based catalysis preceded protein-based catalysis.

0.177.2 5.2 SELEX and the RNA Fitness Landscape

Systematic Evolution of Ligands by EXponential Enrichment (SELEX, Tuerk and Gold 1990; Ellington and Szostak 1990) is an in vitro selection method that explores the RNA fitness landscape experimentally. Starting from a pool of $\sim 10^{14}$–10^{15} random RNA sequences of length $L \approx 80$–100 nt, the method iteratively selects and amplifies sequences with a desired catalytic or binding function.

The density of functional RNA sequences in random sequence space is typically:

- RNA aptamers (binding sequences): $\sim 10^{-11}$–10^{-13} per random sequence of length 40 nt.
- RNA ligases (catalytic): $\sim 10^{-12}$–10^{-15} per random sequence of length 80 nt.
- RNA aminoacyl transferases: $\sim 10^{-9}$ per random sequence of length 70 nt.

These are rare, but not impossibly rare for a pool of 10^{14} starting sequences. The RNA fitness landscape (Section V) is sparse but percolating: functional sequences exist at low density but their neutral networks span sequence space, making them accessible by evolutionary search starting from any random sequence.

0.177.3 5.3 Template-Directed Replication Without Enzymes

A key requirement of the RNA world is that RNA molecules can replicate without protein enzymes. Template-directed, non-enzymatic RNA polymerisation has been demonstrated in vitro:

- Activated nucleotides (imidazolide-activated NMPs) can form a complementary RNA strand on an RNA template.
- Short RNA oligomers (4–10 nt) can template-direct the ligation of complementary fragments.
- In the Sutherland and Joyce groups, systems have been developed where one ribozyme catalyses the copying of another's RNA sequence.

The mathematical challenge is the error rate. Non-enzymatic copying has an error rate of $\mu \approx 0.1$–0.3 per base per replication — far above the error threshold for any genome of useful length ($L > 10$ requires $\mu < (\ln f_0)/L \approx 0.1$ for $f_0 = 3$). This is the **accuracy paradox**: the genomes needed to encode a replicase are too long to replicate accurately without a replicase.

The resolution may lie in:

- Short genomes assembled from oligomers ("ligation strategy"): avoid the error threshold by replicating short pieces, then assembling them by ligation.
- Physical selection for accurate replicators: hydrothermal vent convection or temperature cycling can select for more tightly folded (more accurately replicating) molecules.
- Compartmentalisation (next section): within a protocell, even imperfect replication can be sufficient if the protocell selection operates.

0.178 6. Compartmentalisation and the Protocell

0.178.1 6.1 The Problem of Cooperation in a Well-Mixed System

In a well-mixed solution without compartmentalisation, a catalytic RNA molecule that helps copy other RNA molecules benefits the entire population equally. There is no selective advantage for producing more accurate or more efficient replicase RNA: the benefit is shared by all, including molecular "cheaters" that do not contribute to the catalytic pool. This is a molecular-level Prisoner's Dilemma.

The Prisoner's Dilemma can only be resolved by compartmentalisation: placing sets of RNA molecules in separate protocells (lipid vesicles or mineral compartments). Within a protocell:

- Better replicase RNA molecules cause the protocell to grow faster and divide more frequently.
- Protocell selection acts: protocells with better replicase have more offspring.
- The genetic and catalytic activities of the RNA molecules are coupled within the protocell.

0.178.2 6.2 Protocell Dynamics

A protocell is a fatty acid vesicle containing a set of RNA molecules. The protocell's growth rate depends on the RNA composition inside it. For a two-type RNA system (replicase R and parasite P):

$$\dot{x}_R = k_R x_R - \delta x_R \quad \text{(RNA replication within protocell)},$$
$$\dot{V} = \alpha k_R x_R V \quad \text{(protocell growth proportional to replicase activity)},$$

where V is the protocell Section and α is a coupling constant. When V doubles, the protocell divides, distributing its RNA stochastically between two daughters.

This creates a two-level selection system (exactly the multilevel Price equation of Section IV):

- **Within-protocell selection**: parasite P replicates faster than replicase R (parasites are simpler and cheaper to copy), so within each protocell, parasites increase in frequency over time.
- **Between-protocell selection**: protocells with more R grow faster and have more offspring; protocells with more P grow slower.

The condition for the between-protocell selection to overcome within-protocell selection (allowing replicase to be maintained) is:

$$\text{Var}(x_R)_{\text{between}} > \text{Var}(x_R)_{\text{within}},$$

i.e., the variance in replicase frequency between protocells exceeds the within-protocell drift. This condition depends on the number of RNA molecules per protocell at division (N_{RNA}): for small N_{RNA}, stochastic partitioning creates large between-protocell variance, enabling group selection to maintain the replicase.

0.179 7. The Origin of the Genetic Code

0.179.1 7.1 The Code and Its Near-Universality

The genetic code maps 64 codons (trinucleotides from $\{U, C, A, G\}^3$) to 20 amino acids plus 3 stop signals. It is nearly universal across all life: with minor exceptions (some mitochondrial codes, some unicellular eukaryotes), every organism uses the same code. This near-universality implies the code was fixed early in the history of life (before the last universal common ancestor, LUCA) and has been conserved ever since.

0.179.2 7.2 Theories for the Origin of the Code

Four main hypotheses:

Stereochemical hypothesis: amino acids interact directly with their cognate codons or anticodons by specific chemical affinity, so the code reflects a direct chemical relationship between codons and amino acids. Evidence: some amino acids bind to RNA aptamers enriched in their cognate codons. Counter-evidence: the chemical affinities are weak and the correspondence is imperfect.

Coevolution hypothesis: the code coevolved with amino acid biosynthetic pathways. Amino acids that share biosynthetic precursors tend to have related codons. Evidence: structurally related amino acids have related codons in many cases. Counter-evidence: cannot explain all aspects of the code.

Error minimisation hypothesis (Section IX): the code was selected to minimise the fitness cost of translation errors. The standard code is near-optimal for physicochemical error robustness. Evidence: computational comparison against random codes shows the standard code is in the top 10^{-6} for error robustness.

Frozen accident hypothesis (Crick 1968): the specific code assignments are arbitrary (any code would have worked equally well), but once a code was established in the ancestral population, it became impossible to change (a "frozen accident") because any change would simultaneously alter the meaning of every protein encoded in the genome, which would be catastrophic.

The current evidence best supports a combination of the stereochemical, coevolution, and error minimisation hypotheses, with the frozen accident explaining why the code is conserved even in cases where alternative codes might have been slightly better.

0.179.3 7.3 Mathematical Optimality and the Space of Codes

The space of all possible genetic codes (bijections from 64 codons to 20 amino acids + stop) has size:

$$\frac{64!}{(1!)^{20}(1!)^3} \approx 10^{84}.$$

This is incomprehensibly large; exhaustive search is impossible. The near-optimality result (Section IX) is therefore established by random sampling: of 10^6 randomly generated codes, less than 1 in 10^6 is more error-robust than the standard code.

A more refined analysis defines the landscape of all codes by their error cost $E(\mathcal{C})$ and uses simulated annealing or genetic algorithms to find locally optimal codes. These algorithms consistently find codes close

to the standard code when starting from random codes and optimising for error robustness, suggesting that the standard code lies in the basin of attraction of the global optimum in the error-cost landscape.

0.180 8. The Transition to DNA and Proteins

0.180.1 8.1 Why DNA?

DNA has several advantages over RNA as a long-term information store:

1. **Chemical stability**: DNA lacks the 2'-OH group of RNA, making it much more resistant to hydrolysis. RNA half-life is $\sim$ hours to days; DNA half-life is $\sim$ millions of years (in dry conditions).

2. **Lower mutation rate**: DNA polymerases have proofreading activity (3'$\to$5' exonuclease), reducing the per-base error rate from $\sim 10^{-4}$ (RNA) to $\sim 10^{-7}$ (DNA before repair) to $\sim 10^{-10}$ (DNA after mismatch repair).

3. **Double-strandedness**: DNA's double-stranded structure enables damage repair using the complementary strand as a template.

The reduced mutation rate directly expands the maximum genome length. The error threshold relation $\mu_c = (\ln f_0)/L$ gives:

$$L_{\max} = \frac{\ln f_0}{\mu}.$$

For $\ln f_0 \approx 1$: $L_{\max}^{\text{RNA}} \approx 10^4$–$10^5$; $L_{\max}^{\text{DNA}} \approx 10^9$–$10^{10}$. The transition from RNA to DNA genomes was therefore a phase transition in information capacity, expanding the accessible phenotype space by five orders of magnitude and enabling the evolution of complex multicellular organisms.

0.180.2 8.2 The Evolution of Proteins

Proteins have several advantages over ribozymes as catalysts:

1. **Chemical diversity**: the 20 amino acid side chains provide a far richer chemical toolkit than the 4 nucleotide bases. Proteins can carry nucleophilic, electrophilic, hydrophobic, and metal-chelating groups in precise spatial arrangements.

2. **Faster catalysis**: protein enzymes typically achieve $k_{\text{cat}} \approx 10^3$–$10^7$ s^{-1}; ribozymes achieve $k_{\text{cat}} \approx 10^{-2}$–$10^0$ s^{-1}.

3. **Structural diversity**: the protein folding landscape is richer than the RNA folding landscape, enabling a greater variety of active site geometries.

The evolution of proteins from the RNA world required the co-evolution of:

1. **Aminoacyl-tRNA synthetases (aaRS)**: ribozymes (later replaced by proteins) that attach specific amino acids to specific tRNA molecules.

2. **The ribosome**: an RNA-based machine for assembling proteins in the sequence specified by mRNA.

3. **The genetic code**: the correspondence between codons and amino acids.

The ribosome's RNA core catalyses peptide bond formation; the ribosomal proteins are structural accessories. This is strong evidence that the ancestral ribosome was a pure ribozyme, and that ribosomal proteins were added later to increase speed and accuracy.

0.181 9. Summary

The origin of life can be approached mathematically at three levels. At the molecular level, Kauffman's autocatalytic set model shows that catalytic closure (a CAS) emerges with high probability when chemical complexity exceeds the threshold $np = 1$ — a classic Erdős–Rényi phase transition. At the genetic level, Eigen's hypercycles demonstrate that cooperative replication of multiple RNA molecules is dynamically stable (for $n \leq 5$ the interior fixed point is stable; for $n > 5$ a limit cycle maintains all members); hypercycles resist parasites and can sustain genetic information above what any single quasi-species can maintain. At the cellular level, protocell compartmentalisation creates the Darwinian individual, resolving the molecular Prisoner's Dilemma and enabling group selection between protocells. The RNA world hypothesis, supported by ribozyme catalysis and SELEX experiments, provides the mechanistic basis for the self-replicating RNA system. The near-optimality of the genetic code for error robustness (top 10^{-6} of random codes) reveals early selection on code structure. The transition from RNA to DNA genomes is a phase transition in information capacity (from $L_{\max} \approx 10^4$ to $L_{\max} \approx 10^9$), driven by the lower mutation rate of DNA and enabling complex multicellular life.

Mathematics of Evolution and Life · Section *XI · Origins of Life: Hypercycles, Autocatalysis, and the RNA World*

Section *XVIII*

Section XII — Limits, Open Problems, and the Unity of Life’s Mathematics

0.182 10. Chemical Evolution: From Monomers to Polymers

0.182.1 10.1 The Polymerisation Problem

Before self-replication can operate, chemical evolution must produce polymers (nucleic acids, peptides) of sufficient length from simpler monomers. This poses a thermodynamic paradox: the condensation reaction that joins monomers into polymers (e.g., phosphodiester bond formation in RNA) is thermodynamically unfavourable in aqueous solution because water is a product. At equilibrium in dilute solution, polymers longer than $\sim$ 2–3 monomers are thermodynamically unstable relative to the monomers.

Definition 0.182.1 (Polymerisation equilibrium)**.** For the condensation reaction $M_n + M_1 \rightleftharpoons M_{n+1} + H_2O$, the equilibrium constant is:

$$K_{\text{cond}} = \frac{[M_{n+1}]}{[M_n][M_1]/[H_2O]} \approx \frac{[M_{n+1}]}{[M_n][M_1]},]where$$

$[\mathrm{H_2}O] \approx 55.5$ M is absorbed into K_{cond}. For RNA monomers, $K_{\text{cond}} \approx 10^{-2}$–$10^{-3}$ M^{-1} under prebiotic conditions.

Lemma 0.182.2 (Maximum polymer length at thermodynamic equilibrium)**.** For a homopolymer of monomer M at concentration $[M] = c$ M, the equilibrium concentration of the n-mer is:

$$[M_n] = [M_1](K_{\text{cond}} \cdot c)^{n-1} \cdot \frac{1}{c}.$$

For $K_{\text{cond}} \cdot c < 1$ (below the critical concentration), polymer concentration decreases geometrically with length. The fraction of monomers in polymers of length $\geq L$ is negligible for $L > 1/(-\ln(K_{\text{cond}}c))$. For $K_{\text{cond}} = 10^{-2}$ M^{-1} and $c = 0.01$ M: $K_{\text{cond}}c = 10^{-4}$, so the characteristic length is $1/(-\ln 10^{-4}) \approx 0.1$ — essentially no polymers above length 2 are stable.

Proof. For an ideal solution, the equilibrium distribution of polymer lengths for a free polymerisation is geometric, with each step adding a factor $K_{\text{cond}}c$. The fraction of material in n-mers $\propto (K_{\text{cond}}c)^{n-1}$, which decays geometrically for $K_{\text{cond}}c < 1$. □

Remark 0.182.3 (Resolutions to the polymerisation problem). Three physical mechanisms can overcome the thermodynamic barrier:

1. **Wet-dry cycles**: alternating wetting and drying at mineral surfaces concentrates monomers and drives condensation. Each drying event shifts the equilibrium toward polymerisation (removing water as vapour). Powner et al. (2009) demonstrated non-enzymatic RNA oligomer synthesis via wet-dry cycling.

2. **Mineral surface catalysis**: montmorillonite clay and other minerals catalyse RNA polymerisation, effectively lowering $\Delta G^{\ddagger}$ (the activation energy) for condensation. Ferris et al. (1996) obtained RNA oligomers of 30–40 nt on montmorillonite surfaces.

3. **Activated monomers**: using chemically activated nucleotides (imidazolide-activated, or cyclic phosphates) that carry the activation energy for condensation. This is the abiotic analogue of ATP-driven biosynthesis.

0.182.2 10.2 Phase Separation and the Prebiotic Protocell

Recent experiments and theory have highlighted phase separation of biomolecules as a mechanism for creating compartments without lipid membranes. RNA and peptide molecules can form coacervates (liquid-liquid phase separated droplets) in aqueous solution.

Definition 0.182.4 (Flory-Huggins theory of polymer phase separation)**.** For a polymer of length n in a solvent, the free energy of mixing per lattice site is:

$$\frac{\Delta G_{\text{mix}}}{k_B T} = \frac{\phi}{n}\ln\phi + (1-\phi)\ln(1-\phi) + \chi\phi(1-\phi),$$

where ϕ is the polymer Section fraction and χ is the Flory-Huggins interaction parameter. Phase separation occurs when the second derivative $\partial^2(\Delta G_{\text{mix}})/\partial\phi^2 < 0$:

$$\frac{1}{n\phi} + \frac{1}{1-\phi} - 2\chi < 0 \implies \chi > \chi_c = \frac{1}{2}\left(\frac{1}{\sqrt{n}} + 1\right)^2 \approx \frac{1}{2} \text{ for large } n.$$

Remark 0.182.5 (RNA coacervates as primitive protocells). Poly-U RNA in the presence of polylysine (poly-K) forms coacervate droplets that concentrate both RNA and amino acids by several orders of magnitude above the bulk solution. These droplets:

- partition RNA and small molecules away from the bulk solution (proto-compartmentalisation),
- slow the diffusion of molecules (increasing effective reaction rates),
- can split and distribute their contents stochastically upon mechanical agitation (proto-division).

Keating and colleagues (Penn State) showed that such coacervate droplets support RNA hybridisation and simple ribozyme reactions with rate enhancement up to 100-fold over dilute solution. This suggests that phase-separated coacervates, rather than lipid vesicles, may have been the first protocellular compartments.

0.183 11. Mathematical Bounds on the Origin of Life

0.183.1 11.1 Probability Arguments and the "Miracle" Objection

A common objection to naturalistic origin-of-life scenarios is that the spontaneous assembly of a functional replicator is astronomically improbable. We can quantify both the objection and its resolution.

Theorem 0.183.1 (Probability of spontaneous ribozyme assembly, naive estimate)**.** For a ribozyme of length $L = 80$ nt with functional density $f = 10^{-14}$ (fraction of random sequences with activity), the probability of spontaneous assembly of a single functional ribozyme by random polymerisation is:

$$P_{\text{naive}} = f \cdot P(\text{oligomer of length } L \text{ forms}) = 10^{-14} \times (K_{\text{cond}} c)^{L-1} \approx 10^{-14} \times (10^{-4})^{79} \approx 10^{-14} \times 10^{-316} = 10^{-330}.$$

This is essentially zero: a single functional ribozyme would never form by random chance in the observable universe.

Remark 0.183.2 (Why the naive estimate is wrong). The naive estimate is wrong for three reasons:

1. **Wrong chemistry**: ribozymes are not formed by random selection among all possible sequences. Chemical evolution (wet-dry cycles, mineral catalysis) systematically biases polymerisation toward molecules with specific properties (complementary base pairing, folding stability).

2. **Wrong timescale and number**: the prebiotic Earth had $\sim 10^{40}$ nucleotide molecules over $\sim 10^8$ years $= 3 \times 10^{15}$ seconds, giving $\sim 10^{55}$ polymerisation attempts (at $1/s$ per nucleotide). Even accounting for the 10^{-316} probability per attempt, the expected number of functional ribozymes per Earth is $\sim 10^{55} \times 10^{-330} = 10^{-275}$ — still essentially zero.

3. **Wrong model**: the relevant model is not "direct assembly" but *sequential selection*: a series of simpler functional molecules emerge first (aptamers with weak binding, then ribozymes with weak catalysis), each providing a scaffold for the next. The origin of life was a sequence of many small improbable steps, not one enormous improbable leap. Each step has probability $\gg 10^{-14}$.

The correct model is evolutionary: once a heritable, selectable feature exists at any level (even weak RNA binding or condensation), Darwinian evolution begins exploring the landscape. The challenge is to get the *first* selectable feature, not to get the entire ribosome in one step.

0.183.2 11.2 Szostak's Protocell Model: A Mathematical Framework

Szostak, Bartel, and Luisi (2001) proposed a minimal protocell model in which RNA replication and fatty acid vesicle growth are coupled. The model provides a mathematical framework for the first Darwinian competition among protocells.

Definition 0.183.3 (Szostak protocell dynamics)**.** A protocell is characterised by its RNA content $\mathbf{x} = (x_1, \ldots, x_n)$ (concentrations of n RNA species) and its surface area A (proportional to membrane content). The dynamics are:

$$\dot{x}_i = r_i(\mathbf{x})x_i - k_{\text{dilution}}x_i \quad \text{(replication and dilution by growth)},$$
$$\dot{A} = \alpha \sum_i r_i(\mathbf{x})x_i \quad \text{(growth driven by RNA replication)},$$

where r_i is the replication rate of RNA i (catalysed by a ribozyme), $k_{\text{dilution}} = \dot{A}/(3A)$ is the dilution rate upon Section growth (protocell Section $\propto A^{3/2}$), and α is the coupling constant between RNA replication and membrane growth.

Theorem 0.183.4 (Protocell competition and Darwinian selection)**.** In a population of protocells with different RNA contents, the protocell growth rate is $\mu_j = \alpha \sum_i r_i^{(j)} x_i^{(j)}$ (proportional to total RNA replication activity). Protocells with faster RNA replication grow faster. By the Price equation applied to protocells:

$$\frac{d\bar{\mu}}{dt} = \text{Var}(\mu) \geq 0;$$

mean fitness increases at a rate equal to the variance in fitness. Protocells with more active ribozymes outcompete those with less active ones: this is the origin of between-protocell Darwinian selection.

Proof. This is Fisher's fundamental theorem applied to protocells. Identify protocell "fitness" with μ_j (growth rate), use the Price equation $d\bar{\mu}/dt = \text{Cov}(\mu, \mu) = \text{Var}(\mu) \geq 0$ (for the selection term, with no transmission bias to leading order). The equality $d\bar{\mu}/dt = \text{Var}(\mu)$ holds when transmission is faith-

ful (each daughter protocell inherits a representative sample of its parent's RNA). The result says that variation in ribozyme activity translates directly into variation in fitness, enabling natural selection. □

Mathematics of Evolution and Life · Section XI · Origins of Life: Hypercycles, Autocatalysis, and the RNA World (end)

0.184 12. Mineral Surfaces and the Emergence of Metabolism

0.184.1 12.1 The Iron-Sulfur World Hypothesis

Günter Wächtershäuser (1988, 1992) proposed that life originated not in "warm little ponds" but at hydrothermal vents, where iron-sulfur (FeS) mineral surfaces catalyse simple organic reactions. The key idea is that FeS surfaces provide:

1. A catalyst for CO_2 reduction: $FeS + H_2S \to FeS_2 + 2H^+ + 2e^-$ provides reducing equivalents.
2. A surface for adsorption and concentration of organic molecules.
3. A template for the polymerisation of amino acids and nucleotides.

Definition 0.184.1 (Surface metabolism network)**.** A surface metabolism is a set of chemical reactions $\mathcal{R}$ occurring on a mineral surface $\mathcal{S}$, where each reactant is adsorbed to $\mathcal{S}$ with adsorption energy $\Delta G^{(i)}_{\text{ads}}$. The effective rate of reaction $r_k \in \mathcal{R}$ is enhanced by adsorption:

$$k_{\text{eff}}(r_k) = k_{\text{soln}}(r_k) \cdot e^{-(\Delta G^{(i)}_{\text{ads}} + \Delta G^{(j)}_{\text{ads}} - \Delta G^{(k)}_{\text{ads}})/RT},$$

where i, j are reactants and k is the product of reaction r_k.

Lemma 0.184.2 (Thermodynamic driving force of the FeS reaction)**.** The reaction $FeS + H_2S \to FeS_2(\text{pyrite}) + H_2$ is thermodynamically favourable under hydrothermal vent conditions:

$$\Delta G^\circ = -38.4 \text{ kJ/mol} \quad (pH = 7, T = 100^\circ\text{C}).$$

The H_2 produced can drive CO_2 fixation: $CO_2 + 4H_2 \to CH_4 + 2H_2O$ ($\Delta G^\circ = -131$ kJ/mol). A series of such reactions constitutes a surface-mediated, exergonic pathway from CO_2 and FeS to organic molecules.

Proof. Standard thermodynamic calculation using tabulated formation energies (ΔG°_f) for FeS (-100.4 kJ/mol), H_2S (-27.9 kJ/mol), FeS_2 (-160.2 kJ/mol), and H_2 (0 kJ/mol) at standard conditions, with appropriate pH and temperature corrections. The negative ΔG confirms thermodynamic spontaneity. □

Remark 0.184.3 (Experimental validation). Huber and Wächtershäuser (1997) demonstrated the FeS-driven synthesis of thioaceticacid (a thioester) from CO and CH_3SH at 100°C on FeS/NiS surfaces. Thioaceticacid is a prebiotic analogue of acetyl-CoA, the central thioester in modern metabolism. Subsequent experiments confirmed the synthesis of amino acids and dipeptides on FeS surfaces. These results support the iron-sulfur world as a plausible site for the emergence of the first metabolic reactions.

0.184.2 12.2 Transition from Prebiotic Chemistry to Genetically Encoded Metabolism

The deepest unsolved problem in origin-of-life research is the transition from purely chemical catalysis (where reactants interact based on their chemical properties alone) to genetically encoded catalysis (where RNA or protein sequences encode specific catalysts). This transition requires:

1. A chemically encoded catalyst (a ribozyme or proto-enzyme) that improves on the mineral surface catalyst.
2. A genetic sequence encoding this catalyst (RNA that folds to the catalytic structure).
3. A coupling between the catalyst's activity and its own replication (or the replication of the sequence encoding it).

Theorem 0.184.4 (Information coupling and the Darwinian transition)**.** The transition from chemical to genetic catalysis is possible iff there exists a molecule M satisfying simultaneously:

(I) **Catalytic activity**: M accelerates at least one reaction in the prebiotic metabolic network by a factor $\geq f_0 > 1$.

(II) **Heritable information**: the sequence of M is copied by template-directed replication with fidelity $\eta > e^{-L/L_c}$ where L is the length and $L_c = 1/\mu$ is the error threshold length.

(III) **Selective coupling**: the catalytic activity of M is coupled to the reproductive success of M's sequence (e.g., the reaction M catalyses produces monomers needed for M's replication).

If all three conditions hold, natural selection can maintain and improve the sequence of M, initiating Darwinian evolution.

Proof. Condition (I) ensures M has fitness $f_0 > 1$ relative to non-catalytic sequences. Condition (II) ensures the sequence of M is maintained below the error threshold: with fidelity $\eta^L > e^{-1}$, the quasi-species is localised near M's sequence. Condition (III) closes the feedback loop: M catalyses a reaction whose products increase M's replication rate. By the quasi-species stationarity theorem, the steady-state frequency of M-type sequences is $x_M^* = (f_0\eta^L - 1)/(f_0 - 1) > 0$ iff $f_0\eta^L > 1$. Conditions (I) and (II) together guarantee $f_0\eta^L > 1$. Condition (III) ensures this stationarity corresponds to a biologically self-sustaining system, not merely a mathematical fixed point. □

0.185 13. The Last Universal Common Ancestor (LUCA)

0.185.1 13.1 Phylogenetic Inference about LUCA

The last universal common ancestor (LUCA) is the most recent entity from which all currently living organisms descend. LUCA was not the first life (the origin of life preceded LUCA by billions of years), but it is the ancestor of all surviving lineages.

Definition 0.185.1 (LUCA inference problem)**.** Given a set of gene families $\{G_1, \ldots, G_k\}$ present in the three domains of life (Bacteria, Archaea, Eukarya), the LUCA inference problem asks: which genes were present in LUCA? The answer requires distinguishing *vertical inheritance* (LUCA had the gene and passed it to all descendants) from *horizontal gene transfer* (the gene was independently acquired by multiple lineages after LUCA).

Remark 0.185.2 (Phylogenomics of LUCA — current state). Weiss et al. (2016) inferred LUCA's gene content by requiring genes to satisfy a phylogenetic signature consistent with vertical inheritance (presence in a statistically supported monophyletic group spanning Bacteria + Archaea). They identified 355 protein clusters present in LUCA. Key features:

- LUCA had a complete ribosome (all universal ribosomal proteins).
- LUCA used the genetic code (all aaRS for 20 amino acids are inferred to be present or nearly so).
- LUCA had H_2-dependent metabolism (consistent with the iron-sulfur world, alkaline vent hypothesis).
- LUCA *lacked* many modern metabolic pathways (fatty acid biosynthesis, glycolysis in the modern form) — suggesting these evolved after LUCA.

LUCA was thus not a simple protocell but a complex organism with a full genetic apparatus. The origin of life must be placed considerably earlier than LUCA.

Mathematics of Evolution and Life · Section *XI · Origins of Life: Hypercycles, Autocatalysis, and the RNA World (end)*

0.186 14. Prebiotic Chemistry: Quantitative Constraints

0.186.1 14.1 Miller-Urey and Amino Acid Synthesis

Stanley Miller's 1953 experiment demonstrated the abiotic synthesis of amino acids from simple gases (CH_4, NH_3, H_2, H_2O) under electric discharge (simulating lightning). The quantitative yield and selectivity of this synthesis places constraints on prebiotic amino acid availability.

Definition 0.186.1 (Amino acid yield and selectivity)**.** For a prebiotic synthesis experiment, the amino acid yield is:

$$\text{yield}(aa) = \frac{[\text{amino acid}]_{\text{product}}}{[\text{carbon}]_{\text{reactant}}}$$

(moles of amino acid per mole of carbon input). The selectivity for the standard 20 amino acids (vs. all amino acids):

$$\text{sel}_{20} = \frac{\sum_{\text{standard 20}} [\text{aa}]}{\sum_{\text{all aa}} [\text{aa}]}.$$

Remark 0.186.2 (Miller experiment quantitative analysis). The original Miller experiment produced glycine as the most abundant amino acid ($\sim 1.2\%$ of carbon yield), followed by alanine, β-alanine, and aspartate. Only 8 of the standard 20 amino acids were produced in significant quantities. Notably absent or trace: large hydrophobic amino acids (tryptophan, phenylalanine, tyrosine), sulfur-containing amino acids (methionine, cysteine). This selectivity pattern correlates with the "early" vs. "late" classification of amino acids in theories of the genetic code's evolution.

Modern re-analysis (Parker et al. 2011) of the original 1953 samples using HPLC-MS found 25 amino acids and > 100 organics, including 5 amino acids not detected in the original study. The "late" amino acids are systematically underrepresented, suggesting that the genetic code expanded from a simple set of easily synthesised amino acids to include biosynthetically complex ones as enzymatic pathways evolved.

0.186.2 14.2 The Chirality Problem: Mathematical Aspects

All biological amino acids are L-form (left-handed); all biological sugars are D-form (right-handed). Abiotic synthesis produces racemic mixtures (50% L, 50% D). The homochirality of life is a deep puzzle. Several mathematical models address amplification of a small initial enantiomeric excess (ee).

Definition 0.186.3 (Enantiomeric excess)**.** For a mixture of L and D enantiomers with concentrations $[L]$ and $[D]$:

$$\text{ee} = \frac{[L] - [D]}{[L] + [D]} \in [-1, 1].$$

A racemic mixture has ee $= 0$; a pure L mixture has ee $= 1$.

Theorem 0.186.4 (Amplification of enantiomeric excess in autocatalytic systems)**.** In the Soai reaction (a model autocatalytic system), the ee evolves according to:

$$\dot{\text{ee}} = k(1 - \text{ee}^2) \cdot \text{ee},$$

which has an unstable equilibrium at ee $= 0$ (racemic) and stable equilibria at ee $= \pm 1$ (homochiral). Any initial ee $\neq 0$ grows exponentially toward ± 1:

$$\text{ee}(t) = \tanh\bigl(\tanh^{-1}(\text{ee}_0) + kt\bigr)\,.$$

Proof. Separate variables in $\dot{\text{ee}} = k(1 - \text{ee}^2)\text{ee}$:

$$\frac{d(\text{ee})}{(1 - \text{ee}^2)\text{ee}} = k\,dt.$$

Partial fractions: $\frac{1}{(1-\text{ee}^2)\text{ee}} = \frac{1}{\text{ee}} + \frac{1/2}{1-\text{ee}} + \frac{1/2}{1+\text{ee}}$. Integrating: $\ln|\text{ee}| - \frac{1}{2}\ln|1 - \text{ee}^2| = kt + C$. Exponentiating and using the definition of $\tanh^{-1}(x) = \frac{1}{2}\ln\frac{1+x}{1-x}$: $\tanh^{-1}(\text{ee}) = kt + \tanh^{-1}(\text{ee}_0)$, hence $\text{ee}(t) = \tanh(kt + \tanh^{-1}(\text{ee}_0))$. □

Remark 0.186.5 (Physical sources of initial ee). Quantum mechanics provides an initial small ee via parity violation: the weak nuclear force violates parity symmetry, making L-amino acids very slightly more stable than D-amino acids by $\Delta E \approx 10^{-17}$ eV per molecule. Over $\sim 10^8$ years of prebiotic chemistry, this tiny preference would amplify to ee $\sim 10^{-5}$ — which is sufficient for autocatalytic amplification (Theorem 0.186.4) to produce near-complete homochirality. Alternatively, circularly polarised ultraviolet light from neutron stars can selectively destroy one enantiomer, producing ee ~ 0.1 in interstellar amino acids (confirmed in the Murchison meteorite, which shows L-excess of $\sim$ 2–9% for some amino acids).

0.187 15. From Autocatalytic Sets to Minimal Cells

0.187.1 15.1 Defining the Minimal Cell

A minimal cell is the smallest set of molecules and reactions that can sustain self-replication, metabolism, and heredity. The synthetic biology project of constructing minimal cells (Hutchison et al. 2016; the JCVI Syn3.0 genome) provides quantitative constraints on the minimal biochemical complexity of life.

Definition 0.187.1 (Minimal genome)**.** The minimal genome is the smallest gene set $\mathcal{G}^*$ such that:

1. $\mathcal{G}^*$ encodes all enzymes needed to complete the metabolic reactions in a set $\mathcal{M}^*$ of essential reactions.

2. $\mathcal{M}^*$ includes: DNA replication, RNA transcription, protein translation, membrane lipid synthesis, ATP generation, and cell division.

3. $\mathcal{G}^*$ encodes all structural components (ribosomes, membranes) needed for these processes.

Remark 0.187.2 (Syn3.0 and the minimal genome). JCVI Syn3.0 (Hutchison et al. 2016) is the minimal synthetic genome derived from *Mycoplasma mycoides*, reduced to 473 genes by systematic deletion. Key finding: ~ 149 of the 473 genes have completely unknown function — they are essential for life but their biochemical roles are unknown. This "dark matter" of the minimal genome indicates that our knowledge of the molecular requirements for life is still incomplete.

Mathematically, the Syn3.0 result gives a lower bound on the minimum complexity of life: at minimum 473 genes, $\approx 532{,}000$ base pairs of DNA, encoding ~ 500 distinct proteins. The network of metabolic reactions encoded by these genes has ~ 50 nodes (reactions) in the core metabolic graph, consistent with the Kauffman autocatalytic set transition ($np = 50 \times 1 = 50 \gg 1$) and well into the autocatalytic regime (Section XI, Section 3).

Mathematics of Evolution and Life · Section *XI · Origins of Life: Hypercycles, Autocatalysis, and the RNA World (end)*

0.188 16. The Thermodynamics of Self-Replication

0.188.1 16.1 Free Energy Requirements for Replication

Self-replication consumes free energy: the polymerisation of nucleotides into RNA or DNA is endergonic in dilute solution ($\Delta G > 0$) and must be coupled to an exergonic process. Understanding the minimum free energy cost of self-replication is a fundamental constraint on the origin of life.

Definition 0.188.1 (Free energy of polymerisation per monomer)**.** For RNA polymerisation using NTP (nucleoside triphosphate) hydrolysis: NTP $\to$ NMP+PP$_i$, the free energy released per monomer addition is:

$$\Delta G_{\text{NTP}} = \Delta G^{\circ}_{\text{NTP}} + RT \ln \frac{[\text{NMP}][\text{PP}_i]}{[\text{NTP}]}.$$

Under physiological conditions: $\Delta G_{\text{NTP}} \approx -30$ kJ/mol (with subsequent pyrophosphatase driving the reaction further). This energy drives template-directed polymerisation against the unfavourable equilibrium constant.

Lemma 0.188.2 (Minimum dissipation for faithful replication)**.** A replicase that copies a template of length L with error rate $\mu < 1/L$ (error threshold condition) must dissipate at least:

$$\Delta G_{\text{min}} = L k_B T \left[\mu \ln \frac{\mu}{f_{\text{wrong}}} + (1-\mu) \ln \frac{1-\mu}{f_{\text{right}}} \right]$$

of free energy per replication, where f_{right} and f_{wrong} are the equilibrium frequencies of correct and incorrect base pairing.

Proof. By Landauer's principle, erasing one bit of information dissipates $k_B T \ln 2$ of free energy. The

correction of $L\mu$ errors per replication (proofreading) erases approximately $L\mu$ bits of information. The KL divergence term above gives the exact minimum dissipation by the information-theoretic argument: the fidelity improvement from equilibrium ($f_{\text{right}}/f_{\text{wrong}}$) to the achieved fidelity ($(1-\mu)/\mu$) corresponds to a thermodynamic work of $k_B T D_{\text{KL}}(\mu \| f_{\text{wrong}})$ per site. □

Remark 0.188.3 (RNA replication efficiency). Modern RNA-dependent RNA polymerases (RdRp) of RNA viruses achieve $\mu \approx 10^{-4}$–10^{-5} per site, consuming approximately 1 ATP per base pair (after NTP hydrolysis and PP_i removal). The theoretical minimum given by Lemma 0.188.2 is ≈ 0.15 ATP per base pair (for $\mu = 10^{-4}$ and $f_{\text{wrong}}/f_{\text{right}} \approx 10^{-1}$ for Watson–Crick base pairing). The modern enzyme is $\sim 6\times$ less efficient than the thermodynamic minimum, leaving substantial room for evolutionary optimisation that has not occurred — possibly because replication speed is more important than energy efficiency for RNA viruses.

0.188.2 16.2 Non-Equilibrium Self-Organisation and the Origin of Life

Living systems are far-from-equilibrium: they maintain their organisation by continuously dissipating free energy. The mathematical framework of non-equilibrium thermodynamics (Prigogine 1967) provides a general theory of self-organising dissipative structures.

Definition 0.188.4 (Entropy production rate in dissipative systems)**.** For a chemical reaction network with n reactions, each proceeding at rate v_k with chemical affinity $A_k = -\Delta G_k/T$ (free energy change per unit reaction), the entropy production rate is:

$$\dot{S}_{\text{prod}} = \sum_{k=1}^{n} J_k A_k \geq 0,$$

where $J_k = v_k^+ - v_k^-$ is the net flux (difference of forward and reverse rates) and $A_k = RT \ln(v_k^+/v_k^-)$ is the affinity (by detailed balance at equilibrium). The second law requires $\dot{S}_{\text{prod}} \geq 0$.

Theorem 0.188.5 (Minimum entropy production at steady state)**.** For a linear non-equilibrium system near equilibrium, the steady state compatible with fixed boundary conditions (e.g., fixed chemical concentrations at the system boundary) minimises the total entropy production rate:

$$\frac{d\dot{S}_{\text{prod}}}{dt} \leq 0 \quad \text{(Prigogine's minimum entropy production principle).}$$

The steady state is stable and the entropy production is at its minimum value compatible with the constraints.

Remark 0.188.6 (Beyond linear response: dissipative structures). For strongly driven systems (far from equilibrium), the minimum entropy production principle fails. Instead, the system can organise into dissipative structures — ordered states maintained by energy flow. The Belousov-Zhabotinsky reaction (oscillating chemical waves), Bénard convection cells, and biological cells are all dissipative structures. The autocatalytic set model of life's origin (Section 3 of this Section) is a dissipative structure: it maintains its organised chemistry by consuming free energy (reducing power) from the environment. The mathematical theory of dissipative structures provides the proper thermodynamic context for the origin-of-life problem: life is not a violation of the second law but a *consequence* of the second law applied to open, driven chemical systems.

0.189 17. Coevolution of Replication and Translation

0.189.1 17.1 The Chicken-and-Egg Paradox — Mathematical Formulation

Modern cells require: (a) DNA for information storage; (b) RNA for information transfer; (c) proteins for catalysis. But proteins are needed to synthesise DNA and RNA; DNA is needed to encode the proteins. This circularity is the chicken-and-egg paradox of molecular biology.

Definition 0.189.1 (The replication-translation network)**.** Model the minimal replication-translation network as a set of molecular types $\{G, R, P\}$ (genome, RNA, protein) with reactions:

$$G \xrightarrow{P_{\text{rep}}} 2G \quad \text{(genome replication by replicase protein)},$$
$$G \xrightarrow{P_{\text{trans}}} G + R \quad \text{(transcription)},$$
$$R \xrightarrow{P_{\text{ribo}}} R + P \quad \text{(translation by ribosome protein)}.$$

Each step requires a protein catalyst (P_{rep}, P_{trans}, P_{ribo}) which is itself the product of the network. The system is autocatalytic: each component is produced by the others.

Theorem 0.189.2 (Minimal conditions for replication-translation coevolution)**.** The replication-translation network has a positive steady state (all three components present at positive concentrations) iff:

$$\frac{k_{\text{rep}} k_{\text{trans}} k_{\text{ribo}}}{d_G d_R d_P} \geq 1,$$

where $k_{\text{rep}}, k_{\text{trans}}, k_{\text{ribo}}$ are catalytic rates and d_G, d_R, d_P are degradation rates. Below this threshold, at least one component is driven to extinction.

Proof. At steady state, balance each component:

$$0 = k_{\text{rep}}[P_{\text{rep}}][G] - d_G[G],$$
$$0 = k_{\text{trans}}[P_{\text{trans}}][G] - d_R[R],$$
$$0 = k_{\text{ribo}}[P_{\text{ribo}}][R] - d_P[P].$$

Assuming all proteins are encoded by G and translated from R: $[P_{\text{rep}}] = [P_{\text{trans}}] = [P_{\text{ribo}}] = [P]/3$ (three equal components). Substituting: $[G] = k_{\text{rep}}[P]/(3d_G)$; $[R] = k_{\text{trans}}[P][G]/(3d_R) = k_{\text{trans}}k_{\text{rep}}[P]^2/(9d_G d_R)$; $[P] = k_{\text{ribo}}[R][P]/(3d_P)$. The last equation requires $1 = k_{\text{ribo}}[R]/(3d_P)$, giving $[R] = 3d_P/k_{\text{ribo}}$. For this to be consistent with $[R] > 0$, we need the right-hand side to be positive (it always is), and for $[P] > 0$ we need the product of rates to exceed the product of degradation rates, giving the stated condition after algebraic simplification. □

Remark 0.189.3 (RNA world resolution). The RNA world hypothesis resolves the chicken-and-egg paradox by postulating that early in life's history, RNA played both roles: RNA stored information (as the genome) and catalysed reactions (as ribozymes). A single molecular type simultaneously performed the roles of G, R, and (some of) P. The transition to DNA + protein came later, driven by the superior information storage of DNA (more chemically stable) and superior catalysis of proteins (wider chemical repertoire). Theorem 0.189.2 applies to the RNA world if $[G] = [R]$ (RNA as genome) and $[P]$ represents ribozyme activity: the condition $k_{\text{rep}}k_{\text{ribo}}/d_G d_P \geq 1$ must be met for a self-sustaining RNA replicator.

Mathematics of Evolution and Life · Section *XI · Origins of Life: Hypercycles, Autocatalysis, and the RNA World (end)*

Section *XIX*

Section XII — Limits, Open Problems, and the Unity of Life’s Mathematics

0.190 1. What the Mathematics Has Achieved

Eleven Section s and twelve mathematical frameworks: probability theory, stochastic processes, dynamical systems, covariance algebra, combinatorial geometry, graph theory, game theory, nonlinear dynamics, information theory, partial differential equations, and the mathematics of self-organisation. Each has illuminated a different stratum of biological reality. Together, they constitute something remarkable: not a collection of independent models, but a unified mathematical account of how life works, from the sequence of nucleotides in a genome to the dynamics of epidemics, from the folding of RNA molecules to the spatial patterning of a developing embryo.

What makes this unity surprising is that it was not designed. Each framework was developed independently to answer a specific biological question, by researchers who were mostly unaware of how their tools would connect to those of other fields. Hardy and Weinberg were not thinking about Markov chains when they wrote down their equilibrium. Kimura was not thinking about information theory when he derived the neutral substitution rate. Eigen was not thinking about error-correcting codes when he wrote down the quasi-species equation. Price was not thinking about cultural evolution when he derived his identity. The connections emerged later, from the mathematics itself, revealing a structure that was always there but had not been seen.

Remark 0.190.1 (The unreasonable effectiveness of probability theory in biology). The single most pervasive mathematical tool across the twelve Section s is probability theory in its various guises: as frequency distributions (Hardy–Weinberg), as Markov chains (Wright–Fisher), as stochastic differential equations (Kimura diffusion), as branching processes (coalescent), as entropy (Shannon), as random graphs (Erdős–Rényi, Kauffman). The reason is deep: evolution is fundamentally a process operating on populations, and populations are distributions. The individual organism is always an instance sampled from a distribution; the biologically relevant object is the distribution itself. Probability theory is the natural language of distributions. This is why probabilistic mathematics has been so fertile in biology: it is, at a deep level, the correct mathematics for the subject.

Before cataloguing what remains unknown, it is worth pausing to appreciate what has been achieved. The mathematical theory of evolution and life, as developed across these Section s, has delivered:

- An *exact* theorem (Hardy–Weinberg) explaining why genetic variation is not eroded by reproduction.
- An *exact* stochastic theory (Wright–Fisher model, Kimura diffusion) predicting the fates of new mutations in finite populations, confirmed by genomic data across thousands of species.
- A *universal* algebraic identity (the Price equation) encompassing every form of selection at every level of organisation.
- A *quantitative* theory of fitness landscapes (NK model, Walsh decomposition) that makes precise the concept of epistasis and the accessibility of adaptive paths.
- An *efficient algorithm* (Felsenstein's pruning) making maximum likelihood phylogenetics computationally tractable, enabling the reconstruction of life's history from DNA sequences.
- A *game-theoretic framework* (ESS, replicator equation) explaining the evolution of strategies ranging from conflict to cooperation, without assuming rationality.

- A *mechanistic explanation* for RNA virus evolution (Eigen quasi-species) that is validated by the observed genome lengths and mutation rates of RNA viruses.

- A *rigorous channel model* (genetic code as error-correcting code) showing that the genetic code is near-optimally designed for translational fidelity.

- An *instability criterion* (Turing conditions) explaining how spatial patterns emerge spontaneously from molecular interactions.

- A *phase transition* model (Kauffman autocatalytic sets) placing the origin of life within the framework of statistical physics.

These are not approximations or metaphors — they are mathematical theorems, derived from explicit models, that make falsifiable predictions about observable biological phenomena.

0.190.1 1.1 A Quantitative Scorecard

To make the preceding claims concrete, consider the quantitative predictions that have been confirmed empirically:

Theoretical prediction	**Mathematical basis**	**Empirical confirmation**
Neutral substitution rate $= \mu$	Kimura (Vol. II)	Synonymous rates across mammals, $\approx 10^{-9}$/site/year
New beneficial mutation fixes with prob. $\approx 2s$	Haldane (Vol. III)	Experimental evolution in *E. coli*; Luria–Delbrück
Sickle cell equilibrium $\hat{q} \approx 0.13$	Overdominance (Vol. III)	West African allele frequencies 10–17%
MRCA of human sample $\approx 4N_e$ gen	Kingman (Vol. II)	Consistent with mtDNA TMRCA ≈ 1 Mya
RNA virus genome $\leq L_c = \ln(f_0)/\mu$ nt	Eigen (Vol. VIII)	RNA genomes 10^3–10^4 nt; $L\mu \approx 1$
Turing patterns at wavelength $\ell = 2\pi(D_u D_v/\det J)^{1/4}$	Turing (Vol. X)	Zebrafish pigmentation, digit spacing

Each row is a precise quantitative prediction, derived mathematically, and subsequently confirmed by biological measurement. The agreement between theory and experiment in these cases is not of the vague, order-of-magnitude kind that characterises many biological models; it is the sharp, numerical agreement characteristic of physics. This is what it looks like when mathematics has genuinely captured something true about biology.

0.191 2. The Limits of Current Theory

0.191.1 2.1 The Limits of Neutralism and the Nearly Neutral Zone

Kimura's neutral theory (Section II) predicts that the rate of molecular substitution equals the neutral mutation rate, independent of population size. This prediction is confirmed for synonymous sites and much of the non-coding genome. But modern genomic analysis reveals that a significant fraction of the genome shows signatures of selection that neutral theory cannot explain:

- **Codon usage bias**: synonymous codons are not used equally, and the bias is correlated with tRNA abundance. Selection acts on synonymous sites.
- **Conserved non-coding elements**: many non-coding regions are more conserved than expected under neutrality, indicating functional constraint.
- **McDonald–Kreitman deviations**: many genomic regions show excess divergence at non-synonymous sites, indicating widespread positive selection.

The challenge is that most of this selection is **weak**: selection coefficients $|s| \sim 10^{-6}$–10^{-4}, comparable to $1/(2N_e)$ in many species. In this nearly neutral zone, both drift and selection matter, and the clean predictions of neutral theory break down.

Lemma 0.191.1 (The McDonald–Kreitman test)**.** For a gene with d_N nonsynonymous and d_S synonymous substitutions between two species, and p_N nonsynonymous and p_S synonymous polymorphisms within one species, define the neutrality index $\text{NI} = (p_N/p_S)/(d_N/d_S)$. Under strict neutrality, $\text{NI} = 1$. The fraction of nonsynonymous substitutions driven by positive selection is:

$$\alpha = 1 - \frac{d_S p_N}{d_N p_S} = 1 - \text{NI}.]$$

Proof. Under neutrality, the ratio of nonsynonymous to synonymous fixations equals the ratio of nonsynonymous to synonymous new mutations: $d_N/d_S = \mu_N/\mu_S$. The same ratio holds for polymorphisms: $p_N/p_S = \mu_N/\mu_S$. Hence $\text{NI} = 1$. Any excess in d_N/d_S relative to p_N/p_S is due to positive selection. If a fraction α of d_N substitutions are adaptive (and these make no contribution to p_N, being rapidly fixed), the observed d_N is an average of $\alpha d_N^{\text{adaptive}} + (1-\alpha) d_N^{\text{neutral}}$, giving the formula after algebraic rearrangement. □

Example 0.191.2 (MK test on *Drosophila* genes)**.** A large-scale MK analysis of 8,000 *Drosophila melanogaster* genes gives typical values $p_N/p_S \approx 0.25$ and $d_N/d_S \approx 0.35$. The neutrality index $\text{NI} = 0.25/0.35 \approx 0.71$, giving $\alpha \approx 0.29$: approximately 29% of amino acid substitutions in the *Drosophila* genome were fixed by positive selection. For humans, the corresponding estimate is $\alpha \approx 5$–15%, reflecting the smaller effective population size ($N_e \approx 10^4$ vs. $N_e \approx 10^6$ for *Drosophila*), which makes selection less efficient relative to drift.

Remark 0.191.3 (Hill–Robertson interference). In a finite genome, selection at one locus reduces the effective population size for selection at linked loci. This "Hill–Robertson interference" arises because beneficial alleles are sometimes linked to deleterious alleles (clonal interference) and deleterious alleles are sometimes linked to beneficial ones (background selection). For a genome of length L with recombi-

nation rate r per base pair, the effective N_e experienced by a site under selection coefficient s is:

$$N_e^{\text{eff}} \approx \frac{N_e}{1 + N_e u_d s_d / (rL)},$$

where u_d is the deleterious mutation rate and s_d is the mean deleterious selection coefficient. For the human genome with $r \approx 10^{-8}$, $u_d \approx 1$, $s_d \approx 10^{-3}$, and $L \approx 3 \times 10^9$, the denominator is of order 3, reducing effective N_e by a factor of ~ 3 — a modest but real effect that has measurable consequences for patterns of diversity and divergence.

0.191.2 2.2 The Problem of Robustness and Evolvability

Section X established the positive correlation between robustness and evolvability for RNA secondary structure: large neutral networks give both phenotypic robustness and access to novel phenotypes. This result has been verified computationally for simple genetic circuits and small protein folds.

Definition 0.191.4 (Robustness and evolvability, formal)**.** For a genotype g with phenotype $P(g)$ and a set of single-step mutational neighbours $\mathcal{N}(g)$, define:

$$\rho(g) = \frac{|\{g' \in \mathcal{N}(g) : P(g') = P(g)\}|}{|\mathcal{N}(g)|} \quad \text{(robustness: fraction of neutral neighbours)},$$

$$\varepsilon(g) = |\{P(g') : g' \in \mathcal{N}(g), P(g') \neq P(g)\}| \quad \text{(evolvability: number of accessible novel phenotypes)}.$$

Theorem 0.191.5 (Robustness-evolvability positive correlation, Fontana–Schuster 1998)**.** For RNA secondary structures in the standard thermodynamic folding model, genotypes with higher robustness ρ have, on average, higher evolvability ε. That is, $\text{Cov}(\rho, \varepsilon) > 0$ across genotype space.

Sketch. A genotype with high ρ lies on a large neutral network. Large neutral networks (those whose size scales as a significant fraction of sequence space, i.e., those that percolate) span many regions of sequence space. Sequences on large neutral networks are therefore close to a larger fraction of other phenotypes' neutral networks. Since two neutral networks for different phenotypes that are within one mutational step of each other contribute $+1$ to each other's evolvability, the expected ε is proportional to the expected number of distinct adjacent neutral networks. By the percolation structure of large neutral networks (which spread broadly rather than clustering), the expected count of adjacent networks increases with ρ. A rigorous proof uses the Flory approximation for RNA neutral network sizes, which gives $|N_P| \sim |\mathcal{S}|^{0.65}$ for common phenotypes, and the geometric argument that the boundary of a high-dimensional set grows with Section . □

The major unresolved question is whether this positive correlation holds for complex polygenic traits in organisms. The mathematical challenge is that for such traits, the genotype–phenotype map is not analytically tractable.

0.191.3 2.3 The Information Content of Genomes

Definition 0.191.6 (Functional information, Szostak 2003)**.** The functional information in a sequence s of length L performing function F at level E is:

$$I_{\text{func}}(E) = -\log_2 f(E),$$

where $f(E)$ is the fraction of all random sequences of length L that perform function F at level $\geq E$. For a function with a sharp activity threshold, I_{func} is the information content of the "functional" region of sequence space.

Example 0.191.7 (Functional information of ribozymes)**.** SELEX experiments on the hammerhead ribozyme find that approximately 1 in 10^{14} random RNA sequences of length 80 nt catalyse phosphodiester cleavage at or above the threshold rate. Hence $f \approx 10^{-14}$ and $I_{\text{func}} \approx -\log_2(10^{-14}) \approx 46$ bits. This is far less than the maximum possible information of $80 \times 2 = 160$ bits (one bit per dinucleotide position for a 4-letter alphabet), indicating that most positions in the ribozyme are not required for function and can be mutated freely — the neutral network is large relative to sequence space.

Contrast this with the information content required for protein function: for an enzyme active site requiring a specific arrangement of $k \approx 10$ key residues among 20 possible amino acids, $I_{\text{func}} \approx k \log_2 20 \approx 43$ bits — remarkably similar to the ribozyme case, suggesting a deep similarity in the information requirements for catalytic function in RNA and protein.

0.192 3. Seven Precisely Stated Open Problems

0.192.1 3.1 Stochastic Quasi-species at the Error Threshold

Open Problem 1. The Eigen quasi-species equation is deterministic ($N \to \infty$). In a finite population of effective size N_e, the error threshold becomes a crossover rather than a sharp phase transition. Derive the finite-N_e analogue of the error threshold condition.

[Finite population error threshold] For the two-class quasi-species model (master sequence with fitness $f_0 > 1$, mutants with fitness 1) in a Wright–Fisher population of size N_e, the critical mutation rate satisfies:

$$\mu_c(N_e) = \frac{\ln f_0}{L} + C \cdot \frac{(\ln f_0)^{3/2}}{L^{1/2} N_e^{1/2}} + O\left(\frac{1}{N_e L}\right),$$

where C is a universal constant depending only on the fitness distribution. At $\mu = \mu_c(N_e)$, the master sequence frequency follows a distribution with mean $\langle x_0 \rangle \approx 1/(2\sqrt{N_e \ln f_0})$ and variance of the same order.

The physical picture behind this conjecture: the finite-N_e correction arises because the stochastic version of the error threshold is a noisy first-order phase transition smoothed into a crossover. The width of the crossover scales as the strength of the fluctuations relative to the deterministic force, which in the Wright–Fisher model is $\sim 1/\sqrt{N_e}$. The factor $L^{-1/2}$ enters because the genome consists of L independent sites, and the combined effect of drift at each site gives a $\sqrt{L}$ enhancement of the stochastic correction.

0.192.2 3.2 NK Landscape Topology in the Thermodynamic Limit

Open Problem 2. For the NK random fitness landscape with L loci and K epistatic partners per locus, derive the asymptotic distribution of the number of local fitness maxima as $L \to \infty$ with $\kappa = K/L \in (0, 1)$ fixed.

Lemma 0.192.1 (Expected number of local maxima in the NK model)**.** In the NK model with uniform

random fitness contributions, the expected number of local maxima satisfies:

$$\mathbb{E}[\#\text{local maxima}] = 2^L \cdot P(\text{a given sequence is a local maximum}) = \frac{2^L}{L+1}$$

for $K = L - 1$ (fully epistatic landscape). For $K = 0$ (additive landscape), $\mathbb{E}[\#\text{local maxima}] = 1$ exactly.

Proof. For $K = L-1$: each sequence has L single-step neighbours. A sequence is a local maximum iff it has higher fitness than all L neighbours. Since all $L+1$ fitness values (the sequence and its L neighbours) are i.i.d. uniform on $[0, 1]$, the probability that any particular sequence is the maximum of $L + 1$ i.i.d. uniforms is $1/(L + 1)$. By linearity of expectation, $\mathbb{E}[\#\text{maxima}] = 2^L/(L + 1)$.

For $K = 0$: the fitness $f(\sigma) = \sum_i a_i\sigma_i$ (linear in alleles). The unique maximum is the sequence setting $\sigma_i = 1$ for all i with $a_i > 0$ and $\sigma_i = 0$ otherwise. (Almost surely unique for continuously distributed a_i.) Hence $\mathbb{E}[\#\text{maxima}] = 1$. □

The intermediate case $0 < K < L-1$ remains open. Numerical evidence suggests $\mathbb{E}[\#\text{maxima}] \sim 2^{Lh(\kappa)}$ with h increasing and concave in κ. A rigorous proof requires the cavity method from statistical physics (as used in the analysis of the random energy model and spin glasses).

0.192.3 3.3 Information Geometry of Selection and Drift

Open Problem 3. Develop a complete information-geometric theory of the Wright–Fisher diffusion.

Definition 0.192.2 (Fisher–Rao metric on allele frequency distributions)**.** Consider the family of distributions $\{f(x \mid p) : p \in (0, 1)\}$ where $f(\cdot \mid p)$ is the Wright–Fisher stationary distribution at allele frequency p. The Fisher information metric is:

$$g_{ij}(p) = \mathbb{E}\left[\frac{\partial \ln f}{\partial p_i} \cdot \frac{\partial \ln f}{\partial p_j}\right].$$

For the binomial family $f(k \mid p) = \binom{2N}{k}p^k(1 - p)^{2N-k}$, this gives $g(p) = 2N/[p(1 - p)]$ (scalar in one dimension). The geodesic distance between p_1 and p_2 in this geometry is:

$$d(p_1, p_2) = 2\sqrt{2N}\arcsin(\sqrt{p_2}) - 2\sqrt{2N}\arcsin(\sqrt{p_1}).$$

Theorem 0.192.3 (Natural selection as gradient flow in Fisher geometry)**.** For the codominant selection model $\dot{p} = sp(1 - p)/(2\bar{w})$, the selection dynamics correspond to gradient ascent of mean fitness $\bar{w}(p)$ with respect to the Fisher–Rao metric on the allele frequency simplex.

Proof. The gradient of $\bar{w}$ with respect to the standard metric on $[0, 1]$ is $d\bar{w}/dp = s$ (for the codominant model $\bar{w} = 1 + sp$). The Fisher–Rao metric tensor is $g(p) = 1/[p(1 - p)]$ (normalised). The Riemannian gradient is $\nabla^g\bar{w} = g(p)^{-1}(d\bar{w}/dp) = p(1 - p) \cdot s$. The gradient flow $\dot{p} = \nabla^g\bar{w}$ gives $\dot{p} = sp(1 - p)$, which matches the selection dynamics (up to the $1/\bar{w}$ factor, negligible for small s). □

This theorem connects evolutionary dynamics to differential geometry: selection is navigation on a curved manifold, with the curvature determined by the variance of allele frequencies.

0.192.4 3.4 Global Optimality of the Standard Genetic Code

Open Problem 4. Prove or rigorously disprove that the standard genetic code is a global optimum of error robustness.

Definition 0.192.4 (Code error robustness)**.** For a genetic code $\Gamma : \{A, C, G, U\}^3 \to \mathcal{AA} \cup \{\text{Stop}\}$, the error robustness is:

$$R(\Gamma) = -\sum_{\text{codons } c} \sum_{\text{single mutants } c'} p(c) q(c \to c') d_{\text{aa}}(\Gamma(c), \Gamma(c')),$$

where $p(c)$ is the usage frequency of codon c, $q(c \to c')$ is the misreading rate for the mutation $c \to c'$, and d_{aa} is the physicochemical distance between the amino acids. A more robust code has a smaller $|R|$ (misreading produces chemically similar amino acids).

Example 0.192.5 (Error robustness of the standard code)**.** Computing $R(\Gamma_{\text{standard}})$ over the $64 \times 3 = 192$ possible single-base misreadings, weighted by empirical codon usage frequencies and misreading rates at each position, gives $|R| \approx 0.07$ on the Grantham polarity-Section -composition scale (normalised). Of 10^7 randomly permuted assignments of amino acids to codon blocks, fewer than 1 in 10^6 have $|R| < 0.07$. The code is therefore in the top 10^{-6} quantile of error robustness, which is strong (though not conclusive) evidence for optimisation.

The argument for biological optimality: if the code evolved by a Darwinian process optimising translational fidelity, it would have been refined over $\sim 3 \times 10^9$ years of evolution. The effective population size for early life was enormous ($N_e \sim 10^{10}$–10^{12} for prokaryotes), making selection efficient at detecting very small improvements in translational accuracy. Even a 10^{-6} advantage per codon assignment change would be strongly selected in such populations, so optimality of the code is not implausible on evolutionary grounds.

0.192.5 3.5 The Structured Coalescent at Scale

Open Problem 5. Develop a computationally tractable approximation to the structured coalescent likelihood.

Definition 0.192.6 (Structured coalescent)**.** Consider k subpopulations of sizes $N_1, \ldots, N_k$ with symmetric migration rates m_{ij} (probability per generation that a lineage in population i has its ancestor in population j). A sample of n gene copies, distributed among populations, has a genealogy described by the structured coalescent: a continuous-time Markov chain with two types of events: coalescence of two lineages in the same population (rate $1/(2N_i)$ for each pair in population i), and migration of a lineage from population j to population i (rate m_{ij}).

Lemma 0.192.7 (State space explosion)**.** The number of states in the structured coalescent for n lineages in k populations is:

$$\binom{n + k - 1}{k - 1} = O\left(\frac{n^{k-1}}{(k-1)!}\right),$$

which is the number of ways to distribute n indistinguishable lineages among k populations (ignoring identity of lineages). Including lineage identity multiplies by the multinomial coefficient. For $n = 100$ lineages and $k = 10$ populations, the state space has $> 10^{10}$ states, making exact computation intractable.

Proof. The number of ways to distribute n indistinguishable balls into k urns is $\binom{n+k-1}{k-1}$ by stars-and-bars. For $n = 100, k = 10$: $\binom{109}{9} \approx 4.3 \times 10^{11}$. □

The challenge is to develop approximations that are both statistically valid and computationally feasible. Current approaches (MIGRATE, BPP, StarBeast) use MCMC but scale as $O(n^2 k^2)$ per step, limiting them to $n \lesssim 50$ and $k \lesssim 10$.

0.192.6 3.6 The Scaling Limit of the Mutation–Selection–Drift Equation

Open Problem 6. Derive the complete scaling limit of the mutation–selection–drift dynamics for the full genome.

The Wright–Fisher model and Kimura diffusion describe a *single locus* with selection, mutation, and drift. In reality, the genome contains $L \sim 10^9$ loci, all evolving simultaneously with linkage (recombination). The multi-locus problem has resisted a clean mathematical solution for 80 years. The challenge is that the state space is $[0,1]^L$ (a 10^9-dimensional cube), and the dynamics involve interactions between all pairs of loci through linkage disequilibrium.

Remark 0.192.8 (Known partial results). For $L = 2$ loci with recombination rate c and selection coefficients s_1, s_2, the 4-dimensional diffusion has been analysed in limiting cases:

- $c \gg s_1, s_2$: loci are approximately independent; use two-locus Hardy–Weinberg.
- $c \ll s_1 s_2$: strong epistasis case; treated by the quasi-linkage equilibrium approximation of Kimura (1965) and Nagylaki (1993).
- $c \sim s$: the full 4-dimensional Fokker–Planck equation has no known closed-form stationary distribution.

For $L \geq 3$ loci in the general case, no analytic theory exists.

0.192.7 3.7 A Mathematical Theory of Speciation

Open Problem 7. Develop a mathematically rigorous theory of speciation as a bifurcation in gene flow dynamics.

Remark 0.192.9 (The problem of speciation). Speciation — the splitting of one evolutionary lineage into two reproductively isolated ones — is the source of biological diversity. Despite a century of empirical study, there is no agreed mathematical theory of the rate of speciation or the conditions that favour it. The main challenge is that speciation involves a discontinuity (the emergence of a species barrier) in what is otherwise continuous evolutionary dynamics. The standard models (Bateson–Dobzhansky–Muller incompatibilities, reinforcement, sympatric speciation via assortative mating) have been studied with simulation and local stability analysis, but a global dynamical theory connecting the micro-evolutionary parameters (selection coefficients, migration rates, population sizes) to the macro-evolutionary rate of cladogenesis does not exist.

0.193 4. The Two Unifying Ideas

0.193.1 4.1 Population as Probability Distribution

Looking across all twelve Section s, one structural insight emerges with striking clarity: in every Section , the fundamental object is a **probability distribution over a space of types**, and evolution is a process that changes that distribution.

Section	Entity	Distribution space
I	Genotypes	Hardy–Weinberg simplex $(p^2, 2pq, q^2)$
II	Allele copies	$[0, 1]$ (allele frequency distribution)
III	Alleles under selection	Δ^n (allele frequency simplex)
IV	Organisms with character z	Joint distribution of (w, z)
V	Sequences	$\{0, 1\}^L$ (hypercube)
VI	Lineages	Probability distribution over tree topologies
VII	Strategies	Δ^n (mixed strategy simplex)
VIII	Replicating sequences	Quasi-species distribution on $\{0, 1\}^L$
IX	Symbolic sequences	Probability distribution over message space
X	Gene expression states	Attractor basin structure on $\{0, 1\}^N$
XI	Chemical species	Probability over reaction network states
XII	All of the above	Unified information-theoretic framework

The unification is not merely taxonomic. The same mathematical toolkit — martingales, diffusions, entropy, fixed-point theorems — applies to all these distribution spaces because they are all governed by the same class of dynamics: *stochastic processes on probability simplices*. Evolution, at any level and in any medium, is the dynamics of a probability distribution subject to selection (a force that modifies the distribution according to a fitness function), drift (a stochastic noise term), and transmission (a map from parent to offspring distributions).

0.193.2 4.2 Information as the Conserved Quantity

The second unifying idea is that **information** — in the precise Shannon-theoretic sense — is the quantity that evolution both creates and destroys.

Theorem 0.193.1 (Informal: the information budget of evolution)**.** In a population at mutation–selection–drift balance, the following information flows operate simultaneously:

1. **Selection reduces entropy**: it increases the mean fitness of the distribution, concentrating probability mass on fitter types. Information about the fitness landscape is transferred into the distribution.
2. **Mutation increases entropy**: it spreads the distribution, adding noise and destroying information about the current type.
3. **Drift randomly re-distributes entropy**: in finite populations, fluctuations move probability mass unpredictably, but in expectation neither create nor destroy information.
4. **The error threshold is the condition** under which the entropy production by mutation exceeds the entropy reduction by selection. Above the error threshold, genetic information is destroyed faster than selection can create it.

Precise version for the quasi-species. For the quasi-species evolving on a two-class fitness landscape (master f_0, mutants 1), let $H(t) = -x_0(t)\ln x_0(t) - (1-x_0(t))\ln(1-x_0(t))$ be the entropy of the quasi-species distribution. Selection drives $x_0 \to 1$ (entropy $\to 0$); mutation drives $x_0 \to 1/2$ (entropy $\to \ln 2$). At stationarity (Section 4 of Section VIII), $x_0^* = (f_0(1-\mu)^L - 1)/(f_0 - 1) \to 0$ as $\mu \to \mu_c = \ln(f_0)/L$. The entropy at stationarity satisfies $H(x_0^*) \to \ln 2$ as $\mu \nearrow \mu_c$: the quasi-species transitions from an ordered state (low entropy, concentrated on the master) to a disordered state (maximum entropy, uniform over all sequences). This transition is a second-order phase transition in information-theoretic terms: the order parameter is the information content $I = \ln 2 - H(x_0^*)$ of the quasi-species, which goes to zero at μ_c. □

Remark 0.193.2 (The origin of life as an information phase transition). Theorem 0.193.1 provides a mathematical framing for the origin of life. Before the origin of life, the "population" of chemical species was in the disordered phase: essentially random, with maximal entropy. The origin of life was the transition to the ordered phase: a self-replicating system capable of maintaining genetic information against the mutational noise, i.e., a system with $f_0 > e^{L\mu}$. The Kauffman autocatalytic set transition (Section XI) is the physical mechanism that produced the first system with $f_0 > 1$ (selective advantage of the replicating set); the Eigen error threshold is the condition that maintains the information once it exists. The origin of life is, in this sense, an information phase transition: the emergence of a system capable of resisting entropic degradation.

0.194 5. Synthesis: A Unified Framework

0.194.1 5.1 The Master Equation of Life

The Price equation

$$\bar{w}\,\Delta\bar{z} = \mathrm{Cov}(w, z) + \mathbb{E}[w\,\Delta z] \tag{18}$$

is a candidate for the "master equation" of life. Every evolutionary process studied in this series can be written as a special case or limit of (18). But the Price equation is a kinematic identity, not a dynamical law: it tells you how the mean of z changes given the joint distribution of (w, z), but it says nothing about how (w, z) itself evolves. The dynamical content must be supplied by specifying:

1. The fitness function $w(z)$ or $w(z, \bar{z})$ (direct or frequency-dependent).
2. The transmission map $z \mapsto z'$ (Mendelian, cultural, or other).
3. The stochastic structure (drift, mutation).

Different specifications give different Section s of this series. The Price equation is the algebraic shell; the biological content is in the instantiation.

0.194.2 5.2 The Hierarchy of Mathematical Structures

The mathematical objects in this series form a strict hierarchy, with each level containing the previous as a special case:

Level	Mathematical object	Biological level
1	Probability simplex Δ^n	Allele frequency distribution
2	Markov chain on Δ^n	Wright–Fisher model
3	Diffusion on Δ^n	Kimura approximation
4	Gradient flow on Δ^n	Selection dynamics
5	Replicator equation	Evolutionary game theory
6	Price equation	Universal selection identity
7	Quasi-species equation	Sequence-level selection
8	Reaction-diffusion system	Spatial pattern formation

Moving up the hierarchy adds biological generality but removes mathematical tractability. At level 1–3, exact results (fixation probabilities, stationary distributions) are available. At level 4–6, dynamical results (stability, equilibria) are accessible. At level 7–8, only local stability analysis and numerical simulation are feasible in full generality.

0.195 6. Appendix A: The Five Fundamental Theorems

Theorem 0.195.1 (1: Hardy–Weinberg, 1908)**.** In an infinite panmictic population at a biallelic locus with allele frequencies p and $q = 1 - p$, in the absence of selection, mutation, migration, and drift: (a) genotype frequencies are $p^2, 2pq, q^2$ after one generation of random mating; (b) these frequencies are stable for all subsequent generations; (c) allele frequencies are conserved at p and q.

Proof: Let P_{AA}, P_{Aa}, P_{aa} be the genotype frequencies. After one generation of random mating, the probability that an offspring receives allele A from each parent independently is $p = P_{AA} + P_{Aa}/2$ (allele frequency). By independence of gametes: $P'_{AA} = p^2$, $P'_{Aa} = 2p(1-p)$, $P'_{aa} = (1-p)^2$. The allele frequency in the next generation: $p' = P'_{AA} + P'_{Aa}/2 = p^2 + p(1-p) = p$. By induction, all subsequent generations have the same frequencies. □

Theorem 0.195.2 (2: Neutral Fixation Probability, Kimura 1955)**.** In a neutral Wright–Fisher population of size N, the probability that allele A, starting at frequency p_0, eventually fixes is p_0.

Proof: p_t is a bounded martingale (proved in Section II, Proposition 2.3); by Doob's convergence theorem it converges a.s. to a limit p_∞; since the chain is absorbed at $\{0, 1\}$ a.s., $p_\infty \in \{0, 1\}$; by the optional stopping theorem, $\mathbb{E}[p_\infty] = p_0$; hence $P(p_\infty = 1) = p_0$. □

Theorem 0.195.3 (3: The Price Equation, 1970)**.** For any population with fitness w_i and character z_i: $\bar{w}\,\Delta\bar{z} = \mathrm{Cov}(w, z) + \mathbb{E}[w\,\Delta z]$.

Proof: $\bar{z}' = \sum_i W_i z'_i = \sum_i W_i z_i + \sum_i W_i \Delta z_i = \bar{z} + \mathrm{Cov}(W, z)/\bar{w}^0 + \mathbb{E}[W\Delta z]$; after scaling the first covariance by $\bar{w}$, this yields (18). (Full proof in Section IV, Theorem 2.1.) □

Theorem 0.195.4 (4: Turing Instability, 1952)**.** A two-species reaction-diffusion system with a slower-diffusing activator and faster-diffusing inhibitor can develop spatial patterns from a homogeneous steady state that is stable without diffusion.

Proof: At the steady state (u^*, v^*), the Jacobian J has $\mathrm{tr}(J) < 0$ and $\det(J) > 0$. With diffusion, the dispersion relation gives instability at wavenumbers satisfying $\det(J - k^2 D) < 0$, i.e., $(D_v f_u + D_u g_v)^2 >$

$4D_uD_v \det(J)$ with $D_v f_u + D_u g_v > 0$. Both conditions are satisfiable with $D_v > D_u$ even when $\mathrm{tr}(J) < 0$. (Full proof in Section X, Theorem 3.2.) □

Theorem 0.195.5 (5: Quasi-species Stationarity, Eigen 1971)**.** The stationary distribution of the quasi-species equation $\dot{\mathbf{x}} = (QF - \Phi I)\mathbf{x}$ is the normalised Perron eigenvector of QF.

Proof: QF is a positive matrix (all entries > 0, since the mutation matrix Q has all positive entries). By the Perron–Frobenius theorem, QF has a unique Perron eigenvector $\mathbf{v}_{\max}$ with all positive components, corresponding to the largest eigenvalue $\lambda_{\max}$. Setting $\Phi = \lambda_{\max}$, the equation $\dot{\mathbf{x}} = (QF - \lambda_{\max} I)\mathbf{x} = 0$ has $\mathbf{x} = \mathbf{v}_{\max}/\|\mathbf{v}_{\max}\|$ as its unique positive equilibrium. Lyapunov stability follows from the Perron–Frobenius exponential convergence guarantee. □

0.196 7. Appendix B: Cross Section Mathematical Connections

Section **I** $\to$ Section **II.** Hardy–Weinberg equilibrium is the deterministic fixed point of the allele frequency dynamics. Section II shows what finite-population sampling does to this fixed point: the allele frequency becomes a stochastic process (martingale) that drifts away from equilibrium and is eventually absorbed at fixation or loss. The Hardy–Weinberg distribution is the initial distribution from which the Wright–Fisher process evolves; the $p^2, 2pq, q^2$ genotype probabilities become the initial condition for the diffusion.

Section **II** $\leftrightarrow$ Section **VI.** The Wright–Fisher diffusion, run backwards in time, is the Kingman coalescent. The time to the MRCA ($4N_e$ generations) is the backward version of the fixation time ($4N_e$ generations for a neutral allele). The duality between forward (diffusion) and backward (coalescent) processes is mediated by Kingman's duality theorem: $\mathbb{E}_p[\phi(p_t)] = \mathbb{E}_n[\phi(\text{Beta}(n, 2N - n))]$ for the appropriate starting conditions.

Lemma 0.196.1 (Kingman duality)**.** Let $\{p_t\}$ be the Wright–Fisher diffusion on $[0, 1]$ starting at $p_0 = x$, and let $\{N_t\}$ be the Kingman coalescent starting with n lineages. For any bounded measurable function ϕ:

$$\mathbb{E}_x[p_t^n] = \mathbb{E}_n\left[\binom{N_t}{n}^{-1} \cdot x^{N_t}\right],$$

where N_t is the number of lineages at time t. This duality implies that the probability that all n sampled lineages coalesce by time t equals the probability that the frequency of the ancestral allele, evolving forward t generations, is such that all n samples draw the same ancestral allele.

Section **III** $\to$ Section **VII.** The n-allele selection equation with frequency-dependent fitnesses is precisely the replicator equation of evolutionary game theory. Let n alleles have fitnesses $w_i(\mathbf{p}) = f_i(\mathbf{p})$ (functions of allele frequencies); the selection equation $\dot{p}_i = p_i(w_i - \bar{w})$ becomes the replicator equation $\dot{p}_i = p_i(f_i - \bar{f})$. Population genetics is a special case of evolutionary game theory; evolutionary game theory is population genetics with frequency-dependent selection.

Section **IV** $\to$ **All** Section **s.** The Price equation is the algebraic skeleton of every selection model in the series. Setting $z = w$ gives Fisher's theorem (Vol. III); setting $z = \nVdash[\text{altruism}]$ and interpreting r as regression coefficient gives Hamilton's rule (Vol. IV); taking the continuous-time limit of the Price equation gives the replicator equation (Vol. VII); applying it to sequence identity indicators gives the quasi-species (Vol. VIII).

Section **V** $\rightarrow$ Section **XI.** The neutral network percolation of Section V explains why functional RNA sequences (ribozymes) are accessible from any starting point in the RNA world (Section XI). If the neutral network of a functional structure percolates through sequence space, then any quasi-species evolving on the neutral network of a simpler structure is adjacent to the functional structure's neutral network by a single adaptive mutation. The accessibility of RNA function from random sequences is a consequence of neutral network percolation.

Proposition 0.196.2 (Percolation enables RNA world transition)**.** Let $\mathcal{G}_1$ be the neutral network of a non-catalytic RNA fold of size $|\mathcal{G}_1| = \epsilon_1 \cdot 4^L$, and $\mathcal{G}_2$ the neutral network of a catalytic ribozyme of size $|\mathcal{G}_2| = \epsilon_2 \cdot 4^L$, with $\epsilon_1, \epsilon_2 > 0$. If both neutral networks percolate (with the bond percolation threshold $p_c \approx 1/(2L)$ for the L-dimensional hypercube), then with probability $1 - e^{-\epsilon_1 \epsilon_2 4^L/(2L)}$, there exist sequences in $\mathcal{G}_1$ within Hamming distance 1 of $\mathcal{G}_2$. For large L, this probability approaches 1 for any $\epsilon_1, \epsilon_2 > 0$.

Sketch. Two percolating neutral networks span a constant fraction of the hypercube. For two sets of size $\epsilon_1 4^L$ and $\epsilon_2 4^L$ distributed (approximately independently, by the percolation spreading) in the 4^L-dimensional hypercube with $4L$ neighbours per vertex, the expected number of edges between them is $\epsilon_1 \epsilon_2 4^L \cdot 4L/|\mathcal{S}| \cdot |\mathcal{S}| = \epsilon_1 \epsilon_2 4^L \cdot 4L$. By the Markov inequality, the probability of zero edges is at most $e^{-\epsilon_1 \epsilon_2 4^L \cdot 4L}$, which goes to 0 super-exponentially. □

Section **VIII** $\leftrightarrow$ Section **IX.** The quasi-species error threshold (VIII) is the condition under which the Shannon channel capacity of the genetic replication machinery (IX) drops below the information content of the master sequence. The error catastrophe is an information-theoretic crisis: the channel can no longer reliably transmit the sequence information encoded in the master genotype.

Lemma 0.196.3 (Error threshold equals channel capacity condition)**.** For a binary symmetric channel with error probability μ per base and a genome of length L, the channel capacity is $C = 1 - H_2(\mu) = 1 + \mu \log_2 \mu + (1-\mu)\log_2(1-\mu)$ bits per site. The condition for the quasi-species to be localised (information-maintaining) is:

$$LC > \log_2 f_0 \quad \Leftrightarrow \quad \mu < \mu_c = H_2^{-1}\left(1 - \frac{\log_2 f_0}{L}\right).$$

For small μ: $H_2(\mu) \approx -\mu \log_2 \mu$, and $\mu_c \approx \ln(f_0)/L$ (matching Eigen's error threshold), so the two conditions are identical.

Proof. The quasi-species is localised iff the master sequence frequency is positive at stationarity. From the quasi-species stationarity condition, this requires $(1-\mu)^L f_0 > 1$, i.e., $L\ln(1-\mu) + \ln f_0 > 0$. For small μ, $\ln(1-\mu) \approx -\mu$, giving $\mu < \ln(f_0)/L$. For the information-theoretic condition: the channel capacity C bits per site must exceed the information per site required to specify the master sequence, which is $(\log_2 f_0)/L$ bits/site (the selective advantage sets the minimum information content). Hence $C > (\log_2 f_0)/L$ is necessary and sufficient for localisation. Equating the two expressions for μ_c (both derived from the same underlying condition) demonstrates the equivalence. □

0.197 8. Appendix C: Complete Mathematical Glossary

Allele frequency (p). The fraction of gene copies in a population carrying a specific allele. The fundamental state variable of population genetics.

Autocatalytic set (CAS). A set of molecular species where every member is catalysed by another member and the whole set can be produced from a food set. Emerges with high probability when catalytic connectivity $np > 1$ (Kauffman phase transition, Section XI).

Basic reproduction number ($\mathcal{R}_0$). Expected number of secondary infections caused by one infectious individual in a fully susceptible population. $\mathcal{R}_0 > 1$ is necessary and sufficient for an epidemic. See Section VIII, Section 5.

Coalescent. The stochastic process of lineage merging (coalescence) running backwards in time from a sample of n gene copies. Waiting time for $k \to k-1$ lineages: $\mathrm{Exp}(\binom{k}{2}/(2N_e))$. Time to MRCA: $4N_e(1-1/n)$ generations.

Diffusion approximation. The continuous-time, continuous-state limit of the Wright–Fisher Markov chain (large N_e). SDE: $dp = \sqrt{p(1-p)/(2N_e)}\,dW_t + \mu(p)\,dt$. Stationary distribution (with mutation): $\mathrm{Beta}(4N_e v, 4N_e u)$.

Effective population size (N_e). Size of an idealised Wright–Fisher population with the same allele frequency drift variance as the actual population. For variable-size populations: harmonic mean of historical sizes. For unequal sex ratios: $4N_f N_m/(N_f + N_m)$.

Error threshold. Critical mutation rate $\mu_c = (\ln f_0)/L$ above which the quasi-species delocalises from the fitness peak and genetic information is lost. Equivalently, the condition under which the Shannon channel capacity for genetic replication falls below the information content per site.

Evolutionarily stable strategy (ESS). A strategy $\mathbf{p}^* \in \Delta^n$ that cannot be invaded by any alternative strategy: $f(\mathbf{p}^*, \epsilon\mathbf{q} + (1-\epsilon)\mathbf{p}^*) > f(\mathbf{q}, \epsilon\mathbf{q} + (1-\epsilon)\mathbf{p}^*)$ for small $\epsilon > 0$. Every ESS is a Nash equilibrium; the ESS adds a secondary stability condition.

Fisher–Rao metric. The Riemannian metric on the statistical manifold of parametric probability distributions, defined by the Fisher information matrix $g_{ij}(\theta) = \mathbb{E}[(\partial \ln p/\partial\theta_i)(\partial \ln p/\partial\theta_j)]$. Natural selection is gradient ascent of mean fitness with respect to this metric (Theorem 0.192.3).

Fitness landscape. A function $f : \{0,1\}^L \to \mathbb{R}_{\geq 0}$ on the sequence hypercube. Characterised by its Walsh–Hadamard Fourier spectrum: $f(x) = \sum_S \hat{f}_S \chi_S(x)$. Ruggedness measured by the fraction of variance in high-order ($|S| \geq 2$) coefficients.

Functional information (I_{func}). The information content of a sequence performing a biological function: $I_{\text{func}} = -\log_2 f_{\text{min}}$, where f_{min} is the fraction of random sequences of the same length performing the function at least as well. For ribozymes, $I_{\text{func}} \approx 40$–$50$ bits.

Hamilton's rule. Altruism evolves if $rB > C$, where r is the coefficient of relatedness between actor and recipient, B is the fitness benefit to the recipient, and C is the fitness cost to the actor. Derived from the Price equation with r identified as the regression coefficient of recipient character on actor character (Section IV, Theorem 4.2).

Hardy–Weinberg equilibrium. Genotype frequencies $p^2, 2pq, q^2$ at a biallelic locus, reached in one generation of random mating and maintained indefinitely in the absence of evolutionary forces.

Hill–Robertson interference. The reduction in effective N_e for selection at a locus due to linkage with sites under selection elsewhere in the genome. Reduces the efficiency of both positive and purifying selection in finite, recombining genomes.

Hypercycle. A network of n self-replicating molecules where each catalyses the replication of the next: $\dot{x}_i = x_i(k_i x_{i-1} - \Phi)$. Interior fixed point $x_i^* = 1/n$; stable for $n \leq 5$, Hopf bifurcation to limit cycle for $n > 5$ (Section XI).

Jukes–Cantor distance. The corrected evolutionary distance between two sequences: $d_{JC} = -(3/4)\ln(1 - 4\hat{d}/3)$, where $\hat{d}$ is the observed fraction of differing sites. Corrects for multiple hits; derived from the continuous-time Markov chain for base substitution (Section VI).

Kimura's neutral theory. Most molecular variation within and between species is selectively neutral. Substitution rate equals mutation rate, independent of population size. Confirmed by synonymous site divergence rates across taxa.

Kingman coalescent. See *Coalescent* above.

Linkage disequilibrium (D). Statistical association between alleles at two loci: $D = x_{AB} - pr$. Decays geometrically as $(1-c)^t D_0$ under recombination at rate c. Standardised measures: $D' = D/D_{\max}$; $r^2 = D^2/(pqrs)$.

Martingale. A stochastic process $\{X_t\}$ with $\mathbb{E}[X_{t+1}|\mathcal{F}_t] = X_t$ a.s. The neutral Wright–Fisher allele frequency is a bounded martingale; by the optional stopping theorem, $\mathbb{E}[p_\tau] = p_0$, giving the neutral fixation probability.

McDonald–Kreitman test. Compares rates of protein evolution (d_N/d_S) to within-species polymorphism (p_N/p_S). Neutrality index NI $= (p_N/p_S)/(d_N/d_S)$; fraction of adaptive substitutions $\alpha = 1 - \text{NI}$. Standard test for adaptive molecular evolution.

Molecular clock. The rate of neutral substitution equals the neutral mutation rate μ per site per generation, independent of population size (Kimura 1968).

Mutation-selection balance. Equilibrium frequency of a deleterious allele: $\hat{q} \approx \mu/(hs)$ (partially dominant); $\hat{q} \approx \sqrt{\mu/s}$ (recessive). Haldane's load: genetic load $\approx u$ (genomic deleterious mutation rate), independent of selection coefficients.

Neutral network. Connected subgraph of sequence space consisting of sequences sharing a given phenotype. Percolates through sequence space for common RNA structures; large neutral networks generate the positive robustness–evolvability correlation.

NK model. Kauffman's parametric fitness landscape: L loci each interacting with K others. $K = 0$: unique global maximum. $K = L - 1$: random landscape with $\mathbb{E}[\#\text{local maxima}] = 2^L/(L+1)$.

Perron–Frobenius theorem. A positive matrix has a unique positive eigenvector (Perron vector) with the largest eigenvalue (Perron root), and all positive initial conditions converge to this eigenvector. Applied to the quasi-species equation (Section VIII, Theorem 3.1).

Price equation. $\bar{w}\,\Delta\bar{z} = \mathrm{Cov}(w, z) + \mathbb{E}[w\,\Delta z]$. Exact algebraic identity decomposing character change into selection and transmission terms. Subsumes Fisher's theorem, Hamilton's rule, Robertson's theorem, and the replicator equation (Section IV).

Quasi-species. The stationary distribution of a replicating, mutating population: the normalised Perron vector of QF. A cloud of mutants concentrated near the fitness peak, not a single sequence. Localised for $\mu < \mu_c$ and delocalised (disordered) for $\mu > \mu_c$.

Replicator equation. $\dot{p}_i = p_i(f_i(\mathbf{p}) - \bar{f}(\mathbf{p}))$. Continuous-time ODE for strategy frequencies in an evolutionary game. Mean payoff non-decreasing (symmetric games); ESS are asymptotically stable fixed points.

Robustness–evolvability correlation. Large neutral networks (high robustness) give access to more novel phenotypes (high evolvability), because they span more of sequence space. Proved for RNA secondary structures (Theorem 0.191.5); observed computationally for proteins and GRNs.

Structured coalescent. Extension of the Kingman coalescent to k subpopulations with migration. State space grows as $O(n^{k-1}/(k-1)!)$; computationally intractable for large n, k (Open Problem 5).

Tajima's D. Test statistic comparing $\hat{\theta}_W = S/H_{n-1}$ and $\hat{\theta}_\pi = \pi$. $D < 0$: excess rare variants (recent expansion or selective sweep); $D > 0$: excess intermediate variants (balancing selection or population subdivision).

Turing instability. Diffusion-driven instability of a homogeneous steady state in a reaction-diffusion system. Conditions: ODE stability plus $(D_v f_u + D_u g_v)^2 > 4D_u D_v \det(J)$ and $D_v f_u + D_u g_v > 0$. Pattern wavelength $\ell = 2\pi(D_u D_v/\det(J))^{1/4}$.

Walsh–Hadamard transform. The Fourier transform on $(\mathbb{Z}/2\mathbb{Z})^L$: $f(x) = \sum_{S\subseteq[L]} \hat{f}_S \chi_S(x)$, $\chi_S(x) = (-1)^{\sum_{i\in S} x_i}$. Decomposes fitness variance into additive ($|S| = 1$), pairwise epistatic ($|S| = 2$), and higher-order interaction components.

Wright–Fisher model. Canonical stochastic model of genetic drift: $X_{t+1} \sim \mathrm{Binomial}(2N, X_t/(2N))$. Allele frequency is a bounded martingale; fixation probability of neutral allele = initial frequency; absorption time for new neutral mutation $\approx 4N_e$ generations.

The mathematics of evolution and life is not complete. It is a discipline in active development, with deep open problems and entire biological phenomena for which the mathematical framework is only beginning to be adequate. But what exists already is enough to constitute one of the most beautiful mathematical structures in all of science: the precise, quantitative, and surprisingly unified account of how chance and necessity — drift and selection, mutation and constraint, information and entropy — conspire to generate, over deep time, the extraordinary complexity of the living world.

0.198 9. Appendix D: Major Open Problems — Extended Formulations

0.198.1 9.1 The Missing Heritability Problem

Genome-wide association studies (GWAS) have identified thousands of genetic variants associated with complex traits (height, body mass index, schizophrenia, diabetes). Yet the variants identified explain only a fraction of the trait's heritability estimated from twin studies:

Trait	Twin-study h^2	GWAS-explained h^2	Missing h^2
Human height	0.80	0.25 (2010) / 0.60 (2022)	0.20
BMI	0.70	0.15 / 0.40	0.30
Schizophrenia	0.80	0.30 / 0.55	0.25
Type 2 diabetes	0.50	0.12 / 0.20	0.30

The missing heritability has several candidate explanations, each with precise mathematical content:

1. **Common variants with small effects**: variants with $\beta < 10^{-4}$ standard deviations per allele are below the detection threshold in current GWAS (sample size $n \sim 10^5$–10^6). Power scales as $n\beta^2/2$ (non-central χ^2 approximation); for $n = 10^6$, effects below $\beta = \sqrt{4/10^6} \approx 0.002$ are undetectable at $p < 5 \times 10^{-8}$. Millions of such effects could collectively explain substantial h^2.

2. **Rare variants of large effect**: variants with MAF $< 1\%$ are poorly captured by SNP arrays and have wide confidence intervals. Whole-genome sequencing of biobank-scale cohorts ($n > 5 \times 10^5$) is now recovering some of this variance.

3. **Gene-gene interactions (epistasis)**: if true h^2 includes epistatic variance V_I, but twin studies measure total genetic variance while GWAS measures additive variance V_A, then $h^2_{\text{twin}} = (V_A + V_I)/V_P$ may exceed $h^2_{\text{GWAS}} = V_A/V_P$.

4. **Gene-environment interaction**: if $V_{GE} = \text{Cov}(\text{genotype}, \text{environment})$ contributes to phenotypic variance, twin studies may overestimate h^2 if twins share environments more than the model assumes.

[Precise decomposition of missing heritability] For any complex trait, decompose the missing heritability into its components: rare variants, small-effect common variants, epistasis, and GxE interaction. Develop statistical tests (under specific genetic architecture models) that can distinguish these explanations with genome-scale data. Specifically, quantify the fraction of the missing heritability attributable to epistasis using the Walsh–Hadamard framework of Section V.

0.198.2 9.2 The Evolution of Sex and Recombination

Sexual reproduction is costly: females who reproduce asexually produce twice as many female offspring per generation (no males), so an asexual mutant would have a 2-fold fitness advantage in a sexual population. Yet sex is nearly universal in eukaryotes. The "twofold cost of sex" paradox has been studied for 50 years without complete resolution.

Theorem 0.198.1 (Twofold cost of sex, formal)**.** In a population of N sexual and k asexual females,

where all females have equal fertility f, the fraction of asexuals in the next generation is:

$$\frac{k'}{N'} = \frac{2k}{k+N} > \frac{k}{N},$$

since asexual females produce $2f$ offspring (all female) while sexual females produce $2f$ offspring (half female, half male, of which only the female half reproduce). The asexual fraction increases by factor $(2N + 2k)/(k + N) = 2$ per generation — the 2-fold cost.

Proof. Next generation: asexual females produce $2k \cdot f$ females; sexual females produce $N \cdot f$ females (the male offspring don't reproduce). Total: $(2k + N)f$ females next generation. Asexual fraction: $2k/(2k + N)$. For small k/N: $2k/(2k + N) \approx 2k/N$, a doubling. □

The main hypotheses for sex's persistence:

- **Mutation clearance (Muller's ratchet)**: asexual populations accumulate deleterious mutations irreversibly (each lineage only ever gains new mutations). The "ratchet" clicks forward as the least-loaded class goes extinct by drift. Sex allows recombination to create low-mutation offspring from high-mutation parents.
- **Red Queen dynamics**: coevolution with parasites (host-parasite arms races) generates rapidly changing fitness landscapes. Recombination generates novel genotypes not yet targeted by the current parasite generation.
- **Hill-Robertson interference**: in finite genomes, selection at different loci interferes. Sex (recombination) reduces this interference, increasing the efficiency of selection.

Remark 0.198.2 (Mathematical unresolution). Despite 50 years of theory, no single mechanism clearly explains the universal prevalence of sex. The three main hypotheses give quantitative conditions under which sex is favoured, but these conditions are satisfied only in restricted parameter regimes. A complete mathematical theory of sex would need to quantify the relative magnitudes of mutation clearance benefit, Red Queen benefit, and the 2-fold cost, under biologically realistic parameter distributions. Such a theory does not yet exist.

0.199 10. Appendix E: Historical Sketch of the Mathematical Biology of Evolution

0.199.1 10.1 The Founders: Fisher, Wright, and Haldane (1918–1932)

The mathematical theory of evolution was created in a single decade by three scientists working largely independently:

R.A. Fisher (1890–1962):

- 1918: *The Correlation Between Relatives on the Supposition of Mendelian Inheritance*. First proof that Mendelian genetics can generate the continuous variation observed in quantitative traits. Introduced variance decomposition.

- 1922: First derivation of the Wright–Fisher sampling formula and the concept of effective population size.
- 1930: *The Genetical Theory of Natural Selection*. Proved the Fundamental Theorem of Natural Selection; introduced the concept of fitness as the Malthusian parameter.

Sewall Wright (1889–1988):

- 1921: Introduced the path coefficient method for genetic correlation analysis.
- 1931: *Evolution in Mendelian Populations*. Derived the stationary distribution of allele frequencies under drift, mutation, and selection (the diffusion approximation). Introduced the concept of "adaptive topography" (fitness landscape).
- 1932: The shifting balance theory; the concept of genetic drift as an escape mechanism from local fitness maxima.

J.B.S. Haldane (1892–1964):

- 1924–1932: *A Mathematical Theory of Natural and Artificial Selection* (series of 10 papers). Derived selection equations for diploid organisms, dominance, sex-linked loci; quantified the rate of evolution by selection.
- 1927: The fixation probability of a beneficial mutation ($\approx 2s$, the "Haldane sieve").
- 1932: *The Causes of Evolution*: unified synthesis of genetics and Darwinian evolution.

0.199.2 10.2 The Molecular Era: Kimura and the Neutral Theory (1953–1983)

The discovery of DNA structure (Watson and Crick 1953) transformed evolutionary biology: mutation became a concrete molecular event (base substitution, insertion, deletion), not a statistical parameter.

Motoo Kimura (1924–1994):

- 1955: First rigorous derivation of the probability of gene fixation using diffusion theory.
- 1968: The neutral theory of molecular evolution: most molecular variation is selectively neutral; the substitution rate equals the mutation rate.
- 1969: The infinite-sites model of molecular evolution.
- 1983: *The Neutral Theory of Molecular Evolution*: comprehensive treatment of neutral theory and its mathematical basis.

John Kingman (1939–):

- 1982: The Kingman coalescent. The genealogy of a sample from a large Wright–Fisher population, running backwards in time, is described by a Poisson process of lineage merging. This gave population genetics its backward-time framework and enabled Bayesian phylogeography.

0.199.3 10.3 The Information-Theoretic Turn: Eigen, Price, and Maynard Smith

Manfred Eigen (1927–2019):

- 1971: The quasi-species equation. Evolution operates on distributions of sequences, not on individual sequences; the error threshold places a fundamental limit on genome length at a given mutation rate.

- 1977–78 (with Schuster): The hypercycle.

- Nobel Prize in Chemistry, 1967 (for relaxation methods in chemical kinetics, not for the quasi-species — a frequent misconception).

George Price (1922–1975):

- 1970: The Price equation. Published in a single paper in *Nature* (389 words), it is arguably the most general statement of the mathematics of selection ever derived. Price later moved to London, gave away all his possessions to the homeless, and died of a self-inflicted wound in a squat in London in 1975.

John Maynard Smith (1920–2004):

- 1973 (with Price): The evolutionarily stable strategy. Applied game theory to biology for the first time.

- 1982: *Evolution and the Theory of Games*: the canonical treatment.

- 1995 (with Eörs Szathmáry): The major transitions in evolution.

Remark 0.199.1 (The mathematical character of these contributions). What unites Fisher, Kimura, Price, and Eigen is not a shared topic but a shared method: they all derived *exact algebraic or analytical results* from precise mathematical models, rather than fitting statistical models to data. This tradition of exact results from precise models is what distinguishes mathematical evolutionary biology from descriptive evolutionary genetics. The theorems proved by these researchers — Hardy-Weinberg stability, neutral fixation probability, the Price equation, quasi-species stationarity — are as mathematically rigorous as theorems in number theory or differential geometry.

0.200 11. Towards a Unified Theory: The Mathematics Yet to Be Written

0.200.1 11.1 The Multi-Scale Problem

The central unsolved problem in the mathematics of evolution and life is the **multi-scale problem**: how do molecular-level events (mutations, gene expression noise, protein folding) generate organism-level phenotypes, and how do organism-level phenotypes determine population-level evolutionary dynamics?

Each of the twelve Section s in this series operates at a different scale:

Scale	Timescale	Spatial scale	Section
Molecular (sequence)	Microseconds (folding)	Nanometres (protein)	V, VIII, IX
Cellular (GRN)	Minutes to hours	Micrometres (cell)	X
Developmental	Hours to days	Millimetres (organ)	X, XI
Population	Generations	Metres to km	I–IV, VI–VII
Ecological	Centuries	Continents	VII, VIII
Evolutionary	Millions of years	Biosphere	III, IV, VI

The mathematical links between scales are known in certain limiting cases:

- Molecular $\to$ Population: the distribution of fitness effects (DFE, Vol. V, XII) connects mutation biochemistry to population genetic dynamics.
- Cellular $\to$ Developmental: attractor landscapes (Vol. X) connect gene regulatory network dynamics to cell fate decisions.
- Population $\to$ Evolutionary: the Price equation (Vol. IV) and breeder's equation (Vol. III) connect within-generation fitness differentials to across-generation evolutionary change.

But the full vertical integration — from sequence to phenotype to fitness to population dynamics to long-term evolution — remains mathematically incomplete.

Remark 0.200.1 (The genotype-phenotype map as the missing link). The most acute gap is the **genotype-phenotype (GP) map**: the function $P : G \to \Phi$ from genotype space to phenotype space. For simple molecules (RNA secondary structure, small proteins), the GP map can be computed explicitly using thermodynamic models. For complex organisms, the GP map is unknown, uncomputable, and possibly irreducibly complex (not compressible below the size of the organism itself).

The holy grail of mathematical biology would be a statistical theory of the GP map: not the exact map for any specific organism, but a probabilistic description of the generic properties of GP maps (ruggedness, neutral network structure, phenotypic bias, robustness) that allows evolutionary dynamics to be predicted without knowing the full map. Partial results exist for RNA (Section s V, IX, X) but the generalisation to proteins, regulatory networks, and development is wide open.

0.200.2 11.2 The Extended Evolutionary Synthesis

The Modern Synthesis (Fisher, Wright, Haldane, Dobzhansky, Mayr, 1930s–1950s) unified Darwinian evolution with Mendelian genetics. An Extended Evolutionary Synthesis (EES) has been proposed (Laland et al. 2015; Pigliucci and Müller 2010) to incorporate additional mechanisms not in the Modern Synthesis:

Mechanism	Mathematical framework	Section
Phenotypic plasticity	Waddington potential (Vol. X)	X
Epigenetic inheritance	Non-genetic channels (Vol. IX)	IX
Niche construction	Eco-evolutionary feedback	VII
Cultural evolution	Price equation + social learning	IV, VII
Developmental bias	GP map ruggedness (Vol. V)	V

The mathematical challenge is that each EES mechanism requires extending the core population genetic framework (Section s I–IV) to handle non-genetic inheritance systems. The generalised Price equation (Section 5.3 of Section IV) is the most flexible framework, but deriving quantitative predictions from it requires specifying the transmission rules for each inheritance system, which are poorly characterised.

[Unified theory of extended inheritance] Develop a mathematically precise theory of heredity that encompasses genetic, epigenetic, behavioural, and ecological inheritance within a single dynamical framework. The theory should:

1. Specify the state space for each inheritance system (e.g., methylation patterns for epigenetic; learned behaviours for cultural).

2. Define fitness as a function of all inheritance systems jointly.

3. Derive the dynamics of all systems under selection, mutation, drift, and transmission (including interactions between systems).

4. Make quantitative predictions distinguishable from the predictions of the standard Modern Synthesis with genetic inheritance only.

.1 Appendice Tecnica I: Notazioni e Convenzioni Matematiche

.1.1 I.1 Notazione generale

Nel corso della monografia sono adottate le seguenti convenzioni notazionali uniformi:

Simbolo	Significato	Introdotto
N	Dimensione della popolazione (diploide: $2N$ geni)	Vol. I
p, q	Frequenze allelica ($q = 1 - p$ per locus biallelico)	Vol. I
s	Coefficiente di selezione	Vol. III
μ	Tasso di mutazione per locus per generazione	Vol. II
h	Coefficiente di dominanza ($h = 0$: recessivo; $h = 1$: dominante)	Vol. III
F_{ST}	Indice di struttura di Wright	Vol. I
$\mathcal{N}(\mu, \sigma^2)$	Distribuzione normale con media μ e varianza σ^2	Vol. II
$\mathrm{Cov}(X, Y)$	Covarianza tra variabili aleatorie X e Y	Vol. IV
$\mathbb{E}[X]$	Speranza matematica di X	Vol. II
$\mathcal{O}(\cdot)$	Notazione di Landau (ordine asintotico)	Vol. II
∇, Δ	Gradiente e laplaciano	Vol. X
$\otimes$	Prodotto tensoriale	Vol. VIII

.1.2 I.2 Convenzioni probabilistiche

Tutti gli spazi di probabilità $(\Omega, \mathcal{F}, \mathbb{P})$ sono assunti completi. I processi stocastici a tempo discreto sono indicizzati da $t \in \mathbb{N}_0$; quelli a tempo continuo da $t \in [0, \infty)$. La notazione $X_t \xrightarrow{d} X$ denota convergenza in distribuzione; $X_t \xrightarrow{p} X$ convergenza in probabilità; $X_t \xrightarrow{\text{q.c.}} X$ convergenza quasi certa.

.1.3 I.3 Convenzioni della genetica delle popolazioni

Salvo indicazione contraria: (i) le popolazioni sono diploidi con riproduzione sessuata; (ii) le generazioni sono discrete e non si sovrappongono; (iii) il modello neutro di riferimento è Wright–Fisher; (iv) le frequenze allelica sono misurate nella generazione degli adulti prima della selezione.

—

.2 Appendice Tecnica II: Riepilogo delle Equazioni Fondamentali

.2.1 II.1 Genetica delle popolazioni (Volumi I–IV)

Hardy–Weinberg (Vol. I):

$$P_{AA} = p^2, \quad P_{Aa} = 2pq, \quad P_{aa} = q^2, \qquad (p+q=1)$$

Equazione di selezione a un locus (Vol. III):

$$\Delta p = \frac{p\,q\big[p(w_{AA} - w_{Aa}) + q(w_{Aa} - w_{aa})\big]}{\bar{w}}$$

Equazione di Price (Vol. IV):

$$\bar{w}\,\Delta\bar{z} = \mathrm{Cov}(w, z) + \mathbb{E}[w\,\Delta z]$$

Probabilità di fissazione neutrale (Vol. II):

$$P_{\text{fix}}(p_0) = p_0$$

Tempo atteso di coalescenza (Vol. II):

$$\mathbb{E}[T_{\text{MRCA}}] = 4N\Big(1 - \frac{1}{n}\Big) \quad \text{(campione di } n \text{ individui)}$$

.2.2 II.2 Teoria dell'informazione evolutiva (Vol. VIII)

Entropia di Shannon della distribuzione genotipica:

$$H = -\sum_{i} p_i \log_2 p_i$$

Divergenza di Kullback–Leibler tra distribuzioni allelica:

$$D_{\text{KL}}(P \| Q) = \sum_{i} P(i) \log \frac{P(i)}{Q(i)}$$

.2.3 II.3 Dinamica di reazione–diffusione (Vol. X)

Sistema di Turing (instabilità di Turing):

$$\frac{\partial u}{\partial t} = D_u \nabla^2 u + f(u,v), \qquad \frac{\partial v}{\partial t} = D_v \nabla^2 v + g(u,v)$$

con condizione di instabilità: $D_v f_u + D_u g_v > 2\sqrt{D_u D_v \det J}$.

.2.4 II.4 Equazione delle quasi-specie (Vol. XI)

$$\dot{x}_i = \sum_{j} Q_{ij} f_j x_j - \Phi(t)\, x_i, \qquad \Phi(t) = \sum_{k} f_k x_k$$

—

.3 Appendice Tecnica III: Strumenti Computazionali e Software

.3.1 III.1 Pacchetti software di riferimento

I principali strumenti computazionali citati o implicitamente utilizzati nella monografia sono:

Software	Funzione	Section di riferimento
`ms` (Hudson 2002)	Simulazione coalescente	Vol. II
`msprime` (Kelleher et al. 2016)	Simulazione ARG efficiente	Vol. II
`PSMC` (Li & Durbin 2011)	Inferenza demografica	Vol. II
`BEAST` (Drummond et al. 2006)	Filogenesi bayesiana	Vol. VI
`ADMIXTURE` (Alexander et al. 2009)	Struttura di popolazione	Vol. I
`PLINK` (Purcell et al. 2007)	Analisi GWAS	Vol. I
`iqtree` (Nguyen et al. 2015)	Filogenesi ML	Vol. VI
`SLiM` (Haller & Messer 2019)	Simulazione forward-time	Vol. III
`AlphaFold2` (Jumper et al. 2021)	Struttura proteica	Vol. VIII

.3.2 III.2 Note computazionali

I tempi di calcolo indicati nella monografia si riferiscono a hardware standard da workstation (CPU quad-core, 64 GB RAM). Per genomica comparativa su scala di 10^4–10^5 individui è raccomandato l'uso di cluster HPC. Tutti i codici esemplificativi sono in pseudocodice indipendente dal linguaggio; implementazioni di riferimento sono disponibili nei repository citati.

—

Bibliografia

Bibliography

[1] Alexander, D.H., Novembre, J., & Lange, K. (2009). Fast model-based estimation of ancestry in unrelated individuals. *Genome Research*, 19(9), 1655–1664.

[2] Barton, N.H., & Turelli, M. (1991). Natural and sexual selection on many loci. *Genetics*, 127(1), 229–255.

[3] Bell, G., & Gonzalez, A. (2009). Evolutionary rescue can prevent extinction following environmental change. *Ecology Letters*, 12(9), 942–948.

[4] Bryant, D., & Moulton, V. (2004). Neighbor-Net: an agglomerative method for the construction of phylogenetic networks. *Molecular Biology and Evolution*, 21(2), 255–265.

[5] Bulik-Sullivan, B.K., et al. (2015). LD Score regression distinguishes confounding from polygenicity in genome-wide association studies. *Nature Genetics*, 47(3), 291–295.

[6] Charnov, E.L. (1976). Optimal foraging: attack strategy of a mantid. *The American Naturalist*, 110(971), 141–151.

[7] Ciliberti, S., Martin, O.C., & Wagner, A. (2007). Innovation and robustness in complex regulatory gene networks. *Proceedings of the National Academy of Sciences*, 104(34), 13591–13596.

[8] Coyne, J.A., Barton, N.H., & Turelli, M. (1997). Perspective: a critique of Sewall Wright's shifting balance theory of evolution. *Evolution*, 51(3), 643–671.

[9] Crick, F.H.C. (1968). The origin of the genetic code. *Journal of Molecular Biology*, 38(3), 367–379.

[10] Desai, M.M., Fisher, D.S., & Murray, A.W. (2007). The speed of evolution and maintenance of variation in asexual populations. *Current Biology*, 17(5), 385–394.

[11] Dobzhansky, T. (1937). *Genetics and the Origin of Species*. Columbia University Press, New York.

[12] Drummond, A.J., et al. (2006). Relaxed phylogenetics and dating with confidence. *PLOS Biology*, 4(5), e88.

[13] Eigen, M. (1971). Self-organization of matter and the evolution of biological macromolecules. *Naturwissenschaften*, 58(10), 465–523.

[14] Ewens, W.J. (1972). The sampling theory of selectively neutral alleles. *Theoretical Population Biology*, 3(1), 87–112.

[15] Felsenstein, J. (1981). Evolutionary trees from DNA sequences: a maximum likelihood approach. *Journal of Molecular Evolution*, 17(6), 368–376.

[16] Fisher, R.A. (1930). *The Genetical Theory of Natural Selection*. Clarendon Press, Oxford.

[17] FitzGibbon, C.D., & Fanshawe, J.H. (1988). Stotting in Thomson's gazelles: an honest signal of condition. *Behavioral Ecology and Sociobiology*, 23(2), 69–74.

[18] Frank, S.A. (1996). The design of natural and artificial adaptive systems. In M.R. Rose & G.V. Lauder (Eds.), *Adaptation*, pp. 451–505. Academic Press, San Diego.

[19] Gardner, T.S., Cantor, C.R., & Collins, J.J. (2000). Construction of a genetic toggle switch in *Escherichia coli*. *Nature*, 403(6767), 339–342.

[20] Geritz, S.A.H., Kisdi, E., Meszéna, G., & Metz, J.A.J. (1998). Evolutionarily singular strategies and the adaptive growth and branching of the evolutionary tree. *Evolutionary Ecology*, 12(1), 35–57.

[21] Gould, S.J. (1989). *Wonderful Life: The Burgess Shale and the Nature of History*. W.W. Norton, New York.

[22] Grafen, A. (1985). A geometric view of relatedness. *Oxford Surveys in Evolutionary Biology*, 2, 28–89.

[23] Grafen, A. (1990). Biological signals as handicaps. *Journal of Theoretical Biology*, 144(4), 517–546.

[24] Grant, P.R., & Grant, B.R. (2014). *40 Years of Evolution: Darwin's Finches on Daphne Major Island*. Princeton University Press.

[25] Gutenkunst, R.N., et al. (2009). Inferring the joint demographic history of multiple populations from multidimensional SNP frequency data. *PLOS Genetics*, 5(10), e1000695.

[26] Haldane, J.B.S. (1927). A mathematical theory of natural and artificial selection, part V: selection and mutation. *Proceedings of the Cambridge Philosophical Society*, 23(7), 838–844.

[27] Hamilton, W.D. (1970). Selfish and spiteful behaviour in an evolutionary model. *Nature*, 228(5277), 1218–1220.

[28] Hardy, G.H. (1908). Mendelian proportions in a mixed population. *Science*, 28(706), 49–50.

[29] Houchmandzadeh, B., Wieschaus, E., & Leibler, S. (2002). Establishment of developmental precision and proportions in the early *Drosophila* embryo. *Nature*, 415(6873), 798–802.

[30] Hudson, R.R. (1985). The sampling distribution of linkage disequilibrium under an infinite allele model without selection. *Genetics*, 109(3), 611–631.

[31] Hudson, R.R. (2002). Generating samples under a Wright–Fisher neutral model of genetic variation. *Bioinformatics*, 18(2), 337–338.

[32] Hutchison, C.A., et al. (2016). Design and synthesis of a minimal bacterial genome. *Science*, 351(6280), aad6253.

[33] Jumper, J., et al. (2021). Highly accurate protein structure prediction with AlphaFold. *Nature*, 596(7873), 583–589.

[34] Kauffman, S.A. (1989). Adaptation on rugged fitness landscapes. In D. Stein (Ed.), *Lectures in the Sciences of Complexity*, pp. 527–618. Addison-Wesley, Redwood City.

[35] Kauffman, S.A., & Levin, S. (1987). Towards a general theory of adaptive walks on rugged landscapes. *Journal of Theoretical Biology*, 128(1), 11–45.

[36] Kelleher, J., Etheridge, A.M., & McVean, G. (2016). Efficient coalescent simulation and genealogical analysis for large sample sizes. *PLOS Computational Biology*, 12(5), e1004842.

[37] Kermack, W.O., & McKendrick, A.G. (1927). A contribution to the mathematical theory of epidemics. *Proceedings of the Royal Society A*, 115(772), 700–721.

[38] Kimura, M. (1955). Solution of a process of random genetic drift with a continuous model. *Proceedings of the National Academy of Sciences*, 41(3), 144–150.

[39] Kimura, M. (1968). Evolutionary rate at the molecular level. *Nature*, 217(5129), 624–626.

[40] Kimura, M. (1983). *The Neutral Theory of Molecular Evolution*. Cambridge University Press.

[41] King, J.L., & Jukes, T.H. (1969). Non-Darwinian evolution: random fixation of selectively neutral mutations. *Science*, 164(3881), 788–798.

[42] Kingman, J.F.C. (1982). The coalescent. *Stochastic Processes and their Applications*, 13(3), 235–248.

[43] Laland, K.N., et al. (2015). The extended evolutionary synthesis: its structure, assumptions and predictions. *Proceedings of the Royal Society B*, 282(1813), 20151019.

[44] Lande, R. (1979). Quantitative genetic analysis of multivariate evolution, applied to brain:body size allometry. *Evolution*, 33(1), 402–416.

[45] Lewontin, R.C., & Cohen, D. (1969). On population growth in a randomly varying environment. *Proceedings of the National Academy of Sciences*, 62(4), 1056–1060.

[46] Li, H., & Durbin, R. (2011). Inference of human population history from individual whole-genome sequences. *Nature*, 475(7357), 493–496.

[47] Maynard Smith, J., & Price, G.R. (1973). The logic of animal conflict. *Nature*, 246(5427), 15–18.

[48] Maynard Smith, J., & Szathmáry, E. (1995). *The Major Transitions in Evolution*. W.H. Freeman, Oxford.

[49] Mayr, E. (1942). *Systematics and the Origin of Species*. Columbia University Press, New York.

[50] Metz, J.A.J., Nisbet, R.M., & Geritz, S.A.H. (1992). How should we define "fitness" for general ecological scenarios? *Trends in Ecology & Evolution*, 7(6), 198–202.

[51] Mirarab, S., et al. (2014). ASTRAL: genome-scale coalescent-based species tree estimation. *Bioinformatics*, 30(17), i541–i548.

[52] Moran, P.A.P. (1958). Random processes in genetics. *Proceedings of the Cambridge Philosophical Society*, 54(1), 60–71.

[53] Ohtsuki, H., Hauert, C., Lieberman, E., & Nowak, M.A. (2006). A simple rule for the evolution of cooperation on graphs and social networks. *Nature*, 441(7092), 502–505.

[54] Orr, H.A. (1995). The population genetics of speciation: the evolution of hybrid incompatibilities. *Genetics*, 139(4), 1805–1813.

[55] Orr, H.A. (2002). The population genetics of adaptation: the adaptation of DNA sequences. *Evolution*, 56(7), 1317–1330.

[56] Pigliucci, M., & Müller, G. (Eds.) (2010). *Evolution: The Extended Synthesis*. MIT Press, Cambridge MA.

[57] Price, G.R. (1970). Selection and covariance. *Nature*, 227(5257), 520–521.

[58] Prigogine, I. (1967). *Introduction to Thermodynamics of Irreversible Processes*, 3rd ed. Wiley, New York.

[59] Rissanen, J. (1978). Modeling by shortest data description. *Automatica*, 14(5), 465–471.

[60] Tajima, F. (1989). Statistical method for testing the neutral mutation hypothesis by DNA polymorphism. *Genetics*, 123(3), 585–595.

[61] Turing, A.M. (1952). The chemical basis of morphogenesis. *Philosophical Transactions of the Royal Society B*, 237(641), 37–72.

[62] Waddington, C.H. (1942). Canalization of development and the inheritance of acquired characters. *Nature*, 150(3811), 563–565.

[63] Wagner, A. (2008). Robustness and evolvability: a paradox resolved. *Proceedings of the Royal Society B*, 275(1630), 91–100.

[64] Weinberg, W. (1908). Über den Nachweis der Vererbung beim Menschen. *Jahreshefte des Vereins für vaterländische Naturkunde in Württemberg*, 64, 368–382.

[65] Wright, S. (1931). Evolution in Mendelian populations. *Genetics*, 16(2), 97–159.

[66] Wright, S. (1951). The genetical structure of populations. *Annals of Eugenics*, 15(4), 323–354.